UNIVERSITÉ DE MONTRÉAL

HYDRODYNAMIQUE DES LITS FLUIDISÉS À TROIS PHASES – MÉCANISMES CONVECTIF ET DISPERSIF

SYLVAIN LEFEBVRE
DÉPARTEMENT DE GÉNIE CHIMIQUE
ÉCOLE POLYTECHNIQUE DE MONTRÉAL

THÈSE PRÉSENTÉE EN VUE DE L'OBTENTION
DU DIPLÔME DE PHILOSOPHIAE DOCTOR
(GÉNIE CHIMIQUE)
AVRIL 2006

©Sylvain Lefebvre, 2006.

Library and Archives Canada

Published Heritage Branch

395 Wellington Street
Ottawa ON K1A 0N4
Canada

Bibliothèque et Archives Canada

Direction du Patrimoine de l'édition

395, rue Wellington
Ottawa ON K1A 0N4
Canada

Your file Votre référence
ISBN: 978-0-494-17980-2
Our file Notre référence
ISBN: 978-0-494-17980-2

NOTICE:
The author has granted a non-exclusive license allowing Library and Archives Canada to reproduce, publish, archive, preserve, conserve, communicate to the public by telecommunication or on the Internet, loan, distribute and sell theses worldwide, for commercial or non-commercial purposes, in microform, paper, electronic and/or any other formats.

The author retains copyright ownership and moral rights in this thesis. Neither the thesis nor substantial extracts from it may be printed or otherwise reproduced without the author's permission.

AVIS:
L'auteur a accordé une licence non exclusive permettant à la Bibliothèque et Archives Canada de reproduire, publier, archiver, sauvegarder, conserver, transmettre au public par télécommunication ou par l'Internet, prêter, distribuer et vendre des thèses partout dans le monde, à des fins commerciales ou autres, sur support microforme, papier, électronique et/ou autres formats.

L'auteur conserve la propriété du droit d'auteur et des droits moraux qui protège cette thèse. Ni la thèse ni des extraits substantiels de celle-ci ne doivent être imprimés ou autrement reproduits sans son autorisation.

In compliance with the Canadian Privacy Act some supporting forms may have been removed from this thesis.

While these forms may be included in the document page count, their removal does not represent any loss of content from the thesis.

Conformément à la loi canadienne sur la protection de la vie privée, quelques formulaires secondaires ont été enlevés de cette thèse.

Bien que ces formulaires aient inclus dans la pagination, il n'y aura aucun contenu manquant.

Canada

UNIVERSITÉ DE MONTRÉAL

ÉCOLE POLYTECHNIQUE DE MONTRÉAL

Cette thèse intitulée :

HYDRODYNAMIQUE DES LITS FLUIDISÉS À TROIS PHASES – MÉCANISMES CONVECTIF ET DISPERSIF

présentée par : LEFEBVRE Sylvain
en vue de l'obtention du diplôme de : Philosophiae Doctor
a été dûment soumise au jury d'examen constitué de:

M. TANGUY Philippe, Ph.D., président
M. CHAOUKI Jamal., Ph.D., membre et directeur de recherche
M. CHRISTOPHE Guy., Ph.D., membre et co-directeur de recherche
M. JOLICOEUR Mario, Ph.D., membre
M. WILD Gabriel, Ph.D., membre

DÉDICACE

À Mireille et Sofiane

REMERCIEMENTS

Le doctorat est long périple, rempli d'inattendu. Je remercie mes directeurs, Jamal Chaouki et Christophe Guy, d'avoir été là dans les moments où leur support m'était nécessaire et d'avoir su respecter ma situation particulière. Je leur suis également reconnaissant du soutien financier qu'ils m'ont accordé.

Je remercie également les membres du jury, le Dr. Gabriel Wild, le Dr. Philippe Tanguy et le Dr. Mario Jolicœur d'avoir accepté d'évaluer ma thèse.

J'exprime ma gratitude à l'équipe technique, soit Jean Huart, Robert Delisle, Carol Painchaud, Daniel Dumas et Gino Robin pour l'aide essentielle apportée à la réalisation de mon projet de thèse. Par ailleurs, il me faut souligner toutes les intéressantes conversations avec Jean Huart et Robert Delisle qui ont été présents aux étapes clés liées à la réalisation de ma thèse Merci également aux secrétaires, Brigitte Gagnon, Sabine Plusquellec, Chantal Faubert et Chantal Bénard de m'avoir si gentiment aidé en ce qui concerne les aspects plus administratifs du processus de thèse.

Un grand merci à Pierre Sauriol pour la réalisation des modifications aux programmes de RPT, ce qui a rendu son utilisation plus facile et plus efficace. Je souhaite remercier le Dr. Kennedy et M. Saint-Pierre d'avoir activé les sources radioactives et d'avoir répondu à mes nombreuses questions.

Je remercie mes compagnons d'étude, Yann Courbariaux, Pierre Sauriol, Rachid Mabrouk et Ramin Radmanesh de leur amitié et de leurs encouragements. Merci à mes compagnons de travail, Guillaume Hudon et Alexandre Beaulieu, de m'avoir soutenu et compris tout au long de ces années travail/étude. Je veux exprimer ma gratitude à mon employeur actuel pour son support et à mon directeur, Yves Pépin, pour ses

encouragements. Merci aussi à Michèle, ma sœur, et à Mme Jill Laleg pour les révisions linguistiques.

Compléter une thèse en travaillant à temps plein demande beaucoup de détermination de la part du candidat, mais l'appui de sa famille immédiate est essentiel à l'aboutissement de ladite thèse. Mireille, ma femme, a su comprendre ma volonté d'aller jusqu'au bout de l'aventure qu'a été ce doctorat. Elle m'a donné le soutien dont j'avais besoin. Je te remercie Mireille de ton amour, de ta chaleur et de ta patience. Je souhaite remercier ma fille, Sofiane, d'avoir manifesté une douceur extraordinaire et une maturité déconcertante pour une enfant de 4 ans quand papa lui disait, trop souvent, qu'il ne pouvait pas passer du temps avec elle.

RÉSUMÉ

Les deux objectifs de la thèse étaient d'identifier les caractéristiques clés liées à l'hydrodynamique des phases dans les lits fluidisés à trois phases et de développer un modèle de mélange le plus simple possible, mais qui respecte les caractéristiques clés liées à l'hydrodynamique. Pour répondre en partie au premier objectif, une revue critique de la littérature, ayant permis d'identifier les caractéristiques clés liées à l'hydrodynamique des phases dans les lits fluidisés à trois phases, a été faite. La technique de suivi d'une particule radioactive (RPT) a été utilisée afin de compléter la réponse du premier objectif et d'exploiter le modèle développé lors de la thèse (deuxième objectif). Les expériences ont été effectuées sur deux lits fluidisés de diamètre différent, soit 0.100 et 0.292 m. La plupart des expériences ont été faites avec un lit contenant des billes de verre de 3 mm de diamètre. Des particules de PVC ont aussi été fluidisées ainsi que des systèmes binaires composés de billes de verre de diamètres différents et composés de mélanges de billes de verre et de particules de PVC. L'air a été utilisé comme phase gazeuse et de l'eau municipale a servi à fluidiser les particules. Les plages de vitesses superficielles de gaz et de liquide étaient, respectivement, de 0.010-0.106 m/s et de 0.042-0.065 m/s.

La revue critique de la littérature a montré que le modèle piston-dispersif est trop simple pour simuler le mélange des phases lorsque les cinétiques chimiques sont rapides et les transferts de masse limitants. La phase gazeuse suit un mécanisme de mélange convectif. Autrement dit, la montée des bulles peut être représentée par une série de réacteurs pistons en parallèle. Ce mécanisme doit être différencié du mécanisme de mélange dispersif, caractérisé par un système où les éléments ont un mouvement erratique et dont la vitesse change de façon aléatoire. Une fraction du liquide et du solide, montant avec les bulles dans leur sillage, suit donc un mécanisme de mélange convectif. Une fraction du liquide et du solide suit aussi un mouvement

erratique et ils peuvent s'écouler dans des vortex. Un modèle schématique montrant l'interaction entre les phases et tenant compte des différentes fractions de liquide et de solide a été développé à la revue critique de la littérature. Ce modèle schématique est en fait une mise à jour du « structural wake model ».

Les données de RPT ont permis de quantifier les paramètres du modèle schématique pour la phase solide. Ces paramètres sont liés à la contribution relative du mécanisme convectif sur le mécanisme dispersif. La phase solide a été divisée en trois sous-phases, soit la sous-phase particule-sillage, la sous-phase particule-émulsion-descente et la sous-phase particule-émulsion-vortex. La première sous-phase représente le solide dans le sillage des bulles et suit un mécanisme convectif, i.e. vitesses Lagrangiennes constantes le long de l'axe de la colonne. La deuxième sous-phase représente le solide qui descend en suivant aussi un mécanisme convectif. La dynamique de ce solide descendant découle d'un mouvement compensatoire du solide qui monte dans le sillage des bulles. Le solide dans la sous-phase particule-émulsion-descente est donc indirectement lié à la dynamique des bulles. La troisième sous-phase représente le solide qui suit un mouvement erratique en attendant de passer dans une des deux sous-phases convectives pour parcourir de plus grandes distances axiales.

La distribution de vitesse du solide pour chacune de ces sous-phases a été obtenue. Pour le solide dans la sous-phase particule-sillage, les propriétés de la distribution de vitesse du solide suivent bien celles de la distribution de vitesse des bulles observées dans la littérature. La moyenne et l'écart-type (ÉT) de la distribution de vitesse du solide pour chacune sous-phase ont été obtenus. Pour le solide dans la sous-phase particule-sillage, sa vitesse moyenne passe de 0.11 à 0.35 m/s et augmente avec les vitesses superficielles du gaz et du liquide ainsi qu'avec le diamètre des lits fluidisés. L'ÉT de la distribution de vitesse du solide augmente, pour toutes les sous-phases, avec les vitesses superficielles du gaz et du liquide ainsi qu'avec le diamètre des lits

fluidisés. Une observation intéressante pour une mise à l'échelle est que l'ÉT adimensionnelle (ÉT/vitesse moyenne) n'est fonction que du diamètre du lit fluidisé. Il est de 0.4 et de 0.6 pour, respectivement, le lit de 0.10 et de 0.292 m de diamètre. L'ÉT donne une indication de l'intensité du mélange et l'ÉT des sous-phases convectives par rapport à la sous-phase dispersive représente la contribution du mécanisme convectif sur le mécanisme dispersif en terme d'intensité de mélange.

L'ÉT à lui seul n'est pas suffisant pour caractériser l'importance relative des mécanismes de mélange. La fraction volumique de chacune des sous-phases doit être tenue en compte car elle représente le poids de chaque mécanisme de mélange. La fraction volumique des deux sous-phases convectives combinées varie de 0.13 à 0.64 pour le lit de 0.10 m et de 0.54 à 0.74 pour le lit de 0.292 m. L'effet des paramètres opératoires sur la fraction volumique des sous-phases est plus complexe que pour la moyenne et l'ÉT des distributions de vitesse du solide. Pour le lit de 0.292 m, la fraction volumique de la sous-phase particule-sillage augmente avec la vitesse superficielle du gaz pour de faibles vitesses superficielles du liquide, mais diminue avec la vitesse superficielle du gaz pour de grandes vitesses superficielles du liquide. La fraction volumique de la sous-phase particule-sillage augmente avec le diamètre du lit fluidisé.

Des corrélations ont été développées pour les paramètres (ÉT, vitesse et fractions volumiques des sous-phases) qui viennent d'être décrits. Ces paramètres ont été combinés afin de développer un critère, nommé MMI , permettant de suivre l'importance relative du mécanisme convectif sur le mécanisme dispersif. Le MMI est le rapport de la moyenne de l'ÉT de la distribution de vitesse des sous-phases convectives pondérée par leur fraction volumique sur l'ÉT de la distribution de vitesse de la phase dispersive pondéré par sa fraction volumique. Le MMI a montré que l'effet des conditions opératoires sur l'importance relative du mécanisme convectif sur le

mécanisme dispersif est complexe et suit un comportement semblable à la fraction volumique de la sous-phase particule-sillage. L'importance relative des mécanismes ne suit pas l'intensité de mélange. Autrement dit, lorsque l'intensité de mélange augmente, l'importance relative du mécanisme convectif peut augmenter ou diminuer, selon les conditions opératoires et le diamètre du lit fluidisé.

Un modèle de mélange doit pouvoir suivre tant l'intensité de mélange que l'importance relative des mécanismes de mélange. Le modèle de mélange de la phase solide développé dans cette thèse permet de suivre les deux. Dans le modèle, le mélange de la phase solide est lié à la distribution de vitesse des bulles et tient compte de l'agitation erratique du solide dans la sous-phase dispersive. Les courbes « C_s vs t » générées par le modèle sur diverses positions axiales suivent assez bien les courbes expérimentales. Le modèle de dispersion axiale (modèle piston-dispersif avec vitesse nulle : système en cuvé) suivait moins bien les courbes expérimentales, indiquant qu'un seul paramètre n'est pas suffisant pour représenter le mélange du solide. Les modèles basés sur le « structural wake model » et le modèle de dispersion axiale, étant des cas particuliers du modèle proposé dans cette thèse, ne peuvent suivre mieux les courbes expérimentales. Le modèle de mélange de la phase solide proposé dans cette thèse est celui qui suit le mieux l'intensité du mélange et le seul qui peut suivre l'importance relative des mécanismes de mélange, mais il peut quand même être amélioré. Le modèle pourrait mieux suivre les courbes expérimentales en considérant l'évolution axiale de certains paramètres comme la fraction volumique des sous-phases et les moyennes et ÉT des distributions de vitesse de solide. Le modèle développé dans cette thèse est un modèle général par rapport à ce qui a été proposé dans la littérature, i.e. que le modèle de dispersion axiale peut être obtenu ainsi qu'un modèle de mélange basé sur le « structural wake model ».

ABSTRACT

The two objectives of the thesis were to identify the key hydrodynamic characteristics of the phases in three-phases fluidized bed and to develop a mixing model as simple as possible, but respecting the key hydrodynamic characteristics. In order to reach partially the first objective, a critical literature review, that allowed identifying the key hydrodynamic characteristics for three-phase fluidized bed, was performed. The Radioactive Particle Tracking (RPT) technique was used to reach completely the first objective and to exploit the mixing model developed during the thesis (second objective). Experiments were performed over two fluidized beds of different diameters, i.e., 0.10 and 0.292 m. Most of these experiments were done with a bed containing 3 mm diameter glass beads. PVC particles were also fluidized as well as binary systems composed with glass beads of various diameters and with mixtures of glass beads and PVC particles. The gas phase was air, and water was used to fluidize the particles. Superficial gas and liquid velocity ranges were 0.010-0.106 m/s and 0.042-0.065 m/s, respectively.

The critical literature review shown that the Axial Dispersion Model (ADM) was too simple to simulate the phases mixing when the kinetics were fast and the mass transfers limiting. Gas phase follows a convective mixing mechanism, i.e., the mixing is due to the various velocities of a system containing elements that have constant velocity. In other words, the rise of the bubbles may be represented by a series of plug flow reactors in parallel. This mixing mechanism has to be differentiated from the dispersive mixing mechanism, which is characterized by a system where the elements have an erratic movement and a velocity that changes randomly. A fraction of the liquid and the solid particles, which rise with the bubbles in their wake, follows a convective mixing mechanism. A schematic model showing phases interactions and taking into account various solid and liquid fractions (sub-phases) was developed in the

critical literature review. This schematic model is in fact an update of the structural wake model.

RPT data have allowed quantifying schematic model parameters for the solid phase. These parameters were linked to relative contribution of the convective mixing mechanism to the dispersive mixing mechanism. The solid phase was divided into three sub-phases, i.e., the particle wake sub-phase, the particle downflow-emulsion sub-phase and the particle vortex-emulsion sub-phase. The first sub-phase represented the solid particles in the bubbles wake and followed a convective mixing mechanism, i.e., constant Lagrangian velocity along column axis. The second sub-phase represented the solid particles that go down while also following a convective mixing mechanism. The dynamic of the solid particles in that sub-phase is caused by a compensatory effect of the solid particles rising in the bubbles wake. The solid in the particle downflow-emulsion sub-phase is thus indirectly linked to the bubbles hydrodynamics. Finally, the third sub-phase represented the solid that followed an erratic movement before reaching one of the two other sub-phases for covering larger axial distances.

Solid velocity distribution for each sub-phase was obtained. For the particle wake sub-phase, the solid velocity distribution properties followed well the one of the bubbles' velocity distribution observed in literature. Mean and standard-deviation (STD) of the solid velocity distribution were obtained for each sub-phase. The mean velocity of the solid in the particle wake sub-phase ranged from 0.11 to 0.35 m/s and increased with superficial gas and liquid velocity as well as with fluidized beds diameter.

Solid velocity distribution STD increased, for the all sub-phases, with superficial gas and liquid velocity as well as with fluidized beds diameter. An interesting observation for scale-up was that the dimensionless STD (STD/mean velocity) is a unique function

of the fluidized bed diameter. It was 0.4 and 0.6 respectively for the fluidized beds of 0.10 and 0.292 m in diameter. STD gave an indication of the extent of mixing and the STD of the convective sub-phases, relatively to one of the dispersive sub-phase, represented the contribution of the convective mixing mechanism over the dispersive one in term of mixing extent.

The STD alone was not sufficient to characterize the relative importance of the mixing mechanisms. Sub-phase holdup had to be taken into account because it represents the weight of each mixing mechanism. The convective sub-phases holdup varied from 0.13 to 0.64 for the 0.10 m diameter fluidized bed and from 0.54 to 0.74 m for the 0.292 m diameter fluidized bed. Operating parameters effects on the sub-fraction holdup were more complex than the ones on the solid velocity distribution mean and STD. For the 0.292 m fluidized bed, holdup of the particle wake sub-phase increased with superficial gas velocity for low superficial liquid velocity, but decreased with superficial gas velocity for high superficial liquid velocity. The particle wake sub-phase holdup increased with fluidized bed diameter.

Correlations for the above-described parameters were developed. These parameters were combined in order to develop an indicator, named the Mixing Mechanism Indicator (MMI), allowing to follow the relative importance of the convective onto the dispersive mixing mechanism. The MMI has shown that the effect of the operating conditions on the relative importance of the convective mixing mechanism over the dispersive one was complex and followed a similar behavior as the particle wake sub-phase holdup. Relative importance of the mixing mechanisms did not follow the extent of mixing. In other words, when the extent of mixing increases, the relative importance of the convective mixing mechanism may increase or decrease, depending on the operating conditions and the fluidized bed diameter.

A mixing model has to follow both extent of mixing and relative importance of mixing mechanism. The solid phase mixing model developed in this thesis allowed to follow both. In the model, the solid phase mixing was linked to the bubble velocity distribution and took into account the erratic movement of the solid particles in the dispersive sub-phase. The « Cs vs t » curves generated by the model for various axial positions followed fairly well the experimental curves. The ADM followed badly the experimental curves, indicating that only one parameter is not enough to represent the solid mixing. The ADM and the mixing based on the structural wake model, which are particular cases of the mixing model proposed in the thesis, do not followed better the experimental curves. The solid phase mixing model proposed in the thesis was the one that better followed the extent of mixing and the only one that followed the relative importance of the mixing mechanisms, but it can be improved. The model could follow even better the experimental curves while considering the axial evolution of some parameters such as the sub-phase holdup as well as the mean and STD of the solid velocity distribution. The mixing model developed in the thesis is a more general model relatively of the existing mixing model found in literature, i.e., the ADM and the mixing model based on the structural wake model may be obtained from the mixing model proposed in the thesis.

TABLE DES MATIÈRES

DÉDICACE IV

REMERCIEMENTS V

RÉSUMÉ VII

ABSTRACT XI

TABLE DES MATIÈRES XV

LISTE DES TABLEAUX XIX

LISTE DES FIGURES XXI

LISTE DES SYMBOLES ET ABRÉVIATIONS XXVIII

CHAPITRE 1 : INTRODUCTION 1

1.1 Problématique 1

1.2 But général et objectifs 2

1.3 Structure de la thèse 3

CHAPITRE 2 : REVUE CRITIQUE DE LA LITÉRATURE ET IDENTIFICATION DES CARACTÉRISTIQUES CLÉS DE L'HYDRODYNAMIQUE DES PHASES 5

2.1 Présentation de l'article 5

2.2 Phase Mixing Modeling in Multiphase Reactors Containing Gas Bubble: a Review 6
2.2.1 Abstract 6
2.2.2 INTRODUCTION 7
2.2.3 AXIAL DISPERSION MODEL 9
2.2.4 MIXING MECHANISMS 12
2.2.5 GAS PHASE MIXING MODELS 25
2.2.5.1 Model concept 25
2.2.5.2 Model exploitation 36
2.2.5.3 Conclusion 54
2.2.6 LIQUID PHASE MIXING MODELS 55
2.2.6.1 Model concept 55
2.2.6.2 Model exploitation 69
2.2.6.3 Conclusion 79
2.2.7 SOLID PHASE MIXING MODEL 81
2.2.7.1 Model concept 81
2.2.7.2 Model exploitation 96
2.2.7.3 Conclusion 100
2.2.8 LITERATURE PHASE MIXING MODELS GENERALIZATION 101
2.2.9 OTHER APPROACHES 107
2.2.10 CONCLUSION 113

CHAPITRE 3 : MÉTHODOLOGIE 145

3.1 Méthodologie générale 145

3.2 Montages expérimentaux 146

3.3 Conditions opératoires et systèmes 149

3.4 Technique de suivi d'une particule radioactive (RPT) 152

CHAPITRE 4 : HYDRODYNAMIQUE DE LA PHASE SOLIDE – UN MÉCANISME CONVECTIF/DISPERSIF 156

4.1 Présentation de l'article 156

4.2 Solid Phase Hydrodynamics of a Three-Phase Fluidized Bed – 157

4.2.1 Abstract 157
4.2.2 INTRODUCTION 158
4.2.3 MODEL CONCEPT AND MIXING MECHANISMS 159
4.2.4 EXPERIMENTAL 162
4.2.4.1 Experimental Setups 162
4.2.4.2 Radioactive Particle Tracking (RPT) 164
4.2.5 RPT DATA TREATMENT AND PARAMETER DEFINITION 165
4.2.6 MACROSCOPIC HYDRODYNAMICS - RESULTS 167
4.2.6.1 Solid Velocity 167
4.2.6.2 Particle Phase Holdup and Spending Time 185
4.2.7 MESOSCOPIC HYDRODYNAMICS - RESULTS 195
4.2.8 CONCLUSIONS AND DISCUSSIONS 200
4.2.9 ACKNOWLEDGEMENTS 204
4.2.10 NOMENCLATURE 204
4.2.11 REFERENCES 208

CHAPITRE 5 : HYDRODYNAMIQUE DE LA PHASE SOLIDE – UN MODÈLE CONVECTIF/DISPERSIF 250

5.1 Présentation de l'article 250

5.2 Solid Phase Hydrodynamics of Three-Phase Fluidized Beds – A Convective/Dispersive Mixing Model 251

5.2.1 Abstract 251
5.2.2 INTRODUCTION 251
5.2.3 EXPERIMENTAL 253
5.2.3.1 Experimental setups and operating conditions 253
5.2.3.2 Radioactive Particle Tracking (RPT) 253
5.2.3.3 Mixing data from RPT 254
5.2.4 CONVECTIVE/DISPERSIVE MODEL DEVELOPMENT 255

5.2.4.1 Model concept 255
5.2.4.2 Mathematical formulation 256
5.2.4.3 Model parameters 260
5.2.4.4 Numerical procedure 261
5.2.5 RESULTS AND DISCUSSION 262
5.2.5.1 Limits of the convective/dispersive model 266
5.2.6 CONCLUSION 267
5.2.7 Acknowledgements 268
5.2.8 Nomenclature 268
5.2.9 References 271

CHAPITRE 6 : DISCUSSION GÉNÉRALE 289

6.1 Distributions de vitesse du solide 292

6.2 Fraction volumique des trois sous-phases 294

6.3 Évolution de l'importance relative du mécanisme convectif sur le mécanisme dispersif 295

6.4 Représentation 2D de l'écoulement du solide et des fractions volumiques des sous-phases 296

6.5 Modèle de mélange de la phase solide 297

CHAPITRE 7 : CONCLUSION ET RECOMMANDATIONS 303

7.1 Conclusion 303

7.2 Recommandations 307

RÉFÉRENCES 309

LISTE DES TABLEAUX

Table 2.1: ADM validation relations for small and high dispersion.....17

Table 2.2: Gas phase mixing models.....29

Table 2.3: Gas phase mixing models-Experimental conditions.....31

Table 2.4: Gas phase mixing models-Model exploitation.....37

Table 2.5: Liquid phase mixing models.....56

Table 2.6: Liquid phase mixing models-Experimental conditions.....57

Table 2.7: Liquid phase mixing models-Model exploitation.....71

Table 2.8: Solid phase mixing models.....84

Table 2.9: Solid phase mixing models-Experimental conditions.....86

Table 2.10: Solid phase mixing models-Model exploitation.....97

Table 2.11: possibilities of the general phase mixing model.....104

Tableau 3.1 : Conditions expérimentales.....151

Table 4.1: Experimental conditions.....248

Table 4.2: Effect of superficial gas and liquid velocity on holdup parameters.....249

Table 5.1: Experimental conditions.....286

Table 5.2: Model parameters.....287

Table 5.3: Model parameter values and apparent axial dispersion coefficient.....288

LISTE DES FIGURES

Figure 2.1: Comparison between schematic representation of axial dispersion model and flow observed in (a) bubble columns (Franz et al., 1984) and in three phase fluidized bed (Chen et al., 1994 ; Larachi et al., 1996). (right Figure comes from Larachi et al.(1996)). 11

Figure 2.2: Prediction of some axial dispersion coefficient correlations for the three phases and for some multiphase reactors. Numbers on the upper right graph refer to the flow regime: 1)bubbly flow regime; 2)dispersed (homogeneous) 3)coalesced (heterogeneous). 13

Figure 2.3 : Three mixing mechanisms. 15

Figure 2.4: delta, δ, (defined in eq (5)) as a function of the first *Pe* measured (at L_1) for various sets of positions. 18

Figure 2.5: Example of the purely log-normal convective RTD axial evolution. Parameters used are: σ_u = 0.1 m/s and $\bar{u}$ = 1 m/s (or α = -0.005 and β = 0.0997). 22

Figure 2.6: optimized values of *n* that allows fitting the linear form of equation (17) to the standard-deviation axial evolution compute with equation (11). $\bar{u}$ = 1 m/s, *L* = 1, 2, 3, 4, 5 and 6 m. 24

Figure 2.7: Schematic representation of the gas phase mixing models proposed in literature. 28

Figure 2.8: Comparison of the reactor performance predictions of the SBC-ADM and the TBCMM of Modak et al. (1994). a) Ratio (SBC-ADM / TBCMM) of the predicted conversion. b) Ratio of the predicted selectivity. 53

Figure 2.9: Schematic representation of the liquid phase mixing model proposed by Degaleesan et al. (1996, 1997) 62

Figure 2.10: Schematic representation of the liquid phase mixing model proposed by Rustemeyer et al.(1989). 63

Figure 2.11: Schematic representation of the liquid phase mixing model proposed by (a) Nassar et al (1992) and (b) simplified by Schmidt et al. (1992) 67

Figure 2.12: Concentration time evolution predictions of the Degaleesan et al. (1996,1997) model in a liquid batch industrial slurry bubble column reactor. a) near the injection point. b) away from the injection point. (Degaleesan, 1997) 76

Figure 2.13: Flow representation characterizing solid phase mixing models. (Figure inspired by Murray and Fan, 1989) 82

Figure 2.14: a) experimental and b) predicted average axial mixing times evaluated from the instantaneous axial centroids of solids pulses injected at various heights in the bed. Air/water/glass bead system. Ug = 0.11 m/s, U_L = 0.065 m/s and d_p = 3 mm. (Cassanello et al., 1996). 100

Figure 2.15: Update of the flow representation shown in Figure 2.13. Dash arrows represent transferred solute between phases and the full arrows represent liquid and solid phases exchange between bubble/wake class and

liquid/solid emulsion phase, and between liquid/solid emulsion phase and liquid/solid vortex phase 107

Figure 3.1 : Système de distribution du lit fluidisé à trois phases de 0.10 m. Adapté de Larachi et al. (1996). 147

Figure 3.2 : Système de distribution du lit fluidisé à trois phases de 0.292 m. Les dimensions sont en mm. 148

Figure 3.3 : Arrangement typique des détecteurs à rayon gamma autour d'un lit fluidisé. 153

Figure 4.1: Flow representation characterizing various solid phase mixing models. (Figure inspired by Murray and Fan, 1989). Dash arrows represent transferred solute between phases and the full arrows represent liquid and solid phase exchange between wake and emulsion phases. 220

Figure 4.2: Three mixing mechanisms. 221

Figure 4.3: Update of the flow representation shown in Figure 4.1. Dash arrows represent transferred solute between phases and the full arrows represent liquid and solid phase exchange between bubble/wake class and liquid/solid emulsion phase, and between liquid/solid emulsion phase and liquid/solid vortex phase. 222

Figure 4.4: Distributor of the 0.292 m three-phase fluidized bed. Dimensions are in mm. 223

Figure 4.5: Time series of the traced particle axial position. Particle phase examples. Illustration of the spending time (t_{spend}) and axial trajectory length (l_z). Dc=0.292 m ; GB3mm ; UL=0.042 m/s ; Ug=0.050 m/s. 224

Figure 4.6: Solid Velocity Distribution functions – Downflow-Emulsion Phase, Vortex-Emulsion Phase, Wake Phase and all phases. Fitting quality example for Dc=0.292 m ; GB3mm ; UL=0.042 m/s ; Ug=0.031 m/s. 225

Figure 4.7: Solid Velocity Distribution function – Wake Phase. Operating conditions effect. Dc=0.292 m ; GB3mm. 226

Figure 4.8: Average and standard deviation (STD) of the Solid Velocity Distribution function – Wake Phase. Dc=0.292 m ; GB3mm. 227

Figure 4.9: Relation between the average and standard deviation (STD) of the Solid Velocity Distribution function – Wake Phase. (a) Comparison between Dc=0.10m and 0.292m. (b) Correlation taking into account the column diameter (Dc). 228

Figure 4.10: Relation between the average of the solid velocity distribution function and superficial gas and liquid velocity – Wake Phase. (a) Comparison between Dc=0.10m and 0.292m. (b) Correlation taking into account the column diameter (Dc). 229

Figure 4.11: Relation between the average of the solid velocity distribution function – Wake Phase vs Downflow-Emulsion phase. 230

Figure 4.12: Relation between the Average and Standard Deviation of the Solid Velocity Distribution function – Downflow-Emulsion Phase. (a) Comparison between Dc=0.10m and 0.292m. (b) Correlation taking into account the column diameter (Dc). 231

Figure 4.13: Solid Velocity Distribution function – Vortex Phase. Operating conditions effect. Dc=0.292 m ; GB3mm. 232

Figure 4.14: Standard deviation (STD) of the Solid Velocity Distribution function – Vortex Phase. 233

Figure 4.15: From Lagrangian to Eulerian velocity measurements. Contribution of the three particle phases. 234

Figure 4.16: Particle phase holdup. (a) Wake phase (b) wake phase correlation prediction quality (c) Relation between particle vortex-emulsion phase and particle wake phase holdup. 235

Figure 4.17: Relative contribution of the convective over dispersive mixing mechanism or Mixing Mechanism Indicator (MMI). 236

Figure 4.18: Cumulative distribution function of particle phase spending time. (a) Dc=0.292 m, GB3mm, UL=0.042 m/s, Ug=0.080 m/s (b) Dc=0.10 m, GB3mm, UL=0.065 m/s, Ug=0.069 m/s 237

Figure 4.19: Mean particle phase spending time. (a) Wake phase (b) Vortex-emulsion phase. 238

Figure 4.20: Mean particle wake phase particle spending time versus bed height. 239

Figure 4.21: Relation between particle convective spending time and particle convective phase velocity. Negative values for downflow-emulsion phase and positive values for wake phase. (a) direct plotting. (b) and (c) are the cumulative distribution function vs. convective velocity for the downflow-emulsion phase and wake phase, respectively. Dc=0.292 m, GB3mm, UL=0.042 m/s, Ug=0.080 m/s. 240

Figure 4.22: Solid phase velocity flow field and particle phases holdup field. Dc=0.292 m ; GB3mm ; UL=0.042 m/s ; Ug=0.080 m/s. 241

Figure 4.23: Comparison of the particle vortex-emulsion phase holdup axial profile and the particle occurrence axial profile. Dc=0.292 m ; GB3mm ; UL=0.042 m/s ; Ug=0.080 m/s. 242

Figure 4.24: Solid phase velocity flow field and particle phase holdup field. Dc=0.292 m ; GB3mm ; UL=0.062 m/s ; Ug=0.080 m/s. 243

Figure 4.25: Solid phase velocity flow field and particle phase holdup field. Dc=0.292 m ; GB3mm ; UL=0.042 m/s ; Ug=0.031 m/s. 244

Figure 4.26: Solid phase velocity flow field and particle phase holdup field. Dc=0.100 m ; GB3mm ; UL=0.065 m/s ; Ug=0.032 m/s. 245

Figure 4.27: Solid phase velocity flow field and particle phase holdup field. Dc=0.100 m ; GB3mm ; UL=0.065 m/s ; Ug=0.069 m/s. 246

Figure 4.28: Solid phase velocity flow field and particle phase holdup field. Dc=0.100 m ; PVC5.5mm ; UL=0.058 m/s ; Ug=0.025 m/s. 247

Figure 5.1: Schematics of the solid phase convective/dispersive model. 277

Figure 5.2: Time series of the traced particle axial position. Particle phases examples. Dc=0.292 m ; GB3mm ; UL=0.042 m/s ; Ug=0.050 m/s. 278

Figure 5.3: Convective/dispersive model fitting quality example for GB3mm. (a) run 3: Dc=0.10 m, U_L=0.065 m/s, Ug=0.106 m/s. (b) run 11: Dc=0.292 m, U_L=0.051 m/s, Ug=0.051 m/s. Dot: experimental result, line: model result. 279

Figure 5.4: Convective/dispersive vs axial dispersion model fitting quality example for run 2: GB3mm, Dc=0.10 m, U_L=0.065 m/s, Ug=0.069 m/s. (a) Convective/dispersive model (b) Axial dispersion model. Dot: experimental result, line: model result. 280

Figure 5.5: Axial profile of the mean velocity distribution from RPT data. Run 11 : Dc=0.292 m, U_L=0.051 m/s, Ug=0.051 m/s. 281

Figure 5.6: Particle wake phase Lagrangian velocity (slope of z vs t) vs axial trajectory length. Run 11 : Dc=0.292 m, U_L=0.051 m/s, Ug=0.051 m/s. 282

Figure 5.7: Particle wake phase velocity – fitted vs RPT values. The dashed line has a slope of 1. The solid line is a linear fit of the data and the slope is 0.8. ... 283

Figure 5.8: Fitted particle wake phase velocity vs solid phase holdup 284

Figure 5.9: Fitted exchange coefficient from the particle wake phase to the vortex-emulsion phase vs solid phase holdup 285

LISTE DES SYMBOLES ET ABRÉVIATIONS

Pour le chapitre 2

a	surface d'échange par unité de volume de réacteur ou de bulle (1/m)
A	aire (m^2) ; paramètre défini à la Table 2.8 (mole ou kg/m^2s)
A_e	aire effective de la surface de la sous-phase « particle entrainment » (m^2)
A_d	aire effective de la surface de la sous-phase « particle de-entrainment » (m^2)
B	constante de normalisation dans l'équation (47) (-)
C	concentration (kg ou $mole/m^3$)
C_t	coefficient de variation de la DTS (σ_t/t_m) (-)
C_u	coefficients de variation de la distribution de vitesse (σ_u/u_m) (-)
d_p	diamètre de particule (m)
d_b	diamètre de bulle (m)
D_{ax}	coefficient de dispersion axiale (ADC) (m^2/s)
D_{rad}	coefficient de dispersion radiale (m^2/s)
D_c	diamètre de colonne (m)
$Diff_A$	Coefficient de diffusion de A dans la liquide (m^2/s)
E	espérance mathématique; fonction de transfert dans le domaine du temps ; DTS (s^{-1})
Ez	coefficient de mélange du solide dans la modèle sillage-émulsion (m^2/s)

Ez'	coefficient de mélange du solide défini dans la Table 2.8 (m^2/s)
Ez''	fonction de mélange du solide défini par les équations (62) et (64) (m^2/s)
f	fonction de probabilité ; fonction des paramètres entre parenthèses
f_e	transfert de masse entre deux classes de bulle (s^{-1})
f_s	fréquence de passage des bulles-pistons (« slug ») dans le modèle de Myers et al. (1987) (s^{-1})
f_{wsh}	fréquence de largage de sillage de bulles (« wake shedding frequency ») (s^{-1})
$F_{s_{dw}}$	flux de solide sortant du sillage des bulles (mole ou kg/m^2s)
G	terme de génération nette net dans équation (68)
g	accélération gravitationnelle (m/s^2)
h_{mc}	hauteur de cellule de mélange du modèle de Rustemeyer et al. (1989) (m)
H	constante de Henry
Ha	nombre de Hatta défini à l'équation (34) (-)
H_c	hauteur de réacteur (m)
HWU	hauteur d'une unité de sillage (m)
I	fonction d'interaction entre les phases (équation (62)) (mole ou kg/m^3s)
J^*_A	flux molaire du soluté A à l'interface liquide/gaz ($mole/m^2s$)
k	rapport de la fraction volumique de la sous-phase solide/liquide-sillage sur celle de la phase gazeuse (-) ; constante cinétique

K	coefficient d'échange massique entre les régions de montées et de descente du modèle de Degaleesan et al. (1996, 1997) (m^2/s)
$K_{ls\text{-}w}$	coefficient d'échange massique entre les sous-phases liquide/solide-émulsion et sillage (s^{-1})
k_L	coefficient gaz/liquide d'échange massique du coté liquide (m/s)
K_{La}	coefficient gaz/liquide d'échange massique global du coté liquide (m/s)
L	distance entre deux points de mesure ; longueur de réacteur (m)
L_m	hauteur de la zone ayant une fraction de solide constante dans un lit fluidisé à trois-phase (m)
m	masse (kg)
M	nombre total de particules suspendues (-)
M_{kl}	transfert de quantité de mouvement à l'interface des phases k et l (Pa)
n	exposant de la corrélation de Richardson and Zaki (équation (57)); nombre de cellule de mélange du modèle de Rustemeyer et al. (1989) ; exposant à l'équation (17)
n_b	concentration en nombre de bulles par unité de volume de suspension liquide/solide (« slurry ») (Nb/m^3)
n_{bz}	nombre de point de mesures axiales (-)
n_{bt}	nombre de valeur de DTS (-)
N	nombre de cellule (-)
N_b	nombre de bulles totale dans le système (-)

N_{st}	nombre d'étage de largage de sillage (« wake shedding stages ») après lequel il n'y a plus de solide (-)
P	paramètre optimisé du modèle de Murray and Fan (1989) (P'[xkε_g + (1-ε_g-kε_g)]) ; pression
P'	paramètre de l'équation (59) (défini par l'équation (61))
p	probabilité d'un placement Δz vers la droite (« random walk ») et p+q=1 (-)
Pe	nombre de Peclet (Pe=UL/Dax) (-)
Pe_{eq}	nombre de Peclet équivalent (défini à l'équation (14)) (-)
Q	débit volumique (L ou m^3/h ou s)
q	probabilité d'un placement Δz vers la gauche (« random walk ») et p+q=1 (-)
r	position radiale (m)
r^2	fonction objective défini par l'équation (16) (s^{-2})
R	rayon de colonne (m) ; rayon de courbure de bulle (modèle de Dayan and Zalmanovich (1982)) (m) ; vitesse de réaction
Re_b	nombre Reynolds de bulle ($\rho_L u_{bL} d_b / \mu_L$) (-)
S	source de transfert de quantité de mouvement (toutes les forces externes excluant la force gravitationnelle) (Pa)
Sr	nombre de Strouhal ($f_{wsh} d_b / u_{bL}$) (-)

t	temps ; temps de résidence (s)
t_m	temps de résidence moyen (s)
U	vitesse superficielle (m/s)
$U_{b\infty}$	vitesse terminale de bulle (m/s)
u	vitesse interstitielle (ui = Ui/εi) (m/s) ; vitesse moyenne d'un élément de fluide (voir équations (9) et (10)) (m/s)
$\overline{u}$	moyenne des vitesses moyenne défini à l'équation (12) (m/s)
$\vec{u}$	vecteur vitesse (m/s)
u_b	vitesse moyenne des bulles (m/s)
u_{bL}	vitesse des bulles relative à la vitesse du liquide ($U_g/\varepsilon_g - U_L/\varepsilon_L$) (m/s)
$\hat{u}_{\rho b}$	vitesse moyenne du liquide de la masse (« bulk ») du liquide (m/s)
$\hat{u}_{\rho L}$	vitesse moyenne du liquide de la sous-phase sillage des bulles (m/s)
u_{bp}	vitesse relative à une population de bulles définie par une distribution log-normale (équation (19)) (m/s)
u_{Lls}	vitesse moyenne du liquide dans la phase liquide émulsion (équation (56)) (m/s)
$\hat{u}_L$	vitesse locale moyenne du liquide (m/s)
u_{pe}	vitesse moyenne axiale des particules entraînées (m/s)
u_{ps}	vitesse moyenne de glissement (relative à la vitesse du liquide de la sous-phase émulsion) (m/s)

u_{t0}	vitesse terminale de particule (m/s)
u_m	vitesse moyenne (m/s)
V	volume (L ou m^3) ; fonction de vitesse (équations (62) et (63))
v	débit volumique (L ou m^3/h ou s)
v_e	vitesse moyenne des particules entraînées relative à la vitesse de monté des bulles (m/s)
v_d	vitesse moyenne des particules dé-entraînées relative à la vitesse de monté des bulles (m/s)
v_r	vitesse radiale (relative aux coordonnées sphériques d'une bulle) de particule à la frontière du sillage de la bulle (m/s)
V_p	vitesse de chute d'une particule (équation (55)) (m/s)
w	paramètre de l'équation (8) (-)
W	paramètre adimensionnel ($U_L A/(f^s V^c(1-\varepsilon^{gc}))$) des équations (39)-(42) (-)
x	rapport de la fraction volumique du solide dans la sous-phase sillage sur celle dans la dans la sous-phase émulsion (-)
X	paramètre adimensionnel (V_{LE}/V_{LUF}) des équations (39)-(42) (-)
Y	paramètre adimensionnel ($V_{LE}/(V_c(1-\varepsilon_{gc}))$) des équations (39)-(42) (-)
z	position axiale (m)
Z	paramètre adimensionnel ($V_{LDF}/(V_c(1-\varepsilon_{gc}))$) des équations (39)-(42) (-)

Lettres grecques

α paramètre de la distribution log-normal (équations (10), (15) et (19)) (-); intensité de transition de la sous-phase sillage à la sous-phase de masse du liquide (« bulk phase ») (s^{-1}) ; rapport du débit de gaz dans la région du centre du groupe de bulle (ou de la classe de grosses bulles) sur le débit de gaz totale (-) ; fraction des vitesses de sillage de bulles (équation (54)) (-)

β paramètre de la distribution log-normal (équation (19)); intensité de transition de la sous-phase de masse du liquide (« bulk phase ») à la sous-phase sillage (s^{-1})

Δz intervalle de position axiale (m)

δ fonction de Diract ; paramètre du modèle de Tsutsumi et al. (1992) ; paramètre de l'équation (5) (-)

δ_l distance moyenne de parcours de sillage de bulles à travers la section à partir du point de formation (m)

ε fraction volumique des phases (-)

ϕ représente la dépendance d'une fonction d'une phase ou sous-phase (équations (63) et (64)) (-) ; probabilité par unité de temps pour qu'un élément de fluide change de vitesse (s^{-1})

γ paramètre de l'équation (5) (-)

θ position angulaire (rad ou degré)

θ_w	temps que les particules continues de monter suite au largage du sillage de la bulle (s)
ρ	densité d'une phase (kg/m^3)
σ	écart-type ; tension de surface
σ_o	constante de proportionnalité de l'équation (17) (s)
σ_u	écart-type défini à l'équation (13) (m/s)
σ^2	variance
τ	contrainte de cisaillement (Pa)
$\bar{\bar{\tau}}$	tenseur de contrainte de cisaillement (Pa)
λ_{de}	probabilité par unité de longueur qu'une particule soit expulsée de la région entraînement des bulles (m-1)
λ_{ls}	paramètre du modèle de Turi and Ng (1986) ($u_b A_{enb}/V_p$)
μ	moyenne de la DTS (s) ; viscosité (Pa s)
$\mu_{X(t)}$	moyenne de la distribution de longueur axiale de trajectoire des éléments liquide (Nassar et al., 1992) (m)
$\sigma^2_{X(t)}$	écart-type de la distribution de longueur axiale de trajectoire des éléments liquide (Nassar et al., 1992) (m)
ψ	fonction de probabilité en nombre normalisée (-)
$\zeta_{i,...,}$	propriétés d'une population, exemple : volume, densité

Indice

0	condition d'alimentation
1	région de monté du modèle de Degaleesan et al. (1996, 1997)
2	région de décente du modèle de Degaleesan et al. (1996, 1997)
A	espèce A
a	région prêt du distributeur du modèle de Degaleesan et al. (1996, 1997)
ADM	relié au modèle piston-dispersif (« Axial Dispersion Model »)
b	région de désengagement du mkodèle de Degaleesan et al. (1996, 1997)
c	phase des cellule de mélange du modèle de Myers et al. (1987)
conv	relié au modèle convective
g	phase gazeuse
i	phase gazeuse, liquide ou solide ; position (numéro) de la cellule de mélange du modèle de Myers et al. (1987)
j	relatif à la position d'un détecteur (équations (30) et (31))
k	phase gazeuse, liquide ou solide ; relatif à la position d'un détecteur (équations (30) et (31))
ls	sous-phase émulsion liquide/solide
L	phase liquide
LNC/ADM	relié au modèle log-normal convective/dispersive (ADM)
l	phase gazeuse, liquide ou solide
LDF	liquide descendant du modèle de Myers et al. (1987)

LE	échange de liquide entre la région des bulles-pistons (« slug ») et les cellules de mélange du modèle de Myers et al. (1987)
LUF	liquide montant du modèle de Myers et al. (1987)
N	dernière cellule de mélange du modèle de Myers et al. (1987)
p	relié aux particules
pb	relié à la vitesse du liquide dans la sous-phase sillage de bulles dans un système gaz/liquide
pL	relié à la vitesse de la masse de liquide
R	relié au réacteur
s	phase solide ; sous-phase bulles-pistons (« slug ») du modèle de Myers et al. (1987)
sl	suspension liquide/solide
T	traceur
t	relié au temps de résidence
u	relié à la distribution de vitesse
ub	relié à la distribution de vitesse des bulles
w	sous-phase sillage de bulle

Exposant

*	état d'équilibre
'	pour vitesse et concentration basée sur le volume de réacteur

0	relié à la distribution idéale de vitesse de bulle
a	groupe de bulles sur l'anneau (« annulus ») près des parois
c	groupe de bulles au centre (« core »)
f	condition d'alimentation
I	classe de bulle, i.e. petite (S) et grosse bulle (L) ou groupe de bulles sur l'anneau (a : « annulus ») et au centre (c : « core »)
L	classe des grosses bulles
S	classe des petites bulles
ϕ	phase et sous-phase, peut être gaz, liquide, solide, sillage, masse (« bulk ») du liquide, etc

Pour le Chapitre 4 :

d_b	diamètre équivalent moyen des bulles (m)
d_p	diamètre des particules (m)
D_T	diamètre de colonne (m)
f_b	fonction de poids dépendant des propriétés des bulles (-)
f_{le}	fonction de poids dépendant des propriétés de la phase liquide-émulsion (-)
l_b	longueur de corde de bulle locale (m)
MMI	Mixing Mechanism Indicator (-)
r	position radiale (m)
R	rayon de colonne (m)
t_{spw}	temps passé dans la sous-phase particule-sillage (s)
t_{tot}	temps total de l'expérience (s)
u_b	vitesse moyenne des bulles relatives aux parois (m/s)
u_{br}	vitesse moyenne des bulles relatives à la phase liquide (m/s)
$u_{b_{\phi_i}}$	vitesse de la bulle de la classe ϕ_i (m/s)
u_{pde}	vitesse moyenne du solide dans la sous-phase particule-descente-émulsion (m/s)
u_{pded}	vitesse du solide dans la sous-phase particule-descente-émulsion – distribution log-normale (m/s)
u_{pvd}	vitesse du solide dans la sous-phase particule-vortex-émulsion (m/s)

u_{pve}	vitesse moyenne du solide dans la sous-phase particule-vortex-émulsion (m/s)
u_{pw}	vitesse moyenne du solide dans la sous-phase particule-sillage (m/s)
u_{pwd}	vitesse du solide dans la sous-phase particule-sillage – distribution log-normale (m/s)
u_s	vitesse nette de la phase solide (m/s)
U_g	vitesse superficielle du gaz (m/s)
U_L	vitesse superficielle du liquide (m/s)
U_{sl}	vitesse superficielle du mélange liquide-solide (slurry) (m/s)
v_b	vitesse locale de bulle relative aux parois (m/s)
v_{br}	vitesse locale de bulle relative à la phase liquide (m/s)
v_{le}	vitesse locale de la phase liquide-émulsion (m/s)
V_{ls}	vitesse de la phase émulsion ayant un mouvement net non-nul (m/s)
V_s	vitesse de solide dans une sous-phase spécifiée (m/s)
V_p	vitesse de particule dans la sous-phase particule/liquide émulsion (m/s)

Lettres grecques

α	paramètre de la fonction de distribution log-normale (-)
α_v	rapport $\varepsilon_v/\varepsilon_{ls}$
β	paramètre de la fonction de distribution log-normale (-)
ε	fraction de vide du lit (-)
ε_e	fraction volumique de la sous-phase solide/liquide décente/monté-émulsion (-)

ε_g	fraction volumique de la phase gazeuse (-)
$\varepsilon_{g_{\phi_i}}$	fraction volumique de la classe ϕ_i dans la phase gazeuse (-)
ε_L	fraction volumique de la phase liquide (-)
ε_w	fraction volumique la sous-phase sillage de bulles (-)
ε_{w_s}	fraction volumique du solide dans la sous-phase sillage de bulle (-)
ε_{w_L}	fraction volumique du liquide dans la sous-phase sillage de bulle (-)
$\varepsilon_{w_{\phi_i}}$	fraction volumique de la classe ϕ_i dans la sous-phase sillage de bulles (-)
ε_{ls}	fraction volumique de la sous-phase solide/liquide-émulsion (-)
ε_{ls_L}	fraction volumique du liquide de la sous-phase solide/liquide-émulsion (-)
ε_{ls_s}	fraction volumique du solide de la sous-phase solide/liquide-émulsion (-)
ε_v	fraction volumique de la sous-phase solide/liquide-vortex-émulsion (-)
ε_{v_s}	fraction volumique du solide de la sous-phase solide/liquide-vortex-émulsion (-)
ε_{v_L}	fraction volumique du liquide de la sous-phase solide/liquide-vortex-émulsion (-)
ϕ_{pde}	fraction volumique de la sous-phase particule-descente-émulsion (- or %)
ϕ_{pve}	fraction volumique de la sous-phase particule-vortex-émulsion (- or %)
ϕ_{pw}	fraction volumique de la sous-phase particule-sillage (- or %)

γ	constante généralisée de la viscosité du liquide ($N/s^n m^2$)
κ	paramètre de la fonction de distribution double-exponentielle (m/s)
λ	paramètre de la fonction de distribution double-exponentielle (s/m)
σ	tension de surface (dyne/cm)
σ_{pded}	écart-type de la distribution de vitesse du solide de la sous-phase particule-descente-émulsion (m/s)
σ_{pved}	écart-type de la distribution de vitesse du solide de la sous-phase particule-vortex-émulsion (m/s)
σ_{pwd}	écart-type de la distribution de vitesse du solide de la sous-phase particule-sillage (m/s)
σ_{v_b}	écart-type de la distribution de vitesse des bulles relatif aux parois (m/s)
$\sigma_{v_{le}}$	écart-type de la distribution de vitesse du liquide de la sous-phase émulsion (m/s)
$\sigma_{v_{br}}$	écart-type de la distribution de vitesse des bulles relatif à la vitesse du liquide dans la sous-phase émulsion (m/s)

Pour le Chapitre 5

A	surface de la phase solide, $\frac{D_c \pi}{4} \varepsilon_s$
$C_{pde}\|_{u_{pded}}$	concentration du traceur dans la classe définie par la vitesse du solide dans la sous-phase particule-descente-émulsion u_{pded} (kg/m3)
C_{pve}	concentration du traceur dans la classe définie par la vitesse du solide dans la sous-phase particule-vortex-émulsion (kg/m3)
$C_{pw}\|_{u_{pwd}}$	concentration du traceur dans la classe définie par la vitesse du solide dans la sous-phase particule-sillage u_{pwd} (kg/m3)
C_s	concentration moyenne du solide (kg/m3)
C_∞	concentration du solide à l'homogénéisation – test de traceur en mode cuvé (kg/m3)
$D_{ax_{eff}}$	coefficient de dispersion axiale effectif du modèle de dispersion axiale (m2/s)
$D_{ax_{pve}}$	coefficient de dispersion axiale de la sous-phase particule-vortex-émulsion (m2/s)
D_c	diamètre de colonne (m)
$f\{u_{pded}\}$	distribution de vitesse du solide dans sous-phase particule-descente-émulsion (s/m)
$f\{u_{pwd}\}$	distribution de vitesse du solide dans sous-phase particule-sillage (s/m)

K_{pve-pw}	constante de proportionnallité du transfert de solide de la sous-phase particule-vortex-émulsion à la sous-phase particule-sillage (s-1)
K_{pw-pve}	constante de proportionnallité du transfert de solide de la sous-phase particule-sillage à la sous-phase particule-vortex-émulsion (s-1)
$K_{pve-pde}$	constante de proportionnallité du transfert de solide de la sous-phase particule-vortex-émulsion à la sous-phase particule-descente-émulsion (s-1)
$K_{pde-pve}$	constante de proportionnallité du transfert de solide de la sous-phase particule- descente-émulsion à la sous-phase particule-vortex-émulsion (s-1)
L_f	hauteur de lit fluidisé (m)
MMI	Mixing Mechanism Indicator (-)
u_{pded}	vitesse du solide dans la classe définie par définie par la vitesse du solide dans la sous-phase particule-descente-émulsion u_{pded} (m/s)
u_{pde}	vitesse moyenne de la distribution de vitesse du solide dans la sous-phase particule-descente-émulsion (m/s)
u_{pwd}	vitesse du solide dans la classe définie par définie par la vitesse du solide dans la sous-phase particule-sillage u_{pwd} (m/s)
u_{pw}	vitesse moyenne de la distribution de vitesse du solide dans la sous-phase particule-sillage (m/s)
t	temps (s)
z	position axiale (m)

Lettres grecques

α	paramètre de la fonction de distribution log-normale (-)
β	paramètre de la fonction de distribution log-normale (-)
ε_s	fraction volumique de la phase solide (-)
ϕ_{pde}	fraction volumique de la sous-phase particule-descente-émulsion (-)
ϕ_{pve}	fraction volumique de la sous-phase particule-vortex-émulsion (-)
ϕ_{pw}	fraction volumique de la sous-phase particule-sillage (-)
σ_{pded}	écart-type de distribution de vitesse du solide dans la sous-phase particule-descente-émulsion (m/s)
σ_{pwd}	écart-type de distribution de vitesse du solide dans la sous-phase particule-sillage (m/s)
Δt	intervalle de temps (s)
Δz	intervalle de position axiale (m)

CHAPITRE 1 : INTRODUCTION

1.1 Problématique

Les lits fluidisés à trois phases sont utilisés dans les procédés de pétrochimie, biochimie et minéralogie. Ils consistent en un lit fluidisé liquide-solide où montent des bulles de gaz. Ils sont utilisés dans les applications où un liquide, un gaz et un solide doivent être mis en contact. Les applications les plus populaires sont la synthèse de type Fischer-Tropsch, l'hydrocraquage des huiles lourdes, la production de médicaments à l'aide de microorganismes et la séparation de minerais dans les colonnes de flottaison. Parmi les avantages des lits fluidisés à trois phases, il faut mentionner qu'ils offrent un bon contrôle de la température, utile dans le cas de réactions fortement exothermiques (ex. : synthèse de type Fischer-Tropsch). L'agitation et le transfert gaz/liquide y sont importants tout en ayant des taux de cisaillement faibles par rapport à une agitation mécanique. Ces caractéristiques expliquent leur utilisation dans la production de médicaments à l'aide de microorganismes, sensible aux taux de cisaillement et nécessitant le maintien d'une bonne concentration d'oxygène dissout dans la phase liquide. Pour finir, les colonnes de flottaison tirent avantages du transport des minéraux qu'offrent les bulles qui montent dans le lit fluidisé.

Bien qu'intensivement étudiée depuis plusieurs années, l'hydrodynamique des trois phases des lits fluidisés triphasiques est encore mal comprise. Pour le dimensionnement, la mise à l'échelle et l'optimisation de tels réacteurs, il est nécessaire de bien comprendre l'écoulement et le mélange de chacune des phases.

Une approche souvent employée dans la littérature consiste à supposer les patrons d'écoulement et à y appliquer les bilans de masse appropriés. Cette approche, utilisée dans cette thèse, permet de développer des *modèles de mélange*, plus simples à utiliser

à l'échelle industrielle que les modèles CFD (Computational Fluid Dynamics). Pour ces derniers, la solution des équations de quantité de mouvement et de continuité donne les patrons d'écoulement des phases. Ces modèles ont un grand potentiel pour modéliser efficacement les réacteurs, mais l'utilisation d'équations empiriques de fermeture et des temps de simulations importants limitent, pour l'instant, leur utilisation.

En ce qui concerne les modèles de mélange, afin de supposer les patrons d'écoulement adéquats, une bonne connaissance des caractéristiques clés liées à l'hydrodynamique des phases est nécessaire. Le défi de la modélisation est de développer le modèle le plus simple possible, mais respectant les caractéristiques clés liées à l'hydrodynamique des phases.

1.2 But général et objectifs

Le but général de la thèse est de développer un modèle de mélange de la phase solide. Ce modèle doit suivre non seulement l'intensité de mélange du solide, mais il doit aussi avoir la capacité de suivre l'importance relative des mécanismes de mélange, par exemple des mécanismes convectif et dispersif. Voici les deux objectifs permettant de répondre au but général de la thèse :

- Identifier les caractéristiques clés liées à l'hydrodynamique des phases dans les lits fluidisés à trois phases. Avant de développer un modèle de mélange de la phase solide, il est important de bien comprendre les mécanismes régissant le transport et le mélange de chacune des phases et leurs interactions. À cause des limites des ordinateurs actuels et des limites dans le champ de certaines connaissances fondamentales, par exemple les connaissances relatives au passage de la microéchelle à la mesoéchelle ou à la macroéchelle, un modèle ne peut aujourd'hui tenir en compte tous les mécanismes régissant

l'hydrodynamique des phases. La réalisation d'études empiriques est donc nécessaire afin de développer un modèle ayant des propriétés mathématiques équivalentes aux caractéristiques clés liées à l'hydrodynamique des phases.

- Développer un modèle de mélange de la phase solide le plus simple possible, mais qui respecte les caractéristiques clés liées à l'hydrodynamique. Un modèle de mélange peut respecter plusieurs caractéristiques hydrodynamiques, comme les profils en 3-D de vitesse et de rétention des phases et sous-phases. Cependant, le respect de certaines de ces caractéristiques peut alourdir suffisamment le modèle pour décourager son utilisation et le gain en complexité peut être plus important que l'amélioration du modèle. De plus, négliger certaines caractéristiques n'affecte pas significativement les prédictions de performances des réacteurs. Il est donc important de développer et de valider un modèle de mélange le plus simple possible, mais suivant des caractéristiques clés identifiées pour l'atteinte du premier objectif.

1.3 Structure de la thèse

La revue de la littérature présentée au chapitre 2 constitue un article, déjà publié, de cette thèse. Cette revue a permis de mieux comprendre l'hydrodynamique des trois phases s'écoulant dans les lits fluidisés triphasiques ainsi que d'atteindre en partie le premier objectif de cette thèse, soit d'identifier les caractéristiques clés liées à l'hydrodynamique des phases dans les lits fluidisés à trois phases. La revue a permis de montrer que le modèle piston-dispersif est trop simple pour représenter le mélange des phases dans des systèmes où les réactions sont rapides et les transferts de masse limitants. Des modèles plus phénoménologiques, tirés de la littérature, y sont présentés pour chacune des phases. Les limites et une généralisation des outils permettant de diagnostiquer le mécanisme de mélange dominant (Levenspiel Fitzgerald, 1983) y sont également présentées. Un modèle d'écoulement schématique

plus général, respectant l'interaction entre les phases et donnant la possibilité de représenter les mécanismes dominants, a été proposé. Ce modèle d'écoulement schématique est une mise à jour du « structural wake model » (Fan, 1989).

Le chapitre 3 décrit la méthodologie expérimentale qui a permis d'obtenir les résultats utilisés pour extraire les propriétés du modèle d'écoulement schématique proposé dans l'article de revue. Le calcul et l'analyse de ces propriétés sont présentés au chapitre 4. Ce dernier contient le deuxième article de cette thèse et s'intitule « Hydrodynamique de la phase solide – un mécanisme convectif/dispersif ». Le deuxième article a permis de mieux comprendre l'évolution de l'importance relative du mécanisme convectif sur le mécanisme dispersif et de poursuivre l'atteinte du premier objectif de cette thèse. Les contributions du deuxième article ont conduit au développement du modèle de mélange de la phase solide présenté au chapitre 5. Ce dernier contient le troisième article de cette thèse intitulé « Hydrodynamique de la phase solide – un modèle convectif/dispersif ». Le développement du modèle permet d'atteindre le deuxième objectif de la thèse, soit de développer un modèle de mélange le plus simple possible, mais qui respecte les caractéristiques clés liées à l'hydrodynamique. Ce modèle contient plusieurs paramètres dont une grande partie a pu être estimée à partir de corrélations développées au chapitre 4. Les autres paramètres, trois pour être exact, ont été optimisés sur des résultats de tests de traceur obtenus par la méthode de suivi d'une particule radioactive.

Le chapitre 6 présente la discussion générale portant sur le travail de la présente thèse. Le chapitre 7 contient la conclusion générale de la thèse et les recommandations portant sur des moyens permettant d'améliorer le modèle et sur certains travaux supplémentaires qui permettront de mieux quantifier l'interaction entre les phases.

CHAPITRE 2 : REVUE CRITIQUE DE LA LITÉRATURE ET IDENTIFICATION DES CARACTÉRISTIQUES CLÉS DE L'HYDRODYNAMIQUE DES PHASES[1]

2.1 Présentation de l'article

La première étape permettant de répondre au premier objectif de cette thèse était de réaliser une revue critique de la littérature. L'idée, entre autres, était de généraliser et de tester la méthode des moments utilisée pour diagnostiquer les mécanismes purs de mélange, soit les mécanismes convectif, dispersif et turbulent. Afin d'identifier les caractéristiques clés de l'hydrodynamique des phases, les modèles de mélange autres que le modèle piston-dispersif ont été revus pour chaque phase. Les mécanismes de mélange dominant pour chaque phase et la façon dont les mécanismes d'une phase peuvent interférer sur les mécanismes des autres phases ont été étudiés. La synthèse des modèles de mélange des phases a permis de proposer un modèle schématique représentant les liens entre les phases.

---

[1] Publié dans « International Journal of Chemical Reactor Engineering ». *Vol. 2, 2004, Review* R_2.

2.2 Phase Mixing Modeling in Multiphase Reactors Containing Gas Bubble: a Review

Lefebvre, S., Chaouki, J. and Guy, C.

2.2.1 Abstract

Multiphase reactors are often used as petrochemical, biological and pharmaceutical reactors. Understanding the mixing mechanism responsible for phase mixing is necessary for modeling purposes. Phase mixing may considerably affect reactor performance. In the literature, each phase mixing was often described by the Axial Dispersion Model (ADM), without physical justification. Some authors doubted the validity of the ADM and that it could represent the mixing of the phases and instead proposed other models. Also, some authors studied the fundamental mechanism responsible for phase mixing. For conversion and selectivity prediction purposes, the use of more complex phenomenological phase mixing models is essential when the kinetics are rapid and the interfacial mass transfer is limited. Many literature reviews concerning multiphase reactors have been published. These reviews, however, discuss phase mixing modeling based on the ADM and do not deal with the other phase mixing models. The aim of this work is to review the literature on phase mixing modeling, based on a mechanistic approach, for three kinds of multiphase reactors: the bubble column (solid free), slurry bubble column (small/light particles) and three phase fluidized bed (large/heavy particles) reactors. The common feature of these reactors is the presence of gas bubbles, which considerably influence the phase hydrodynamic. Hence, a mixing model proposed for one of these reactors may be conceptually representative of the mixing of the two others.

2.2.2 INTRODUCTION

Multiphase reactors are used among others in the chemical, petrochemical and biological industry. Although these reactors have been widely studied for several decades, no model is available to accurately predict the reactors' performances (conversion and selectivity). Hence, some problems arise when designing and scaling up multiphase reactors. Optimization is also problematic. Difficulties originate from the many flow characteristics that have to be taken into account and modeled.

Many reviews have been published concerning bubble column hydrodynamics (Shah et al., 1978; Joshi and Shah, 1981; Shah et al., 1982; Deckwer and Schumpe, 1987; Deckwer and Schumpe, 1993) or the slurry bubble column and three phase fluidized bed (Epstein, 1981; Wild et al., 1984; Muroyama and Fan, 1985; Tarmy and Coulaloglou, 1992; Nacef et al., 1992; Kim and Kang, 1997). These reviews mainly deal with modeling the phase holdup, heat and mass transfer and phase mixing, mainly using the Axial Dispersion Model (ADM). More recently, Fan and Yang (2002) published an update of Fan's previous book (1989). The later review is about bubble dynamics, transport phenomena and CFD for gas/liquid and gas/liquid/solid reactors. Fan and Yang (2002) dealt with the effect of pressure on hydrodynamic properties. Moreover, Joshi (2001) and Joshi et al. (2002) reviewed CFD modeling for bubble columns.

For the last decade, the CFD approach increased in popularity as a mean to model phase flow in multiphase reactors. For this approach, microscopic momentum balance (with microscopic mass balance used as a constraint) and/or force balance on discrete phases are solved in order to find many hydrodynamic parameters including local velocity field. However, the CFD approach is time consuming and is difficult to use at industrial scale. The present article reviews mainly mixing models which are more global and closer to industrial model and designers needs. For the mixing modeling

approach, flow patterns are assumed and usually validated with appropriated mass balances and mixing data. This approach necessitates a good knowledge of the phase flow dynamic in order to identify the pertinent flow patterns for reactors scale-up. The mixing modeling approach is less fundamental than CFD, but the former is actually more easily applicable to industrial scale.

The ADM is the most popular mixing model used. However, some authors doubted that the ADM could adequately represent phase mixing and proposed different models. Also, some authors studied the fundamental mechanism responsible for phase mixing. For conversion and selectivity prediction purposes, the use of more complex phenomenological phase mixing models is essential when the kinetics are rapid and the interfacial mass transfer is limited. These phase mixing models have never been compared in a review article. The aim of this work is to review the literature on phase mixing modeling, based on a mechanistic approach, for three kinds of multiphase reactors: the bubble column (solid free), slurry bubble column (small/light particles) and three phase fluidized bed (large/heavy particles) reactors. These types of reactors have the same key characteristics, i.e. a gas phase in bubble form (space discontinuity) rising in a liquid phase and all phases move. This leads us to think that a model validated for one reactor type may be generalized to the others.

This article is structured as follows. ADM and mixing mechanisms are briefly described. For each phase, the mixing models proposed in the literature are discussed based on some flow characteristics (mixing mechanisms). These models are classified in view of their assumed dominant flow characteristic. Each phase mixing model section is divided into two subsections. The first one presents the mixing models and the second discusses the authors' model exploitation. This structure will give the reader a quick overview of the phase mixing model if one reads only the first subsection of

each phase section. A generalization of the phase mixing models is proposed and the other modelling approaches are briefly described.

2.2.3 AXIAL DISPERSION MODEL

Due to its simplicity, the ADM is often used. In some instances (hydrodynamics are not limiting) this model may give rough predictions of the multiphase reactors' performance. ADM is used to model phase mixing by almost ninety-five percent of authors.

ADM assumes that mass transport is in plug flow and mixing is a diffusion-like process represented by a Fickian term. According to this model, the mass balance of a reacting species (A) in an unsteady-state is written as follows:

$$\frac{\partial C_A}{\partial t} = Dax\frac{\partial^2 C_A}{\partial z^2} - U\frac{\partial C_A}{\partial z} - R_A \qquad (1)$$

Where R_A is the kinetic term of the species A. The Axial Dispersion Coefficient (ADC) value depends on the definition of the velocity "U" used. The mean bubble velocity ($U=Ug/\varepsilon_g$) is often used for the gas phase. The velocity defined for the liquid phase is often the interstitial liquid velocity ($U=U_L/\varepsilon_L$). A difference of two velocities is used for the solid phase, one represents the upflow velocity of the particles, while the other represents their downflow velocity. For the case of the solid phase the ADM is rather called the sedimentation-dispersion model. Jean et al. (1989) identified several definitions of the upflow and downflow particle velocities used in the literature.

Several ADC correlations were proposed in the literature for each phase and multiphase reactor. These correlations are either empirical, semi-empirical or theoretical (a few). The last two are based on different flow representations. Some correlations are based

on turbulence theory, analogy with other systems, such as fixed bed and porous soils in hydrogeology, and analogy with the Taylor-Aris relation that takes into account the velocity profile effect. Turbulence theory is the most popular approach used.

A comparison between the schematic representation of the ADM and the flow observed in three phase fluidized beds (Chen et al., 1994 ; Larachi et al., 1996) and bubble columns (Franz et al., 1984) is shown in Figure 2.1. The liquid and solid phase rise in a helicoidal manner in the center of the column and go down near the column wall. Moreover, the mobile vortices are observed between the upflow and downflow region. Fischer et al. (1994) showed that the bubbles also swarm and rise in a helicoidal manner. A liquid and solid part are attached to the bubbles in their wake and rise at the various bubble velocities (Fan, 1989; Lubbert and Larson, 1990, Schmidt et al., 1992a and b). The liquid and solid phases in the emulsion phase are also affected by the bubble and wake interfacial momentum transfer and wake shedding. It is obvious that the ADM is too simple to adequately represent all of these transport and mixing phenomena. All of these must be "absorbed" in the ADC. Therefore, the ADC is reactor sensitive. When obtained for a reactor, its value is only valid for this reactor. The mathematical structure of the ADM does not follow the changes of the reactor's flow structure depending on its configuration and operating conditions. The ADM represents one type of mixing mechanism among others, i.e. axial dispersive mechanism. Mixing mechanisms are presented in the next section.

Figure 2.2 shows ADC predictions for each phase and some multiphase reactors. The sources of the ADC correlation are not included in the Figure for visibility purposes. It is only shown to illustrate the disagreement between the evolutions and predictions of the ADC phase. It raises one question: is it a lack of information inside the ADC correlations that is essential to understand and correctly predict the ADC, or is the ADM not able to adequately represent the phase mixing in multiphase reactors? The

authors of the present article assumed the second possibility to be correct. Some authors doubted the validity of the ADM to represent the phase mixing and/or proposed others types of phase mixing models (El-Temtamy and Epstein, 1980; Dayan and Zalmanvich, 1982 ; Levenspiel and Fitzgerald, 1983 ; Shah et al., 1985 ; Myers et al., 1987 ; Tang and Fan, 1989; Murray and Fan, 1989 ; Rustemeyer et al., 1989; Tsutsumi et al., 1992 ; Nassar et al., 1992 ; Shetty et al., 1992 ; Modak et al., 1993 et 1994 ; Hyndman and Guy, 1995 ; Kantak et al., 1995 ; Cassanello et al., 1995 ;Cassanello et al., 1996 Larachi et al., 1996 ; Degaleesan et al., 1996 and 1997). These mixing models are reported and analyzed in view of the following mixing mechanisms.

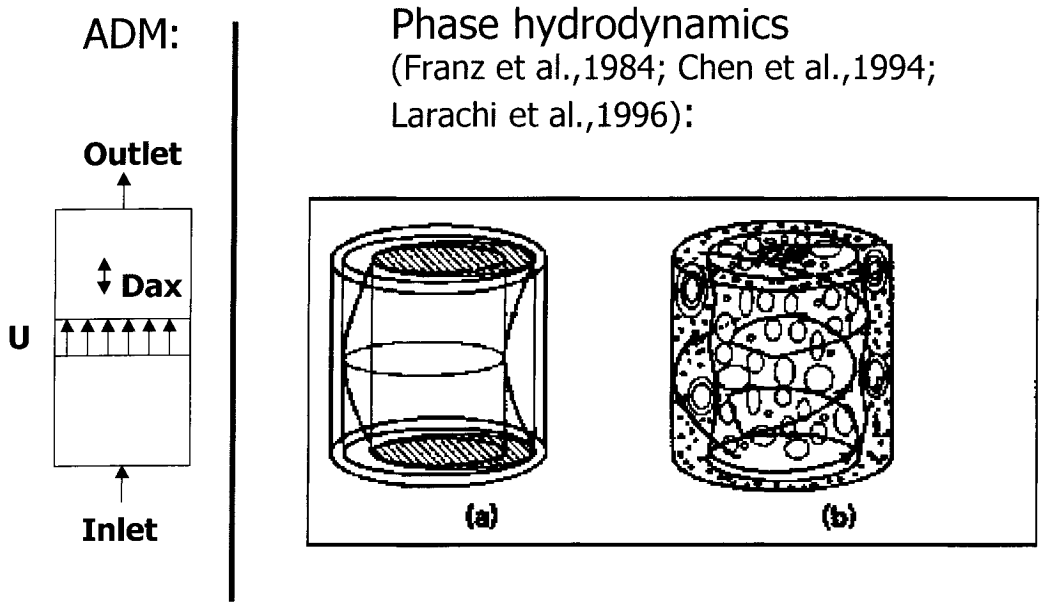


Figure 2.1: Comparison between schematic representation of axial dispersion model and flow observed in (a) bubble columns (Franz et al., 1984) and in three phase fluidized bed (Chen et al., 1994 ; Larachi et al., 1996). (right Figure comes from Larachi et al.(1996)).

2.2.4 MIXING MECHANISMS

It is possible to define three types of mixing mechanisms: dispersive, convective and turbulent mixing mechanisms (Levenspiel and Fitzgerald, 1983; Grossmann and Procaccia 1984; Lubbert and Larson, 1990). The former mechanism represents the behavior of a system containing particles (or fluid elements) where velocity changes occur at random along their path in the reactor (Nauman 1981). Figure 2.3 shows a schematic representation of the three mixing mechanisms discussed. Using Eulerian measurements, the dispersion mechanism may be confused with the convective one. The latter is characterized by particles whose velocities do not change along their path. Mixing is caused by the various velocities of the particles traveling within the reactor (segregation effect; see Figure 2.3). Thus, when a particle velocity distribution is Gaussian, it is possible to mistake its residence time distribution (also Gaussian) with a Gaussian residence time distribution obtained with ADM (Levenspiel and Fitzgerald, 1983). A turbulent mixing mechanism can also be identified. This mechanism is characterized by particles that are transferred from eddies to eddies (Figure 2.3). This mechanism needs to be represented in at least 2-D. Obviously, a dispersive mechanism would be represented in 1-D. The three mechanisms may be confused if measured between only two points. However, they are characterized by their relations equations linking the residence time standard deviation (σ_t) to the length between measuring points (or reactor's length) (L). Levenspiel and Fiztgerald (1983) showed that the following equation could be applied for the dispersive mechanism:

$$\sigma_t \propto L^{1/2} \tag{2}$$

It should be noted that this proportionality was derived from the variance equation ($\sigma_t^2 = \frac{2Dax}{U^3} L$) obtained for a system with small dispersion (Pe>100), giving a

Gaussian RTD (Levenspiel, 1999). The variance equation is not the same for a highly dispersive system. This equation for an open/open system is:

$$\sigma_t = \sqrt{\frac{2Dax}{U^3}L + \frac{8Dax^2}{U^4}} \tag{3}$$

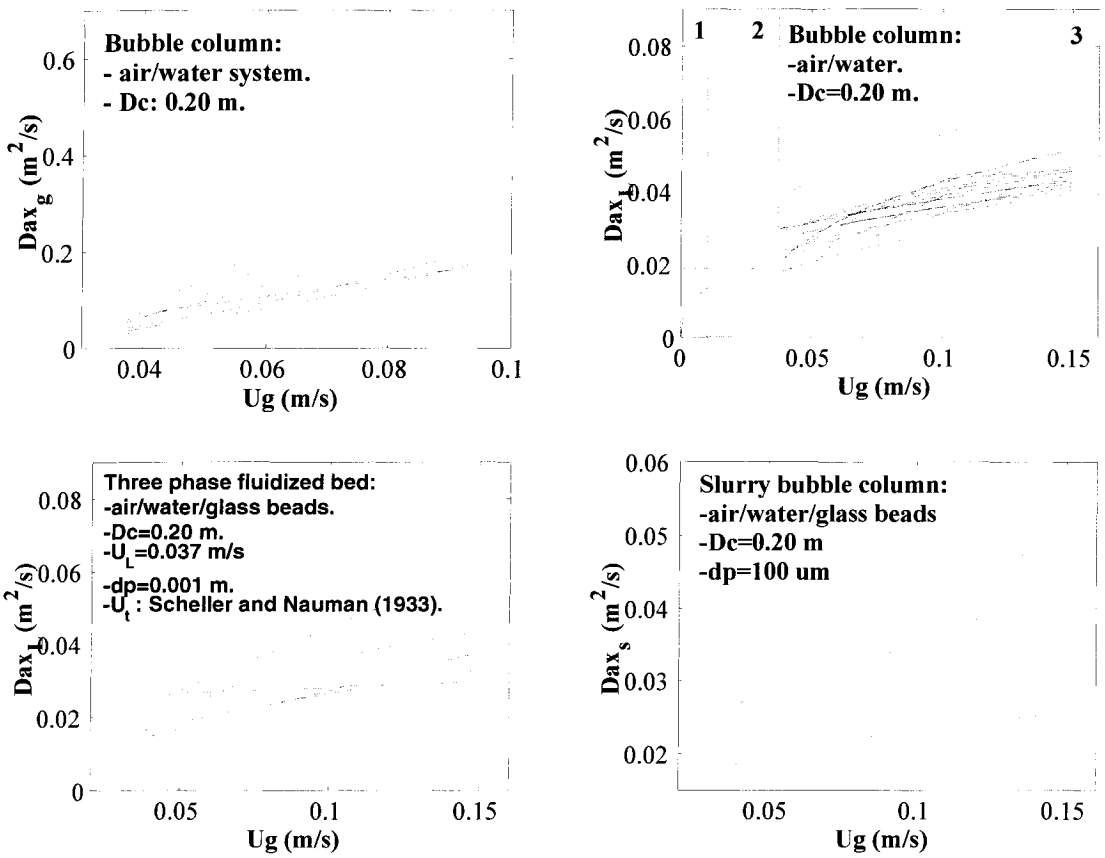


Figure 2.2: Prediction of some axial dispersion coefficient correlations for the three phases and for some multiphase reactors. Numbers on the upper right graph refer to the flow regime: 1)bubbly flow regime; 2)dispersed (homogeneous) 3)coalesced (heterogeneous).

This difference was never underlined and equation (2) was always used in the literature to validate dispersive mechanisms. The following question should be answered: is the dispersive mechanism conclusion the same if one uses the equation for small dispersion in a highly dispersive system? In order to answer this question, the following equation was written:

$$\sqrt{\gamma\frac{2Dax}{U^3}}L^{\delta/2} = \sqrt{\frac{2Dax}{U^3}L + \frac{8Dax^2}{U^4}} \tag{4}$$

Where δ: deviation from exponent ½ (erroneous invalidation) and γ: deviation from the mixing to transport parameters ratio. Rearranging equation (4) gives:

$$\sqrt{\gamma}L^{\delta/2} = \sqrt{L + \frac{4}{Pe}L} = \sqrt{1 + \frac{4}{Pe}}L^{1/2} \tag{5}$$

By analogy, because the Peclet number (Pe) is a function of L, it is possible to write:

$$\delta \neq 1 \tag{6}$$

Therefore, the proportionality shown in equation (2) is not true for a highly dispersive system. Obviously, $\delta \rightarrow 1$ when Pe is high.

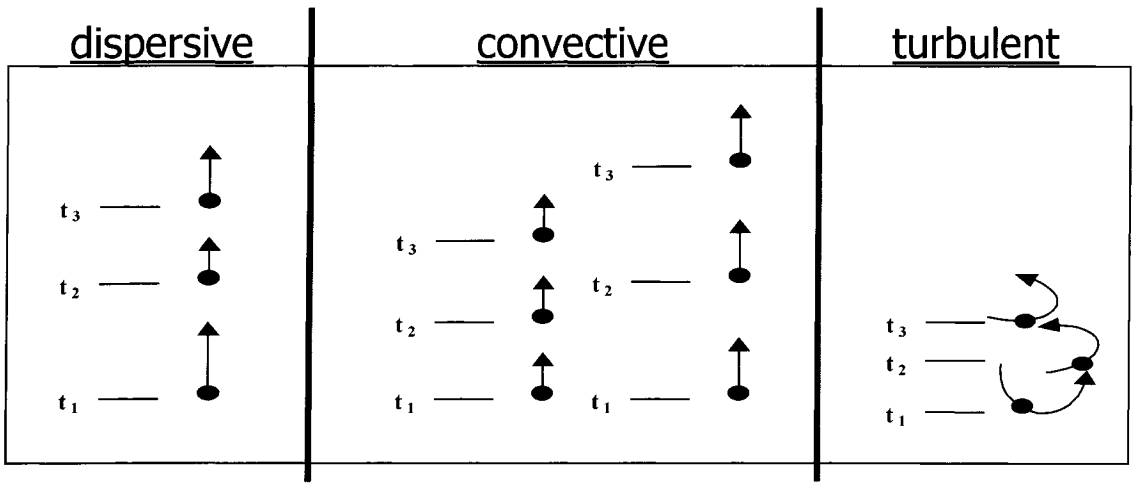


Figure 2.3 : Three mixing mechanisms.

There are four ways (techniques) to validate the dispersive mechanism with the second moment method. The possibility of fitting the equation between the variance or the standard-deviation of the RTD and the axial position constitute two techniques, respectively, $\sigma^2 \propto L$ and $\sigma \propto L^{1/2}$ techniques. The other two techniques are to verify if the appropriate ratio of variance or standard-deviation to distance between measuring points is constant for various distances between measuring points, respectively, $\Delta\sigma^2 \propto \left(L_2 - L_1\right)$ and $\Delta\sigma \propto \left(L_2^{1/2} - L_1^{1/2}\right)$ techniques. Table 2.1 shows the useful equations for the four techniques for small and high dispersion. Also, in the same Table the deviation equations when small dispersion equations are used for a high dispersion system are given. Equations for the $\sigma^2 \propto L$ technique are not shown because of its equivalence with $\sigma \propto L^{1/2}$.

A question which may be asked: how different is δ from one? Figure 2.4 shows δ as a function of the first Pe measured (at the L_1) for various sets of positions. δ was obtained by fitting equation **(17)** onto σ vs L data generated by equation (3); $\delta = n/(½)$. The δ value depends on the measured system configuration. It is clear that a wrong

invalidation of the ADM is observed in most cases. However, the fitted *n*-value is lower than ½ and no mistake can be made from the convective (eq (7)) or turbulent (eq (8)) mechanisms. Furthermore, the linear form of equation **(17)** (Ln(σ)-Ln(L)) is obviously not observed for low *Pe*.

The $\Delta\sigma \propto \left(L_2^{1/2} - L_1^{1/2}\right)$ technique is also a case where the dispersive mechanism is erroneously invalidated when the small dispersion equation is used for a highly dispersive system. The deviation equation obtained in this case shows the obvious tendency to give a correct conclusion when dispersion is small ($Dax/U \rightarrow 0$; see Table 2.1). Moreover, the conclusion will be correct when the first RTD measurement is taken far away from the reactor entrance (L_1 is large). The $\Delta\sigma^2 \propto \left(L_2 - L_1\right)$ technique does not depend on the extent of mixing (see Table 2.1). Therefore, this technique is recommended to validate the ADM, because it gives the same conclusion despite the extent to which the system is mixed.

For the convective mechanism, the standard-deviation of the RTD is a linear function of L (Levenspiel and Fiztgerald, 1983):

$$\sigma_t \propto L \tag{7}$$

Grossmann and Procaccia (1984) showed that the following equation applies for the turbulent mechanism:

$$\sigma_t \propto L^{3/2+w} \tag{8}$$

Where $w = 0$ for isentropic turbulence.

Table 2.1: ADM validation relations for small and high dispersion.

Technique	Small dispersion ($Pe > 100$)	High dispersion ($Pe < 100$)	Deviation relations when small dispersion relation is used for high dispersion system[1,2,3]
$\sigma \propto L^{1/2}$	$\sigma = \frac{2Dax}{U^3} L^{1/2}$	$\sigma = \sqrt{\frac{2Dax}{U^3} L + \frac{8Dax^2}{U^4}}$	$\delta \neq 1$[4]
$\Delta\sigma \propto \left(L_2^{1/2} - L_1^{1/2}\right)$	$\Delta\sigma = \sqrt{\frac{2Dax}{U^3}} \left(L_2^{1/2} - L_1^{1/2}\right)$	$\Delta\sigma = \sqrt{\frac{2Dax}{U^3} L_2 + \frac{8Dax^2}{U^4}} - \sqrt{\frac{2Dax}{U^3} L_1 + \frac{8Dax^2}{U^4}}$	$\frac{\Delta\sigma\vert_{HD}}{\sqrt{\frac{2Dax}{U^3}} \left(L_2^{1/2} - L_1^{1/2}\right)} = \frac{\sqrt{L_1 + \frac{4Dax}{U} + \Delta L} - \sqrt{L_1 + \frac{4Dax}{U}}}{\left(\sqrt{L_1 + \Delta L} - \sqrt{L_1}\right)}$
$\Delta\sigma^2 \propto \left(L_2 - L_1\right)$	$\Delta\sigma^2 = \frac{2Dax}{U^3} \Delta L$	$\Delta\sigma^2 = \frac{2Dax}{U^3} \Delta L$	$\frac{\Delta\sigma^2\vert_{HD}}{\frac{2Dax}{U^3} \Delta L} = 1$

[1] δ is defined in equation (5)

[2] the deviation term shown in case of the $\Delta\sigma^2$ (and $\Delta\sigma$) technique is obtained by dividing the high dispersion (subscript HD) expression of $\Delta\sigma^2$ (or $\Delta\sigma$) in the expression valid for small dispersion cases. Should equal to one to have correct validation conclusion.

[3] the deviation terms shown in case of the $\Delta\sigma^2$ (and $\Delta\sigma$) technique and δ shown in case of the σ^2(and σ) technique allow quantifying the erroneous mixing mechanism conclusion that may be yield when small dispersion relations are used in high dispersion system.

[4] see Figure 2.4

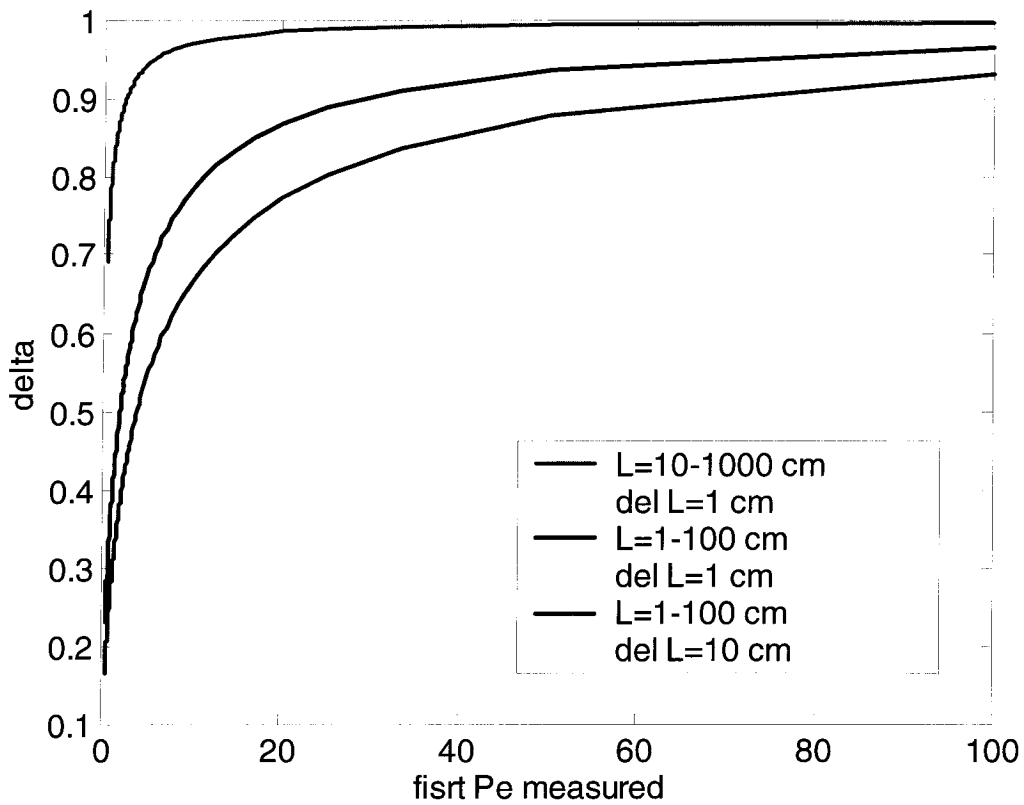


Figure 2.4: delta, δ, (defined in eq (5)) as a function of the first *Pe* measured (at L_1) for various sets of positions.

The standard-deviation equations shown here represent "pure" mechanism. A combination of these pure mechanisms (or other mechanisms) will give other standard-deviation equations with reactor length.

A novel Log-Normal-Convective/ADM model (LNC/ADM model) is shown here in order to illustrate a system following a superposition of a convective on a dispersive mechanism and to give a more general form of the Levenspiel and Fitzgerald (1983) mixing mechanism typology.

For a system following a dispersive mechanism, the RTD is represented by equation (9) for an open/open system. Equation (9) is the analytical solution of equation (1) with R_A=0 (Levenspiel, 1999). It should keep in mind that when several RTD are measured along column axis, systems between measuring point are open/open.

$$E_{ADM}(t) = \frac{u}{\sqrt{4\pi Dax\, t}} \exp\left(-\frac{(L-ut)^2}{4\pi t} \right) \tag{9}$$

The Log-normal distribution is chosen to represent the fluid element velocity distribution because it is often used to represent fluid element population in multiphase reactors (Matsuura and Fan 1984; Hyndman and Guy 1995a). The Log-normal distribution is shown in equation (10).

$$f(u) = \frac{1}{\beta u \sqrt{2\pi}} \exp\left(-\frac{(\ln u - \alpha)^2}{2\beta^2} \right) \tag{10}$$

The simulated system contains fluid elements each of them having a *mean* velocity (u) following a log-normal velocity distribution. The fluctuation between the mean velocity of each fluid element is due to a purely random process following a dispersive mechanism. In other words, the system contains various classes of fluid element having their own RTD. The RTD of the whole population is developped in the appendix and the final result is shown in equation (11).

$$E_{LNC/ADM}(t) = E(t) = \frac{1}{\pi\beta\sqrt{8Dax\, t}} \int_0^\infty \exp\left[-\frac{(Ln(u)-\alpha)^2}{2\beta^2} - \frac{(L-uL)^2}{4Dax\, t} \right] du \tag{11}$$

The RTD obtain for the LNC/ADM model is expressed by equation (11) and contains three parameters, i.e. *Dax*, α and β. The parameters α and β are link to the *average* velocity ($\bar{u}$; see eq (12)) of the fluid element mean velocity and to the standard-deviation of the log-normal mean velocity distribution (σ_u; see eq (13)).

$$\bar{u} = \exp\left(\alpha + \frac{\beta^2}{2}\right) \tag{12}$$

$$\sigma_u = \bar{u}\sqrt{\exp\left(\beta^2\right) - 1} \tag{13}$$

An equivalent Peclet number may be defined in equation (14).

$$Pe_{eq} = \frac{\bar{u}L}{Dax} \tag{14}$$

The RTD width obtained from the LNC/ADM model depend on β and *Dax*. To represent a purely dispersive model, the standard-deviation of the velocity distribution has to go to zero (($\sigma_u \rightarrow 0$, i.e. $\beta \rightarrow 0$). To represent a purely convective model, the axial dispersion coefficient has to go to zero (Dax $\rightarrow$ 0). Between these limits the LNC/ADM model represent a system following a convective/dispersive mechanism. Therefore, fitting the LNC/ADM model to RTD data allows for the diagnosis of the mixing mechanism (between the convective and dispersive mechanisms only) followed by the fluid elements of a system.

Simulations were made in order to illustrate the diagnosis capability of the LNC/ADM model. First of all, axial evolution of the purely convective model RTD was generated.

The RTD function obtained from a convective system following a log-normal velocity distribution was derived by Hyndman and Guy (1995a) and is given in equation (15).

$$E_{conv}(t) = \frac{1}{\beta t\sqrt{2\pi}} \exp\left(-\frac{(\ln t - \ln L + \alpha)^2}{2\beta^2} \right) \tag{15}$$

Figure 2.5 shows the results for $\sigma_u = 0.1$ m/s and $\bar{u} = 1$ m/s (α= -0.005 and β= 0.0997). The ADM (eq (9)) was fitted to the purely convective model RTD at each axial position in order to obtain u and Dax. The value of Dax varied, according to the axial position, from 0.005 to 0.0299 m^2/s (Pe_{eq} = 200). This result obviously invalidates the ADM to represent the mixing of the system following the convective mechanism. The increasing of Dax is linear as expected. Indeed, the combination of equation (3) for Pe>100 and equation (7) shows the linear dependence between Dax and L.

Now, it is important to verify if by fitting the parameters of equation (11) the expected parameters value will be obtained, i.e. Dax = 0, α= -0.005 and β= 0.0997. As a first step, RTD at each axial position was fitted individually. Unfortunately, optimized parameter values change along the reactor length. Also, the value of the optimized parameters depends on the initial guess of the fitting procedure. Indeed, many parameter sets gives the same RTD. In order to overcome this situation, the fitting should be performed on the all RTD at the same time. The following objective function (r^2) was used:

$$r^2 = \sum_{j=1}^{j=nbz} \sum_{i=1}^{i=nbt} \left(E_{conv_i} - E_{LNC/ADM_i} \right)_j^2 \tag{16}$$

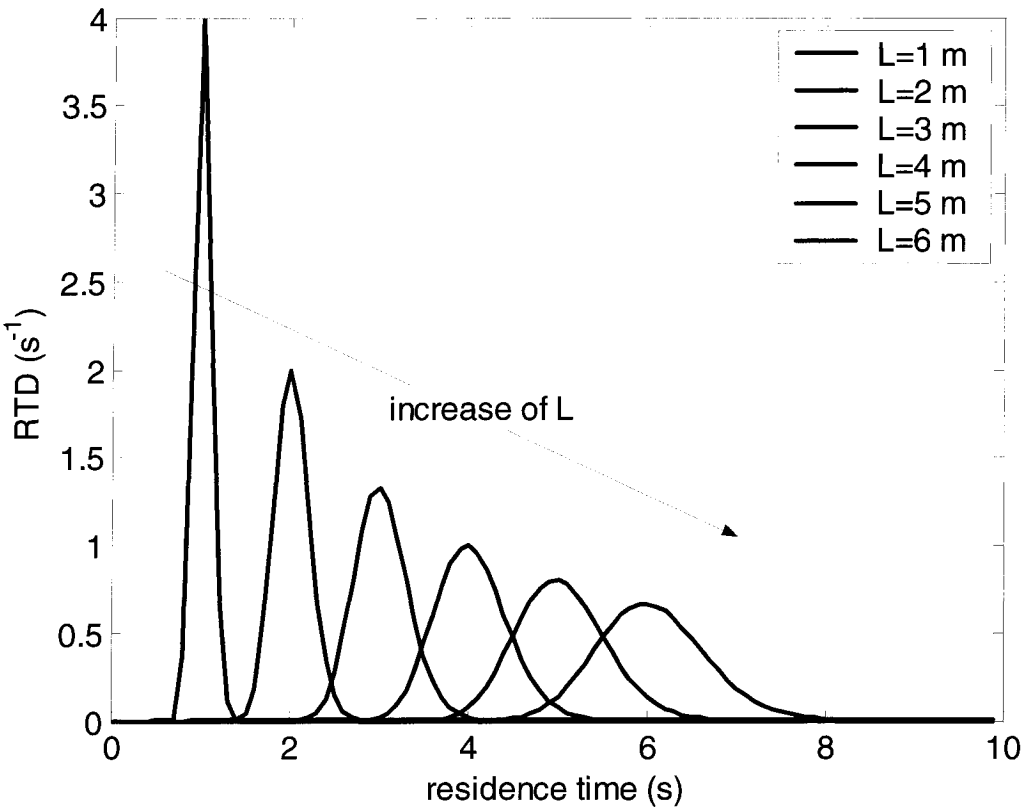


Figure 2.5: Example of the purely log-normal convective RTD axial evolution. Parameters used are: $\sigma_u = 0.1$ m/s and $\overline{u} = 1$ m/s (or $\alpha = -0.005$ and $\beta = 0.0997$).

Where "*j*" represents the RTD of the various axial positions, "*i*" represents the RTD value for a giving residence time, *nbz* and *nbt* are, respectively, the number of axial measurement positions and the number of RTD value. This objective function force the optimization procedure to obtain the parameter set respecting not only the RTD form but also the axial evolution of the RTD. This parameter set is unique. The expected value of α and β were obtained and the value of *Dax* was 4.7×10^{-6} m^2/s (≈ 0).

System following a superposition of the convective and dispersive mixing mechanism was simulated. The axial (L = 1 to 6 m) RTD evolution of that system (eq (11)) was computed for $\overline{u}$ = 1 m/s, β ranging from 0.01 to 0.5 and *Dax* ranging from 0.001 to 1 m^2/s. The linear form ($\ln(\sigma_t)$-$\ln(L)$) of the following equation was fitted:

$$\sigma_t = \sigma_o L^n \tag{17}$$

Where σ_t is the RTD standard-deviation.

Figure 2.6 shown the fitted value of *n* obtained for each parameter set. It is observed that the value of *n* may be below 0.5 for *Dax* value exceeding 0.01 m^2/s (Pe_{eq}<100 for L=1m). This was expected according to equation (5) and Figure 2.4 for purely dispersive system. Moreover, for *Dax* value higher than 0.01 m^2/s, the value of *n* increases and decreases as β increases. In fact, the linear form of equation (17) does not apply for Pe_{eq}<100, i.e. a bias exist between the linear form of equation (17) and the computed relation of σ_t vs L. This bias is shown in equation (5) representing a purely dispersive system, but, it is clear now that the bias exist also for a convective/dispersive system with low Pe_{eq}. Furthermore, a system having a great contribution of convective mechanism may result in standard-deviation axial evolution with a *n*-value of 0.5, giving an impression of a purely dispersive system. Therefore, it is not always possible to identify the relative importance of the mixing mechanisms with equation (17) for a system following a superposition of the convective and the dispersive mixing mechanisms. Indeed, equation of the type of equation (11) combined with a fitting algorithm using objective function define by equation (16) will give a more efficiency method to identify mixing mechanism.

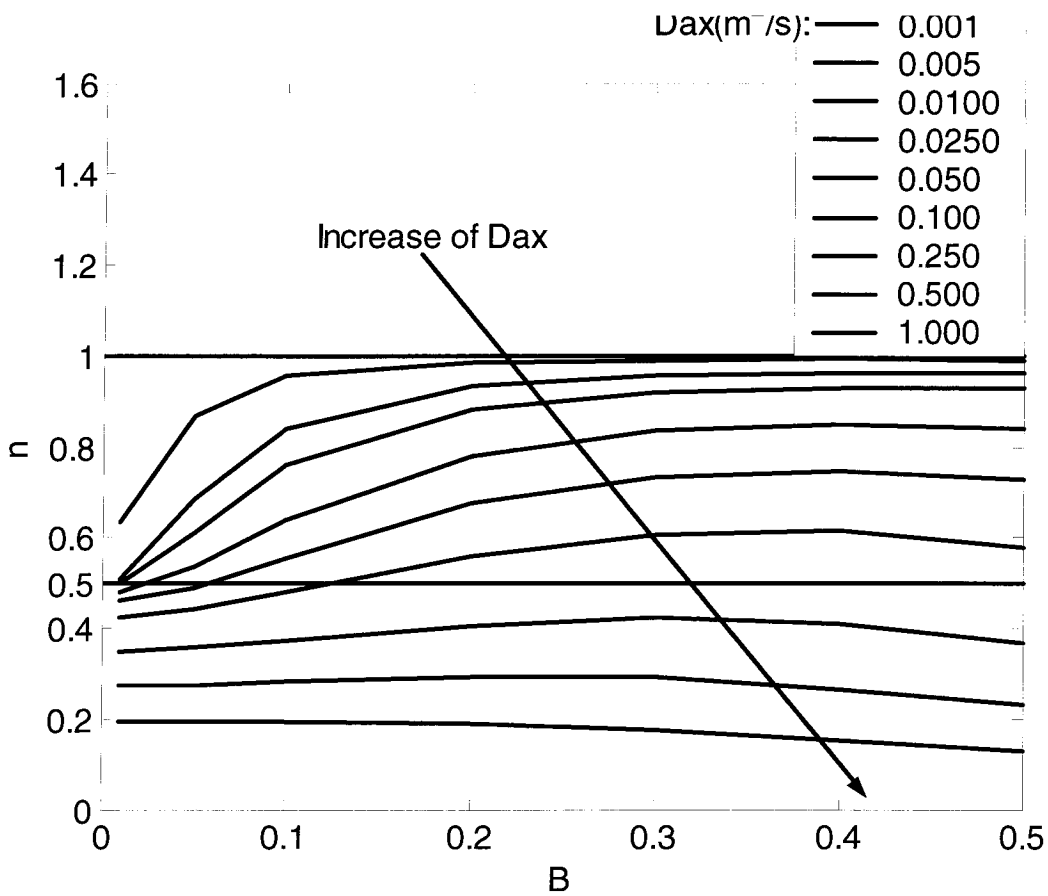


Figure 2.6: optimized values of n that allows fitting the linear form of equation (17) to the standard-deviation axial evolution compute with equation (11). $\overline{u}$ = 1 m/s, L = 1, 2, 3, 4, 5 and 6 m.

The LNC/ADM model allows for generalization of the Levenspiel and Fitzgerald (1983) finding, i.e. the LNC/ADM model is not restricted to the two limiting cases: convective and dispersive mechanism. However, the LNC/ADM model is limited to a system where the convective contribution is represented by a log-normal velocity distribution. Equation (10) may be replaced by an other distribution form, such as a beta distribution, if the convective contribution follows an other distribution form and applying the treatment show here.

The LNC/ADM model represents a system containing a population of fluid elements having various mean velocity that fluctuate randomly. The model assumes that the probability of velocity fluctuation is the same for all fluid elements in the population and does not depend on time and position of fluid elements. Also, the model assumes no exchange between fluid elements.

As it will be seen, these assumptions are not always valid in multiphase reactors. It is obvious that mixing models need to respect the main mixing mechanism(s) for design and scaled-up purposes. For each phase, models are proposed in the literature to represent their mixing. The assumed relative importance of the mixing mechanisms varied widely from one model to the other. These models are reviewed in the following sections while keeping in mind the above mixing mechanisms.

2.2.5 GAS PHASE MIXING MODELS

2.2.5.1 Model concept

Gas phase mixing models were mostly proposed for bubble columns. Even if bubble interactions, such as bubble coalescence/breakup dynamic, are different in reactors containing solid particles, the models may be conceptually similar for the multiphase reactors discussed here, i.e. bubble column, slurry bubble column and three phase fluidized bed. Most of the models are based on the two bubble class flow representation of the gas phase hydrodynamics in the coalesced flow regime. Bubbles rising in the reactor are separated into two bubble classes, i.e. small and large bubble classes (Siram and Mann, 1977 ; Vermeer and Krishna, 1981 ; Schumpe and Deckwer, 1982 ; Godbole et al., 1982 et 1984 ; Kelkar et al., 1983 ; Joseph and Shah, 1984 ; Schumpe and Grund, 1986 ; Patel et al., 1989 ; Hyndman et al., 1997).

Schematics a, b, c and d in Figure 2.7 show the Two-Bubble-Class-Mixing-Models (TBCMM) representation. This type of model assumes that bubbles may be separated into a small bubble class, which is influenced by liquid mixing (small bubbles are driven by liquid flow), and a large bubble class, which is slightly influenced by liquid mixing (Shah et al., 1985a ; Shetty et al., 1992 ; Kantak et al., 1995 ; Modak et al., 1993 and 1994). As a limiting case, Shetty et al. (1992) and Kantak et al. (1995) assumed that the ADC of the small bubble class equals the ADC of the liquid phase. In the TBCMM each bubble class has its own mean velocity, large bubbles rising faster than small bubbles. The large bubble class is assumed to follow a plug flow behavior. Shah et al. (1985a) assumed a perfect mixing for small bubbles, while the other authors used the ADM to represent small bubbles mixing. Modak et al. (1993, 1994) are the only ones that consider an interaction between bubble classes, represented by a mass exchange coefficient (f_e). This cross-mixing term is a representation of the mass exchange between the two bubble classes due to the bubble coalescence/breakup. The bubble coalescence/breakup is a widely recognized phenomenon, thus it is more realistic to take into account the bubble class interactions if the bubble coalescence/breakup occurs the whole length of the reactor. Kawagoe et al. (1989) considered instead one bubble class flowing in the column center (core region) and another flowing near the column wall (annulus region). Each of these classes is represented by the ADM. Table 2.2 summarizes the gas phase mixing models. Model parameters are also given in the Table. Table 2.3 presents experimental conditions used by the authors. The most general equation of the proposed models may be written to represent the various behaviors assumed for bubble class "*I*" on a tracer in an unsteady-state regime (tracer mass balance):

$$\frac{\partial C_{Tg}^{I}}{\partial t} = Dax_g^I \frac{\partial^2 C_{Tg}^{I}}{\partial z^2} - \frac{U_g^I}{\varepsilon_g^I}\frac{\partial C_{Tg}^{I}}{\partial z} + \frac{1}{\varepsilon_g^I} f_e \left(C_{Tg}^{I+1} - C_{Tg}^{I}\right) \tag{18}$$

The models assumed no axial variation of gas flow and holdup. TBCMM is a superposition of a convective mechanism (transport at two velocities) onto a dispersive mechanism (Fickian term in the ADM). The last mechanism is, however, assumed to be dominant to describe the bubble mixing.

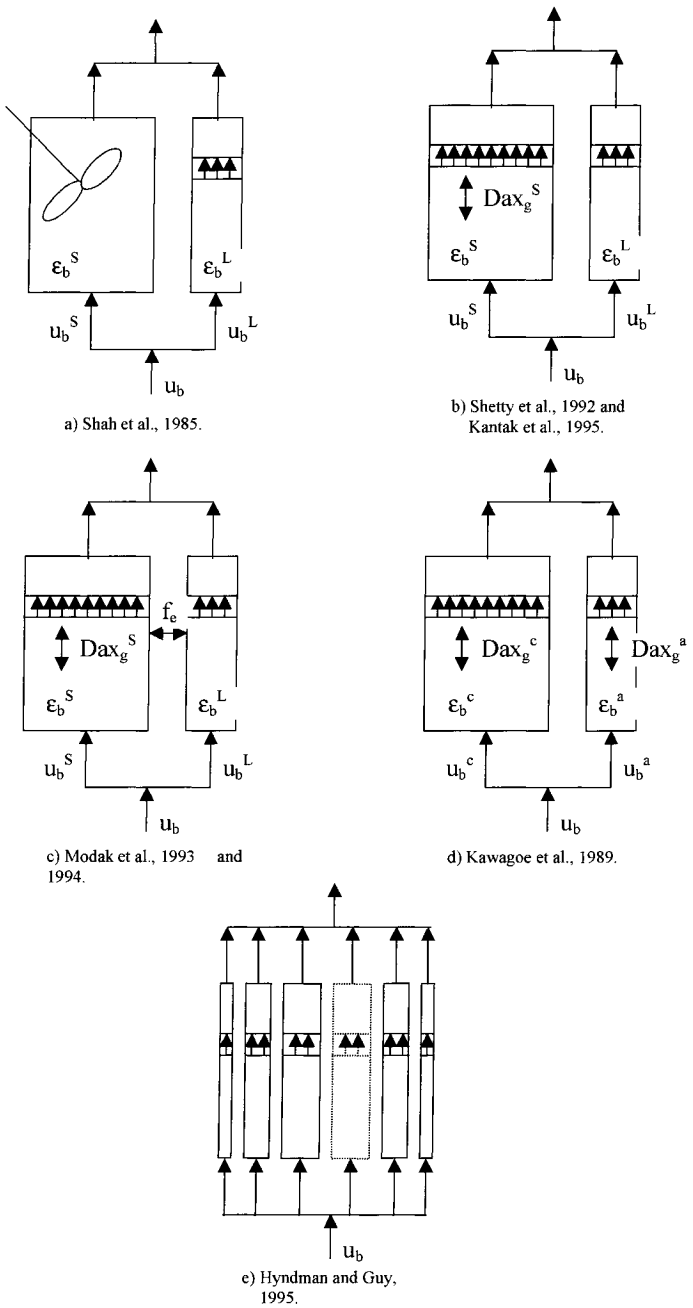


Figure 2.7: Schematic representation of the gas phase mixing models proposed in literature.

Table 2.2: Gas phase mixing models.

Article	Model for		Mixing model parameters[1, 2 3]	Fig.	Equations
	Small bubbles	Large bubbles			
Shah et al. (1985)	Perfectly mixed	Plug flow	➢ ε_g^S ➢ ε_g^L ➢ u_b^S ➢ u_b^L Transfer parameters: ➢ $(K_La)^S$ ➢ $(K_La)^L$	8a	(18) with I=S, L Dax_g^L=0 $Dax_g^S \to \infty$ f_e=0
Kawagoe et al. (1989)	ADM[4]	ADM	➢ ε_g^c ➢ ε_g^a ➢ u_b^c ➢ u_b^a ➢ Dax_g^c ➢ Dax_g^a	8d	(18) with I=c, a[5] f_e=0
Shetty et al. (1992) and Kantak et al. (1995)	ADM	Plug flow	➢ ε_g^S ➢ ε_g^L ➢ u_b^S ➢ u_b^L ➢ Dax_g^S Transfer parameters: ➢ $(K_La)^S$ ➢ $(K_La)^L$	8b	(18) with I=S, L Dax_g^L=0 f_e=0
Modak et al. (1993) and Modak et al. (1994)	ADM	Plug flow[6]	➢ ε_g^S ➢ ε_g^L ➢ u_b^S ➢ u_b^L ➢ Dax_g^S ➢ f_e	8c	(18) with I=S, L Dax_g^L=0
Hyndman and Guy (1995a and b)	Log-normal bubble velocities distribution for the whole bubbles population (purely convective model).		➢ α[7] ➢ β	8e	(19)

(Table 2.2 continued)

Article	Model for		Mixing model parameters[1, 2 3]	Fig.	Equations
	Small bubbles	Large bubbles			
Hyndman et al. (1997)	Purely convective model up to the transition point between dispersed and coalesced flows.	Plug flow (coalesced flow regime only)	➢ $f(u_{bp})_{trans}$ (depend on α and β) ➢ ε_g^S ➢ ε_g^L ➢ u_b^S ➢ u_b^L	Not show	(19)-(22)

[1] In some model representations, the fraction of the large bubble class holdup is used as the model parameter instead of the large bubble class holdup. The two representations are equivalent and both need to know the global gas holdup and a measure of the holdup fraction of each bubble class i.e. two measurement techniques. The same could be mentioned for the large and small bubble velocity.

[2] S: small bubble class and L: large bubble class.

[3] The k_La is not a gas phase mixing model parameters or characteristic, but it permits to take into account the tracer interfacial mass transfer (a way to overcome an experimental problem).

[4] ADM: Axial Dispersion Model.

[5] c: core region and a: annulus region.

[6] The authors proposed ADM for the mixing representation of the large bubble class, but assume that the Dax_g^L is negligible i.e. assume a plug flow behavior for the large bubbles.

[7] The averaged bubble velocity and the standard deviation of the bubble velocity distribution are function of α and β (eq (12) and (13)).

Table 2.3: Gas phase mixing models-Experimental conditions.

Article	Setup	Fluid/solid system	Operating conditions
Shah et al. (1985)	Column: ➢ Dc: 0.108 m ➢ Hc: 1.94 m ➢ Perforated plate: ➢ 76 orifices ➢ 0.001 mϕ_o ➢ triangular pitch	➢ N_2-water ➢ N_2-water-10wt% glass beads (48.5μmϕ)	➢ Ug: 0.09-0.30 m/s
Kawagoe et al. (1989)	Column I: ➢ Dc: 0.159 m ➢ *Hc*: 2.00 m ➢ Perforated plate: ➢ 61 orifices ➢ 0.002 mϕ_o Column II: ➢ Dc: 0.290 m ➢ *Hc*: 2.00 m ➢ Perforated plate: ➢ 198 orifices ➢ 0.002 mϕ_o	➢ air-water ➢ air-sodium sulfate aq. solution (1/3Kmol/m^3) ➢ air-CMC aq. solution (0.5wt %)	➢ Ug: 0.005-0.1 m/s
Shetty et al. (1992) and Kantak et al. (1995)	Column I: ➢ Dc: 0.15 m ➢ *Hc*: 2.7 m (3.0) ➢ Perforated plate and wire-mesh packing in series Column II: ➢ Dc: 0.20 m ➢ *Hc*: 2.7 m (3.0) ➢ Perforated plate and wire-mesh packing in series	➢ air-water ➢ air-CMC soln (0.05-0.5 wt%) ➢ air-ethanol soln (0.2 wt%) ➢ air-n-butanol soln (0.0012-0.36 wt%)	➢ Ug: 0.01-0.16 m/s ➢ U_L: 0.005-0.03 m/s

(*Table 2.3 continued*)

Article	Setup	Fluid/solid system	Operating conditions
Modak et al. (1993) and Modak et al. (1994)	➢ They used RTD data from Kawagoe et al. (1989) ➢ They used results of Schumpe and Grund (1986) for the repartition of gas holdup and gas velocity between the large and small bubbles. Schumpe and Grund (1986) experimental characteristics: <u>Column</u>: ➢ Dc: 0.30 m ➢ *Hc*: 4.4 m ➢ I-ring distributor: ➢ 56 orifices ➢ 0.001 mϕ_o ➢ II-perforated plate: ➢ 616 orifices ➢ 0.001 mϕ_o	➢ air?-water	➢ Ug: ? to 0.20 m/s
Hyndman et al. (1997)	Bubble column is the same as Hyndman and Guy (1995a and b)	➢ air-water	➢ Ug: 0.009-0.16 m/s

Hyndman and Guy (1995a) proposed, for bubble columns, a model describing gas phase mixing as a superposition of many bubble plug flows. Hence, each bubble rises at constant velocity along a column axis and mixing (or segregation) is caused by the difference in bubble velocity. Figure 2.7e shows a schematic representation of the model. This model is the first representation of a purely convective gas mixing. It is conceptually very different compared to a dispersive mixing represented by the ADM.

A convective model needs to be characterized by a velocity distribution. The authors proposed a log-normal form for the global bubble axial velocity distribution:

$$f(u_{bp}) = \frac{1}{\beta u_{bp}\sqrt{2\pi}} \exp\left(-\frac{(\ln u_{bp} - \alpha)^2}{2\beta^2}\right) \tag{19}$$

The choice of this form was based on data obtained by Matsuura and Fan (1984) in three phase fluidized beds. Their model is an adapted version of the one outlined by Aufderheide and Vogelphohl (1986) for dispersed phase flow in a liquid-liquid system. Hyndman and Guy (1995a) used tests based on residence time variance evolution using the length between two measuring points ($\Delta\sigma^2 \propto (L_2 - L_1)$) technique shows in Table 2.1). They invalidated the ADM to represent gas phase mixing and validated their purely convective model.

Hyndman et al. (1997) modified the previous convective model. They made population balance on bubbles and found the following equation for dispersed flow regime:

$$f(u_{bp}) = \frac{f^0(u_{bp})}{1 + \frac{\overline{u_b}}{\sigma^2_{u_b}}(\overline{u_b} - u_{bp})\varepsilon_g} \tag{20}$$

and for coalesced flow regime:

$$f(u_{bp}) = (u^L_{bp} - \overline{u}_b)\frac{f^0(u_{bp})}{(u^L_b - u_{bp})} + \frac{\varepsilon^L_g}{\varepsilon_g}\varepsilon_g \delta\{u^L_{bp} - u_{bp}\} \tag{21}$$

Where δ is a delta Dirac function and $f^{0}(u_{bp})$ is an ideal bubble velocity distribution with no bubble/bubble interaction. This distribution may be found with the following equation:

$$f^{0}(u_{bp}) = f(u_{bp})\Big|_{trans}\left[1+\frac{\overline{u}_{b}}{\sigma^{2}}(\overline{u}_{bp}-u_{bp})\varepsilon_{g}\right]\Big|_{trans} \tag{22}$$

Where $f(u_{bp})\Big|_{trans}$ is the log-normal bubble velocity distribution (eq (19)) at the transition flow regime.

That is, for the coalesced flow regime, the model assumed a plug flow behavior for the large bubble class and a convective (multiple plug flow) mixing for the small bubble class. In other words, the global bubble velocity distribution is assumed to be represented by a combination of a modified log-normal velocity distribution (for the small bubble class at the transition point) and a Dirac function (distribution) contribution attributed to the large bubble class velocity. Furthermore, the first formulation of the model assumes that when two bubbles rise at the same velocity they do not accelerate and when two bubbles interact, the slower bubble accelerates to the velocity of the faster bubble. This approach is consistent with that of Krishna et al. (1994). However, this derivation of the purely convective model and the CSTR-small-bubble/PFR-large-bubble model is inconsistent with gas phase mixing experimental observations. Indeed, increasing the superficial gas velocity increases the large bubble holdup that increases the plug flow behavior of the gas phase. This contradicts the usual observation that the gas phase mixing increases with the superficial gas velocity.

The purely convective model and the ADM (dispersive mechanism) represent two extreme mixing mechanisms. The former assumes a constant velocity for each bubble and the latter assumes a random change of velocity, which is the same for each bubble. In other words, following only one bubble exhibiting a dispersive mechanism is enough to know all about the system dynamic. However, for bubbles exhibiting a convective mechanism, it is necessary to follow all of the bubbles in order to understand the system dynamics. According to visual observations and experimental evidence observed in the bubble column, slurry bubble column and three phase fluidized bed reactors, the bubbles' behavior is clearly intermediate between convective and dispersive mechanisms. Based on that, Briens et al. (1995) proposed a stochastic model (Monte-Carlo model: discussed at the end of this review) that allows representing various fluid (it may be bubbles, drops, particles or liquid elements) dynamics between convective and dispersive mechanims. The model assumes a Gaussian velocity distribution followed by the fluid elements. A fluid element has a probability per unit time to change its velocity and all of the fluid elements have the same probability. Furthermore, the fluid elements *exchange* their velocity in order to conserve the same fluid element velocity distribution along the reactor. The model has therefore three parameters: the mean fluid element velocity, the variance of the fluid element velocity distribution and the probability per unit time to change the velocity of a fluid element.

This model is of interest when all fluid elements have the same dynamic, which is not the case for the bubble population in the multiphase reactor, mainly in a coalesced flow regime. Indeed, the "history" of the velocity changes of a bubble depends on the bubble size. Concerning the relative importance of the buoyancy force compared to the drag, Basset and added mass forces depend on the bubble size. In other words, the smallest bubbles will follow more closely the liquid flow than the largest bubbles. Moreover, for the slurry bubble column and three-phase fluidized bed the coalescence/breakup dynamic due to the solid phase will change from one bubble to another, according to

the bubble size. Furthermore, Briens et al. (1995) assumed a stochastic behavior for the velocity changes, which may not be applied to bubbles as observed in some literature results, indicating a determinist chaos behavior to the bubble flow in a single orifice system (Nguyen et al., 1996; Luewisutthichat et al., 1997), in a bubble column (Kikuchi et al., 1997) and in a three-phase fluidized bed (Kikuchi et al., 1996). Stochastic modeling should not represent determinist chaos. It should be represented by non-linear determinist relations (Hilborn, 2000), such as deterministic forces acting on bubbles. However, Kikuchi et al. (1997) observed a significant increase in the random contribution on bubble motion. It should be noted that this random contribution was calculated from the delay between two successive bubble time series and not from a bubble velocity time series. It is clear that more studies about the diagnosis of bubble dynamic behavior are needed.

Finally, Molerus and Kurtin (1986) described the gas phase Residence Time Distribution (RTD) form. The delay at the beginning of the RTD corresponds to the fastest rising bubbles. The steep slope of the shortest residence times on the RTD originates in the motion of large bubbles. The long tail of the RTD is due to the partial recirculation of small bubbles. The authors used a log-normal distribution to represent the gas phase RTD.

2.2.5.2 Model exploitation

Gas phase mixing models were used or validated in various ways, depending on the authors. Some validated their models with hydrodynamic data. They often compared model predictions with the ADM ones. Other authors used their models to simulate multiphase reactor performances (conversion and selectivity) assuming chemical reactions. Table 2.4 summarizes model exploitations according to the various authors. The following text discusses some models exploitation in more detail.

Table 2.4: Gas phase mixing models-Model exploitation.

Article	Validation/simulation [1]	Interfacial tracer mass transfer [2]	Optimized parameter(s)
Shah et al. (1985)	➢ Simu-one	➢ N.a.	➢ *None*
Kawagoe et al. (1989)	➢ RTD-one	➢ Negl	➢ α ➢ Dax_g^a ➢ Dax_g^c
Shetty et al. (1992) and Kantak et al. (1995)	➢ RTD-one	➢ K_La	➢ *None* and ➢ α
Modak et al. (1993)	➢ RTD-one	➢ Negl	➢ f_e ➢ Dax_g^L
Modak et al. (1994)	➢ Simu-some	➢ N.a.	➢ *None*
Hyndman and Guy (1995a)	➢ RTD-some	➢ T-sat	➢ α ➢ β
Hyndman et al. (1997)	➢ εg-struc	➢ T-sat	➢ *None*

[1] RTD-one: model is validated with a RTD measured at one axial location.

RTD-some: model is validated with RTD measured at some axial locations.

εg-struc: model holdup structure predictions is compared with holdup structure measurement.

Simu-one: model is used to simulate reactor conversion assuming one chemical reaction.

Simu-some: model is used to simulate reactor conversion and selectivity assuming a desired, undesired series and parallel chemical reactions.

[2] N.a.: not applicable.

K_La: authors included in their mixing model the tracer interfacial mass transfer. They assumed $K_La(C^*_{TL}-C_{TL})$ model for transfer rate and used Henry's law relation for the thermodynamic liquid saturated tracer concentration evaluation.

T-sat: authors feed continuously a stream of radioactively inactivated gaseous tracer (Ar) to saturate the liquid phase in order to reduce the dynamic transfer rate.

Negl: authors assumed that the tracer interfacial mass transfer is negligible.

2.2.5.2.1 Residence Time Distribution

Most authors (Molerus and Kurtin 1986; Kawagoe et al., 1989; Shetty et al., 1992; Modak et al., 1993; Kantak et al., 1995; Hyndman and Guy 1995a) used RTD data to validate their gas phase mixing model.

First of all, it is important to discuss gas/liquid interfacial mass transfer of the gas phase tracer. Indeed, the idealized tracer marks only the gas phase, i.e. no interaction or affinity with the other phases. Unfortunately, gases are partially soluble in liquid. A fraction of the gaseous tracer is thus transferred to the liquid phase, resulting in misleading gas phase mixing data. These data contain information about the extent of gas phase mixing and the mass transfer rate, instead of only one hydrodynamic aspect. The solubility of the gaseous tracer often causes a long tail on the RTD, which gives a misleading appearance of a higher extent of mixing. In addition to the conventionally necessary properties of a tracer, a gas phase tracer should be insoluble as much as possible in the liquid phase.

Shetty et al. (1992) experimentally studied the effect of whether or not to consider the interfacial mass transfer with the Single-Bubble-Class-ADM (SBC-ADM). The unsteady tracer mass balance was then written as follows:

$$\frac{\partial C_{Tg}}{\partial t} = Dax_g \frac{\partial^2 C_{Tg}}{\partial z^2} - \frac{U_g}{\varepsilon_g}\frac{\partial C_{Tg}}{\partial z} - \frac{1}{\varepsilon_g} K_L a\left[C_{TL}^* - C_{TL}\right] \tag{23}$$

According to equation (23), Shetty et al. (1992) should consider a liquid mixing model, because C_{TL} should be determined in order to solve equation (23). For simplification purposes they considered that the liquid is perfectly mixed. The unsteady aqueous tracer mass balance is then:

$$\frac{\partial C_{TL}}{\partial t} = -\frac{1}{L}\frac{U_L}{1-\varepsilon_g} C_{TL} + \frac{1}{L}\frac{1}{1-\varepsilon_g} K_L a \int_0^L \left[C_{TL}^* - C_{TL}\right] dz \tag{24}$$

They used their own data (He tracer) and the data of Towell and Ackerman (1972) (Freon-12 tracer) and Field and Davidson (1980) (Ar-41 tracer) in order to find the gas phase ADC and the mass transfer coefficient. The mass balance of both phases is dimensionalized and data were fitted by Shetty et al. (1992) to find the optimized value of Pe_g (Dax_g) and St (K_La). The model fits the literature data better than the ADM alone; the gas phase RTD tail is better fitted. This may be due to the fact that a two-parameter-model fits the data easily. However, it is well known that an interfacial mass transfer of the tracer induces a tail in the gas phase RTD. They observed a difference between the Peclet number calculated while taking and also not taking into consideration the interfacial mass transfer (about 40 %). However, the model is not really sensitive to the Stanton number variation. This is due to the weak interfacial mass transfer of the weak soluble tracer. Furthermore, the Stanton number is related to the RTD tail, which is small and shows this weak sensitivity.

Kantak et al. (1995) (the same team as Shetty et al., 1992) also used the SBC-ADM with an interfacial mass transfer term. They studied the effect of three different gas tracers (He, Ar and CO_2) on optimized parameters (Pe and St). The more soluble tracer (CO_2) gives obviously the longer RTD tail. However, for a given experimental condition, the axial dispersion coefficients obtained have approximately the same values for each tracer and the mass transfer coefficients change with the tracer solubility.

Joseph and Shah (1986) theoretically studied the solubility effect of the tracer. They used the SBC-ADM with an interfacial mass transfer rate term. They studied the impact

of this mass transfer on the first two moments of the residence time distribution, with the assumption that the liquid phase is perfectly mixed. They found that the assumption of neglecting the interfacial mass transfer induces a significant deviation from the expected moments, even for a relatively insoluble gas, such as helium in water. The gas phase Peclet number is underestimated in such a way that the true value, i.e. the extent of mixing, seems higher. They also found that Henry's constant must be higher than 1000 to allow the interfacial mass transfer to be neglected. However, Wachi and Nojima (1990) found, also through theoretical calculation, that the interfacial mass transfer is negligible for H > 10. However, the last authors used the ADM for the liquid phase instead of the CSTR model and simulated for only one set of hydrodynamic parameters, while changing the Henry constant. The conditions allowing the tracer interfacial mass transfer to be neglected are not yet clear. It is clear, however, that caution concerning tracer transfer should be used when gas phase tracing techniques are used.

The models of Kawagoe et al. (1989), Shetty et al. (1992) and Kantak et al. (1995) assumed there were no interactions between bubble classes. Two RTDs are then calculated independently, one for each bubble class. Because RTD data represent mixing of all bubbles, bubble class RTDs should be combined. Therefore, according to their model representation, Kawagoe et al. (1989) calculated, for a set of experimental conditions, one RTD with the ADM (unsteady tracer mass balance written with eq (18) using $f_e = 0$ and I = a) for the annulus bubble group ($E^a(t)$) and one with the ADM (eq (18) using $f_e = 0$ and I = c) for the core bubble group ($E^c(t)$). They thus combined the two bubble class RTDs with the following equation:

$$E(t) = \alpha E^c(t) + (1-\alpha)E^a(t) \tag{25}$$

Where "α" is the ratio of the gas flow rate of the core bubble group to the total gas flow rate. This model considers two bubble regions rather than two bubble classes. Indeed, this model separates the gas holdup into two regions: gas at the upflow region (r/R=[0 to 0.7], Ueyama and Miyauchi (1979)) and at the downflow region (r/R=[0.7 to 1.0]) of the column. The upflow region is called the core region and the downflow region is the annulus region.

Shetty et al. (1992) and Kantak et al. (1995) took into account the interfacial mass transfer of the tracer in their tracer mass balance. The unsteady-state mass balance for each bubble class is then:
For large bubbles:

$$\frac{\partial C_{Tg}^{L}}{\partial t} = -\frac{U_g^L}{\varepsilon_g^L}\frac{\partial C_{Tg}^{L}}{\partial z} - \frac{1}{\varepsilon_g^L}(K_L a)^L\left[\left(C_{TL}^{*}\right)^L - C_{TL}^{L}\right] \tag{26}$$

For small bubbles:

$$\frac{\partial C_{Tg}^{S}}{\partial t} = Dax_g^S\frac{\partial^2 C_{Tg}^{S}}{\partial z^2} - \frac{U_g^S}{\varepsilon_g^S}\frac{\partial C_{Tg}^{S}}{\partial z} - \frac{1}{\varepsilon_g^S}(K_L a)^S\left[\left(C_{TL}^{*}\right)^S - C_{TL}^{S}\right] \tag{27}$$

The interfacial mass transfer flux term should not be considered as a model characteristic, but as a tool or way to overcome an experimental problem: the liquid solubility of the tracer. The gas phase model characteristics are to consider two bubble classes and the different mixing characteristics for each class.

A liquid phase mixing model should be used when considering the tracer interfacial mass transfer. As will be seen, modeling liquid phase mixing is not obvious and many liquid phase mixing models are available in the literature. Shetty et al. (1992) and

Kantak et al. (1995) assumed that the ADM represents the liquid phase mixing. Shetty et al. (1992) used two liquid phase ADMs, i.e. one associated with the large bubble class and the other associated with the small bubble class. This calculation procedure has bad consequences. It does not consider any interaction between the liquid associated with each bubble class. The liquid is continuous in space (except if the liquid in the bubbles wake is considered), the small and large bubbles rise into only *one* phase bulk liquid. There is no clear zone where the small and large bubbles rise that is completely separate. The same team (Kantak et al., 1995) modified the model of Shetty et al., but did not underline this modification. Kantak et al. (1995) used only one ADM for the liquid phase and added the two interfacial mass transfer flux terms in the liquid ADM:

$$\frac{\partial C_{TL}}{\partial t} = Dax_L \frac{\partial^2 C_{TL}}{\partial z^2} - \frac{U_L}{1-\varepsilon_g}\frac{\partial C_{TL}}{\partial z} - \frac{1}{1-\varepsilon_g}\sum_{I=S,L}(K_L a)^I \left[(C_{TL}^*)^I - C_{TL}\right] \tag{28}$$

The continuity of the liquid phase is then respected; this is more realistic. A model does not necessarily consider all physical characteristics, but should take into account the most important mechanisms. The modeling challenges are to identify these key mechanisms and find out how to mathematically represent them. Shetty et al. (1992) and Kantak et al. (1995) used equation (25) to combine the two bubble class RTDs.

Modak et al. (1993) proposed a model that assumes, like Shetty et al. (1992), a plug flow behavior for the large bubble class and a dispersive mixing mechanism for the small bubble class represented by the ADM. However, their model is the first to consider bubble/bubble interaction. They represented this interaction as a cross-mixing, with a cross-mixing coefficient, f_e. The unsteady tracer mass balance is written as equation (18) with I = L and $Dax_g^L = 0$ for the large bubble class and as equation (18) with I = S for the small bubble class. It should be noted that the liquid solubility of the

tracer is not considered. A differential equation system is solved and bubble class RTDs are combined with equation (25). They fitted the residence time distribution measured by Kawagoe et al. (1989) that used He as the tracer (very low liquid solubility).

For all experimental conditions, the optimized values of f_e tend to infinity (very large value of f_e). Since time and the spatial derivative of the tracer concentration are not infinite, the tracer concentration in both bubble classes should be equal. A complete cross-mixing is then assumed by the authors. The authors' results may be interpreted in a different way. If a uniform concentration distribution of the tracer upstream of the gas distributor is assumed, bubbles formed across the distributor have the same tracer concentration. According to this, mass exchange might be zero and is not necessarily equal to infinity. Indeed, bubble coalescence/breakup does not occur enough in the air/water system (Stewart, 1995). However, the conclusion that the bubble class concentrations are equal remains the same. They thus combined their bubble class tracer mass transfer balance, with an axial dispersion coefficient for the large bubbles, into a single equation:

$$\frac{\partial C_{Tg}}{\partial t} = -\frac{U_g}{\varepsilon_g}\frac{\partial C_{Tg}}{\partial z} + \left(Dax_g^L \frac{\varepsilon_g^L}{\varepsilon_g} + Dax_g^S \frac{\varepsilon_g^S}{\varepsilon_g} \right) \frac{\partial^2 C_{Tg}}{\partial z^2} \tag{29}$$

This equation has the same shape as the ADM, but the representation of the dispersive constant is different. The authors used $Dax_g^L = 0$. The value of the ADC of the small bubbles is higher than the overall gas ADC of the SBC-ADM, because the overall extent of mixing is represented by a fraction of the gas phase volume. With the Dynamic Gas Disengagement (DGD) data used, the ratio (Dax_g^S)Modak et al.'s model/$(Dax_g)^{ADM}$ varies from 1 at the transition point to 1.7 at superficial gas velocity of 0.25 m/s.

Some authors estimated and/or measured and/or fitted their model parameters. Table 2.2 gives a list of the model parameters and Table 2.4 indicates which model parameters were fitted. Kawagoe et al. (1989) integrated the well known quadratic radial gas holdup profile relation used for bubble columns in the core region ($0<r/R<0.7$) and in the annulus region ($0.7<r/R<1.0$) to find the relative holdup of each bubble group. They then optimized three parameters with their gas phase RTD data. The three parameters optimized are the ADC of each bubble group (Dax_g^c and Dax_g^a) and the ratio of the core-bubble-group gas flow rate to the total gas flow rate (α). The other authors using TBCMM employed the DGD technique to find the relative bubble-class holdup and relative bubble-class gas velocity. Modak et al. (1993) used the RTD data of Kawagoe et al. (1989) to fit two parameters, i.e. the small bubble class ADC (Dax_g^S) and the cross-mixing coefficient (f_e).

Both sets of authors said that their model fit the experimental data better than the SBC-ADM. This is obviously due to the number of parameters of each model. Their model has two or three parameters to be optimized, whereas the ADM has only one (if the measured value of Ug/ε_g is used). The quality of the fitting is not always (rarely) a good criterion to validate a model. The ability of a model to fit RTD data is an essential model characteristic, but it is not a sufficient model characteristic. Many different mathematical equations may fit a RTD. Also, the choice of the optimization technique used to find the parameters value is very important. Indeed, depending on the model mathematical form, some optimization techniques are capable of fitting data and others are not. Furthermore, some optimization techniques generate a local minimum yielding various sets of parameters having the same objective function (to be minimized) value. Therefore, when many parameters have to be optimized, a correlation matrix should be calculated (Gunst and Mason, 1980).

Shetty et al. (1992) and Kantak et al. (1995) also used DGD data. Literature data was used to estimate the interfacial mass transfer coefficients. Because the small bubbles are carried by the liquid phase, the authors assumed that the small bubbles axial dispersion coefficient is equal to that of the liquid phase. This assumption is not realistic. The small bubbles cannot exactly follow the liquid flow, because, among other reasons, the buoyancy force is far from being zero. Moreover, the bubbles are carried by liquid eddies equal in size to or bigger than the bubbles' size; the global liquid ADC represents the mixing of all scales. The bubbles are not mixed with the liquid at a smaller scale than their size. Fan (1989) stipulated that the gas axial dispersion coefficient is two to ten times greater than the liquid one. Furthermore, Zahradnik and Fialova (1996) showed that the gas phase Peclet number is one order of magnitude higher than that of the liquid phase. That is, the gas phase follows a behavior closer to plug flow than the liquid phase; the gas phase is obviously less backmixed than the liquid phase.

TBCMM was validated with only one overall RTD data. As mentionned above lots of mathematical equations may fit RTD data. However, the evolution of the RTD along the axial position is more specific to the mixing mechanism (see section on "mixing mechanism"). Thus, the number of mathematical equations that may represent this evolution are less numerous and should have mathematical properties closer to flow properties.

Hyndman and Guy (1995a) proposed the first purely convective gas phase mixing model for a bubble column. They first diagnosed the gas phase mixing mechanism as will be discussed below. A purely convective model may be visualized as a multiple-plug-flow model. Each bubble follows a plug flow behavior, i.e. each bubble rises at a time and space constant velocity. Thus, a bubble velocity distribution shape must be assumed. A log-normal bubble velocity distribution was used (eq (19)).

They used an unsteady tracer technique to obtain gas phase mixing data. Radioactive argon (tracer) interfacial mass transfer was not considered in the model formulation, but the authors used an experimental strategy to reduce the solubility effect of the tracer. Indeed, gas argon (not radioactive marked) is supplied with the input airflow. Thus, the liquid is always saturated in argon. The authors said that, even if the interfacial mass transfer is a dynamic process, the interfacial exchange of the radioactive argon becomes negligible.

Hyndman and Guy (1995a) developed statistic tests based on the mechanistic approach by Levenspiel and Fitzgerald (1983) described above. These statistic tests allow them to identify the predominant mixing mechanism responsible for gas phase mixing. They compared a dispersive mechanism (SBC-ADM) with a convective mechanism. The statistic tests need gas phase RTD measurements obtained between different axial distances along the bubble column axis. If the gas phase mixing mechanism is dispersive, the following criteria should be respected (see Table 2.1):

$$\frac{\left(\sigma_k^2-\sigma_j^2\right)}{\left(L_k-L_j\right)}=cte=2\left(\frac{\varepsilon_g}{U_g}\right)^3 Dax_g \tag{30}$$

If the gas phase follows a convective mechanism, the following criteria should be respected:

$$\left(\frac{1}{\left(L_k-L_j\right)}\right)\left(\frac{\mu_k^4}{\left[\mu_k^2+\sigma_k^2\right]^{1.5}}-\frac{\mu_j^4}{\left[\mu_j^2+\sigma_j^2\right]^{1.5}}\right)=cte=\exp\left(-\alpha\right) \tag{31}$$

where μ and σ are, respectively, the first moment (or mean) and the standard deviation of the RTD; j and k are indices relative to the axial position. Hyndman and Guy (1995a) also compared the average bubble velocity obtained from the fit of both model and the average bubble velocity calculated from an independent measurement (U_g/ε_g): input gas flow rate and global gas hold-up.

For the SBC-ADM validation, the Peclet number and the mean residence time were optimized. The average bubble velocities optimized by the SBC-ADM were more than 30 % lower than the U_g/ε_g values. The criteria (eq (30)) were not respected. Indeed, the variability obtained with the expression (eq (30)) was between 12 and 18 %. These two tests invalidated the SBC-ADM.

Equation (19) converted into a RTD form was also fitted to find the α and β parameters. The model estimations of the averaged bubble velocities and the U_g/ε_g values were almost the same. This model property is necessary, but not sufficient. The criteria (eq (31)) were respected with a variability of less than 5 %.

The gas phase mixing mechanism seems to be a convective one. Zahradnik and Fialova (1996) also obtained the same conclusion in an air/water bubble column. They found that the *n*-exponent value in equation (17) is about 0.95, which indicates a mostly convective mechanism for the gas phase mixing. In view of the bubble dynamic, it would be interesting to study the effect of the presence of solid on the mixing mechanism in addition to the extent of mixing. For example, the presence of large/heavy particles induces a vigorous coalescence/breakup intensity that perhaps causes a more stochastic (dispersive) behavior, i.e. bubble velocity changes along the reactor length. The effect of liquid and solid properties on the dominant mixing mechanism would be an interesting study that should be examined before studying how these phase properties affect the extent of gas phase mixing.

Equation (19) was used by Hyndman et al. (1997) to predict their DGD results. The model predictions at the transition point correspond to the DGD data associated with the small bubbles class in the coalesced flow regime. This was observed for all superficial gas velocities used in the coalesced flow regime. The small bubble flow structure is thus constant in the coalesced flow regime. The averaged bubble flow structure may be represented by the superposition of a volume-saturated small bubble population that maintains a constant behavior onto a large bubble population, whose volume increases with the superficial gas velocity.

Hyndman et al. (1997) developed a hydrodynamic model that describes the gas phase holdup structure. This model is capable of predicting the global gas holdup in both flow regimes, the fraction of large bubble in the coalesced flow regime and a superficial gas velocity range of the transition flow regime zone. The convective model accurately predicts the holdup structure data in the bubble columns.

The stochastic (Monte-Carlo) model proposed by Briens et al. (1995) was used to generate RTD for various coefficients of variation of velocity distribution ($C_u=\sigma_u/u_m$) and various probabilities per unit time to change the velocity of a fluid element (ϕ). The authors observed weak RTD (weak $C_t=\sigma_t/t_m$) when ϕ increases (more dispersive) for the same velocity distribution (same C_u). Briens et al. (1995) also studied the erroneous RTD measured by a through-the-wall average concentration technique in an open/open boundary system and based their calculations on input/output signal deconvolution. Remember that fluid elements cross and re-cross the boundary in an open/open boundary system, thus rendering it impossible to directly measure the real RTD using a through-the-wall average concentration measurement (Nauman and Buffham, 1983). The famous case of this phenomenon is the ADM solution obtained for an open/open boundary system vs. the one obtained for the case of a closed/closed boundary system.

Hence, Briens et al. (1995) extend the analysis to a more general case, i.e. various convective/dispersive mechanisms. They found that the error (deviation) yield on the mean residence time obtained by deconvolution is a strong function of ϕ and C_u (particularly). This error is not bijective (for measured values of Ct, there are many possible error values) and the calculated error is up to 1000 %. Although the error (deviation) yield on the C_t obtained by deconvolution is less sensitive to the model parameters, it is not negligible for the high value of the "real" C_t. The authors did not compare their model to experimental measurements. They proposed, however, some local measurement techniques, which allowed them to obtain the real RTD of the reactor.

2.2.5.2.2 Simulation

Shah et al. (1985) and Van der Laan et al. (1999) simulated multiphase reactor performance with the TBCMM assuming plug flow and perfectly mixed behavior for the large and small bubble classes, respectively. The second group of authors simulated slurry bubble column reactors where Fisher-Tropsch synthesis occurs. However, they did not compare their model with other models. The first group of authors assumed there was one simple reaction and predicted the conversions for various reaction rates and superficial gas velocities. Predictions were made with the SBC-plug flow model and their TBCMM. Their main simulation conclusions are compared later with those of Modak et al. (1994) who used another version of a TBCMM. The Modak et al. (1994) model also assumes a plug flow behavior for the large bubble class, but assumes that the ADM may represent the mixing of the small bubble class.

Modak et al. (1994) explain their simulation here in more detail. They simulated the following virtual chemical reactions occurring in a bubble column:

The desired reaction:

$$A_{(g)} + B_{(L)} \xrightarrow{k_B} C_{(L)}$$

the undesired series reaction:

$$A_{(g)} + C_{(L)} \xrightarrow{k_C} D_{(L)}$$

and the undesired parallel reaction:

$$A_{(g)} + A_{(g)} \xrightarrow{k_A} E_{(L)}$$

The three chemical reactions are elementary. They laid out that the first reaction is fast and linked to the interface. The other two reactions are slow and occur in the liquid phase.

For the gas phase, the Modak et al. (1993) model (eq (29) with $Dax_g^{\,L} = 0$ and $\partial C_{Tg}/\partial t = 0$ (steady state)) was used. This model assumes a high interaction (high mass exchange) between the two bubble classes. In other words, component concentrations in both bubble classes are identical. It should be noted that if mass exchange (f_e) is not infinite (as may be assumed, see above comment), component concentration of each bubble class should be not equal. The steady-state gas phase mass balance of A is written as:

$$-\frac{U_g}{\varepsilon_g}\frac{\partial C_{Ag}}{\partial z} + Dax_g^{\,S}\frac{\varepsilon_g^S}{\varepsilon_g}\frac{\partial^2 C_{Ag}}{\partial z^2} = \frac{1}{\varepsilon_g}\left[\left(J_A^*\right)^L a^L + \left(J_A^*\right)^S a^S\right] \tag{32}$$

The last two right hand side terms represent the interfacial mass transfer of both bubble classes. An interfacial mass transfer model should be assumed. They used the Danckwerts surface renewal theory and obtained:

$$\left(J_A^*\right)^I = k_L^I \sqrt{1+\left(Ha^I\right)^2}\left[C_{AL}^* - \frac{C_{AL}}{1+\left(Ha^I\right)^2}\right] \tag{33}$$

I = L (large bubble class), S (small bubble class). C_A^*: concentration of "A" at the gas-liquid interface, found with Henry's law.

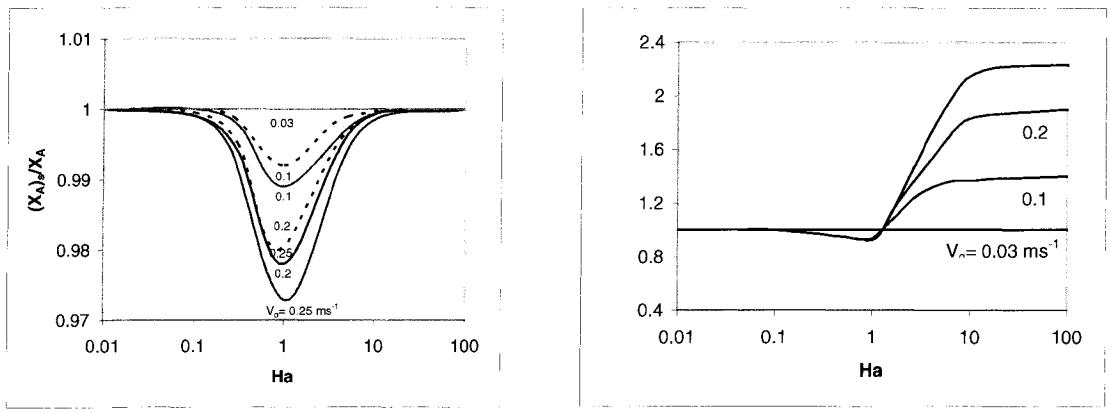
Where Ha^I is:

$$Ha^I = \left[\frac{\{Diff_A\}k_B C_{BL}}{\left(k_L^I\right)^2}\right]^{1/2} \tag{34}$$

Where $Diff_A$ is the diffusivity of A in the liquid phase, k_B is the kinetic constant of the desired reaction and k_L^I is the transfer coefficient of bubble class I. Hence, Ha is the ratio of the chemical rate of the desire reaction to the gas/liquid interfacial mass transfer rate. Furthermore, a liquid phase mixing model should be used. Model-simulation-exploitation induces extra difficulties, but gives an interesting type of investigation about the model's (or the mixing mechanism) effect on the reactor's performance predictions. The choice of the interfacial mass transfer model and liquid phase mixing model affects the gas phase mixing model validation. For simplification purposes the authors considered that the liquid phase is perfectly mixed.

These mass balances were written for the other species and the system of equation was solved. The TBCMM predictions were compared to the SBC-ADM predictions using

equivalence relationships. The hydrodynamic parameters found by Modak et al. (1993) were used. Figure 2.8 shows their simulation results. Figure 2.8a and 8b show, respectively, the ratio of conversion predicted by the SBC-ADM to the one predicted by the TBCMM and the ratio of the selectivity predicted. Conversions of A obtained by the two models were not that different for $Ha >> 1$ and $Ha << 1$. The ADM slightly underestimates (less than 3 %) that the conversion of A at Ha value ranged from 0.3 to 3.0. This difference was higher at large superficial gas velocities. The selectivities predicted by both models were almost the same for $Ha << 1$. However, for $Ha > 1$ the predicted selectivities were quite different, especially for $Ha > 3$ (rapid kinetic relative to interfacial mass transfer). The model selectivity ratio was asymptotic with Ha and increased with the superficial gas velocity. At a superficial gas velocity of 0.25 m/s and at the asymptote, the selectivity predicted by the ADM was more than twice the selectivity predicted by their TBCMM. Modak et al. (1994) attributed this difference to the large difference between the small and large bubble class mass transfer coefficient. Indeed, they imposed the same total mass transfer coefficient (k_L) for both models ($k_L^S a^S + k_L^L a^L = k_L a$) and found that the relative predicted selectivity was the ratio of the square mass transfer coefficient ($(k_L^S)^2 a^S + (k_L^L)^2 a^L$) sum of the TBCMM to the square mass transfer coefficient of the ADM ($k_L^2 a$).



(a) (b)

Figure 2.8: Comparison of the reactor performance predictions of the SBC-ADM and the TBCMM of Modak et al. (1994). a) Ratio (SBC-ADM / TBCMM) of the predicted conversion. b) Ratio of the predicted selectivity.

It should be noted that Shah et al. (1985) observed significantly different predicted conversions between a SBC-plug flow model and a TBCMM (large bubble class: plug flow; small bubble class: perfectly mixed), contrary to Kantak et al (1995). However, it should be mentioned that Shah et al. (1985) seem not to have used similar mass transfer rates for both model predictions. They also showed that the difference between the two model conversion predictions decreased with the superficial gas velocity, contrary to Kantak et al (1995). This decrease in difference is simply due to the increasing large bubble fraction with the superficial gas velocity that "artificially" increases the plug flow behavior of the gas phase, as discussed above.

Another important point should be mentioned here. Shah et al. (1985) and Van der Laan et al. (1999) used the CSTR relations to model the liquid phase mixing. Only gaseous reactants are transferred into the liquid phase; no product is transferred into the gas phase. Conversion and selectivity predictions will, therefore, not differ whatever

the gas phase mixing model used for the same interfacial mass transfer rate. Indeed, reaction rates in CSTR do not depend on how the reactants are fed, i.e. the CSTR "sees" the integration of the feeds. Conversion and selectivity predictions are different when products are transferred into the gas phase and/or some reactions take place at the gaz/liquid interface, as in the case of Kantak et al (1995).

The above discussion shows that the choice of the mixing model is, for some operating conditions and chemical reaction(s), obviously critical to design and scaled-up purposes. A comparison between the mixing model predictions and chemical performance data obtained with different experimental set-ups and/or in different industrial reactors is then needed to find a validated range for each mixing model.

2.2.5.3 Conclusion

First of all, it should be noted that the bi-modal representation of the bubble population is questionable. Indeed, local measurements of bubble property distribution reported in the literature (Matsuura and Fan, 1984; Lee et al., 1990) do not show bi-modal properties of the bubble population. Moreover, some authors (Deshpande et al., 1995; Dudukovic et al., 2002) doubt the validity of the DGD technique used to quantify the bi-modal bubble population properties. Assuming continuity in the bubble properties is obviously closer to the bubble flow pattern observed.

As it was seen, the gas phase mixing mechanism has an important convective mixing component. However, the literature data concerning bubble flow pattern and visual observation of this flow pattern indicate that the bubble velocity changes along the reactor because of phase interactions. For example, bubble/bubble interactions may induce bubble coalescing and particle/bubble interaction may promote bubble breakup. Also, in bubble/liquid interaction, small bubbles are driven by liquid flow. Therefore, according to the bubble size, some bubbles change their velocity often (dispersive

mechanism) and some larger bubbles do not change their velocity and path a lot (convective mechanism). Hence, the mixing mechanism may be different depending on the bubble size. Bubble size distribution is, thus, an important parameter and the relationship of the bubble size to the probable mixing mechanism is also important. The purely convective model for the gas phase has to be improved in order to include the bubble coalescence/breakup and the distribution of bubbles following convective mixing as well as other mixing mechanisms. These behaviors depend on phase properties that favor coalescence or breakup and depend on interfacial momentum transfer. It would be interesting to identify the mixing mechanisms of the gas phase under various conditions instead of studying the extent of mixing under various conditions. Comparing the extent of mixing for two systems that do not follow the same mixing mechanism is equivalent to comparing two different things.

Furthermore, it is clear that using only one global RTD to validate and/or identify the gas phase dynamic is not sufficient. Using several global RTDs along an axis yields a higher level of description (identification). However, this is not sufficient to clearly identify, from the numerous possible descriptions of bubble behaviors, the gas phase dynamic. Therefore, the next level of description should be obtained by local measurements using time series analysis.

2.2.6 LIQUID PHASE MIXING MODELS

2.2.6.1 Model concept

Most liquid mixing models differentiate between mixing caused by liquid recirculation and mixing caused by other aspects, such as turbulence and material exchange between various regions and/or phases. However, the liquid phase mixing models proposed in the literature are less homogeneous in their form than gas phase mixing models. Table 2.5 summarizes models and Table 2.6 shows the experimental conditions used.

Table 2.5: Liquid phase mixing models.

Article	Mixing mechanism contribution		Mixing model parameters	Fig.	Equations
	Dispersive	Convective			
Myers et al. (1987)	Slug/cell liquid exchange	Global liquid recirculation	➢ f_s ➢ V_s ➢ V_{LDF} (Q_{LDF}/f_s) ➢ V_{LUF} ➢ V_{LE} (Q_{LE}/f_s) ➢ V_c ➢ ε_{gc}	-	(39)-(42)
Rustermeyer et al. (1989)	Turbulence i.e Fickian term and perfectly mixed regions	Radial profile of mean axial liquid velocity	➢ $Dax_L(r)$ ➢ $\hat{u}_L(r)$ ➢ n ➢ h_{mc}	2.10	(46) and CSTR zones
Degaleesan et al. (1996,1997)	Turbulence i.e. Fickian term, upflow/downflow liquid exchange and perfectly mixed at inlet and outlet regions	Global liquid recirculation	➢ Dax_1 ➢ Dax_2 ➢ u_1 ➢ u_2 ➢ K ➢ A_1 ➢ A_2 ➢ V_a ➢ V_b ➢ v_1 ➢ v_2 ➢ ε_{ga} ➢ ε_{gb}	2.9	(43)-(45)
Nassar et al. (1992)	Wake/bulk liquid exchange and turbulence in bulk liquid	Bubble (wake) velocity distribution	➢ α ➢ β ➢ σ^2_{pb} ➢ σ^2_{pL} ➢ $\hat{u}_{pb}$ ➢ $\hat{u}_{pL}$	2.11a	(47)-(49)
Schmidt et al. (1992a)	Wake/bulk liquid exchange and turbulence in bulk liquid	Bubble (wake) velocity distribution	➢ α ➢ β ➢ $\hat{u}_{pb}$ ➢ $\hat{u}_{pL}$	2.11b	(47)-(49) with $\sigma^2_{pb} = 0$ $\sigma^2_{pL} = 0$

(Table 2.5 continue)

Article	Mixing mechanism contribution		Mixing model parameters	Fig.	Equations
	Dispersive	Convective			
Schmidt et al. (1992b)	Wake/bulk liquid exchange and turbulence in bulk liquid	Bubble (wake) velocity distribution	➢ α ➢ β ➢ σ^2_{pb} ➢ $\hat{u}_{pb}$ ➢ $\hat{u}_{pL}$	-	(47)-(49) with $\sigma^2_{pL} = 0$

Table 2.6: Liquid phase mixing models-Experimental conditions.

Article	Setup	Fluid/solid system	Operating conditions
Myers et al. (1987)	Column: ➢ Dc: 0.19, 0.29, 0.38, 0.48, 0.57 m ➢ Hc: 2.44 m (for Dc:0.19m)	➢ Air/water	➢ Ug: 0.10-0.30 m/s ➢ U_L: 0.005-0.01m/s
Rustermeyer et al. (1989)	Column I: ➢ Dc: 0.15 m ➢ Hc: 2.57 m ➢ Perforated plate: - Free area:0.63% - 0.001mϕ_o Column II: ➢ Dc: 0.20 m ➢ Hc: 6.18 m ➢ Perforated plate: - Free area:0.63% - 0.001mϕ_o	➢ Air/water	➢ Ug: 0.02-0.10 m/s

(Table 2.6 continue)

Article	Setup	Fluid/solid system	Operating conditions
Degaleesan et al. (1996,1997)	Myers et al. (1987)'s RTD data for the 0.19 m diam. bubble column And Industrial methanol synthesis reactor: ➢ Dc: 0.46 m ➢ Hc: 15.24 m ➢ Internals	➢ Air/water ➢ Synthesis gas/oil/ catalyst (powder)	➢ Ug: 0.10-0.36 m/s ➢ U_L: 0-0.01m/s ➢ Solid loding: 45wt% ➢ P: 3.6 and 5.2 Mpa (indust.)
Nassar et al. (1992)	Airlift: D_{riser}: 0.10 m H_{riser}: 2.00 m $D_{airlift}$: 0.14 m $H_{airlift}$: 2.5 m	➢ Air/water	➢ ε_g: 0.053-0.106
Schmidt et al. (1992a)	Airlift same as Nassar et al. (1992)	➢ Air/water	➢ Ug: 0.01-0.11 m/s
Schmidt et al. (1992b)	Airlift same as Nassar et al. (1992)	➢ Air/water	➢ Ug: 0.0265-0.053 m/s

Myers et al. (1987) proposed a model assuming a series of liquid cells along the column axis (flow model proposed by Joshi and Sharma, 1979). The cells contain a pseudo-homogeneous dispersion of small bubbles in liquid. The liquid and small bubbles are transported by slugs (in its wake) going through the liquid cells. Liquid in the cells and slugs is assumed to be completely mixed. Some liquid slugs are transferred in the bulk liquid contained in each cell. The liquid rises with the slug velocity. It is exchanged with the bulk liquid in the cells. The liquid then goes down from cell to cell when slugs cross the boundaries between cells. In this representation, slugs are responsible for liquid transport and mixing. The following equations are the mathematical representations of the model:

for the cell phase:

$$V_c\left(1-\varepsilon_{gc}\right)\frac{dC_{ci}}{dt}=Q_{LE}\left[C_{si}-C_{ci}\right]+Q_{LDF}\left[C_{c(i+1)}-C_{ci}\right] \tag{35}$$

and for the slug phase:

$$V_{LUF}\frac{dC_{si}}{dt}=Q_{LE}\left[C_{ci}-C_{si}\right] \tag{36}$$

It should be noted that in this section, symbol "*C*" always refers to the concentration of the *tracer* (not to the reacting species). The subscript "T" is thus omited.

The following global mass balances were used:

$$U_g A=f_s V_s \tag{37}$$

And

$$U_L A=f_s V_{LUF}-f_s V_{LDF} \tag{38}$$

Equations (35) and (36) were approximated with a forward finite difference scheme. This makes it possible to obtain algebraic equations for cell and slug liquid. The following equations were obtained for the tracer concentration in cells:
for the first cell (i = 1):

$$C_{c1}^{'}=\left(1-W-Z\right)C_{c1}+WC_0+ZC_{c2} \tag{39}$$

for cell i ($2 \leq i \leq N-1$):

$$C'_{ci} = (1-Y-Z)C_{ci} + YC_{s(i-1)} + ZC_{c(i+1)} \tag{40}$$

for the last cell (i = N):

$$C'_{ci} = (1-Y-Z)C_{cN} + YC_{s(N-1)} + ZC_{sN} \tag{41}$$

The following equations are obtained for the tracer concentration in slugs (for the slug in cell $i \geq 2$):

$$C_{si} = (1-X)^{i-1} C_{c1} + X \sum_{j=2}^{i} (1-X)^{i-j} C_{cj} \tag{42}$$

Where X, Y and Z are dimensionless numbers define they as follows: $X = V_{LE}/V_{LUF}$; $Y = V_{LE}/(V_c(1-\varepsilon_{gc}))$; $Z = V_{LDF}/(V_c(1-\varepsilon_{gc}))$; $W = U_L A/(f_s V_c(1-\varepsilon_{gc}))$. The prime (') on C'_{ci} means after slug passage.

According to Schlüter et al. (1992) this type of model is equivalent to the ADM from a finite difference point of view. However, it has better flexibility when internal structures, such as a heat exchanger are taken into account.

Degaleesan et al. (1996, 1997) proposed another type of model. Figure 2.9 shows a schematic representation of the model. The liquid phase is separated into four regions, i.e. the inlet (near the distributor) and outlet (bubble disengagement) regions and upflow and downflow regions. The first two regions are assumed to be perfectly mixed. This assumption is based on observations of a high mixing intensity in that regions

caused by a change in the direction of the liquid flow. Mixing the upflow (core) and downflow (annulus) regions are represented by the ADM. A mass exchange is considered between these two regions. Thus, liquid mixing is mainly caused by the overall liquid recirculation (Devanathan et al., 1990) superimposed on micromixing attributed to turbulence caused by rising bubbles. Mass exchange between upflow and downflow regions may be considered as radial liquid mixing. They named their model "Recycle and Cross Flow with Dispersion" (RCFD). The model was described by the following differential equations:

upflow region and downflow region:

$$\frac{\partial C_i}{\partial t} = Dax_i \frac{\partial^2 C_i}{\partial z^2} - u_i \frac{\partial C_i}{\partial z} - \frac{K}{A_i}\left(C_i - C_{i\pm1}\right) \tag{43}$$

Where i = 1 for the upflow region and i = 2 for the downflow region

inlet region:

$$V_a \varepsilon_{g_a} \frac{\partial C_a}{\partial t} = v_0 C_0 - v_1 C_a + v_2 C_2\big|_{z=0} \tag{44}$$

Disengagement region:

$$V_b \varepsilon_{g_b} \frac{\partial C_b}{\partial t} = v_1 C_1\big|_{z=L} - v_2 C_b - v_0 C_b \tag{45}$$

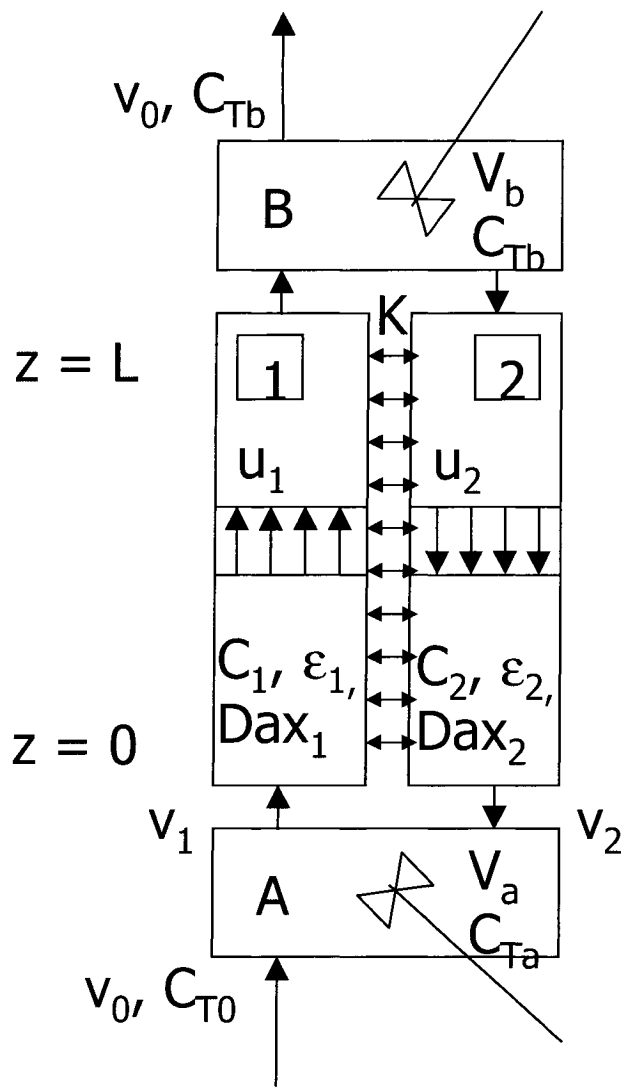


Figure 2.9: Schematic representation of the liquid phase mixing model proposed by Degaleesan et al. (1996, 1997)

This model may be viewed as a particular case of the Rustemeyer et al. (1989) model. This model suggests that liquid mixing is caused by a superposition of the axial liquid velocity profile (Ueyama and Miyauchi, 1979 ; Yao et al., 1991 ; Groen et al., 1996 ; Mudde et al., 1997) segregation effect (convective mechanism) onto the micromixing

attributed to turbulence. Figure 2.10 shows the model. It was described by the following equation:

$$\frac{\partial C_T}{\partial t} = Dax_L(r)\frac{\partial^2 C_T}{\partial z^2} + |\hat{u}_L(r)|\frac{\partial C_T}{\partial z} \tag{46}$$

Where $C_T = f(z,r,t)$.

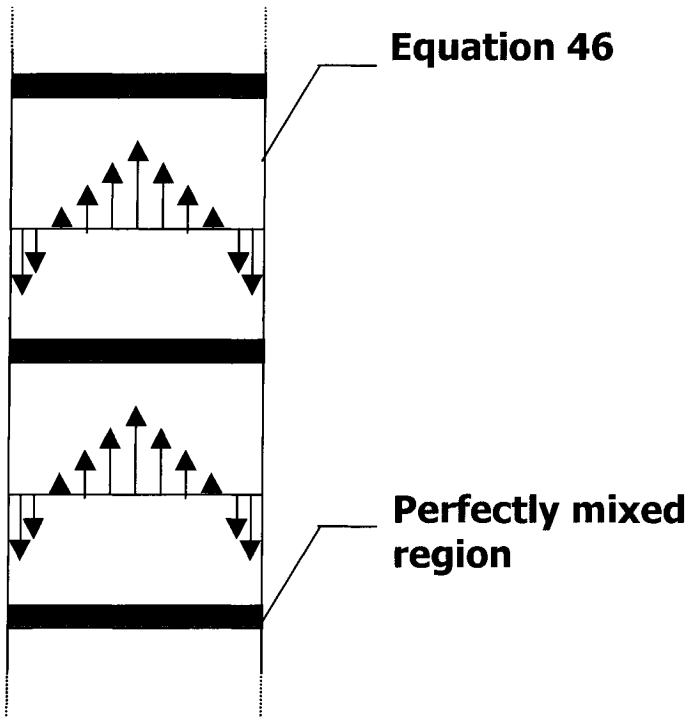


Figure 2.10: Schematic representation of the liquid phase mixing model proposed by Rustemeyer et al.(1989).

Note that radial mixing is allowed by perfectly mixed regions (may be viewed as radial transport in vortices) distributed along the column axis. Perfectly mixed regions and regions represented by equation (46) (only axial mixing assumed) are alternating along

the column. For the regions represented by equation (46), the assumption of neglecting radial dispersion while considering radial velocity profile is questionable. When the reactor column is not divided up into annular volume elements, such as the ADM, assuming negligible radial dispersion is justified when the radial dispersion coefficient is negligible or when the tracer is uniformly distributed over the cross section (with no chemical reaction or interfacial mass transfer). However, in the case of continuous fluid, as the liquid phase in the bubble column, it is difficult to accept equation (46) without any exchange term between the annulus volume elements.

Previous liquid mixing models assumed a combining contribution of the dispersive and convective mixing mechanism. The relative contribution of one mixing mechanism and the scale at which it occurs varies from one model to another, from average liquid recirculation to radial velocity profile. Some authors have diagnosed the liquid mixing mechanism in multiphase reactors with local mixing data.

Lübbert and Larson (1990), Schmidt et al. (1992a et b), and Nassar et al. (1992) have studied mesomixing (representative of a scale ranging from millimeters to about ten centimeters) in a gas/liquid airlift riser. At this scale the mixing mechanism is easily assumed to be very similar for many reactor types containing rising bubbles. Authors used tests based on equations (2), (7), (8) and (17). According to their results the liquid mixing mechanism is a superposition of convective and dispersive ones with predominance of the convective mixing mechanism. The latter mechanism arises from the liquid transported in the bubble wake at their various velocities, i.e. due to bubble velocity distribution. The dispersive mixing mechanism arises from stochastic flow in the liquid bulk phase.

Unpublished results (discussed by Lübbert and Larson, 1990) draw similar conclusions for bubble column reactors. For this type of reactor, Lefebvre and Guy (1999) observed

the same phenomena while comparing liquid mesomixing data and bubble velocity distributions. Also, for the bubble column, Yang et al. (1993) analyzed the Hurst exponent calculated with Computer-Automated Radioactive Particle Tracking (CARPT) and found a convective/dispersive mixing mechanism for the liquid phase in the axial and azimuthal (θ) direction. They obtained Hurst exponent value above 0.5, representing a superdispersive behavior (movement is faster than Brownian motion), and atribute it to a convective mixing contribution. The convective/dispersive mixing mechanism in the azimuthal direction may be attributed to the helicoidal rising of bubbles (Fischer et al., 1994). In the radial direction a dispersive mechanism was identified (Lübbert and Larson, 1990; Yang et al., 1993). While Lübbert and Larson (1990) did not find an axial mixing mechanism evolution with superficial gas velocity, Yang et al. (1993) observed that a more dispersive mechanism is approached when the superficial gas velocity increases. Schmidt et al. (1992a) calculated the exponent "n" of "$\sigma \propto \bar{t}^{n}$" (equation (17) with $L = t/u$, where $u \neq f(z)$) and obtained a value around 0.5 near riser wall, where gas holdup is weak. The axial mixing mechanism may thus vary according to radial position. Cassanello et al. (2001) also used CARPT and showed that the marked particle following the liquid phase often rises with a high *constant* velocity in the bubble column. This phenomenon is attributed to the liquid transport into the bubble wake. The authors computed the wake velocity distribution and found that it becomes larger in a larger column diameter. It was often observed that the extent of liquid mixing increases with the column diameter and it was attributed to a more pronounced radial profile of the average axial velocity and/or to a higher turbulence. Now, it is possible to interpret this column diameter effect on liquid mixing in another way: when the column diameter increases, the bubble velocity distribution becomes larger and the overall liquid velocity distribution also becomes larger due to the liquid transport in the bubble wake. Furthermore, Schmidt et al. (1992b) measured that the liquid in the wake and concluded that it may be accurately assumed to have a perfectly mixed flow.

Figure 2.11a illustrates the model proposed by Nassar et al. (1992) based on the above described representation of the liquid mixing in a bubble/liquid flow. The authors assumed a Gaussian distribution of the axial length trajectory followed by liquid elements at the mesoscale:

$$f(t, L) = \frac{B}{\sqrt{2\pi\sigma^2_{X(t)}}} \exp\left(- \frac{\left(L - \mu_{X(t)}\right)^2}{2\sigma^2_{X(t)}} \right) \tag{47}$$

Population balances allowed the authors to obtain equations of the Axial Liquid Trajectory Length Distribution (ALTLD; eq (47)) variance and mean. It was assumed that a liquid element was lifted in the bubble wake phase at some time (rises in a certain length). The liquid element is hence transferred to the bulk phase and rises a certain time in this phase (rises in a certain length). Wake and bulk liquid velocities Gaussian distribution were assumed for each phase. Thus, the liquid elements rise but never go down; note that the study was made in the riser of an airlift reactor. Mean liquid length trajectory ($\mu_{X(t)}$) is a mean weighed by liquid bulk and wake volume fraction, respectively, "$\frac{\alpha}{\alpha+\beta}$" and "$\frac{\beta}{\alpha+\beta}$":

$$\mu_{X(t)} = \hat{u}_{pL} \frac{\alpha}{\alpha+\beta} t + \hat{u}_{pb} \frac{\beta}{\alpha+\beta} t \tag{48}$$

Where α: transition intensity from the wake phase to the bulk phase, β: transition intensity from the bulk phase to the wake phase, $\hat{u}_{pL}$: mean velocity of the liquid in bulk phase, $\hat{u}_{pb}$: mean velocity of the liquid in bubble wake phase.

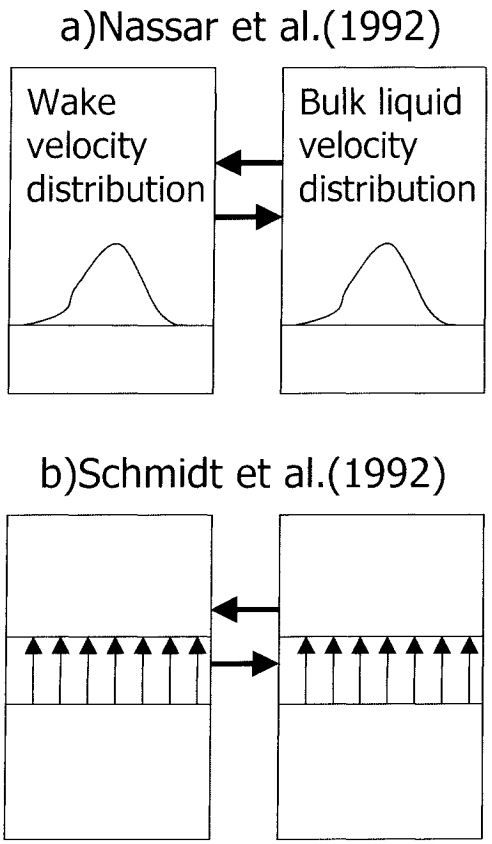


Figure 2.11: Schematic representation of the liquid phase mixing model proposed by (a) Nassar et al (1992) and (b) simplified by Schmidt et al. (1992).

The following equation for the ALTLD variance was found:

$$\sigma^2_{X(t)} = E\left(\hat{u}_{pbi} - \hat{u}_{pLi}\right)^2 \frac{2\alpha\beta}{(\alpha+\beta)^4}\left[(\alpha+\beta)t - 1 + e^{-(\alpha+\beta)t}\right] + \sigma^2_{pb}\left[\frac{t^2\beta}{(\alpha+\beta)(1+\alpha t)}\right] + \sigma^2_{pL}\left[\frac{t^2\alpha}{(\alpha+\beta)(1+\beta t)}\right] \quad (49)$$

Where E: expectancy (average), σ^2_{pL}: variance of the liquid velocity distribution in bulk phase, σ^2_{pb}: variance of the liquid velocity distribution in bubble wake phase.

The second term of equation (49) represents the mixing caused by the various bubble wake velocities and the third term is *supposed* to represent the dispersed mixing contribution in the bulk liquid. The word "*supposed*" means that equation (49) does not respect this representation. According to equation (49), the dispersive mechanism arises only from the bulk/wake exchange term. Indeed, when (α+β) is large (high bulk/wake exchange) and the value of "*t*" is high, one obtained the equation related to the dispersive mechanism, i.e. $\sigma^2_{X(t)} \propto t$. Moreover, when $\alpha >> \beta$ (high contribution of bulk liquid mixing mechanism) one obtained the equation related to the convective mechanism, i.e. $\sigma^2_{X(t)} \propto t^2$. This is in contradiction to the mixing mechanism proposed by the Lubbert team, i.e. the convective mechanism is due to the velocity distribution of the bubble wake and the dispersive mechanism is due to the stochastic flow of the bulk liquid. The mathematical model formulation will respect the proposed mechanism if a fluid element changing velocity probability was attributed to the bulk liquid phase (Nauman, 1981) while the population balance was developed. It is obvious that the mathematical formulation of a model should be verified to respect the conceptual (schematic) formulation of the model.

The authors used a distribution of local *instantaneous* bubble (wake) velocities to represent the convective mixing contribution of the liquid phase instead of a radial profile (spatial distribution) of local *average* liquid velocity used by the Rustemeyer et al. (1989) model. Both are conceptually different. In one case liquid velocity arises from the liquid attached to bubbles and in the other case the liquid velocity arises from the average liquid bulk flow. They also have statistically different meanings, i.e. Lübbert's team model used instantaneous velocities and the Rustemeyer et al. (1989) model used average velocities. Furthermore, the former implies a space discontinuity (wake is more or less bounded). This representation complexifies mixing and transfer

phenomena. Among other reasons, this is due to the frequent wake shedding. Fan (1989) and Fan and Tsuchiya (1990) discussed bubble wake dynamics.

Schmidt et al. (1992) simplified equation (49) while only considering liquid exchange between the wake and bulk liquid phase ($\sigma^2_{pb}=\sigma^2_{pL}=0$). Figure 2.11b shows the simplified model.

2.2.6.2 Model exploitation

All of the liquid phase mixing models proposed were validated with tracer data. According to the authors, steady-state and/or unsteady-state tracer techniques were used. For the former technique, an axial tracer concentration profile was obtained while continuously injecting a stream of liquid tracer into the system near the liquid overflow (Myers et al., 1987). The unsteady-state tracer technique, with a pulsed input function, was used to obtain the liquid phase overall RTD in a continuous liquid system (Myers et al., 1987; Degaleesan et al., 1996) and to obtain time-concentration-evolution until homogenization in a batch liquid system (Rustemeyer et al., 1989; Degaleesan et al., 1997). Also, mesoscale liquid phase RTD was obtained with the Thermal Pulsed Anemometry (TPA) technique (Lübbert's team). Some authors measured unsteady tracer data at one axial position (Myers et al., 1987; Degaleesan et al., 1996) and others measured it at various axial (Degaleesan et al., 1997, Lübbert's team) and radial (Rustemeyer et al., 1989) positions. Often, one to four parameters were optimized to fit the mixing models on experimental data and the other parameters were measured or estimated.

Table 2.7 summarizes tracer techniques used by the various authors and gives the fitted parameters.

Myers et al. (1987) used both steady and unsteady state liquid tracer techniques to validate their mixing model (eq (39)-(42)). It contains seven parameters (see Table 2.5). Fitting all parameters would be a non-pertinent and non-obvious task. Thus, the authors evaluated six of the seven parameters on the basis of physical reasoning, their experimental data and literature data. The value of f_s was set to 2 s^{-1} (Ohki and Inoue, 1970). V_{LDF} was found with a simplified velocity profile model of Ueyama and Miyauchi (1979) (integration of the downflow profile until time $1/f_s$). V_s and V_{LUF} were obtained, respectively, from gas and liquid overall mass balance (eq (37) and (38)). Based on observations, the height of a cell was set to the column diameter value. Thus V_c = A*Dc. The DGD technique was used to find the ε_{gc} value ($\varepsilon_g^S/(1-\varepsilon_g^L)$). Thus, only one parameter was fitted, i.e. the liquid volume exchange between bulk and slug liquid (V_{LE}).

Table 2.7: Liquid phase mixing models-Model exploitation.

Article	Tracer pattern	Measuring point(s) for unsteady data	Optimized parameter(s)
Myers et al. (1987)	➢ Steady-state[1] ➢ Unsteady-state[2]: - RTD[3]	➢ Axial: 1	➢ V_{LE}
Rustermeyer et al. (1989)	➢ Unsteady-state: - TCE[4]	➢ Axial: 2 ➢ Radial: 9	➢ $Dax_L(r)$ ➢ n ➢ h_{mc}
Degaleesan et al. (1996,1997)	➢ Unsteady-state: - RTD - TCE	➢ Axial: 1 (RTD) ➢ Axial: 7 (TCE)	➢ Dax_1 ➢ Dax_2 ➢ K
Nassar et al. (1992)	➢ Unsteady-state - RTD	➢ Axial: 1 (mesoscale)	➢ α ➢ β ➢ σ^2_{pL} ➢ $\hat{u}_{pL}$
Schmidt et al. (1992a)	➢ Unsteady-state - RTD	➢ Axial: some ? (mesoscale)	➢ α ➢ β ➢ $\hat{u}_{pL}$
Schmidt et al. (1992b)	➢ Unsteady-state - RTD	➢ Axial: some ? (mesoscale) ➢ Radial: 15 (mesoscale)	➢ *None*

[1] tracer is continuously injected at the liquid overflow.

[2] in all cases a pulsed injection is used as input function.

[3] RTD: Residence Time Distribution obtained in liquid continuous flow system.

[4] TCE: Time Concentration Evolution obtained in liquid batch system.

An exponentially-decaying tracer concentration from the point of tracer injection is often observed for a steady-state liquid phase tracer experiment in either a bubble column, slurries bubble column or three phase fluidized bed reactors (Towell and Ackerman, 1972; El-Temtamy et al., 1979a; Kara et al., 1982; Kelkar et al., 1983; Myers et al., 1987). The ADM is also characterized by this type of equation. Equation (1) is reduced with the appropriated boundary conditions to the following equation for a steady-state condition:

$$C(z) = C_0 \exp\left(-\frac{U_L/\varepsilon_L}{Dax_L} z \right) \tag{50}$$

However, many mathematical equations are capable of taking the form of the axial tracer concentration profile. In addition, the higher the extent of mixing is, the lower the slope of the semi-log graph is (concentration is more uniform in space). Discrimination of the model is thus more difficult in that case. In fact, a pulsed unsteady-state tracer experiment gives more information on system dynamics.

The Myers et al. (1987) model represents well the tracer concentration profile. The authors presented a relationship between their mixing parameter (liquid volume exchange) and the ADC. They also fitted the slug and cell model to one pulsed tracer experimental data. Their model fitted the RTD data well. Their model and the ADM gave equivalent predictions in both the steady and unsteady tracer experiments. However, the authors said that the two models gave different hydrodynamic predictions when the tracer was injected at the midpoint of a tall bubble column into the batch liquid. The ADM response was symmetric and the slug and cell model response was not symmetric. Even if the models were similar in their hydrodynamic predictions, the slug and cell model is easier to compute, i.e. repeated calculation of algebraic equations. Furthermore, the authors stipulated that their model may only be used for highly liquid phase mixing close to a completely backmixed flow.

Degaleesan et al. (1996) used the pulsed tracer data of Myers et al. (1987) (both sets of authors are part of Dudukovic's team) to fit their mixing model (eq (43)-(45)). It has 13 parameters (see Table 2.5). The upflow and downflow axial dispersion coefficient (Dax_1 and Dax_2) and the exchange coefficient (K) were fitted onto the RTD data. The other parameters were obtained from CARPT and Computer assisted Tomography (CT) measurements.

The three-parameter-model fitting was obviously good, likewise for the ADM. The authors calculated the mixing parameters (Dax_1, Dax_2, and K) with the CARPT data, which are independent of the tracer data. The K and ADC values were represented, respectively, by the radial and axial averaged Lagragian turbulent eddy diffusivity. Even if the fitted and the CARPT-calculated values were somewhat different, the model prediction with the CARPT-calculated values showed good agreement with the RTD data, i.e. a least-square sum of 0.0724 compared to the fitting one of 0.0366. Ratios of the CARPT-calculated ADC to the fitted one for the upflow and the downflow region were 2.5 and 1.8, respectively. Ratio of the CARPT-calculated radial exchange coefficient to the fitted one was 0.62. According to the authors, this difference is due to the fact that the model does not consider the liquid velocity and holdup radial profile, but only the average flow in the upflow and downflow regions. K values (fitted and calculated) were one order of magnitude lower than ADCvalues. Also, in both cases the ADCs in the downflow region were 1.5 (calculated) to 2 (fitted) times higher than in the upflow region. According to the authors this is due to the rising bubbles in an inverse direction to that of the liquid flow. This result may also be viewed as a consequence of the liquid vortex between the upflow and near-the-wall downflow regions observed by Chen et al. (1994) and Larachi et al. (1996) (see Figure 2.1b).

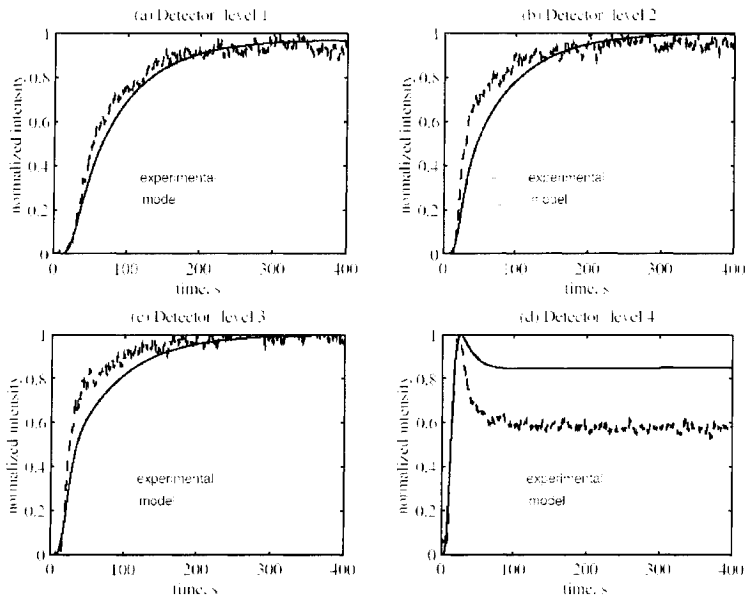
The authors also simulated a pulsed tracer experiment in a liquid batch bubble column with their model (eq (43)-(45) with $v_0 = 0$). They used the CARPT data of Devanathan (1991). They showed tracer concentration time evolution in various parts of the column. The model predicts the overshoot observed near the injection point. Moreover, Degaleesan et al. (1997) used their previous model (Degaleesan et al., 1996) to predict a pulsed tracer response at various axial positions in a liquid batch industrial slurry bubble column reactor. This reactor is operating with methanol synthesis. The

tracer was injected at two midpoint axial positions and at either the upflow or downflow regions. Time response was monitored at seven axial positions. Model parameters found by Degaleesan et al. (1996) were extrapolated to the operational conditions of the industrial reactor studied. Figure 2.12 shows an example of their results (Degaleesan, 1997). Their model *predicts* well the various types of tracer concentration time evolution measured at the various axial distances with the injection point, i.e. sigmoid and overshoot curve. The time of the overshoot seems to be well predicted.

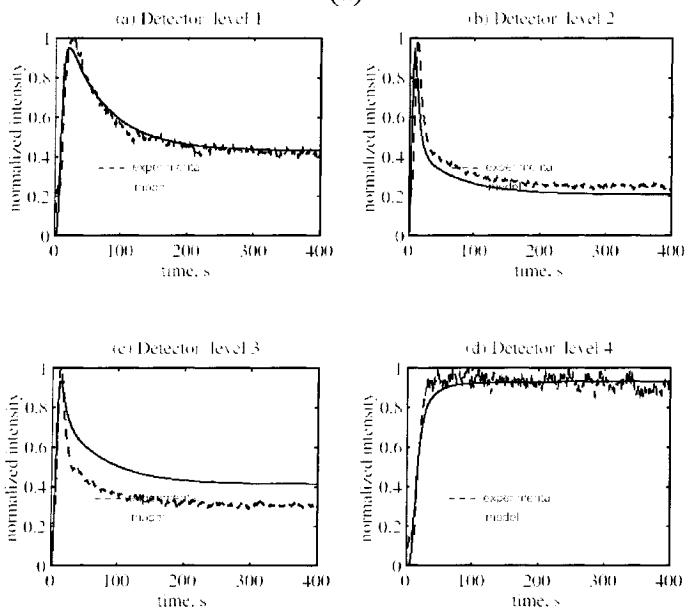
The number of the Rustemeyer et al. (1989) model (eq (46) and CSTR regions) parameters (see Table 2.5) depends on the mesh size used for the axial liquid velocity radial profile. Authors used velocity profiles measured by Franz et al. (1984) (same team as Rustemeyer et al. (1989)). Thus, the parameters to be fitted were the ADCs, the number of mixing cells and their height. The unsteady-state tracer technique was used. The tracer was injected over the cross-section (five injection tubes) at the liquid surface top. Tracer concentration time evolution was monitored at two axial positions and at nine radial positions on a radius. Their results showed the time-concentration overshoot near the injection position. Their model represented well this behavior and the fits were good.

The ADCs did not change a lot with the radial position. However, ADCs tended to increase away from the column center. Degaleesan et al. (1996) found that the ADC was higher in the downflow region. Lefebvre and Guy (1999) also found the same tendency for an ADC (Measured with Thermal Pulsed Anemometry; Lübbert and Larson, 1987) increasing away from the column center at mesoscale. It could be noted, however, that mesoscale ADC was a hundred times lower in order of magnitude than the one found for overall tracer experiments. Indeed, when the average concentration time evolution is monitored, measured behavior represents (depends on) phenomena at

all scales (from microscale to macroscale). When average time delay is measured for each thermal pulsed between two measuring points separated by a few centimeters, the mixing data obtained give information on a scale between microscale (small eddies) and macroscale (overall flow pattern, such as liquid vortex). It is thus interesting to remark that the ADC obtained from global or local measurements followed the same trend even if their order of magnitude was different (Lefebvre and Guy, 1999).



(a)



(b)

Figure 2.12: Concentration time evolution predictions of the Degaleesan et al. (1996,1997) model in a liquid batch industrial slurry bubble column reactor. a) near the injection point. b) away from the injection point. (Degaleesan, 1997).

Lübbert's team (Lübbert and Larson, 1990; Nassar et al., 1992; Schmidt et al., 1992a and b) used mesoscale mixing data obtained in the two phase flow riser of an airlift reactor to diagnose the mixing mechanism and propose a liquid phase mixing model. As previously mentioned the mesomixing mechanism may be easily assumed to be very similar for many reactor types containing rising bubbles. Lübbert and Larson (1990) calculated the exponent on an equation similar to equations (2), (7), (8) and (17). They found that the liquid mixing is caused by the superposition of a convective mechanism, due to the various velocities of the liquid transported in the bubble wake, onto a dispersive mechanism attributed to the mixing in the bulk phase.

Nassar et al. (1992) proposed a stochastic model representing this behavior (eq (47)-(49)). Equation (49) represents the time evolution of the Axial Liquid Trajectory Length Distribution (ALTLD) variance. It presents two time-limiting cases when parameters are time independent. For small time close to zero (small scale; eq (48)), the variance of ALTLD becomes proportional to time squared ($\sigma^2_{X(t)} \propto t^2$). The mechanism is, thus, more convective at a smaller scale. For large time close to infinity (large scale; eq (48)), the variance of ALTLD becomes proportional to time ($\sigma^2_{X(t)} \propto t$; note: $t = L/u$ and $u \neq f(z)$). The mechanism is, thus, more dispersive at a larger scale. However, when time tends to zero, the scale tends to the microscale. Thus, turbulence and the Brownian movement (molecular scale) dominate even in the liquid bubble wake and the mechanism should not be convective. It may be more plausible that the convective mechanism is dominant at an intermediate time scale (mesoscale).

The Lübbert team fitted their model to the mesomixing data obtained with the TPA technique. The model has six parameters (see Table 2.5). Variance and mean bubble velocity distribution (liquid wake velocity distribution) was measured with the ultrasound-Doppler technique (Larson, 1988; Lübbert et al., 1983). Nassar et al. (1992)

fitted the four following parameters: α, β, $\hat{u}_{pL}$, σ^2_{pL}. Schmidt et al. (1992a) stated that $\sigma^2_{pL} = 0$ and $\sigma^2_{pb} = 0$. There was, thus, only one velocity for liquid wake and one for bulk liquid. (Note the conceptual similitude with the Myers et al. (1987) model.) The last two right hand side terms of equation (49) are equal to zero. They fitted the three following parameters: α, β, and $\hat{u}_{pL}$. In both cases, the authors obtained almost the same fitted parameter values. This makes it possible to think that the last two right hand side terms of equation (49) are negligible. Indeed, according to the parameter values it is possible to show that the second and third term are, respectively, 100000 and 10000 times lower than the first term.

Schmidt et al. (1992b) stated that $\sigma^2_{pL} = 0$ and estimated parameters (α, β, $\hat{u}_{pL}$) instead of optimizing them. They hydrodynamically fixed an ellipsoidal bubble for various sizes (4-8 mm) with a downflow liquid. For this system, they measured "α" with the RTD of the *liquid inside the wake and measured the relative wake size* ($k=\varepsilon_w/\varepsilon_g$) *to calculate "$\beta$"* from local gas holdup data obtained with a single point conductivity probe ($\beta/(\alpha+\beta) = k\varepsilon_g$). They also estimated the bulk liquid velocity as the difference between the measured mean bubble velocity and a terminal bubble velocity calculated with a correlation. The authors did not discuss the RTD prediction quality, but showed the ALTLD variance time-evolution predictions quality. The agreement was good.

According to the three Lübbert team articles the following was found: $\beta/(\alpha+\beta)$ = 10-17%; k = 1.3-3.2; $\hat{u}_{pb}/\hat{u}_{pL}$ = 1.8-2.8; $\sigma^2_{pb}/\sigma^2_{pL}$ = 1.8-2.8. It should be noted that k-values were smaller than the ones obtained for large spherical-cap bubbles (Fan and Tsuchiya, 1990). Liquid in the bubble wake is obviously transported at a higher velocity than bulk liquid. Variance of liquid velocity distribution is principally due to the bubble velocity distribution. α and β-values measured by Schmidt et al. (1992b) were one order of magnitude higher than the ones optimized by Nassar et al. (1992) and Schmidt et

al. (1992a). The former finds $1/\alpha = 0.2\text{-}0.3$ and $1/\beta = 1.4\text{-}2.0$ seconds. It should be noted that the α-value has the same order of magnitude as the wake shedding frequency (Fan and Tsuchiya, 1990). Since there is little time spent in the wake and bulk liquid , the wake/bulk exchange is very dynamic (very frequent). Even if liquid elements spend less time in the wake phase, they are transported at a higher and larger velocity distribution. The global effect is a dominant convective mixing mechanism at a mesoscale.

It should be noted that the wake effect on liquid mixing was often shown for large spherical-cap bubbles (Fan and Tsuchiya 1990) and it was also shown for smaller ellipsoidal bubbles in the multi-bubble system of Lubbert's team work.

2.2.6.3 Conclusion

In summary there are many mixing mechanisms in competition at various scales and which ones predominate in which situation is not clear. The effect of the wake (bubble) velocity distribution causing the transport of liquid elements at various velocities was too often forgotten in the liquid phase mixing model. The importance of this mesoscale effect depends on the time the liquid element spends in the bubble wake between its entrance and expulsion. This time is among due to the wake shedding frequency and the liquid-wake-entrance-and-expulsion mechanism. Also, the relative volume of the liquid in the bubble wake is an important parameter. These two parameters increase or decrease the convective contribution of the liquid phase mixing mechanism. The lower the wake shedding frequency is and the higher the relative liquid volume in the wake is, the higher the similitude is between the mixing mechanism of the liquid and gas phase. Furthermore, knowledge of the liquid phase micromixing in the wake may be important depending on the chemical reaction kinetics. The movement of the liquid elements outside the wakes depends on the local "monophasic" (bulk liquid) flow pattern. Their movement is more random. However, they follow the main streamline (macroscopic

recirculation) caused by the average density profile (gas holdup profile). The movement of the liquid elements in the bulk liquid phase also depends on the turbulence (microscale) caused by the average liquid movement and the bubble/liquid interfacial momentum transfer. One important contribution to the liquid mixing that was forgotten in all liquid phase mixing models is the liquid vortex between the upflow region and the downflow region near the wall. A liquid element entrained inside a vortex will stay therefore a certain time and it is more or less isolated from the rest of the bulk liquid phase. This should have an effect on the reactor performance. As a limiting case, if a liquid vortex is completely isolated, the reactant concentration and the reaction rate will decrease with time. Also, the undesirable products will have more time to be produced. Liquid elements flowing inside the vortex may be called the liquid vortex phase. The hydrodynamics of this liquid vortex phase should to be included in the liquid phase mixing model. In addition to studying the mixing mechanism followed by the liquid wake, liquid bulk (emulsion) and liquid vortex phases, it would be interesting to study the mechanisms responsible for the liquid element transfer between these liquid phases. The result of this type of study will make it possible to obtain the relative times spent by the liquid elements in the various phases. These times are the times spent in the liquid phases between one output and input (or frequency of changing phases) and are not the mean time spent in liquid phases. Knowledge of these times, of the relative volume of the liquid phases and of the mixing mechanism followed by these liquid phases will make it possible to obtain a more general liquid phase mixing model representing various mixing mechanisms.

The presence of solid particles may have an effect on the mixing mechanism of each liquid phase (wake, emulsion/bulk and vortex liquid phases) and on the mechanism responsible for the liquid exchange between liquid phases. Since the mixing mechanism followed by the liquid in the wake phase is close to the one of the gas phase, previous discussion on the effect of particle properties on the gas phase mixing

mechanism also applies to the liquid wake phase. Moreover, the solid affects the wake dynamic depending on the solid holdup and properties (Fan and Tsuchiya, 1990); it is discussed in more detail in the next section. The overall liquid recirculation is also affected by the solid effect on the gas holdup profile (Linneweber and Blass, 1983; Lee and De Lasa, 1987). The effects of the presence of solid on the liquid phase mixing mechanism are related to the bubble dynamics. However, the solid also has a direct influence on the hydrodynamics of the emulsion and vortex phases. The solid properties influence the liquid turbulence because it absorbs some energy from the liquid phase. It would be interesting to study this influence and the effect of solid properties on the liquid vortex behavior. Hence, the solid phase properties may influence in various ways not only the extent of mixing, but also the liquid mixing mechanisms. This last influence should be investigated as a first step. Unfortunately, there has been no convincing study done on the local liquid velocity in three-phase fluidized beds. The lack of literature on this particular topic is significant and the task of measuring it is not an easy one.

2.2.7 SOLID PHASE MIXING MODEL

2.2.7.1 Model concept

The solid phase mixing models that have been proposed were inspired by the flow representation of Bhatia and Epstein (1974), modified by Fan (1989), and called the structural wake model. Figure 2.13 shows the flow representation used to elaborate the solid phase mixing models. Liquid and solid are both in a wake and liquid/solid emulsion phase. A dynamic exchange occurred between these two phases. Each phase flows at a unique constant velocity.

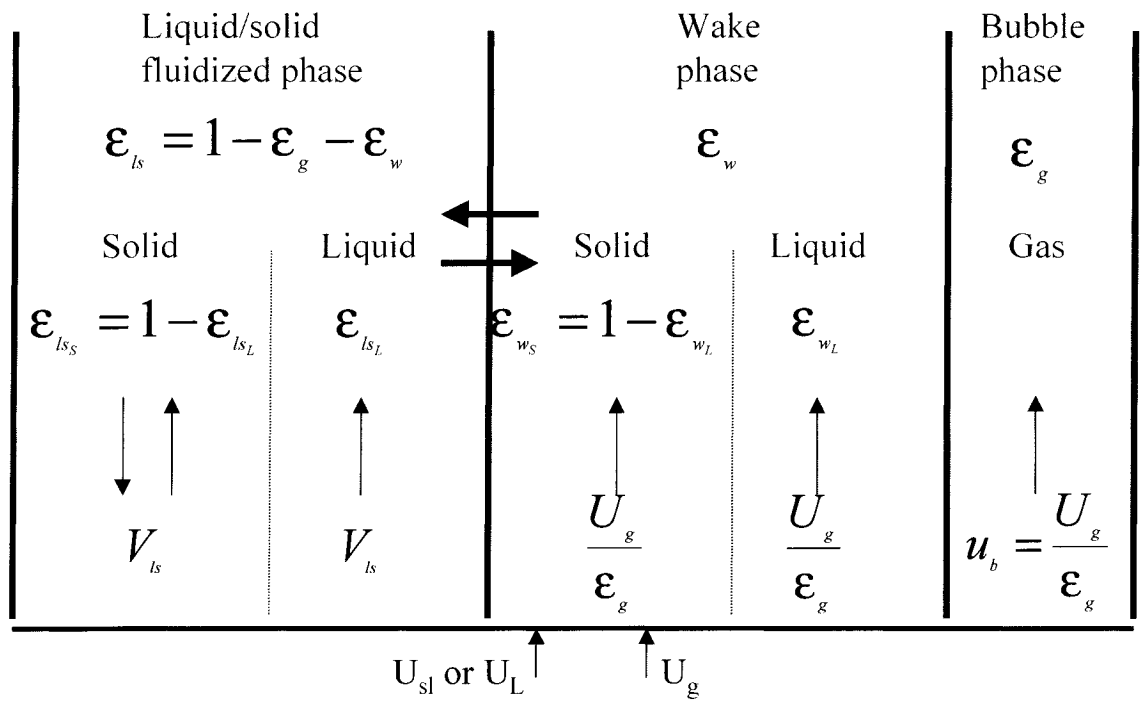


Figure 2.13: Flow representation characterizing solid phase mixing models. (Figure inspired by Murray and Fan, 1989).

Solid phase mixing models assume that particles are entrained in the bubble wake and rise following a plug flow behavior at the average bubble velocity. They also go down following a plug flow behavior with a falling particle velocity. A wake/emulsion solid exchange is considered as the dominant solid phase mixing mechanism. Table 2.8 summarizes the models and Table 2.9 gives the experimental conditions used. This representation was used for various systems. El-Temtamy and Epstein (1980) were the first ones to propose this type of solid phase mixing model. They used it to describe solid fraction axial profile in a three phase fluidized bed freeboard. The wake/emulsion mixing model was also used by Tang and Fan (1989) to calculate the axial solid concentration profile in a three phase fluidized bed containing light-density particles (from 1050 to 1300 kg/m^3) in water.

The solid concentration axial profile of slurry bubble columns was represented by the wake/emulsion mixing model by Dayan and Zalmanvich (1982); Murray and Fan (1989); Tsutsumi et al. (1992). Turi and Ng (1986) used this model for slurry bubble columns, but assumed a drift effect for rising particles instead of bubble wake entrainment. Unsteady state mixing data were modeled with the help of the wake/emulsion mixing model in a three phase fluidized bed containing glass beads by Cassanello et al. (1996).

Table 2.8: Solid phase mixing models.

Article	E'_z [1]	u_{ps} [2]	A [1]	Mixing model parameters
El-Temtamy and Epstein (1980)	N.a. [3]	R-Z	N.a. [3]	➢ ε_g ➢ u_{Lls} ➢ u_{ps} ➢ k ➢ x ➢ HWU ➢ N_{st}
Dayan and Zalmanovich (1982)	$0.258\left(1+u_{Lls}/u_{ps}\right)g^{1/2}R^{3/2}$	T-V	0	➢ u_{Lls} ➢ u_{ps} ➢ R
Turi and Ng (1986)	$\frac{V_p}{\lambda_{de}-\lambda_{ls}}$ [4]	T-V	0	➢ λ_{de} ➢ λ_{ls} ➢ M
Tang and Fan (1989), Murray and Fan (1989)	$\frac{V_R u_b \varepsilon_w x}{N_b\left[\frac{v_e A_e}{V_p}-\frac{v_d A_d \varepsilon_f}{u_b \varepsilon_w}\right]}$	R-Z	Tang and Fan (1989): 0 Murray and Fan (1989): Last term of eq (59)	➢ ε_g ➢ ε_{g0} ➢ u_{Lls} ➢ u_{ps} ➢ E_z ➢ K ➢ x ➢ $A(or\ P)$ ➢ L_m
Tsutsumi et al. (1992)	$-\frac{V_p}{Log\left(\frac{x}{1+\frac{u_{ps}}{u_{Lls}}}\right)}\delta l$ [5]	T-V	0	➢ ε_g ➢ u_{Lls} ➢ u_{ps} ➢ k ➢ x ➢ HWU ➢ δl
Cassanello et al. (1996)	$\frac{u'_b u'_{s_{ls}}}{K_{ls-w}}$ [6]	N.a. [7]	0	➢ $K_{ls\text{-}w}$ ➢ u'_b ➢ u'_{sls}

[1] global parameter expression of the following relations: $E'_z \frac{dC_s}{dz} = V_p C_s + A$

[2] particle velocity in liquid/solid emulsion phase (V_p) is written with the slip velocity of the particles (u_{ps}), i.e particle velocity relative to the liquid velocity in the emulsion phase, and this emulsion liquid velocity (u_{Lls}): $V_p = u_{Lls} - u_{ps}$. According to the flow model shown in Figure 2.1, u_{Lls} is obtained by mass balance on the liquid phase (general case shown in eq (56)). Two representations of the particle slip velocity (u_{ps}) are assumed according to the authors and are specified in the Table. R-Z: Richardson-Zaki (eq (57)) and T-V: terminal velocity of the particles (one particle in a stagnant liquid; authors used Stoke's law i.e. eq (58))

[3] the proposed model is not continuous in its mathematical form. Authors defined stages where a wake shedding occurs. They made solid mass balance on each stage and used x in the same manner as using thermodynamics equilibrium constant (K-value) for the design of an immiscible liquid-liquid or one-solute-stripping/absorption column.

[4] model was written originally in the following form: $C_s = C'\exp(-C'_z z)$. This equation was substituted into the differential equation of comment 1 to obtain the E'_z value. For the original form: $C' = \dfrac{4\Lambda M}{\pi D_c^2\left(1-e^{-\Lambda L}\right)}$ and $C'_z = \Lambda$ where $\Lambda = \lambda_{de} - \lambda_{ls}$.

[5] same as comment 4. For the original form: $C' = C|_{z=0}$ and $C'_z = -Log\left(x \Big/ 1+\dfrac{u_{ps}}{u_{Lls}}\right)\Big/\delta l$

[6] From equations related in Cassanello et al. (1996), if steady-state is assumed and constant velocity relative to the axial position is also assumed, a differential equation having the form of the one in comment 1 may be used and E'_z expression obtained is shown in the Table.

[7] the model proposed is written for unsteady state tracer mass balance by the authors. If steady-state is set the value of E'_z (see equation in comment 1) is obtained (assuming solid in batch) and $V_p = u'_b - u'_{sls}$. However, for the fluidized bed used (large/heavy particles), solid concentration gradient is equal to zero.

The wake/emulsion mixing model assumes negligible interaction between bubbles. The flow of the emulsion phase does not interact with the wake phase. Random motion of particles is not considered. The ratio of the volumetric fraction of the solid phase contained in the wake phase to the one contained in the emulsion phase (x) and the ratio of the wake volume to the bubble volume (k) were assumed to be weak functions of the

axial position and were assumed constant along the column axis. Furthermore, the wakes are perfectly mixed.

Table 2.9: Solid phase mixing models-Experimental conditions.

Article	Setup	Fluid/solid system	Operating conditions
El-Temtamy and Epstein (1980)	Column: ➢ Dc: 0.152 m ➢ Hc: 4.5 m	➢ Air/water/ ➢ Glass beads: - d_p: 214-893 μm - ρ_p: 2745 kg/m3	➢ Ug: 0.013-0.052 m/s ➢ U_L: 0.0041-0.045 m/s
Dayan and Zalmanvich (1982)	Tank: ➢ Base: 0.20x0.184 m ➢ Hc: 0.20 m ➢ Single nozzle with solenoid valve	➢ Air/water/ ➢ Copper powder: - d_p: 8.11-15.7 μm - ρ_p: ? kg/m3	➢ Bubble frequency: $0.37s^{-1}$
Turi and Ng (1986)	Column: ➢ Dc: 0.102 m ➢ Hc: 1.07 m ➢ Perforated plate: - For gas: - 88 orifices - 0.000794 mϕ_o - For liquid: - 9 orifices - 0.00953 mϕ_o	➢ Air/water/ ➢ Glass beads: - d_p: 44-105 μm - ρ_p: 2420 kg/m3	➢ Ug: 0.012-0.032 m/s ➢ U_L: 0 m/s
Tang and Fan (1989)	Column: ➢ Dc: 0.0765 m ➢ Hc: 1.285 m ➢ Distributor: - Packed-bed - PMMA porous plate: Pore: 30 μm	➢ Air/water/ ➢ Polystyrene ➢ Acetate ➢ Acrylic ➢ Nylon - d_p: 1000-6350μm - ρ_p: 1050-1300kg/m^3	➢ Ug: 0.0069-0.028 m/s ➢ U_L:0-0.016 m/s

(Table2.9 continued)

Article	Setup	Fluid/solid system	Operating conditions
Murray and Fan (1989)	Column: ➢ Dc: 0.076 m ➢ Hc: 1.5 m ➢ Tube-shell type: - bliquid (tube): - Length : 0.04 m - 0.008 mϕ_t - Gas (shell): - 0.0014 mϕ_o	➢ Air/water ➢ Glass beads ➢ Binary mixture - d_p: 44-177 µm - ρ_p: 2450-2990 kg/m3	➢ Ug: 0.033-0.17 m/s ➢ U_{sl}: 0-0.031 m/s
Tsutsumi et al. (1992)	Column: - Use data of Suganuma and Yamanishi (1969), Farkas and Leblond (1969), Kato and al. (1972), Tsutsumi and al. (1987)	➢ Air/water ➢ Dowex particles ➢ Glass beads ➢ Sand particles ➢ Alumina ➢ Coal - d_p: 17-700 µm - ρ_p: 1300-2580 kg/m^3	➢ Ug: ? m/s ➢ U_L: 0 m/s
Cassanello et al. (1996)	Column: ➢ Dc: 0.10 m ➢ Hc: 1 m ➢ Distributor: - Porous tubes - Packed-bed - Perforated plate	➢ Air/water ➢ Glass beads ➢ PVC ➢ Binary mixture - d_p: 1000-5500 µm - ρ_p: 1320-2500 kg/m3	➢ Ug: 0.01-0.11 m/s ➢ U_L: 0.058-0.065 m/s

Turi and Ng (1986) proposed that a particle might be in one of the four states (free, engaged, wake-entrained and captured particle) described below. When the trajectory of a particle is not influenced by a bubble (no bubble/particle interaction), the particle is "*free*" and goes down in the emulsion phase. There are three ways for a bubble to induce a rising movement of a particle. A particle may be *engaged* by the flow around the bubble and rise with it. This includes the drift effect. If the particle is entrained into the closed wake, the authors call it the *wake-entrained* particle and there is no exchange

with the emulsion phase. However, it is well known that according to bubble shapes and dynamics, wake shedding and formation occur (Fan and Tsuchiya, 1990). Moreover, a particle in a wake may be expulsed by the centrifugal force acting on it. Therefore, the *wake-entrained* state has to be improved in order to account for the possibility of wake/emulsion exchange. A particle may be intercepted by a bubble and attached or "*captured*" at its surface (flotation process). Another state should be added: the *vortex* state. Indeed, as previously discussed liquid vortices between the upflow regions and downflow regions near the wall transport particles (Chen et al., 1994; Larachi et al., 1996; see Figure 2.2b) and may have great influence on reactor performances.

The relative importances of these particle states depend on particle size and density as well as the nature of the liquid phase and bubbles. The *captured-particles* state will be favored for hydrophobic (non-wettable) particles with low terminal velocity. Hydrophilic (wettable) particles with low terminal velocity will easily follow the liquid flow induced by the rising bubbles and favor the *engaged-particles* state. The *wake-entrained* state will be favored by a high wake size relative to the bubble size (k-value range: $k = \varepsilon_w / \varepsilon_g = 1-10$) combined with a high gas holdup, a high solid holdup in the wake (x_w-value range: $x_w = \varepsilon_{w_s} / \varepsilon_{ls_s} = 0.5-1$; measuring in the wake), a weak wake shedding frequency (f_{wsh}-value range: f_{wsh} = 3.5-6 s^{-1}) and a small ratio of the radial velocity near the wake circumference to the tangential velocity (small centrifugal force). (Almost all giving data come from Fan and Tsuchiya (1990)) Particles with high terminal velocity (high density and size) have an increasing effect on wake size, but have a decreasing effect on solid holdup in the wake (verified for dp<1 mm). A high global solid holdup increases the solid holdup in the wake. The effect of solid properties on wake shedding frequency is weak. Moreover, the particles with large terminal velocity will be more frequently expulsed from the wake because of centrifugal force. The overall positive or negative effect of the particle properties on the

wake-entrained state is not obvious and would be at the simple-case parabolic phenomena. Furthermore, the superficial gas and liquid velocity has an influence on the wake properties mentioned above, which means on the relative importance of the *wake-entrained* state. As for the previous state, the *vortex* state will be favored when the volume of the vortices relative to the volume of the emulsion phase is high, the solid holdup in the vortices is high and the expulsion of the particles due to the centrifugal force is not too frequent. The *free* state is favorable when the other states are less favorable.

For simplicity purposes, all the authors used only two states. The free particle state (emulsion phase) was always used. The engaged particle state (drift effect) was used by Turi and Ng (1986) and the other authors used a wake entrainment with a solid exchange between the wake and emulsion phase.

The mechanisms of the particle wake entrainment/de-entrainment are complex (Fan and Tsuchiya, 1990). The wake formation/shedding is, almost always, the assumed main mechanism responsible for the particle entrainment/de-entrainment in the proposed mixing models. This mechanism is in itself very complex. Particle entrainment/de-entrainment may also be caused by gravitational and centrifugational (particle driven by eddies in the wake) forces. Moreover, there is no clear frontier between the wake and/or drift phase and the emulsion phase. The wake and flow around bubbles are highly dynamic (Fan and Tsuchiya, 1990) and not easy to model. Authors proposing the wake/emulsion mixing model used various models to represent the solid flux across the wake and emulsion phase virtual frontier. Dayan and Zalmanovich (1982) evaluated the radial (relative to the spherical coordinate of a bubble) velocity (v_r) of a particle at the wake frontier. Flux of solid discharged from the wake ($F_{s_{dw}}$) was written as follows:

$$F_{s_{dw}} = v_r C_{w_s} \tag{51}$$

It was assumed that there was no flux of solid from the emulsion phase to the wake phase. In this case, the solid discharges were an irreversible process. Tang and Fan (1989) and Murray and Fan (1989) used similar flux terms. They used average particle entrainment (v_e) and de-entrainment (v_d) velocities relative to bubble rise velocity. Also, they assumed two different effective areas, one for the de-entrainment (A_e) and one for the entrainment (A_d). These authors assumed, thus, a reversible process for the solid exchange. Turi and Ng (1986) used a probability parameter, i.e. λ_{de} representing the probability per unit length that a particle is discharged from the drift bubble region, to model the solid discharged flux. This solid discharged flux was assumed proportional to λ_{de} and the axial velocity (u_{pe}) of the entrained particles:

$$dF_{s_{de}} = \lambda_{de} u_{pe} C_{e_s} dz \tag{52}$$

Cassanello et al. (1996) used a $K_L a$ type flux mass transfer term. The driving force was assumed to be represented by the solid concentration difference between the wake and emulsion phase. These concentrations were defined as the number of particles per *total* reactor volume (C'_{si}). Flux was represented by the following equation:

$$dF'_{s_{dw}} = K_{ls-w}\left(C'_{ls_s} - C'_{w_s}\right) dz \tag{53}$$

Mechanisms assumed in the case where a driving force is used for modeling purposes are far from the ones responsible for solid exchange between wake and emulsion. The driving force representation is thus questionable and may not be a valid mechanism for the wake/emulsion solid exchange.

The above flux terms assume a continuous solid discharge. El-Temtamy and Epstein (1980) and Tsutsumi et al. (1992) used instead a Height Wake Unit (HWU). The solid is discharged by a wake shedding discontinuous mechanism. The particles are discharged after they rise an average distance represented by the HWU. Note the similarity with the HEPT (Height Equivalent to a Theoretical (equilibrium) Plate) approach used for the design of the packed bed separation process. Tsutsumi et al. (1992) proposed the following equation:

$$HWU = \frac{(U_g/\varepsilon_g)}{f_{wsh}} + \alpha(U_g/\varepsilon_g)\theta_w \tag{54}$$

Where f_{wsh} represents the wake shedding frequency. Thus, the first right hand side term represents the rising distance traveled by the particles in the bubble wake before wake shedding occurs. Only this term was used by El-Temtamy and Epstein (1980). The second term represents the rising distance traveled by the particles in the wake shed and continuing to rise over a certain time "θ_w". Due to the viscous decay, particles should decelerate from the rising wake velocity to the falling particle velocity (V_p). However, the authors used a constant velocity after shedding and represented it by a fraction of the wake velocity "α".

The falling particle velocity used by the various authors may be generalized. This velocity may be written as the difference between a slip particle velocity "u_{ps}" (relative to the liquid emulsion phase velocity) and a velocity of the liquid in the emulsion phase "$u_{L_{ls}}$":

$$V_p = u_{L_{ls}} - u_{ps} \tag{55}$$

From the flow model represented in Figure 2.13 liquid mass balance gives the following equation for the velocity of the liquid in the emulsion phase (Murray and Fan, 1989):

$$u_{L_{ls}} = \frac{U_{ls}\left(1-\varepsilon_s^f\right)-\left(U_g/\varepsilon_g\right)\left(1-x\varepsilon_{ls_s}\right)k\varepsilon_g}{\left(1-\varepsilon_g-k\varepsilon_g\right)\left(1-\varepsilon_{ls_s}\right)} \tag{56}$$

Note that for a three phase fluidized bed, $U_{ls} = U_L$ and $\varepsilon_s^f = 0$ (solid concentration in the slurry phase feed). If the liquid is batch (U_{sl} or $U_L = 0$), liquid flow is co-current to the particle (a negative velocity is set to downflow). Dayan and Zalmanovich (1982), Turi and Ng (1986) and Tsutsumi et al. (1992) used slurries and neglect the particle volume in the emulsion phase ($1>>\varepsilon_{ls_s}$). The other authors (except Murray and Fan, 1989; slurry bubble column) used three-phase fluidization and obviously did not assume a negligible volume of the particles.

For the slip particle velocity, some authors (seeTable 2.8) used the Richardson and Zaki (1954) equation:

$$u_{ps} = u_{t0}\left(1-\varepsilon_{ls_s}\right)^{n-1} \tag{57}$$

Where u_{t0} is the terminal particle velocity. The other authors (seeTable 2.8) directly used the particle terminal velocity estimated by Stoke's law:

$$u_{ps} = u_{t0} = \frac{2}{9}\frac{d_s^2}{4}\frac{\left(\rho_s-\rho_L\right)}{\mu}g \tag{58}$$

Notice that the authors neglecting particle volume are the same ones that directly used particle terminal velocity. It is coherent with the Richardson and Zaki correlation. Note

also that when particle volume is not negligible, downward particle velocity (V_p) becomes a function of the axial position, i.e. $\varepsilon_{ls_s} = f(z)$, for intermediate particle size. That is, contrary to the case of the ADM, the steady-state differential equation (see comment 1 in Table 2.8) may be not solved by simple variable separation. The differential equation becomes a non-linear first-order differential equation. This equation should be solved with a numerical method.

Wake/emulsion mixing models give a realistic description of solid phase mixing, but they are incomplete, i.e. they do not consider axial mixing caused by the various wake velocities (bubble velocity distribution). Indeed, the wake/emulsion mixing models proposed were validated in most cases in the dispersed flow regime (narrow bubble size and velocity distribution). Also, they do not consider axial mixing of the falling particles. Furthermore, mathematical form of the models is similar to that of the ADM in steady state. For example, Murray and Fan (1989) developed the following mathematical form in steady state for a continuous slurry bubble column:

$$E_Z \frac{dC_S}{dz} = V_p C_S + P' U_{sl} C_S^f \left[xk\varepsilon_g + \left(1 - \varepsilon_g - k\varepsilon_g\right)\right] \tag{59}$$

Where:

$$E_Z = \frac{V_R u_b \varepsilon_w x}{N_b \left[\frac{v_e A_e}{V_p} + \frac{v_d A_d \varepsilon_{ls}}{u_b \varepsilon_w} \right]} \tag{60}$$

And

$$P' = \frac{v_d A_d}{u_b \varepsilon_w \left[\frac{v_e A_e}{V_p} + \frac{v_d A_d \varepsilon_{ls}}{u_b \varepsilon_w} \right]} \tag{61}$$

For three phase fluidized beds and semi-batch slurry bubble columns (U_{sl}=0) only the two first terms of equation (59) represent the solid mixing model often used. The term representing solid phase mixing is the Fickian one as in the ADM. The mixing coefficient interpretation is, however, clearer. This coefficient depends among other things on bubble wake mean velocity, relative amount of solid transported in the wake and solid exchange between wake and emulsion phases. The similarity of this model with the liquid phase mixing model proposed by Myers et al. (1987) should be noted. This model is also numerically equivalent to the ADM (Schlüler et al., 1992). However, if V_p is a function of the axial position, E_z is also a function of the axial position, i.e. $E_z = f(V_p)$; equation (60).

Cassanello et al. (1995) used statistical analysis tools, such as rescaled range (R/S) statistical analysis and ones based on determinist chaos. These tools were applied on Lagrangian Radioactive Particle Tracking (RPT) time-series data obtained among other in a three phase fluidized bed containing glass beads (dp > 1 mm). These tools allowed them to give indications about characteristics that need to be described by solid phase models. The authors found that the correlation of the particle fluctuating velocities is persistent in time. This means a superdispersive (movement is faster than Brownian motion) axial solid phase mixing. This means that the Fickian term included in the ADM does not represent the solid phase axial mixing. Fluctuating particle steps in horizontal directions were not correlated. The solid phase mixing is then dispersive in horizontal directions. In these directions the solid phase mixing may be represented by a Fickian term. Recall however that Yang et al. (1993) found superdispersive azimudal and dispersive radial liquid phase mixing with RPT data. Cassanello et al. (1995) also

showed that particle movement is chaotic, i.e. their following paths are very sensitive to initial conditions and are not random. Particle chaotic movement is more pronounced when superficial gas velocity is high and at the coalesced flow regime.

Larachi et al. (1996) observed with RPT data obtained in a three phase fluidized bed (dp>1mm) that the axial velocity of rising particles is constant along their paths. Upflow solid velocity distribution may be represented by a log-normal distribution as in the case of the bubble velocity distribution showed previously. Also, particles rise in a helicoidal manner, like bubbles (Fischer et al., 1994). Hence, axial solid mixing follows a convective mechanism and the solid phase flow is intimately linked to the bubbles flow behavior. Particles that go down also have a constant axial velocity along their paths. The downflow solid mixing mechanism of large/heavy particles also seems to be convective (Larachi et al., 1996). This may not be the case for small/light particles, because they follow smaller eddies in the liquid phase and the ratio of viscous force to buoyancy force is higher for such particles. The mechanistic solid mixing model may be different among reactor types, i.e. three phase fluidized beds or slurry bubble columns. For generalized purposes the mixing mechanism assumed in a solid phase mixing model should depend on the ratio of viscous force to buoyancy force. Furthermore, axial particle velocity fluctuates when the particles follow vortices observed in the liquid phase between the upflow and downflow region (Chen et al., 1994). This increases the complexity of the solid phase axial mixing mechanism. The mixing mechanism follows by a particle change with time.

The wake/emulsion mixing model is, thus, coherent with some determinant aspects of the solid phase flow. However, this model is only descriptive and may not accurately predict the reactor performances related to a solid catalyst behavior. This model needs to be modified in order to take into account the other main solid flow behaviors, such as the wake velocity distribution and the dynamic of the liquid vortex.

2.2.7.2 Model exploitation

Except Cassanello et al. (1996), all authors used steady-state axial solid concentration profile data to validate their mixing model. The data was thus obtained in systems characterized by an axial profile of the solid concentration, i.e a slurry bubble column, a three phase fluidization of light particles (density close to that of the liquid phase) and in the freeboard of a three phase fluidized bed containing particles that are not too large (dp < 1 mm). As for the liquid phase, the axial solid concentration profile has an exponential form and may be described by the ADM (see eq (50)). As discussed, global steady-state data give poor information about mixing mechanisms (a lot of models may represent this kind of data). Cassanello et al. (1996) used, among others, systems containing large/heavy particles (ex.: glass beads with dp > 1 mm). These systems exhibit a flat solid concentration axial profile. These authors used RPT data to compute solid pulses from the particle trajectory histories. Their model was thus validated with unsteady-state data. This kind of data gives a high level of information about the flow dynamics (see the end of the last sub-section).

Some model parameters were optimized and others were measured directly or estimated (seeTable 2.10). The gas holdup was always measured. The evaluation of V_p was already discussed in the previous sub-section. When k and x were used, they were either optimized (Tang and Fan, 1989; Tsutsumi et al., 1992) or evaluated (El-Temtamy and Epstein, 1980, Murray and Fan (1989), Tsutsumi et al., 1992). The correlations used are based on the work of Bhatia and Epstein (1974), El-Temtamy and Epstein (1978) and Miyahara et al. (1990).

The wake shedding frequency used for HWU (eq (54)) was evaluated with equations between the Strouhal number ($Sr = f_{wsh} d_b / u_{bL}$) and the bubble Reynolds number ($\mathrm{Re}_b = \rho_L u_{bL} d_b / \mu_L$), where u_{bL} is the velocity of the bubble relative to the liquid phase

velocity ($u_{bL} = U_g/\varepsilon_g - U_L/\varepsilon_L$). El-Temtamy and Epstein (1980) used the results of Lindt and de Groot (1974) and Tsutsumi et al. (1992) used those of Fan and Tsuchiya (1990) to evaluate the wake shedding frequency. Tsutsumi et al. (1992) used the results obtained by Lindt (1972) and Rigby et al (1970) to evaluate, respectively, the value of α and θ_w.

Table 2.10: Solid phase mixing models-Model exploitation.

Article	Mixing measurement	Optimized parameter
El-Temtamy and Epstein (1980)	Steady-state [1]	➢ N_{st}
Dayan and Zalmanvich (1982)	Steady-state	None
Turi and Ng (1986)	Steady-state	$\Lambda = \lambda_{de} - \lambda_{ls}$ (E'_z)
Tang and Fan (1989)	Steady-state	➢ E_z ➢ k ➢ x ➢ L_m
Murray and Fan (1989)	Steady-state	➢ E_z ➢ $C_s\|_{z=0}$ ➢ A *(or P)*
Tsutsumi et al. (1992)	Steady-state	➢ E'_z *(or x)*
Cassanello et al. (1996)	Unsteady-state [2]	➢ $K_{ls\text{-}w}$

[1] Authors used steady-state axial solid concentration profile.

[2] Authors used RPT (Radioactive Particle Tracking) data to generate particle pulses from tracer histories. Solid concentration time evolutions and mixing times are obtained.

Dayan and Zalmanovich (1982) and Turi and Ng (1986) used a model representing the flow around the bubble based on microscopic momentum balance to evaluate some mixing model parameters. Assuming that the main mechanism responsible for the particle de-entrainment from the wake is due to gravitational and inertial forces, the former authors developed an equation of particle velocity around the bubble and the bubble wake. They assumed that the flow around a bubble is irrotational and found an

expression of the tangential (relative to the spherical coordinate of a bubble) velocity of a particle influenced by the liquid flow induced by the rising of a bubble. A force balance on a particle made it possible to find an expression of the radial velocity of the particle. They found that the tangential velocity of a particle is 30 times greater than its radial velocity. That is, a particle is de-entrained from the wake only if it is very close to the external surface of the wake at the radial velocity estimated (see eq (51)). Note that the particle radial velocity is proportional to the square of the particle diameter and that the authors used very small particles: dp = 8-16 μm. A particle only 5.5 times larger has a radial velocity 30 times greater, giving the same order of magnitude as the tangential velocity. Turi and Ng (1986) assumed that above the bubble equator, the flow field might be described by the potential flow model (supported by the work of Bhaga and Weber, 1981; Weber and Bhaga, 1982). Below the equator the particle velocity was evaluated by a wake velocity correlation obtained by Bhaga and Weber (1980). This made it possible to estimate the engagement time, i.e. the duration of the particle engagement with the bubble (influenced by the drift effect). The engagement time makes it possible in turn to estimate the probability per unit length that a particle is discharged from the drift bubble region (λ_{de} in eq (52)).

In spite of the equation developed for E_z (or E'_z), which gives more physical meaning to the mixing parameter than the ADC (see Table 2.8), almost all the authors (see Table 2.10) optimized the mixing parameters. In fact, the equations of the mixing parameters contain parameters that are very difficult to estimate or measure. These parameters are related to wake dynamics.

All the wake/emulsion mixing models obviously fitted the steady-state experimental data well. In addition to fitting their model on data obtained for monodispersed particle systems, Murray and Fan (1989) predicted the solid concentration axial profile of binary mixtures. They used model parameters optimized for a monodispersed system

and predicted the solid concentration axial profile for various combinations of these monodispersed systems with their model. This procedure assumes no interaction between particles and can be made for a slurry reactor where the solid holdup is not high (averaged distance between particles is higher). There was good agreement for the continuous and the batch slurry bubble columns.

As mentioned, Cassanello et al. (1996) computed from RPT data the solid concentration axial profile time evolutions and axial mixing times. Figure 2.14 shows a result of the measured and predicted time evolution of the solid centroid injected at various axial positions in the bed. It is evident that the predicted mixing time was over-estimated. The measured and predicted mixing times were closer for glass beads (dp = 3 mm) at a high U_L/U_g ratio (dispersed flow regime). The wake/emulsion mixing model does not consider among others axial mixing of the particle caused by the wake velocity distribution, nor does it consider the axial mixing of the particle in the emulsion phase, such as the effect of the liquid vortex.

Wake/emulsion mixing models were able to represent well the steady-state solid concentration axial profile. However, it is not acceptable to predict the dynamic of the solid phase. Knowledge about solid dynamics is important to predict catalysis performance (catalysis deactivation) in some industries.

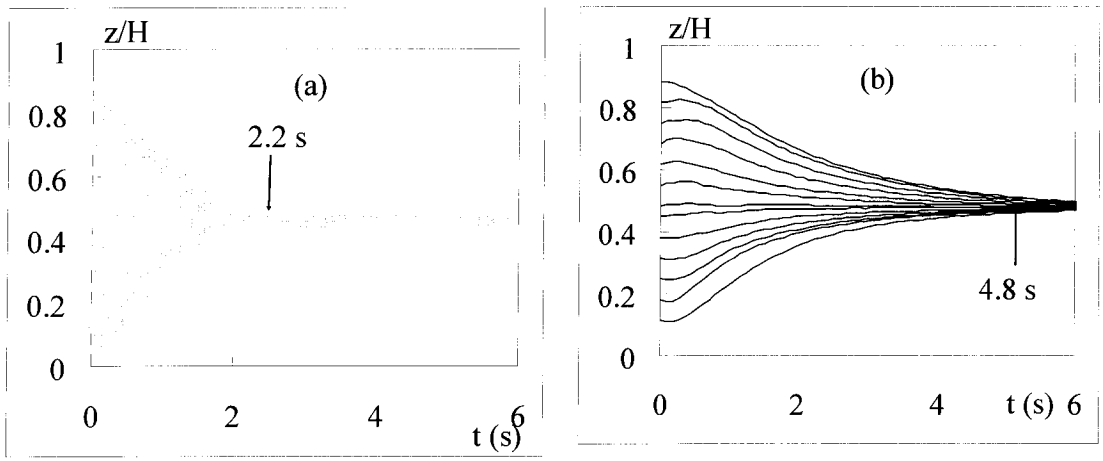


Figure 2.14: a) experimental and b) predicted average axial mixing times evaluated from the instantaneous axial centroids of solids pulses injected at various heights in the bed. Air/water/glass bead system. $Ug = 0.11$ m/s, $U_L = 0.065$ m/s and $d_p = 3$ mm. (Cassanello et al., 1996).

Instead of the solid RTD, the solid Trajectory Length Distribution (TLD) (Villermaux, 1996) may be used as an approach to understand the solid hydrodynamics. The TLD is obtained with Lagrangien data. For the solid phase this data may be obtained by tracking a marked particle. Various trajectory lengths may be computed between planes or points and give the TLD. It gives local information on the flow pattern of the concerned discrete phase. Kiared et al. (1997) used this approach to study the solid mixing in a three-phase fluidized bed.

2.2.7.3 Conclusion

As discussed for the liquid phase, the various velocities of the wake (bubble velocity distribution) should be included in solid phase mixing models. The effect of the vortices on particle mixing should be studied and included in the solid phase mixing model. Also, mechanisms responsible for the particle exchange between solid phases or states (engaged, wake-entrained, captured, emulsion and vortice-entrained) should be

studied and modeled in order to obtain the changing frequency of states. The study of mixing mechanisms followed by particles in various states should be interesting. Solid properties, such as size, density and wettability, may affect these mixing mechanisms. Indeed, particles are driven by the liquid at scales having a similar or larger size than the particle size. The scales that are smaller than the particle size influence the solid/liquid interfacial momentum transfer. Also, forces acting on particles depend on their size and, mostly for small particles, on their chemical surface properties, such as wettability. For example, it was shown that the large downflow glass beads (larger than 1 mm), whose buoyancy force is high, followed a convective mechanism. When the buoyancy force and the particle size are smaller, particles may follow the liquid random motion more (higher contribution of the solid/liquid drag force and effect of the liquid flow at a smaller scale). Furthermore, large/heavy particles are closer to each other in a fluidized bed, inducing high particle/particle hydrodynamic forces and collision that may result in a higher interaction between mixing mechanisms in the various solid phases and regions (e.g. downflow and upflow regions).

2.2.8 LITERATURE PHASE MIXING MODELS GENERALIZATION

As presented above the phase mixing models proposed in the literature take various forms. Models assumed either a purely dispersive mechanism, a purely convective mechanism or a combination of both mechanisms (dispersive/convective mechanism). In the latter case, the contribution of each mechanism varied widely. The models proposed in the literature may be generalized in a simple way. This general model should be able to represent a convective mechanism as well as a dispersive mechanism. The following model does not pretend to generalize all the mixing models that may be proposed, it does, however, generalize most of the phase mixing models discussed in this review. It may be possible to write an unsteady-state tracer balance for a specific phase (gas, liquid, solid, wake, emulsion, bubble class or vortex):

$$\frac{\partial C}{\partial t} = \frac{\partial}{\partial z}\left(E_Z^{"} \frac{\partial C}{\partial z} \right) - \frac{\partial (VC)}{\partial z} + I \tag{62}$$

Where I is a function representing the interaction between phases (for example, a mass transfer function between phases). It may be between the bubble class, the wake and emulsion phase or the gas and liquid, etc. Instead of assuming $E_Z^{"}$ and V are only functions of time and position, these parameters may be assumed to also be functions of phases. In a more general way it may be stated that:

$$V = f_V(\phi, t, r, z, \theta) \tag{63}$$

And

$$E_Z^{"} = f_{E_Z^{"}}(\phi, t, r, z, \theta) \tag{64}$$

Where ϕ represents the dependence of the parameters on the phases. For example, in the TBCMMs proposed for the gas phase, the ADC depends on the bubble class (see Table 2.2). Shetty et al. (1992) used the following equation:

$E_Z^{"} = Dax_g^S \quad \forall r, z, \theta, t$ for ϕ = small bubble class

$E_Z^{"} = 0 \quad \forall r, z, \theta, t$ for ϕ = large bubble class

And

$V = u_b^S \quad \forall r, z, \theta, t$ for ϕ = small bubble class

$V = u_b^L \quad \forall r, z, \theta, t$ for ϕ = large bubble class

Equation should be written as the number of times equal to the number of phases. For the last example, it should be written twice. Thus, equation (62) with $I = 0$ ($f_e = 0$ in eq (18)) is obtained twice. For the Modak et al. (1993, 1994) model, I is equal to the last term on the left in equation (18). In the Rustemeyer et al. (1989) liquid phase mixing model, the mixing parameter function and the velocity function depend on the radial position, i.e. $E_Z'' = Dax_L(r)$ and $V = \hat{u}_L(r)$. If an exchange between annulus regions is added to the model, it is possible to replace I with the radial dispersion term, i.e. $I = D_{rad}\frac{1}{r}\frac{\partial}{\partial r}\left(r\frac{\partial C}{\partial r}\right)$. The mathematical form of the liquid phase mesomixing model proposed by Lubbert's team is not produced. It may be only conceptually produced (dispersive/convective mixing model), because they used an approach other than the conventional mass balance. The other approaches are briefly described in the next section.

Functions of the phase holdup should be known to compute the concentration in the reactor while combining the concentration in each phase (a weight average of the concentration). For example, in the case of the purely convective model of the gas phase proposed by Hyndman and Guy (1995), the relationship between the holdup of each bubble class 'ϕ_i' (the continuous bubble class may be discretized) and their velocity ($\varepsilon_{g_{\phi_i}} = f_{\varepsilon_{g_{\phi_i}}}(V_i)$) may be found as follows:

$$\varepsilon_{g_{\phi_i}} = \varepsilon_g \int_{V_{i-1/2}}^{V_{i+1/2}} f_{distr}(V_i)\,dV \tag{65}$$

Where $f_{distr}(V_i)$ is the equation (19).

Depending on the function of E''_Z and V, equation (62) may be represented as a convective, dispersive or dispersive/convective mechanism (various relative importances of the mechanisms). If $E''_Z = 0$ and V is not a function of the axial position with a non-zero variance, the model represents a convective mechanism. If the variance of a velocity function is zero ($\sigma^2_v = 0$) and does not depend on the axial position, the model becomes the ADM that makes it possible to go from a plug flow to a CSTR behavior. Table 2.11 shows various situations that the general model may represent and contains the references that proposed these kinds of mixing models. Various forms of functions f_V and $f_{E_Z''}$ may be imagined.

Table 2.11: possibilities of the general phase mixing model.

Parameters tend to		Model tends to	Phase	Authors
E_z''	σ_v			
0	0	Plug flow	➢ Gas	A lot
0	∞	Depend on V function	None	None
0	free	Purely Convective	➢ Gas	➢ Hyndman and Guy (1995a,b) ➢ Hyndman et al. (1997)
∞	0	CSTR	➢ Liquid ➢ solid	A lot
∞	∞	Depend on the relation between V and E_z''	None	None
∞	free	Multiple CSTR in parallel	None	None

(*Table2.11 continued*)

Parameters tend to		Model tends to	Phase	Authors
E_z''	σ_v			
free	0	ADM if E_Z'' and V are not functions of axial position	➢ Gas ➢ Liquid ➢ Solid	A lot (see the section about the ADM)
		Wake/emulsion model	➢ Liquid	➢ Myers et al. (1987) ➢ Schmidt et al. (1992a)
		Note: in fact there are 2 velocities (upflow and downflow) but the two velocities are combined.	➢ Solid	➢ El-Temtamy and Epstein (1980) ➢ Dayan and Zalmanvich (1982) ➢ Turi and Ng (1986) ➢ Tang and Fan (1989) ➢ Murray and Fan (1989) ➢ Tsutsumi et al. (1992) ➢ Cassanello et al. (1996)
free	∞	Depend on the relation between V and E_z''	None	None
free	free	Dispersive/convective (may be multiple ADM in parallel; see eq (11))	➢ Gas	TBCMM: ➢ Shah et al. (1985) ➢ Kawagoe et al. (1989) ➢ Shetty et al. (1992) ➢ Kantak et al. (1995) ➢ Modak et al. (1993) ➢ Modak et al. (1994)
			➢ Liquid	➢ Rustermeyer et al. (1989) ➢ Degaleesan et al. (1996,1997) ➢ Nassar et al. (1992) ➢ Schmidt et al. (1992b)

Equation (62) may be extended to other kinds of mixing models. For example, it is possible to set $E''_Z = 0$ and propose a function for the velocity (eq (63)). It is possible to assume a continuous change of the bubble velocity along the column axis and assume various functions according to the bubble size. Indeed, smaller bubbles follow

the liquid flow more than the larger bubbles (ex.: small bubbles may be entrained by the downflow of the liquid phase). The changing velocity of the bubbles should not be the same for the whole bubble size distribution. It may also be possible to take into account the bubble coalescence/breakup while proposing a function for the holdup of each bubble class (bubble size), i.e. $\varepsilon_{g_{\phi_i}} = f(\phi_i, z)$ with the following constraint: $\sum \varepsilon_{g_{\phi_i}} = 1 \ (or \ \varepsilon_g)$ for each axial position.

Equation (62) may be applied for each of the considered phases, e.g. liquid-vortex phase, solid-wake phase, bubble class, etc. Now, considered phases have to be identified. There are a large number of possible sets of phase arrangements and interactions. According to the present review Figure 2.15 presents a proposed set of phase arrangements and interactions. This set is an update of the flow representation found in Figure 2.13. This new flow representation makes it possible to take into account the various bubble class properties and their liquid/solid wake association. The distribution of a bubble/wake class is shown in Figure 2.15. It is possible to attribute different characteristics (e.g. mixing mechanism) to each bubble/wake class depending on bubble size. Moreover, a liquid/solid vortex phase is shown in Figure 2.15. This phase could have an important impact on catalysis desactivation and on reactor conversion and selectivity. This flow representation makes it possible to respect some important recent observations made on phase hydrodynamics, such as the link between the mixing mechanism of the gas phase and that of the liquid/solid phases, the convective mixing mechanism contribution in the gas phase hydrodynamic and the liquid/solid vortex observed in the bubble colomn, slurry bubble column and three-phase fluidized bed reactors. Moreover, this flow representation allows a mechanism of gas/liquid interfacial mass transfer proposed by Schmidt et al. (1994b) to be shown. They measured the local oxygen concentration around a stationary bubble. They found that the oxygen is mainly transferred from the bubble to the liquid in the wake (high

turbulence) and that the oxygen transferred into the liquid at the front of the bubble is really low. The oxygen is then transferred into the emulsion (bulk) phase when wake shedding occurs. Therefore, interfacial mass transfer is mainly caused by the presence of the wake.

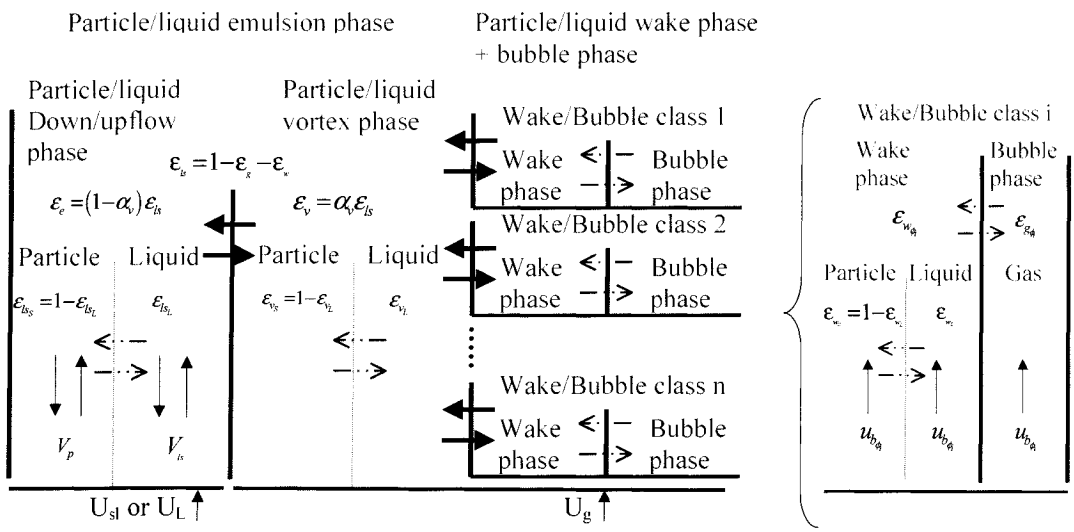


Figure 2.15: Update of the flow representation shown in Figure 2.13. Dash arrows represent transferred solute between phases and the full arrows represent liquid and solid phases exchange between bubble/wake class and liquid/solid emulsion phase, and between liquid/solid emulsion phase and liquid/solid vortex phase

Flow representation shown in Figure 2.15 may also be used for other modeling approaches, such as population balance and the Monte-Carlo simulation. These other approaches are briefly described in the following section.

2.2.9 OTHER APPROACHES

This section briefly discuss the others modeling approaches in order to compare they with the mixing modeling approach.

Basically, to make a Eulerian mixing model a velocity field or function must be taken and included in the continuity equation (in this case without a reaction rate term):

$$\frac{\partial \rho_k}{\partial t} + \nabla \cdot \rho_k \vec{u}_k = 0 \tag{66}$$

A more fundamental approach is to evaluate the velocity field with the microscopic momentum balance:

$$\frac{\partial \rho_k \vec{u}_k}{\partial t} + \nabla \cdot \rho_k \vec{u}\vec{u} = -\varepsilon_k \nabla P - \nabla \cdot \varepsilon_k \bar{\bar{\tau}} + \sum_{l=1}^{N} \vec{M}_{kl} + \vec{S}_k + \rho_k \vec{g} \tag{67}$$

This approach, called Computational Fluid Dynamics (CFD), is complex and presents some important problems. The main problem is the utilization of closing equations. The momentum transfer at the interface of the phases and turbulence are not a well know mechanism and are difficult to model. Correlations (or closing equations) were used to represent this mechanism allowing equation (67) (eq (66) is the constraint of eq (67)) to be solved. Numerical methods, such as finite elements, were used. Computing times for solving the differential equations may be very high, i.e. it may take several weeks for one simulation representing a few seconds. Also, the solution was sometimes very sensitive to the initial conditions. When the problems associated with this approach are solved, it would be a powerful tool to obtain accurate predictions of the reactor performance. CFD is out of the scope of this review. However, for readers that are interested in CFD for the multiphase reactor the following references are given: Becker et al., 1994 ; Sokolichin and Eigenberger, 1994 ; Lapin and Lübbert, 1994 ; Sokolichin et al., 1997 ; Delnoij et al., 1997 ; Mudde and Simonin, 1999 ; Sanyal et al., 1999 ; Cockx et al., 1999 ; Pfleger et al., 1999 ; Joshi (2001) ; Joshi et al. (2002) ; Fan and Yang (2002).

As for the case of the mixing model, equations (66) and (67) assume a space continuity of the phases. The presence of bubbles and particles is obviously punctual in space. For the discrete phases, it is possible to write a force balance on each particle (or bubble). Forces can be classified into three categories. The first category includes the forces function of phase *properties*, the second category includes the forces function of relative *velocity* between the phases, the third includes the forces function of relative velocity between the phase *acceleration*. The buoyancy force is part of the first category and represents the apparent weight of the discrete element. The drag force is part of the second category and represents the fluid friction acting on the discrete element and is proportional to the square of the relative velocity between the phases. The add mass force is part of the third category and represents the resistance of the fluid mass accelerating with the discrete element (fluid mass and discrete element have the same acceleration). The Basset force is also part of the third category and represents the past acceleration (history of the relative velocity acceleration). Another force may be applied to the discrete element, such as electromagnetic field.

In this Lagragian approach, interfacial momentum transfer and the mechanism of particle interactions, such as collision, should be known. Unfortunately, these mechanisms are only approximated by correlations and the accuracy of the solution is not guaranteed. For the discrete phase, a Lagragian approach is more realistic, but has similar limitations to the CFD Eulerian approach. For interested readers the following references are given: Delnoij et al., 1997 ; Sokolichin and Eigenberger, 1997 ; Lapin and Lübbert, 1994 ; Li et al., 1999 ; Fan and Yang, 2002.

Another approach is briefly described here. Particles and bubbles have a more or less random behavior, a stochastic behavior. It is possible to represent this behavior with probabilities. Nauman (1981) used the discrete random walk approach to describe the

RTD in a system represented by the ADM. The movement of particles (or bubbles) following a dispersive mechanism may be described by simple probabilities. Hence, a particle has a probability "p" to move Δz to the right and has a probability "q = 1-p" to move Δz to the left. The particle movement is symmetric when $p = q = ½$ and represents a pure diffusion process in a stationary fluid, also described by the continuous equation (1) with $U = R_A = 0$. If $p > q$, the particle has more chance to move to the right and this description is equivalent to the ADM representing a continuous process.

The random walk approach (also called the Monte Carlo simulation) may be used to give a Lagragian description in 1-D, 2-D and 3-D of particles or bubbles in multiphase reactors with a more sophisticated stochastic description. The trajectory of the particles (or bubbles) may be obtained if and only if the behavior is stochastic in nature. If not (e.g. determinist chaos), only mean (and higher moments) flow behavior may be obtained. Rogalewicz and Fort (1991) used this Monte-Carlo simulation to describe a 2-D flow pattern of bubbles in an agitated gas/liquid reactor. Their model allowed them to obtain the position, size and velocity of each bubble with time. Grandjean et al. (1995) proposed a model describing the stochastic behavior of the bubbles in a bubble column. The probabilities used depended on the position of the bubble (various regions were defined). The Monte Carlo simulation was also used by Fan and Chang (1979) to describe the mixing of particles in a liquid/solid fluidized bed. Grandjean and Chaouki (1993) developed a stochastic description of the particle mixing in a circulation-fluidized bed. The probabilities used depended on the particle position (various regions were defined).

This approach allows a Lagragian description of the discrete phases and gives a dynamic description of the flow pattern of these phases if it is stochastic in nature. It was used a few times for multiphase reactors discussed in this article. The main

difficulty is to determine the many parameters needed to simulate the phase mixing in multiphase reactors. Parameters, probabilities, and/or parameters of the probability functions were computed with a data set obtained by measurements that are indirect to the stochastic particles path, i.e. the measurements are Eulerian and have to represent a Lagragian process. Thus, it is difficult to verify if a Monte-Carlo model accurately represents the Lagragian stochastic process. The Monte-Carlo simulation needs more computing time than some conventional mixing models. However, it often needs less computing time than the CFD approach and it is easier to compute.

The population balance is another statistical approach used in literature. This approach allows making a balance on an entire population characterized by a set of properties. Instead of applying a balance on one property (the mass for example: mass balance), the balance is made on a normalized number of probability functions ($\psi(t,x,y,z,\zeta_1,\zeta_2,...,\zeta_i,...,\zeta_m)$ depending on population properties (ζ_1, ζ_2,..., ζ_i,..., ζ_m e.g. volume, density, etc.), spatial coordinates (x,y,z) and time (t). The general form of the population balance on a volume element is written below (Villermaux, 1993):

$$\frac{\partial \psi}{\partial t} + \nabla \cdot \psi \vec{u} + \sum_{i=1}^{m} \frac{\partial}{\partial \zeta_i}\left(\psi \frac{\partial \zeta_i}{\partial t}\right) - G = 0 \qquad (68)$$

Where G is the net generation term and $\vec{u}$ is the velocity vector. This approach was used, for example, to model bubble coalescence and breakup in the bubble column (Colella et al., 1999) and was combined with the CFD approach (Olmos et al., 2001).

Various modeling approaches may thus be used that imply some assumptions. Some are more representative of the flow physics. It is yet to be determined which assumptions may be used to obtain simple models that respect the essential physical aspects of the phase flow. The chosen modeling approach depends on the wanted level

of description (spatial and temporal). For a local dynamic description, the *dynamic behavior* should be known, i.e. deterministic, deterministic chaos, periodic, quasi-periodic or stochastic (Hilborn, 2000). Such a dynamic behavior may be discriminated with the following parameters obtained with time series data: Lyaponov exponent, Kolmogorov-Sinai (K-S) entropy, Hurst exponent, number of dimensions within a stated space (degree of freedom obtained by the embedding technique) and fractal dimension (Hilborn, 2000). Fourier power spectra and surrogate data technique may also be used (Theiler et al., 1992; Kennel and Isabelle, 1992; Prichard and Theiler, 1994). Actual overall (from average flow pattern to the reactor output) mixing models are not able to discriminate between such dynamic behaviors. However, a mixing model represents one or more mixing mechanisms respecting those of the wanted level of description, e.g. overall RTD should respect the relationship between the RTD-variance and reactor length.

In other words, local flow may be exhibiting deterministic chaos even if the reactor output is determinist. A question may be asked: what is the influence of the local dynamic behavior on the reactor output, i.e. conversion and selectivity? The conversion and selectivity of two reactors may be the same no matter what the local dynamic behavior is, deterministic chaos or stochastic, and may be predicted by a simple overall mixing model. Another question may be asked: under what conditions is the choice of the modeling approach essential to accurately predict conversion and selectivity?

Moreover, the level of description determines the measuring technique needed. When the local dynamic must be modeled, it is obvious that local measuring techniques should be used. However, global measuring techniques may be combined with local ones, because global measuring techniques give the results of the spatio-temporal local dynamic. In all cases, models should be validated with appropriate data and validation-methods.

2.2.10 CONCLUSION

The Axial Dispersion Model (ADM) is too simple to represent the phase mixing relative to the complex phase hydrodynamics. Moreover, the Axial Dispersion Coefficient (ADC) correlations proposed in the literature contradict themselves. Using the ADM may be justified when the kinetics are slow (limiting). In a limiting case, the simple plug flow and CSTR models may give very close performance predictions. However, in the case of limiting hydrodynamics, multiphase reactor design should be made with mixing models better representing the flow pattern of the phases. A phase mixing model closer to the physics of the phase flow was proposed in the literature. The objective of this article was to review these mixing models for the gas, liquid and solid phases in a bubble column, slurry bubble column (small/light particles) and three-phase fluidized bed (large/heavy particles) reactors. The common feature of these reactors is the presence of gas bubbles, influencing considerably the flow pattern. Thus, a model proposed for one of these types of reactors may be conceptually similar to the others.

There are various visions of the main mixing mechanism to be considered in model formulation. For the gas phase, two main visions were proposed. The majority of authors assumed that the bubble may be separated into two bubble classes. One is the large bubble class (coalescing bubbles in the coalesced flow regime) and the other is the small bubble class. The large bubbles rise faster than the small bubbles and are not really influenced by the liquid phase flow pattern. They are assumed to follow a plug flow behavior. The small bubbles were driven by the liquid streams, eddies and vortices. Small bubbles are then mixed and assumed to be either perfectly mixed or partially mixed. In the last case the ADM was used to represent the small bubble class mixing. For this Two Bubble Class Mixing Model (TBCMM), the main mechanism responsible for the gas phase mixing is a dispersive one (random movement of the bubbles). One team has another vision. They first diagnosed the main gas phase mixing

mechanism with tests based on the RTD evolution along the column axis. According to their results they proposed a purely convective model for the gas phase. This model assumes that each bubble rises at a constant velocity along the column axis and the mixing is caused by the bubble velocity distribution, i.e. it may be seen as a segregation effect or a multiple-plug flow behavior. The purely convective model was validated for the bubble column. The presence of particles influences the bubble coalescence/breakup dynamic. For reactors containing particles increasing this dynamic, the purely convective model has to be validated. Indeed, the bubble velocity would change a lot when they rise along the column axis. Since mixing smaller bubbles may follow a more dispersive mechanism than the larger ones, the investigation of the mixing mechanism of the various bubble sizes will be interesting. Indeed, visual observation of the bubble dynamics in reactors leads to the assumption that the mixing mechanism of the small bubbles is not purely convective and that the mixing mechanism depends on bubble size in the overall bubble population.

For the solid phase, the mixing models proposed are conceptually homogenous. Particles were assumed to be entrained by the bubble wake (or drift effect) at only a one upward velocity, the mean bubble velocity. These particles are discharged from the wake to the emulsion phase. According to the authors, various main discharged mechanisms are assumed. Wake shedding and centrifugal force may be assumed to be these main mechanisms. Some authors assumed an irreversible process of the particle discharge and others assumed that the particles in the emulsion phase are re-entrained in the wake. Particles in the emulsion phase go down at only one velocity, a particle falling velocity. That is, the particle rises and goes down in a plug flow manner. The main mechanism assumed responsible for the solid mixing is the solid wake/emulsion exchange. However, if convective mixing of the gas phase is assumed, the particle in the wake should also follow a convective mixing mechanism. Particles are transported at various velocities (following the bubble velocity distribution) in the wake phase and

are discharge/re-entrained at various levels in the bed. Axial mixing of the falling particles should also be considered. Liquid vortex between the upflow and downflow (close to the wall) would have an important effect on solid mixing and would be included in a solid phase mixing model.

Various kinds of liquid phase mixing models were proposed in the literature. However, they all assumed a dispersive/convective mixing mechanism. The relative importance of a dispersive to convective mechanism varies widely. Some models assumed an overall liquid recirculation superposed onto micromixing attributed to turbulence and represented by the ADM. The dispersive mechanism was the main mechanism assumed in that case. The contribution of the liquid axial velocity profile superposed onto turbulence (ADM) was also assumed. The assumption that the main mixing mechanism may be attributed to the liquid transported in the bubble wake at the various bubble velocities was also taken into account. Modeling the liquid phase mixing is more difficult because, among other things, of the scale continuity to be studied. However, the liquid phase mixing model should include the bubble wake velocity distribution effect and take into account the dynamic of the vortices.

The presence of the liquid and solid transported in the bubble wake should not be ignored. In this way, liquid and particles partially follow the mixing mechanisms of the bubbles. However, if wake shedding and solid discharge are high, they may drive the mixing and it would become more dispersive.

Almost all the phase mixing models were validated according to the experimental data, even if they assumed various mechanisms. Methods of model validation should be questioned. A model was often validated on the basis of the fitting quality. This is not a sufficient criterion even if it is a necessary one. For liquid and solid phases, the steady-state solid concentration axial profile data was, respectively, sometimes and often used.

This kind of data gives global and static information on mixing, which is a dynamic process. The Axial profile of the liquid phase tracer and solid phase has an exponential form (for the solid phase, the particle should be light and/or small). A lot of mathematical forms may fit the axial profile. A higher level of information is obtained with unsteady-state measurements. The pulse input function gives the larger quantity of dynamic information on a continuous system. However, the RTD obtained at one axial position may not be fitted by a unique function. There are a lot of mathematical forms that are able to fit the RTD. Measuring various RTDs along the reactor column gives more detailed information on the mixing mechanism. The number of mathematical forms that follow this RTD axial evolution is reduced. Moreover, local measurement allows making a stricter model validation.

A model should be based on phase flow behavior identified with flow measurements, because the mixing is a consequence of the flow structure. In addition to the difficulty of elaborating a simple phenomenological model, three other kinds of difficulties are presented. First, as discussed, the choice of the model validation method(s) is important. Second, a lot of difficulties arise when measuring techniques are used. Two questions are always present: what is really being measured and what is the accuracy of the data? An example of that is the gas phase tracer liquid solubility. Some authors included in their model an interfacial mass transfer term and other authors used experimental strategies to overcome this problem. Another example is the output signal deconvolution to extract the instrumental effect from the measured RTD data to obtain the real RTD. Third, some mathematical difficulties are presented: a) fitting method (optimized method); b) numerical method to solve differential equation(s) and c) model sensibility to the parameters. a) There exist a lot of fitting methods, some are more adequate than others to fit certain relationships. Thus, if a fit is not good, this may be due to an inadequate fitting method and not necessarily to the model itself. b) If no analytical solution exists for the differential equations, a numerical method should be

used. It should be verified that this numerical method is stable, convergent and consistent. c) If the model is very sensitive to some of its parameters, their accuracy may be poor.

The purpose of a mixing model is to design or make scaled-up (or scaled-down) or optimized reactors. For this reason, the influences of reactor geometry, experimental conditions and phase properties on the model prediction need to be known. Those influences are related to the model parameters, and relationships (correlations) between these parameters and the above mentioned conditions are needed to predict the reactors' performances. However, a model having a bad representation of the flow pattern (mathematical properties are different from the flow properties) does not contain parameter(s) that may correctly follow the influences of reactor geometry, experimental conditions and phase properties. This is the case of the ADM in which various ADC correlations were proposed and contradict themselves. Hence, the first step is to identify a mixing model that follows the phase flow pattern (mixing mechanisms) well and not develop ADC correlations based on flow pattern. The main mixing mechanisms may change according to the reactor geometry, experimental conditions and phase properties. For example, the flow regime depends on these conditions and the main mixing mechanism depends on the flow regime. Different models may be proposed for various classes of flow pattern. Or, a general model containing weighted terms representing the various classes of flow pattern may also be proposed. After that, the influence of reactor geometry, experimental conditions and phase properties on the model parameters will be studied. These parameters will have a better opportunity to follow the phase hydrodynamic according to the various mentioned conditions and will give adequate predictions of the multiphase reactor performances.

ACKNOWLEDGMENTS

The authors gratefully acknowledge financial support from the Natural Sciences and Engineering Research Council of Canada and the Fonds pour la Formation de Chercheurs et à la Recherche (Québec).

NOTATION

A	interfacial area per unit reactor volume or per unit bubble volume
A	area; parameter defined in Table 2.8
A_e	effective area of the particle entrainment
A_d	effective area of the particle de-entrainment
B	normalization constant in equation (47)
C	concentration
$\boldsymbol{C_t}$	coefficients of variation of RTD ($\sigma t/tm$)
C_u	coefficients of variation of velocity distribution (σ_u/u_m)
d_p	particle diameter
d_b	bubble diameter
Dax	Axial Dispersion Coefficient (ADC)
D_{rad}	radial dispersion coefficient
Dc	column diameter
$Diff_A$	Coefficient of diffusivity of A in the liquid phase
E	mathematical expected value; time domain transfer function or RTD
E_z	solid phase mixing coefficient of the wake/emulsion mixing model
E_z'	solid phase mixing coefficient defined in Table 2.8
E_z''	phase mixing function defined by equations (62) and (64)
f	probability function; function of the parameter in parentheses
f_e	mass transfer coefficient between two bubble classes
f_s	slug frequency Myers et al. (1987) model

f_{wsh} wake shedding frequency

$F_{s_{dw}}$ flux of solid discharged from the wake

G net generation term (in eq (68))

g gravitational acceleration

h_{mc} height of mixing cells of the Rustemeyer et al. (1989) model

H Henry constant

Ha Hatta number (define in eq (34))

Hc reactor height

HWU height of a wake unit

I phase interaction function (equation (62))

J^*_A molar flux of solute A at the gas-liquid interface

k ratio of the wake volume on the bubble volume; kinetic constant

K mass exchange coefficient between upflow and downflow regions of the Degaleesan et al. (1996, 1997) model

$K_{ls\text{-}w}$ solid mass transfer coefficient between the liquid/solid emulsion phase and the wake phase

k_L liquid side mass transfer coefficient

K_La global interfacial mass transfer coefficient, liquid side resistance

L distance between two measuring points; reactor length

L_m constant solids holdup height in a three-phase fluidized bed

m mass

M total number of solid particles suspended

M_{kl} momentum transfer at the interface of phase k and l

N Richardson and Zaki correlation exponent (equation (57)); number of mixing cells of the Rustemeyer et al. (1989) model; exponent in eq (17)

n_b number concentration of bubbles per unit volume of slurry

nbz the number of axial measurement positions

nbt the number of RTD value

N number of cells

N_b total number of bubbles in the system

N_{st} number of wake shedding stages after wich no solid are present

P fitted parameter of the Murray and Fan (1989) model ($P'[xk\varepsilon_g + (1-\varepsilon_g - k\varepsilon_g)]$); pressure

P' parameter of the equation (59) (define in equation (61))

p probability to move Δz to the right (random walk) and $p+q=1$

Pe Peclet number ($Pe=UL/Dax$)

Pe_{eq} Peclet number (define in equation (14))

Q flow rate

q probability to move Δz to the left (random walk) and $p+q=1$

r radial position

r^2 objective function define in eq (16)

R column radius; bubble radius of curvature (Dayan and Zalmanovich (1982)'s model); Reaction rate

Re_b bubble Reynolds number ($\rho_L u_{bL} d_b / \mu_L$)

S momentum source (all external force excluding the gravitational force)

Sr Strouhal number ($f_{wsh} d_b / u_{bL}$)

T time; residence time

t_m mean residence time

U superficial velocity

$U_{b\infty}$ bubble terminal velocity

u interstitial velocity ($u_i = U_i/\varepsilon_i$); mean velocity of fluid a element (see eq (9) and (10))

$\overline{u}$ average of the mean velocity (define in eq (12))

$\vec{u}$ velocity vector

u_b mean bubble velocity

u_{bL} velocity of the bubble relative to the liquid phase velocity $(U_g/\varepsilon_g - U_L/\varepsilon_L)$

$\hat{u}_{\rho b}$ mean velocity of the liquid in bulk phase

$\hat{u}_{\rho L}$ mean velocity of the liquid in bubble wake phase

u_{bp} velocity relative to a bubble population according to the log-normal bubble velocity distribution (equation (19))

u_{Lls} mean velocity of the liquid in the emulsion phase (equation (56))

$\hat{u}_L$ time-average local liquid velocity

u_{pe} mean axial velocity of the entrained particles

u_{ps} mean slip particle velocity (relative to the liquid emulsion phase velocity)

u_{t0} terminal particle velocity

u_m mean velocity

V volume; velocity function (equations (62) and (63))

v flow rate

v_e mean particle entrainment velocity relative to bubble rise velocity

v_d mean de-entrainment velocity relative to bubble rise velocity

v_r radial velocity (relative to spherical coordinate of a bubble) of a particle at the wake frontier

V_p falling particle velocity (equation (55))

w parameter in equation (8)

W dimensionless parameter ($U_L A/(f_s V_c(1-\varepsilon_{gc}))$) of equations (39)-(42)

x ratio of the volumetric fraction of the solid phase contained in the wake phase on the one contained in the emulsion phase

X dimensionless parameter (V_{LE}/V_{LUF}) of equations (39)-(42)

Y dimensionless parameter ($V_{LE}/(V_c(1-\varepsilon_{gc}))$) of equations (39)-(42)

z axial position

Z dimensionless parameter $(V_{LDF}/(V_c(1-\varepsilon_{gc}))$ of equations (39)-(42)

Greek letters

α parameter of the log-normal distribution (equations (10), (15) and (19)); transition intensity from the wake phase to the bulk phase; ratio of the gas flow rate of the core bubble group (or large bubble class) on the total gas flow rate; fraction of the wake velocity (equation (54)).

β parameter of the log-normal distribution (equation (19)); transition intensity from the bulk phase to the wake phase

Δz step in the z direction

δ delta Dirac function; parameter of the Tsutsumi et al. (1992)'s model; parameter in equation (5)

δl average traveling distance of bubble wake passing through the column cross section from the formation point

ε phase volumetric fraction

ϕ represents the dependence of a function to the phase (equation (63) and(64)); probability per unit time to change the velocity of a fluid element

γ parameter in equation (5)

θ angular position

θ_w time that a particles, previously in a wake, continue to rise after wake shedding

ρ phase density

σ standard-deviation; surface tension

σ_o constant of proportionality of eq (17)

σ_u standard-deviation define in eq (13)

σ^2 variance

τ shear stress

$\bar{\bar{\tau}}$ shear stress tensor

λ_{de} probability per unit length that a particle is discharged from the drift bubble region

λ_{ls} parameter of the Turi and Ng (1986) model (= $u_b A_e n_b / V_p$)

μ mean value of the residence time distribution; viscosity

$\mu_{X(t)}$ mean of the liquid elements length axial trajectory (Nassar et al., 1992)

$\sigma^2_{X(t)}$ variance of the liquid elements length axial trajectory (Nassar et al., 1992)

ψ normalized number of probability functions

$\zeta_i,...,$ population properties, e.g. volume, density, etc.

Subscript

0 inlet conditions

1 upflow region of the Degaleesan et al. (1996, 1997) model

2 downflow region of the Degaleesan et al. (1996, 1997) model

A specie A

a near distributor region of the Degaleesan et al. (1996, 1997) model

ADM relative to the Axial Dispersion Model

b disengagement region of the Degaleesan et al. (1996, 1997) model

c cell phase of the Myers et al. (1987) model

conv relative to the convective model

g gas phase

i gas, liquid or solid phase; cell position (number) in the Myers et al. (1987) model

j relative to a detector position (equations **(30)** and**(31)**)

k gas, liquid or solid phase; relative to a detector position (equations **(30)** and**(31)**)

ls liquid/solid emulsion phase

L	liquid phase
LNC/ADM	relative to the log-normal convective/dispersive (ADM) model
l	gas, liquid or solid phase
LDF	downflow liquid of the Myers et al. (1987) model
LE	liquid exchange between slug and cell liquid of the Myers et al. (1987) model
LUF	upflow liquid of the
N	last cell in the Myers et al. (1987) model
p	relative to particle
pb	relative to the velocity of the liquid in the bubble wake phase in gas/liquid system
pL	relative to the velocity of the bulk liquid phase
R	relative to the reactor
s	solid phase; slug phase of the Myers et al. (1987) model
sl	slurries
T	tracer
t	relative to residence time
u	relative to velocity distribution
u_b	relative to the bubble velocity distribution
w	bubble wake phase

Exponent

*	equilibrium state
'	for velocity and concentration based on reactor volume
0	relative to ideal bubble velocity distribution
a	annulus bubble group
c	core bubble group
f	feed conditions

I bubble class i.e. small (L) and large bubble class (S) or annulus (a) and core (c) bubble group

L large bubble class

S small bubble class

ϕ phase, should be gas, liquid, solid, wake, bulk, etc.

REFERENCES

AUFDERHEIDE, E. and A. VOGELPOHL, "Convective model to interpret dispersed-phase residence time measurements in pulsed liquid/liquid extractors.", Chemical Engineering Science, Vol. 41, 1747-1757 (1986).

BECKER, S., A. SOKOLICHIN and G. EIGENBERGER, "Gas-liquid flow in bubble columns and loop reactors: part II. Comparison of detailed experiments and flow simulations.", Chemical Engineering Science, Vol. 49, 5747-5762 (1994).

BHAGA, D. and M. WEBER, "Bubbles in viscous liquids: shapes, wakes and velocities.", Journal of Fluid Mechanics, Vol. 105, 61-85 (1981).

BHAGA, D. and M. E. WEBER, "In-line interaction of pair of bubbles in a viscous liquid.", Chemical Engineering Science, Vol. 35, 2467-2474 (1980).

BHATIA, V. K. and N. EPSTEIN (1974). Three-phase fluidization: a generalized wake model. Fluidization and its application. H. Angélino, Couderc,J.P., Gilbert, H. Laguérie, C. Toulouse, France, Cépaduès-Editions: 380-392.

BRIENS, C. L., A. MARGARITIS and G. WILD, "A new stochastic model and measurement errors in residence time distributions of multiphase reactors.", Chemical Engineering Science, Vol. 50, 279-287 (1995).

CASSANELLO, M., F. LARACHI, C. GUY and J. CHAOUKI, "Solids mixing in gas-liquid-solid fluidized beds: experiments and modelling.", Chemical engineering Science, Vol. 51, 2011-2020 (1996).

CASSANELLO, M., F. LARACHI, A. Kemoun, M. H. Al-Dahhan and M. P. DUDUKOVIC, "Inferring liquid chaotic dynamics in bubble columns using CARPT.", Chemical Engineering Science, Vol. 56, 6125-6134 (2001).

CASSANELLO, M., F. LARACHI, M.-N. MARIE, C. GUY and J. CHAOUKI, "Experimental characterization of the solid phase chaotic dynamics in three-phase fluidization.", Industrial and Engineering Chemistry Research, Vol. 34, 2971-2980 (1995).

CHEN, R. C., J. REESE and L. S. FAN, "Flow structure in a three-dimensional bubble column and three-phase fluidized bed.", American Institute of Chemical Engineering Journal, Vol. 40, 1093-1104 (1994).

COCKX, A., Z. DO-QUANG, A. LINE and M. ROUSTAN, "Use of computational fluid dynamics for simulating hydrodynamics and mass transfer in industrial ozonation tower.", Chemical Engineering Science, Vol. 54, 5085-5090 (1999).

COLELLA, D., D. VINCI, R. BAGATIN, M. MASI and A. B. E. BAKR, "A study on coalescence and breakage mechanisms in three different bubble columns.", Chemical Engineering Science, Vol. 54, 4767-4777 (1999).

DAYAN, A. and S. ZALMANOVICH, "Axial dispersion and entrainment of particles in wakes of bubbles.", Chemical Engineering Science, Vol. 37, 1253-1257 (1982).

DECKWER, W.-D. and A. SCHUMPE, "Bubble columns - the state of the art and current trends.", International Chemical Engineering, Vol. 27, 405-422 (1987).

DECKWER, W.-D. and A. SHUMPE, "Improved tools for bubble column reactor design and scale-up.", Chemical Engineering Science, Vol. 48, 889-911 (1993).

DEGALEESAN, S., "Fluid dynamic measurements and modelling of liquid mixing in bubble columns", Department of chemical engineering, Saint-Louis, Washington university (1997)

DEGALEESAN, S., M. P. DUDUKOVIC, B. A. TOSELAND and B. L. BHATT, "A two-compartment convective-diffusion model for slurry bubble column reactors.", Industrial and Engineering Chemistry Research, Vol. 36, 4670-4680 (1997).

DEGALEESAN, S., S. ROY, B. KUMAR and M. P. DUDUKOVIC, "Liquid mixing based on convection and turbulent dispersion in bubble columns.", Chemical Engineering Science, Vol. 51, 1967-1976 (1996).

DELNOIJ, E., J. A. M. KUIPERS and W. P. M. VAN SWAAIJ, "Computional fluid dynamics applied to gas-liquid contactors.", Chemical Engineering Science, Vol. 52, 3623-3638 (1997).

DESHPANDE, N. S., M. DINKAR and J. B. JOSHI, "Disengagement of the gas phase in bubble columns.", Int J Multiphase Flow, Vol. 21, 1191-1201 (1995).

DEVANATHAN, N., D. MOSLEMIAN and M. P. DUDUKOVIC, "Flow mapping in bubble columns using CARPT.", Chemical Engineering Science, Vol. 45, 2285-2291 (1990).

DUDUKOVIC, M. P., F. LARACHI and P. L. MILLS, "Multiphase catalytic reactors: a perspective on current knowledge and future trends.", catalysis reviews, Vol. 44, 123-246 (2002).

EL-TEMTAMY, S. A., Y. O. EL-SHARNOUBI and M. M. EL-HALWAGI, "Liquid dispersion in gas-liquid fluidized beds Part I: Axial dispersion. The axially dispersed plug-flow model.", The Chemical Engineering Journal, Vol. 18, 151-159 (1979a).

EL-TEMTAMY, S. A. and N. EPSTEIN, "Bubble wake solids content in three-phase fluidized beds.", Int J Multiphase Flow, Vol. 4, 19-31 (1978).

EL-TEMTAMY, S. A. and N. EPSTEIN, "Simultaneous solids entrainment and de-entrainment above a three-phase fluidized bed.", Fluidization, Vol., 519-528 (1980).

EPSTEIN, N., "Three-phase fluidization : some knowledge gaps.", The Canadian Journal of Chemical Engineering, Vol. 59, 649-657 (1981).

FAN, L.-S., "Gas-liquid-solid fluidisation engineering", Butterworths, Massachusetts Institute of Technology, (1989).

FAN, L.-S. and K. TSUCHIYA, "Bubble wake dynamics in liquid and liquid-solid suspensions", Butterworths, Massachusetts institute of technology, (1990).

FAN, L.-S. and G. Yang (2002). Gas-liquid-solid three-phase fluidization. Handbook of fluidization and fluid-particle systems. Y. a. D. Wen-Ching, M. Chapter 27.

FAN, L. T. and Y. CHANG, "Mixing of large particles in two-dimesional gas fluidized beds.", The Canadian Journal of Chemical Engineering, Vol. 57, 88-97 (1979).

FIELD, R. W. and J. F. DAVIDSON, "Axial dispersion in bubble columns.", Institution of Chemical Engineers, Vol. 58, 228-236 (1980).

FISCHER, J., H. KUMAZAWA and E. SADA, "On the local gas holdup and flow pattern in standard-type bubble columns.", Chemical Engineering and Processing, Vol. 33, 7-21 (1994).

FRANZ, K., T. BÖRNER, H. J. KANTOREK and R. BUCHHOLZ, "Flow structures in bubble columns.", German Chemical Engineering, Vol. 7, 365-374 (1984).

GODBOLE, S. P., M. F. HONATH and Y. T. SHAH, "Holdup structure in highly viscous newtonian and non-newtonian liquids in bubble columns.", Chemical Engineering Communications, Vol. 16, 119-134 (1982).

GODBOLE, S. P., S. JOSEPH and Y. T. SHAH, "Hydrodynamics and mass transfer in a bubble column with an organic liquid.", The Canadian Journal of Chemical Engineering, Vol. 62, 440-445 (1984).

GRANDJEAN, B. P. A. and J. CHAOUKI, "Application of a monte carlo method to solid flow pattern visualization in CFB.", Chemical Reactor Technology for Environmentally Safe Reactors and Products, Vol., 537-546 (1993).

GRANDJEAN, B. P. A., C. HYNDMAN and C. GUY, "A monte-carlo simulation of gas phase hydrodynamics in bubble columns.", Chemical Engineering Communications, Vol. 133, 93-105 (1995).

GROEN, J. S., R. G. C. OLDEMAN, R. F. MUDDE and H. E. A. VAN DEN AKKER, "Coherent structures and axial dispersion in bubble column reactors.", Chemical Engineering Science, Vol. 51, 2511-2520 (1996).

GROSSMAN, S. and I. PROCACCIA, "Unified theory of relative turbulent diffusion.", Physical review, Vol. A29, 1358-1365 (1984).

GUNST, R. F. and R. L. MASON, "Regression analysis and its application", Dekker, (1980).

HILBORN, C., "Chaos and nonlinear dynamics", Oxford university press, (2000).

HYNDMAN, C. and C. GUY, "Gas phase flow in bubble columns: a convective phenomenon.", The Canadian Journal of Chemical Engineering, Vol. 73, 426-434 (1995a).

HYNDMAN, C. and C. GUY, "Gas-phase hydrodynamics in bubble columns.", Transactions of the Institute of Chemical Engineers, Vol. 73, 302-307 (1995b).

HYNDMAN, C., F. LARACHI and C. GUY, "Understanding gas-phase hydrodynamics in bubble columns: a convective model based on kinetic theory.", Chemical Engineering Science, Vol. 52, 63-77 (1997).

JEAN, R. H., W. T. TANG and L.-S. FAN, "The sedimentation-dispersion model for slurry bubble columns.", American Institute of Chemical Engineering Journal, Vol. 35, 662-665 (1989).

JOSEPH, S. and Y. T. SHAH, "Errors caused by tracer solubility in the measurement of gas phase axial dispersion.", The Canadian Journal of Chemical Engineering, Vol. 64, 380-386 (1986).

JOSEPH, S., Y. T. SHAH and B. G. KELKAR, "Simple experimental technique to measure gas phase dispersion in bubble columns.", Chemical Engineering Communications, Vol. 28, 223-230 (1984).

JOSHI, J. B., "Computational flow modeling and design of bubble column reactors.", Chemical Engineering Science, Vol. 56, 5893-5933 (2001).

JOSHI, J. B. and Y. T. SHAH, "Hydrodynamic and mixing models for bubble column reactors.", Chemical Engineering Communications, Vol. à voir, 165-199 (1981).

JOSHI, J. B. and M. M. SHARMA, "A circulation cell model for bubble columns.", Transactions of the Institute of chemical Engineers, Vol. 57, 244-251 (1979).

JOSHI, J. B., V. S. VITANKAR, A. A. KULKARNI, M. T. DHOTRE and K. EKAMBARA, "Coherent flow structures in bubble column reactors.", Chemical Engineering Science, Vol. 57, 3157-3183 (2002).

KANTAK, M. V., R. P. HESKETH and B. G. KELKAR, "Effect of gas and liquid properties on gas phase dispersion in bubble columns.", The Chemical Engineering Journal, Vol. 59, 91-100 (1995).

KARA, S., B. KELKAR, Y. T. Shah and N. L. CARR, "Hydrodynamics and axial mixing in a three-phase bubble column.", Industrial and Engineering Chemistry. Process Design and Development, Vol. 21, 584-594 (1982).

KAWAGOE, M., T. OTAKE and C. W. ROBINSON, "Gas-phase mixing in bubble columns.", Journal of Chemical Engineering of Japan, Vol. 22, 136-142 (1989).

KELKAR, B. G., S. P. GODBOLE, M. F. HONATH, Y. T. SHAH, N. L. CARR and W.-D. DECKWER, " Effect of addition of alcohols on gas holdup and backmixing in bubble columns.", American Institute of Chemical Engineering Journal, Vol. 29, 361-369 (1983).

KENNEL, M. B. and S. ISABELLE, "Method to distinguish possible chaos from noise and determine embeedding parameters.", Physical review A., Vol. 46, 3111-3118 (1992).

KIARED, K., F. LARACHI, C. GUY and C. CHAOUKI, "Trajectory length and residence-time distributions of the solids in three-phase
fluidized beds.", Chemical Engineering Science, Vol. 52, 3931-3939 (1997).

KIKUCHI, R., A. TSUTSUMI and K. YOSHIDA, "Fractal aspect of hydrodynamics in a three-phase fluidized bed.", Chemical Engineering Science, Vol. 51, 2865-2870 (1996).

KIKUCHI, R., T. YANO, A. TSUTSUMI, K. YOSHIDA, M. PUNCHOCHAR and J. DRAHOS, "Diagnosis of chaotic dynamics of bubble motion in a bubble column.", Chemical Engineering Science, Vol. 52, 3741-3745 (1997).

KIM, S. D. and Y. KANG, "Heat and mass transfer in three-phase fluidized-bed reactors- an overview.", Chemical Engineering Science, Vol. 52, 3639-3660 (1997).

KRISHNA, R., J. W. A. DE SWART, D. E. HENNEPHOF and J. ELLENBERGER, "Influence of increased gas density on hydrodynamics of bubble-column reactors.", American Institute of Chemical Engineering Journal, Vol. 40, 112-119 (1994).

LAPIN, A. and A. LÜBBERT, "Numerical simulation of the dynamics of two-phase gas-liquid flows in bubble columns.", Chemical Engineering Science, Vol. 49, 3661-3674 (1994).

LARACHI, F., M. CASSANELLO, J. CHAOUKI and C. GUY, "Flow structure of the solids in a 3-D gas-liquid-solid fluidized bed.", American Institute of Chemical Engineering Journal, Vol. 42, 2439-2452 (1996).

LARACHI, F., M. CASSANELLO, M.-N. MARIE, J. CHAOUKI and C. GUY, "Solids circulation pattern in three-phase fluidized beds containing binary mixtures of particles as inferred from RPT.", Transactions of the Institute of Chemical Engineers, Vol. 73, 263-268 (1995).

LEE, S. L. P. and H. I. DE LASA, "Phase holdups in three-phase fluidized beds.", American Institute of Chemical Engineering Journal, Vol. 33, 1359-1370 (1987).

LEE, S. L. P., A. SORIA and H. I. DE LASA, "Evolution of bubble length distributions in three-phase fluidized beds.", American Institute of Chemical Engineering Journal, Vol. 36, 1763-1767 (1990).

LEFEBVRE, S. and C. GUY, "Characterization of bubble column hydrodynamics with local measurements.", Chemical Engineering Science, Vol. 54, 4895-4902 (1999).

LEVENSPIEL, O., "Chemical reaction engineering", John Wiley & Sons, Oregon state university (1999).

LEVENSPIEL, O. and T. L. FITZGERALD, "A warning on the misuse of the dispersion model.", Chemical Engineering Science, Vol. 38, 491-493 (1983).

LI, Y., J. ZHANG and L.-S. FAN, "Numerical simulation of gas-liquid-solid fluidization systems using a combined CFD-VOF-DPM method: bubble wake behavior.", Chemical Engineering Science, Vol. 54, 5101-5107 (1999).

LINDT, J. T., "On the periodic nature of the drag on a rising bubble.", Chemical Engineering Science, Vol. 27, 1775-1781 (1972).

LINDT, J. T. and R. G. F. DE GROOT, "Drag on a single bubble accompanied by periodic wake.", Chemical Engineering Science, Vol. 29, 957-962 (1974).

LINNEWEBER, K. W. and E. BLASS, "Measurement of local gas and solid hold-ups in three-phase bubble columns.", German Chemical Engineering, Vol. 6, 28-33 (1983).

LÜBBERT, A. and B. LARSON, "A new method for measuring local velocities of the continous liquid phase in strongly aerated gas-liquid multiphase reactors.", Chemical Engineering and technologies, Vol. 10, 27-32 (1987).

LÜBBERT, A. and B. LARSON, "Detailed investigations of the multiphase flow in airlift tower loop reactors.", Chemical Engineering Science, Vol. 45, 3047-3053 (1990).

LUEWISUTTHICHAT, W., A. TSUTSUMI and K. YOSHIDA, "Chaotic hydrodynamics of continuous single-bubble flow systems.", Chemical Engineering Science, Vol. 52, 3685-3691 (1997).

MATSUURA, A. and L.-S. FAN, "Distribution of bubble properties in a gas-liquid-solid fluidized bed.", American Institute of Chemical Engineering Journal, Vol. 30, 894-903 (1984).

MIYAHARA, T., M. KURIHARA, M. ASODA and T. TAKAHASHI, "Gas-liquid interfacial area and liquid-phase mass transfer coefficient in sieve plate columns without downcomer operating at high gas velocities.", Journal of Chemical Engineering of Japan, Vol. 23, 280-285 (1990).

MODAK, S. Y., V. A. JUVEKAR and V. C. RANE, "Dynamics of the gas phase in bubble columns.", Chemical Engineering technologies, Vol. 16, 303-306 (1993).

MODAK, S. Y., V. A. JUVEKAR and V. C. RANE, "Comparison of the single-bubble-class and modified two-bubble-class models of bubble column reactors.", Chemical Engineering and technologies, Vol. 17, 313-32 (1994).

MOLERUS, O. and M. KURTIN, "Modelling of residence time distributions of the gas phase in bubble columns in the liquid circulation regime.", Chemical Engineering Science, Vol. 41, 2693-2698 (1986).

MUDDE, R. F., J. S. GROEN and H. E. A. VAN DEN AKKER, "Liquid velocity field in a Bubble Columns: LDA experiments.", Chemical Engineering Science, Vol. 52, 4217-4224 (1997).

MUDDE, R. F. and O. SIMONIN, "Two- and three-dimensional simulation of bubble plume using a two-fluid model.", Chemical Engineering Science, Vol. 54, 5061-5069 (1999).

MUROYAMA, K. and L.-S. FAN, "Fundamentals of gas-liquid-solid fluidization.", American Institute of Chemical Engineering Journal, Vol. 31, 1-34 (1985).

MURRAY, P. and L.-S. FAN, "Axial solid distribution in slurry bubble column.", Industrial and Engineering Chemistry Research, Vol. 28, 1697-1703 (1989).

MYERS, K., M. P. DUDUKOVIC and P. A. RAMACHANDRAN, "Modelling churn-turbulent bubble columns - I. Liquid-phase mixing.", Chemical Engineering Science, Vol. 42, 2301-2311 (1987).

NACEF, S., G. WILD, A. LAURANT and S. D. KIM, "Scale effects in gas-liquid-solid fluidisation.", International Chemical Engineering, Vol. 32, 51-72 (1992).

NASSAR, R., J. SCHMIDT and A. LÜBBERT, "A stochastic dispersion model in gas-liquid flow systems.", Chemical Engineering Science, Vol. 47, 3657-3664 (1992).

NAUMAN, E. B., " Residence time distribution in systems governed by the dispersion equation.", Chemical engineering Science, Vol. 36, 957-966 (1981).

NAUMAN, E. B. and B. A. Buffham, "Mixing in continuous flow systems", John Wiley & Sons, (1983).

NGUYEN, k., C. S. DAW, P. CHAKKA, M. CHENG, D. D. BRUNS, C. E. A. FINNEY and M. B. KENNEL, "Spatio-temporal dynamics in a train of rising bubbles.", The Chemical Engineering Journal, Vol. 65, 191-197 (1996).

OHKI, Y. and H. INOUE, "Longitudinal mixing of the liquid phase in bubble coumns.", Chemical Engineering Science, Vol. 25, 1-16 (1970).

OLMOS, E., C. GENTRIC, C. VIAL, G. WILD and N. MIDOUX, "Numerical simulation of multiphase flow in bubble column reactors. Influence of bubble coalescence and break-up.", Chemical Engineering Science, Vol. 56, 6359-6365 (2001).

PATEL, S. A., J. G. DALY and D. B. BUKUR, "Holdup and interfacial area measurements using dynamic gas disengagement.", American Institute of Chemical Engineering Journal, Vol. 35, 931-942 (1989).

PFLEGER, D., S. GOMES, N. GILBERT and H.-G. WAGNER, "Hydrodynamics simulations of laboratory scale bubble columns fundamental studies of the eulerian-eulerian modelling approach.", Chemical Engineering Science, Vol. 54, 5091-5099 (1999).

PRICHARD, D. and J. THEILER, "Generating surrogate data for time series with several simultaneaously measured variables.", Physical review letters, Vol. 73, 951-954 (1994).

RICHARDSON, J. F. and W. N. ZAKI, "Sedimentation and fluidization-Part 1.", Transactions of the Institute of Chemical Engineers, Vol. 32, 35-53 (1954).

RIGBY, G. R., G. P. VAN BLOCKLAND, P. E.H. and C. E. CAPES, "Properties of bubbles in three phase fluidized beds as measured by an electroresistivity probe.", Chemical Engineering Science, Vol. 25, 1729-1741 (1970).

ROGALEWICZ, V. and I. FORT, "Stochastic model of an agitated gas-liquid system.", Computers Chemical Engineering, Vol. 15, 437-444 (1991).

RUSTEMEYER, U., J. PAULI, T. MENZEL, R. BUCHHOLZ and U. ONKEN, "Liquid-Phase Mixing Model for Hydrodynamics of Bubble Columns.", Chemical Engineering and Processing, Vol. 26, 165-172 (1989).

SANYAL, J., S. VASQUEZ, S. ROY and M. P. DUDUKOVIC, "Numerical simulation of gas-liquid dynamics in cylindrical bubble column reactors.", Chemical Engineering Science, Vol. 54, 5071-5083 (1999).

SCHLÜTER, S., A. STEIFF and P. M. WEINSPACH, "Modeling and simulation of bubble column reactors.", Chemical Engineering and Processing, Vol. 31, 97-117 (1992).

SCHMIDT, J., R. NASSAR and A. LÜBBERT, "Influence of the wakes in bubble driven multiphase flow systems.", Chemical Engineering Science, Vol. 47, 2295-2300 (1992a).

SCHMIDT, J., R. NASSAR and A. LÜBBERT, "Local dispersion in the liquid phase of gas-liquid reactors.", Chemical Engineering Science, Vol. 47, 3363-3370 (1992b).

SCHUMPE, A. and W.-D. DECKWER, "Gas holdups, specific interfacial areas, and mass transfer coefficients of aerated carboxymethyl cellulose solutions in a bubble column.", Industrial and Engineering Chemistry. Process Design and Development, Vol. 21, 706-711 (1982).

SCHUMPE, A. and G. GRUND, "The gas disengagement technique for studying gas holdup structure in bubble columns.", The Canadian Journal of Chemical Engineering, Vol. 64, 891-896 (1986).

SHAH, Y. T., S. JOSEPH, D. N. SMITH and A. J. RUETHER, "Two-bubble class model for churn-turbulent bubble-column reactors.", Industrial and Engineering Chemistry. Process Design and Development, Vol. 24, 1096-1104 (1985a).

SHAH, Y. T., S. JOSEPH, D. N. SMITH and A. J. RUETHER, "On the behavior of the gas phase in bubble column with ethanol-water mixtures.", Industrial and Engineering Chemistry. Process Design and Development, Vol. 24, 1140-1148 (1985b).

SHAH, Y. T., B. G. KELKAR, S. P. GODBOLE and W.-D. DECKWER, "Design parameters estimation for bubble column reactors.", American Institute of Chemical Engineering Journal, Vol. 28, 353-379 (1982).

SHAH, Y. T., G. J. STIEGEL and M. M. SHARMA, "Backmixing in gas-liquid reactors.", American Institute of Chemical Engineering Journal, Vol. 24, 369-400 (1978).

SHETTY, S. A., M. V. KANTAK and B. G. KELKAR, "Gas-phase backmixing in bubble-columns reactors.", American Institute of Chemical Engineering Journal, Vol. 38, 1013-1026 (1992).

SIRAM, K. and R. MANN, "Dynamic gas disengagement: a new technique for assessing the bahaviour of bubble columns.", Chemical Engineering Science, Vol. 32, 571-580 (1977).

SOKOLICHIN, A. and G. EIGENBERGER, "Gas-liquid flow in bubble columns and loop reactors: part I. Detailed modelling and numerical simulation.", Chemical Engineering Science, Vol. 49, 5735-5746 (1994).

SOKOLICHIN, A., G. EIGENBERGER, A. LAPIN and A. LÜBBERT, "Dynamics numerical simulation of gas-liquid two-phase flows.", Chemical Engineering Science, Vol. 52, 611-626 (1997).

STEWART, C. W., "Bubble interaction in low-viscosity liquids.", International Journal of Multiphase Flow, Vol. 21, 1037-1046 (1995).

TANG, W. T. and L.-S. FAN, "Hydrodynamics of a three-phase fluidized bed containing low-density particles.", American Institute of Chemical Engineering Journal, Vol. 35, 355-364 (1989).

TARMY, B. L. and C. A. COULALOGLOU, "Alpha-omega and beyond industrial view of gas/liquid/solid reactor development.", Chemical Engineering Science, Vol. 47, 3231-3246 (1992).

THEILER, J., S. EUBANK, A. LONGTIN, B. GALDRIKIAN and J. DOYNE F., "Testing for nonlinearity in time series: the method of surrogate data.", Physica D, Vol. 58, 77-94 (1992).

TOWELL, G. D. and G. H. ACKERMAN, "Axial mixing of liquid and gas in large bubble reactors.", Proceeding of the symposium on chemical reaction engineering, Vol., Amsterdam, Holland, B3-1-B3-13. (1972).

TSUTSUMI, A., T. CHARINPANITKUL and K. YOSHIDA, "Prediction of solid concentration profiles in three-phase reactors by a wake shedding model.", Chemical Engineering Science, Vol. 47, 3411-3418 (1992).

TURI, E. and K. M. NG, "Axial distribution of soid particles in bubble column slurry reactors in the bubble flow regime.", Chemical Engineering Communications, Vol. 46, 323-345 (1986).

UEYAMA, K. and T. MIYAUCHI, "Properties of recirculating turbulent two phase flow in gas bubble columns.", American Institute of Chemical Engineering Journal, Vol. 25, 258-266 (1979).

VAN DER LAAN, G. P., A. A. C. M. BEENACKERS and R. KRISHNA, "Multicomponent reaction engineering model for Fe-catalyzed Fischer-Tropsch synthesis in comercial scale slurry bubble column reactors.", Chemical Engineering Science, Vol. 54, 5013-5019 (1999).

VERMEER, D. J. and R. KRISHNA, " Hydrodynamics and mass transfer in bubble columns operating in the churn-turbulent regime.", Industrial and Engineering Chemistry. Process Design and Development, Vol. 20, 475-482 (1981).

VILLERMAUX, J., "Génie de la réaction chimique : conception et fonctionnement des réacteurs", Paris : Tec & Doc Lavoisier, (1993).

VILLERMAUX, J., "Trajectory length distribution (TLD), a novel concept to characterize mixing in flow systems.", Chemical Engineering Science, Vol. 51, 1939-1946 (1996).

WACHI, S. and Y. NOJIMA, "Gas-phase dispersion in bubble columns.", Chemical Engineering Science, Vol. 45, 901-905 (1990).

WEBER, M. E. and D. BHAGA, "Fluid drift caused by a rising bubble.", Chemical Engineering Science, Vol. 37, 113-116 (1982).

WILD, G., M. SABERIAN, J.-L. SCHWARTZ and J.-C. CHARPENTIER, "Gas-liquid-solid fluidized-bed reactors. State of the art and industrial possibilities.", International Chemical Engineering, Vol. 24, 639-678 (1984).

YANG, Y. B., M. P. DUDUKOVIC and M. P. DUDUKOVIC, "Liquid backmixing in bubble column via computer-automated radioactive particle tracking (CARPT).", Experiments in fluids, Vol. 16, 1-9 (1993).

YAO, B. P., C. ZHENG, H. E. GASCHE and H. HOFMANN, "Bubble behaviour and flow structure of bubble columns.", Chemical Engineering and Processing, Vol. 29, 65-75 (1991).

ZAHRADNIK, J. and M. FIALOVA, "Effect of bubbling regime on gas and liquid phase mixing in bubble column reactors.", Chemical Engineering Science, Vol. 51, 2491-2500 (1996).

APPENDIX

The present appendix contains the development of the Log-Normal-Convective/ADM model (LNC/ADM model). The following relation (eq A1) defines the fraction of the fluids elements (of the whole population) having a residence time between t and $t+dt$.

$$E(t)\,dt = \textit{fraction of the fluids elements (of the whole population) having a residence time between } t \textit{ and } t+dt \qquad \text{(A1)}$$

The following relation (eq A2) defined the fraction of the fluids elements having a mean velocity between u and $u+du$.

$$f(u)\,du = \textit{fraction of the fluids elements having a mean velocity between } u \textit{ et } u+du \qquad \text{(A2)}$$

The following relation (eq A3) defined the fraction of a RTD having a residence time between t and $t+dt$ and conditional to a fluid element having the mean velocity u.

$$E_{ADM}(t,u)\,dt = \textit{fraction of a RTD having a residence time between } t \textit{ and } t+dt \textit{ and conditional to a fluid element having the mean velocity } u \qquad \text{(A3)}$$

Equation (A4) may thus be written. It represents the fraction of fluids elements having a residence time between t and $t+dt$ due to fluids element having a mean velocity between u et $u+du$.

$$\left[E(t)\,dt\right]_u = \left[E_{ADM}(t,u)\,dt\right]\left[f(u)\,du\right] \tag{A4}$$

In order to obtain the total fraction of the RTD having a residence time between t and $t+dt$, equation (A4) is integrated over the all fluids elements mean velocity (see eq (A5)).

$$E(t)\,dt = \int_0^\infty \left\{f(u)\,E_{ADM}(t,u)\,dt\right\} du \tag{A5}$$

RTD of the fluids elements population ($E(t)$) is obtained by integration and derivation (relative to t) of equation (A5) combined with equations (9) and (10) and by using the Fubini theorem. The final result is shown in equation (11).

$$E_{LNC/ADM}(t) = E(t) = \frac{1}{\pi\beta\sqrt{8Dax\,t}} \int_0^\infty \exp\left[-\frac{\left(Ln(u)-\alpha\right)^2}{2\beta^2} - \frac{\left(L-uL\right)^2}{4Dax\,t}\right] du \tag{11}$$

CHAPITRE 3 : MÉTHODOLOGIE

3.1 Méthodologie générale

En première étape de l'atteinte du premier objectif de la thèse, la revue critique de la littérature présentée au chapitre précédent a été réalisée. Les caractéristiques clés liées à l'hydrodynamique des phases (et leurs interactions) dans un lit fluidisé à trois phases ont été identifiées. De plus, les méthodes et outils utilisés afin de diagnostiquer les mécanismes de mélange ont été généralisés et leurs limites ont été soulevées. La revue critique de la littérature a permis de développer un modèle d'écoulement schématique tenant en compte l'interaction entre les mécanismes de mélange des trois phases.

En deuxième étape de l'atteinte du premier objectif, le modèle d'écoulement schématique a été exploité à l'aide de données obtenues grâce à la technique de suivi d'une particule radioactive (RPT : « Radioactive Particle Tracking »). Les données de RPT viennent de deux montages contenant chacun un lit fluidisé à trois phases de diamètres différents. Ces données ont permis de quantifier des paramètres hydrodynamiques des phases dans un lit fluidisé à trois phases. Cela a offert une meilleure compréhension de l'hydrodynamique de la phase solide et a permis de compléter l'atteinte du premier objectif de la thèse.

Basé sur les résultats des études ayant permis d'atteindre le premier objectif, un modèle de mélange de la phase solide, le plus simple possible mais respectant les caractéristiques clés liées à l'hydrodynamique, a été développé afin de répondre au deuxième objectif de la thèse. Le modèle a été exploité à l'aide des données de RPT mesurées sur les deux lits fluidisés à trois phases. La majorité des paramètres du modèle ont été évalués à l'aide de relations et d'estimations obtenues en deuxième étape de l'atteinte du premier objectif. Les autres paramètres, trois pour être exact, ont

été estimés par régression sur des résultats de tests de traceur de la phase solide obtenus par la méthode de RPT.

Les prochaines sections décrivent les montages expérimentaux, les conditions opératoires et la technique de RPT.

3.2 Montages expérimentaux

Les expériences ont été réalisées sur deux montages contenant chacun un lit fluidisé co-courant à trois phases de diamètre différent. Les colonnes des deux lits fluidisés étaient en plexiglass. Le plus petit lit fluidisé avait un diamètre de 0.10 m. Pour ce dernier, les résultats de RPT ont été obtenus grâce à des travaux antérieurs à la présente thèse et ont déjà fait l'objet de publications, comme par exemple Larachi et al. (1995), Cassanello et al. (1995), Larachi et al. (1996) et Kiared et al. (1997). Un nouveau montage contenant une colonne de 0.292 m de diamètre a été dimensionné et construit durant la présente thèse. Il faut remarquer qu'il y a peu d'études réalisées avec un lit fluidisé de cette taille. La plupart des études ont été réalisées avec des lits fluidisés de 0.20 m et moins, pour lesquels les effets de parois sont plus importants qu'à 0.292 m.

La colonne de 0.10 m a une hauteur de 1.5 m. Le distributeur des phases liquide et gazeuse est montré à la Figure 3.1 et se décrit comme suit. Le liquide est alimenté par la base conique de 0.15 m de haut et qui contient un lit fixe de billes de verre de 5 mm de diamètre. Le liquide passe ensuite à travers une plaque perforée ayant une surface ouverte de 5.5 %, ainsi que des orifices de 0.74 mm de diamètre espacés de 2 mm et suivant un arrangement triangulaire. La plaque perforée supporte un autre lit fixe de 0.20 m de haut, mais constitué de billes de verre ayant un diamètre de 2 mm. Les billes de 2 mm sont retenues par un grillage fin. Les particules composant le lit fluidisé s'appuient sur ce grillage fin. Le gaz passe à travers trois tubes poreux (le diamètre des pores est de 20 μm) situés juste sous la plaque perforée. Les tubes poreux sont

distancés par un angle de 120°. Le liquide et le gaz sont donc pré-mélangés avant d'entrer dans le lit fluidisé.

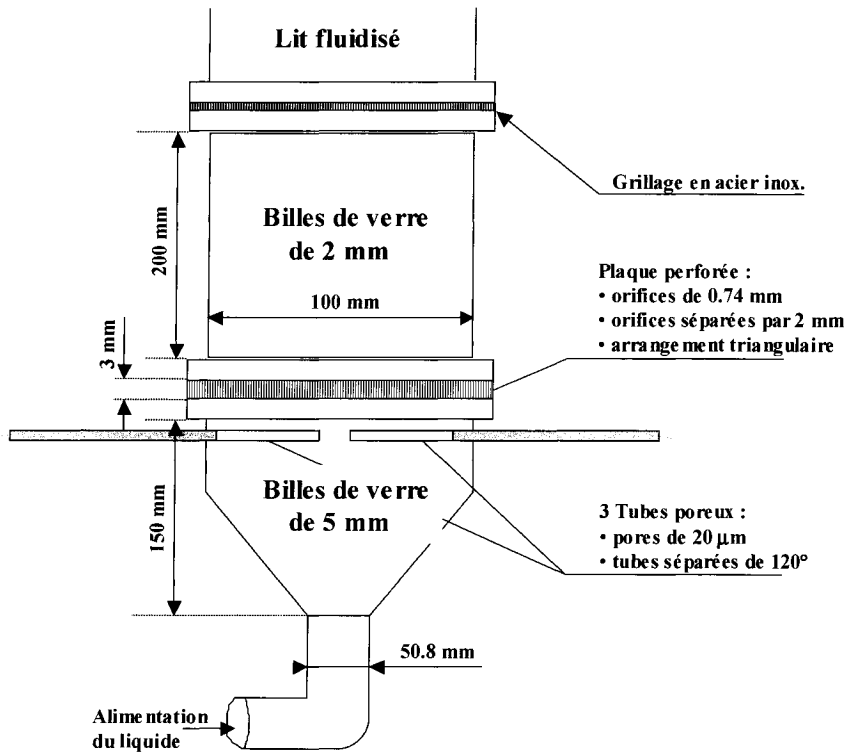


Figure 3.1 : Système de distribution du lit fluidisé à trois phases de 0.10 m. Adapté de Larachi et al. (1996).

La colonne de 0.292 m a une hauteur de 2.7 m. Contrairement au lit fluidisé de 0.10 m, l'alimentation du liquide et du gaz se fait séparément. La Figure 3.2 montre le dessin du distributeur. Le liquide est alimenté par une base conique (non montré sur la figure), puis passe à travers les 268 orifices de 2 mm de diamètre d'une plaque perforée (4000 orifices/m^2). Un arrangement rectangulaire de 9x27 mm sépare les orifices. La vitesse du liquide à travers les orifices est de 4 m/s pour une vitesse superficielle de 0.05 m/s. Cette vitesse est supérieure a celle retrouvée sur les distributeurs décrits dans

la littérature, soit de 1 à 1.5 m/s. Une vitesse de 4 m/s est donc adéquate pour opérer une pression dans la base conique suffisamment grande pour que le liquide passe uniformément à travers tous les orifices.

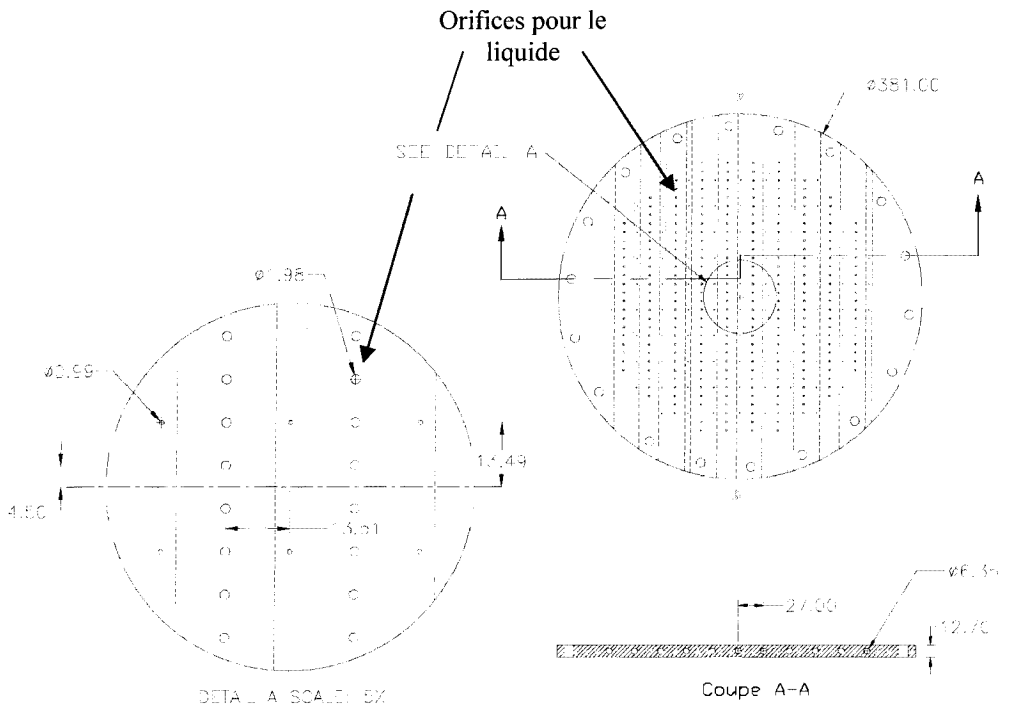


Figure 3.2 : Système de distribution du lit fluidisé à trois phases de 0.292 m. Les dimensions sont en mm.

Le gaz est alimenté par 11 conduites horizontales de 6.35 mm de diamètre percées à travers la plaque perforée, entre les orifices du liquide. Le gaz est alimenté sur chaque côté des conduites et entre dans le lit fluidisé à travers 94 orifices de 1 mm de diamètre (1400 orifices/m^2). Les orifices sont espacées de 27 mm en un arrangement

carré. Le distributeur du gaz a été dimensionné de façon à respecter le critère (Nigam and Schumpe, 1996) suivant basé sur le nombre de Weber :

$$\frac{u_{go}^2 d_o \rho_g}{\sigma} \geq We_{go,crit} = 2$$

où u_{go} est la vitesse du gaz à travers les orifices, d_o est le diamètre des orifices où passe le gaz, ρ_g est la densité du gaz, σ est la tension de surface. Un distributeur qui a un nombre de Weber plus grand que le critère ($We_{go,crit}$) de 2 permet d'avoir des bulles qui se forment à chaque orifice.

Des inspections visuelles et des tests de fluidisation ont permis de constater que ce type de distributeur donne une bonne distribution du gaz et du liquide.

Chaque montage permet de faire circuler le liquide en boucle fermée. Dans le haut des colonnes, un système de trop plein sépare le gaz du liquide. Ce dernier est acheminé à un bassin tampon qui alimente la pompe de façon à respecter ces spécifications. Des rotamètres sont utilisés pour contrôler et mesurer les débits de gaz et de liquide pour le montage contenant le lit fluidisé de 0.10 m. Des plaques à orifices ont été dimensionnées et construites afin de contrôler et de mesurer les débits de gaz et de liquide pour le montage contenant le lit fluidisé de 0.292 m.

3.3 Conditions opératoires et systèmes

De l'eau municipale a été utilisée comme liquide de fluidisation et de l'air compressé a été utilisé comme phase gazeuse. Les expériences ont été réalisées aux conditions ambiantes.

Le Tableau 3.1 contient les conditions expérimentales des différents tests effectués. L'intervalle des vitesses superficielles du gaz et du liquide est de 0.010-0.106 m/s et 0.042-0.065 m/s, respectivement. Les systèmes de particules utilisés sont :

(1) Systèmes de particule simple : billes de verres de 3 mm (GB3, 2475 kg/m^3) ; particules en PVC de 5.5 mm (PVC5.5, 1320 kg/m^3)
(2) Systèmes binaires de particule : GB3GB0.9; GB3GB5; GB3PVC5.5

Le Tableau 3.1 donne quelques propriétés des particules utilisées. Il faut noter que les particules en PVC ont une forme hexagonale et ont été rendues hydrophiles à l'aide d'un traitement chimique dans une solution aqueuse de H2SO4/K2Cr2O7 selon la procédure de Linek et al. (1974).

Tableau 3.1 : Conditions expérimentales.

Run	UL	Ug	Système de particules [1]	Masse totale du lit [2]	$Umf_{Ug=0}$ [3]	u_t [4]
(#)	(m/s)	(m/s)		(kg)	(m/s)	(m/s)
Dc = 0.10 m						
1	0.065	0.032	GB3	4.0	0.036	0.37
2	0.065	0.069	GB3	4.0	0.036	0.37
3	0.065	0.106	GB3	4.0	0.036	0.37
4	0.065	0.106	{GB3}GB0.9	2.8	{0.036}0.009	{0.37}0.14
5	0.058	0.010	PVC5.5	0.8	0.023	0.23
6	0.058	0.025	PVC5.5	0.8	0.023	0.23
7	0.065	0.032	{GB3}GB5	3.0	{0.036}0.051	{0.37}0.47
8	0.065	0.032	GB3{GB5}	3.0	0.036{0.051}	0.37{0.47}
9	0.065	0.032	{GB3}PVC5.5	1.7	{0.036}0.023	{0.37}0.23
Dc = 0.292 m						
10	0.042	0.031	GB3	88	0.036	0.37
11	0.042	0.050	GB3	88	0.036	0.37
12	0.042	0.080	GB3	88	0.036	0.37
13	0.051	0.031	GB3	88	0.036	0.37
14	0.051	0.051	GB3	88	0.036	0.37
15	0.051	0.080	GB3	88	0.036	0.37
16	0.062	0.031	GB3	88	0.036	0.37
17	0.062	0.051	GB3	88	0.036	0.37
18	0.062	0.080	GB3	88	0.036	0.37

[1] GB: Billes de verre. Le nombre attaché indique le diamètre de la particule en mm. { }: indique la particule suivie.

[2] Pour les systèmes binaires, le ratio volumique est d'environ 1:1. 1.10 kg de billes de verre et 0.62 kg de particule en PVC compose les systèmes GB/PVC. La fraction de vide au repos est d'approximativement 0.41 et 0.61 pour, respectivement, les billes de verre et les particules en PVC.

[3] La vitesse minimale de fluidisation du système liquide-solide a été calculé par la corrélation de Grace (1982). Valider pour les billes de verre dans le lit de 0.292 m.

[4] La vitesse terminale des particules dans l'eau a été calculée à l'aide de la corrélation de Schiller and Nauman (1933).

3.4 Technique de suivi d'une particule radioactive (RPT)

La technique non-intrusive de suivi d'une particule radioactive développée par l'équipe du professeur Chaouki (Larachi et al., 1994) a été utilisée. Cette technique se nomme en anglais « Radioactive Particle Tracking » (RPT). Elle permet de suivre une particule radioactive (émettant des rayons gamma) ayant les mêmes densité et diamètre que les particules constituant le lit fluidisé. Les trois coordonnées spatiales (x,y,z) sont obtenues en fonction du temps.

La technique de RPT consiste à installer des détecteurs cylindriques à scintillation (NaI(TI)) autour de la colonne contenant le lit fluidisé. La Figure 3.3 montre un arrangement typique. Huit détecteurs (dimension 76x76 mm) ont été utilisés pour le lit de 0.10 m. Sur une vue de dessus, les détecteurs ont été distancés par des angles de 90° (quatre détecteurs doivent être enlevés sur la vue de dessus de la Figure 3.3). Il y a deux niveaux de détecteurs, et la position axiale de chaque détecteur est variable et ajustée de manière à couvrir le plus grand volume possible dans le lit. Pour le lit fluidisé de 0.292 m, seize détecteurs ont été installés autour de la colonne. Il y avait aussi deux niveaux et les détecteurs étaient distancés par des angles de 45° (vue de dessus de la Figure 3.3). La position axiale de chaque détecteur a aussi été ajustée de manière à couvrir le plus de zones possibles dans le lit.

Une particule (GB ou PVC) contenant du ^{46}Sc (isotope) a été utilisée. Le ^{46}Sc a été obtenu par bombardement aux neutrons sur du ^{45}Sc dans le réacteur nucléaire Slowpoke de l'école polytechnique de Montréal. L'activité du ^{46}Sc était de 50 et de 200 μCi pour les lits de 0.10 et de 0.292 m, respectivement. L'intensité des rayons gamma (ou le compte de photons) émis par le ^{46}Sc a été mesurée par les détecteurs à scintillation. L'intensité lue par un détecteur dépend de la distance entre la particule radioactive dans le lit et le détecteur, du facteur de vue de la particule sur le détecteur et de l'atténuation du lit. En utilisant la lecture de chaque détecteur, une technique de

triangulation a été utilisée afin de trouver la position instantanée de la particule à toutes les 30 ms. La position de la particule a été suivie durant 5 à 6 heures pour chaque expérience.

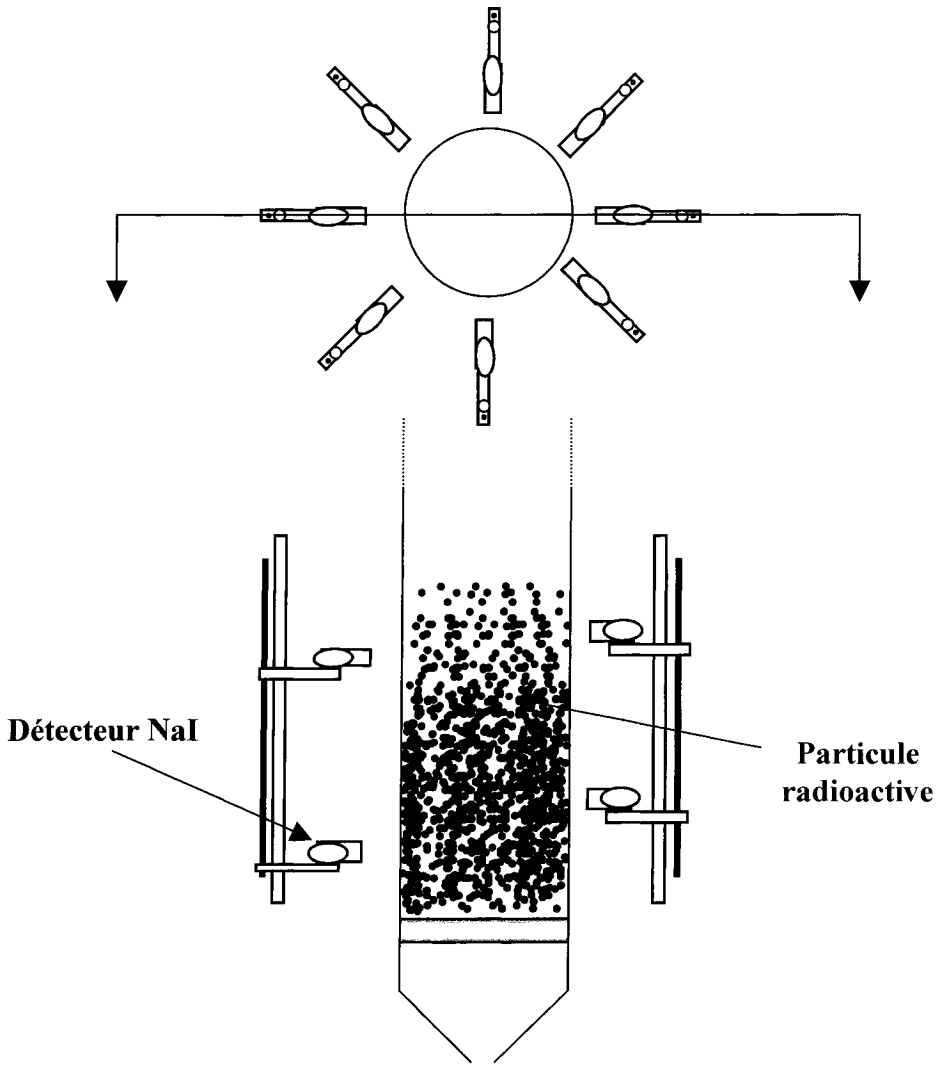


Figure 3.3 : Arrangement typique des détecteurs à rayon gamma autour d'un lit fluidisé.

Pour chaque expérience, une calibration des détecteurs a été effectuée. Le lit était fluidisé aux conditions de l'expérience et l'intensité de chaque détecteur était mesurée pour 150 positions connues de la particule radioactive dans le lit fluidisé. Quinze tubes, traversant à tour de rôle tout le diamètre de la colonne, ont servi à positionner la particule radioactive. Les tubes étaient placés sur trois rangées suivant l'axe de la colonne. Les trois rangées étaient distancées par des angles de 45°. Trois paramètres du modèle quantifiant l'intensité des détecteurs étaient optimisés par régression pour chaque détecteur, soit le coefficient d'atténuation linéaire du milieu gaz-liquide-solide, le temps mort du détecteur et l'activité de la source radioactive.

Une activité de 200 μCi a été utilisée pour le lit de 0.292 m au lieu du 50 μCi utilisé pour le lit de 0.10 m. Une activité de 200 μCi a été utilisée à cause de la longueur d'atténuation qui est plus importante dans le lit 0.292 m lorsque la particule radioactive se trouve au centre de la colonne. En effet, à 50 μCi, l'intensité lue par les détecteurs est trop faible pour donner une position précise de la particule radioactive. Cependant, à 200 μCi, un détecteur situé trop près de la particule radioactive est « saturé ». Dans ce cas, lorsque la réponse du détecteur ne change plus quand la particule radioactive se rapproche, le détecteur est dit non-paralysable. Pour ce type de détecteur, lorsqu'un photopic est détecté, il ne répond pas pour une période correspondant à son temps mort. Lorsque la particule radioactive est très près d'un tel détecteur, un nouveau photopic est détecté juste après le temps mort. L'intensité mesurée par le détecteur non-paralysable donne une valeur maximale qui ne varie plus en fonction de la distance entre la particule et le détecteur. Un détecteur peut être paralysable. Dans ce cas, plusieurs photopics qui se superposent sur des périodes couvrant le temps mort comptent pour un seul compte. Dans ce cas, l'intensité lue par le détecteur paralysable diminue au fur et à mesure que la particule radioactive se rapproche du détecteur à une distance inférieure à la distance de « saturation ». La réponse de ces deux types de détecteurs peut être modélisée (Knoll, 1994).

Les programmes compris dans la technique de RPT ont dû être modifiés afin de tenir en compte de ces deux types de détecteurs à cause de la forte activité de la source utilisée pour le lit de 0.292 m. Lors des calculs de calibration (régression), le programme choisissait le modèle représentant le mieux chacun des 16 détecteurs. Les programmes calculant la position de la particule radioactive ont aussi été modifiés. Lorsque la particule source est à l'intérieur de la distance de saturation des détecteurs non-paralysables, ce dernier n'est pas utilisé dans la procédure de positionnement de la particule. Pour les détecteurs paralysables, la procédure de positionnement tient en compte la lecture du détecteur même quand la particule est à l'intérieur de la zone où l'intensité diminue au fur et à mesure que la particule se rapproche du détecteur. Il faut noter que presque tous les détecteurs ont été identifiés comme étant paralysables.

CHAPITRE 4 : HYDRODYNAMIQUE DE LA PHASE SOLIDE – UN MÉCANISME CONVECTIF/DISPERSIF [2]

4.1 Présentation de l'article

Le modèle schématique proposé à la revue critique de la littérature a permis de répondre qualitativement au premier objectif de la thèse. Afin de répondre quantitativement au premier objectif, des données sur la phase solide mesurées à l'aide de la technique de suivie d'une particule radioactive (RPT) ont été obtenues sur le nouveau lit fluidisé à trois phases de 0.292 m de diamètre. Des données de RPT mesurées avant cette thèse pour un lit fluidisé à trois phases de 0.10 m ont été traitées. Cela a permis d'étudier l'effet de davantage de conditions opératoires. Les paramètres du modèle schématique ont été estimés pour la phase solide. L'analyse de ces paramètres a permis de mieux comprendre l'effet des conditions opératoires sur l'importance relative des mécanismes de mélange entre eux et sur l'intensité de mélange de la phase solide pour les lits fluidisés à trois phases.

---

[2] Soumis dans « International Journal of Chemical Reactor Engineering ».

4.2 Solid Phase Hydrodynamics of a Three-Phase Fluidized Bed –

Lefebvre, S., Chaouki, J. Guy, C.

4.2.1 Abstract

The objective of this work was to investigate the relative contribution of the convective and dispersive mixing mechanisms to the overall solid phase mixing mechanism for three-phase fluidized bed reactors. Noninvasive Radioactive Particle Tracking (RPT) data were obtained at various operating conditions, reactor diameters and particle systems. The structural wake model was updated and consists of three sub-phases: the particle wake and downflow-emulsion phase following the convective mixing mechanism and the vortex-emulsion phase following the dispersive mixing mechanism. The particle velocity mean and STD increased with the superficial liquid and gas velocity as well as the reactor diameter for each particle phase. Therefore, the extent of mixing increased under these operating parameters. The particle phase's holdup and a new Mixing Mechanism Indicator (MMI), however, exhibited a much more complex trend. For the larger reactor (Dc = 0.292 m), the convective mixing mechanism dominated and at low superficial liquid velocity the contribution of the convective mixing mechanism increased with superficial gas velocity. This trend, however, was reversed when the superficial liquid velocity increased. For the smaller reactor (Dc = 0.10 m), the random movement of the solid dominated. Therefore, the extent of mixing and the mixing mechanism did not follow the same trend. The CFD and the mixing model have to follow both those hydrodynamic properties. Relations to estimate mean and STD particle velocity distribution as well as particle phase holdup were developed. Solid in the established region mainly followed the convective mixing mechanism. Random movement of the solid was mostly observed at the top of the bed, but it was also present in the established region and at the bed bottom. The volume of

each region depended on the operating conditions, reactor diameter and particle system. Furthermore, the particle wake expulsion frequency range was similar to the wake shedding frequency found in literature. It is, thus, possible to assume that wake shedding was mainly responsible for the solid exchange between particle phases.

4.2.2 INTRODUCTION

Applications for three-phase fluidized bed reactors are varied. Petrochemical, chemical, biological and mineral industries often use three-phase fluidized bed reactors in their processes. There is no model in the literature that is able to accurately predict these reactors' performance (conversion and selectivity) when the kinetics are fast and the mass transfer is limiting. This may be easily explained by an obvious observation: the existing models do not take into account the fundamental mixing mechanisms characterizing three-phase fluidized bed reactors.

The CFD model calculates flow pattern with microscopic momentum balance and/or with force balance on discrete elements. Microscopic mass balance is used as a constraint. The momentum and mass balance equations are fundamental relations, but empirical closure relations have to be used in order to solve the system of equations. These empirical closure relations often come from singlephase systems and are adapted to multiphase reactors. This type of relation dilutes the fundamental nature of CFD modeling because closed relations are not fundamentals relations. For the mixing model, the flow pattern is assumed instead of calculated and mass balance is applied based on that flow pattern. This approach requires a good knowledge of hydrodynamics. This article helps to understand better the solid phase hydrodynamics that will be incorporated in a new phenomenological mixing model (demonstrated in a future paper). This article also contains useful data for CFD modeling and shows the phenomenology that must be taken into account in the CFD modeling.

More precisely, for mixing and CFD models, knowing the relative importance of the convective mixing mechanism to the dispersive mixing mechanism is essential for the reactor's prediction performance, design and scale-up. The study of parameters affecting the relative importance of mixing mechanisms is investigated in this article. Analysis of the effect of the operating conditions, column diameter and particle system on such parameters is reported and relations are proposed. These relations give information to help develop models that follow not just mixing extent, but also the mixing mechanisms versus various situations. In other words, the ***objective*** of this work is to compute parameters that will investigate the relative contribution of the convective and dispersive mixing mechanisms on the overall solid phase mixing mechanism.

4.2.3 MODEL CONCEPT AND MIXING MECHANISMS

The sedimentation-dispersion model is widely used to represent solid phase mixing. This model is a modified version of the Axial Mixing Model (ADM). A plug flow behavior superimposed onto a diffusion-like process (Fickian term) is assumed. The velocity used is the difference between the upflow and downflow velocity of the particles. Jean et al. (1989) identified several definitions of the upflow and downflow particle velocities used in literature.

Another widely used solid phase mixing model family was inspired by the flow representation of Bhatia and Epstein (1974) and was later modified by Fan (1989). This flow representation is called the structural wake model and is shown in Figure 4.1. The solid phase is divided into two particle phases. Note that in order to reduce the confusion between the solid phase (equivalent to the liquid and gas/bubble phase) and the divisions of the solid phase, the divisions will be called ***particle phases***. With such nomenclature, the structural wake model divides the solid phase into the ***particle wake phase*** and the ***particle emulsion phases***. The structural wake model has been used by

various authors (El-temtamy and Epstein, 1980; Dayan and Zalmanvich, 1982; Turi and Ng, 1986; Tang and fan, 1989; Murray and fan, 1989; Tsutsumi et al., 1992 and Cassanello et al., 1996, Knesebeck and Guardani, 2004) in order to develop a solid phase mixing model for three-phase fluidized bed and slurry reactors. Lefebvre et al. (2004) reviewed the literature on phenomenological gas, liquid and solid mixing models, i.e., other than the axial dispersion model. This literature review made the link between fundamental mechanisms followed by the gas, liquid and solid phases.

The solid phase mixing models based on the structural wake model assumed that the solid in the particle wake phase rises at the average bubble velocity and follows a plug flow behavior. Depending on the conditions, such as the solid concentration at the liquid inlet, the solid in the particle emulsion phase may go up or down. The solid phase mixing model developed for a three-phase fluidized bed often assumed that the solid went down at the settling particle velocity and also followed a plug flow behavior. A wake/emulsion solid exchange is considered as the dominant solid phase mixing mechanism, which is equivalent to the dispersive mixing mechanism.

Since solid is transported into the bubble wake, it is natural to assume that the solid in the particle wake phase follows the same mixing mechanism as the gas phase. Therefore, it is important to understand the gas phase mixing mechanism. Bubbles do not rise at only one velocity. Bubbles rise at various velocities following a log-normal velocity distribution in the three-phase fluidized bed (Matsuura and Fan, 1984). Hyndman and Guy (1995a) have shown that the bubble phase follows a convective mixing mechanism (Levenspiel and Fitzgerald, 1983) in bubble column reactors. This means that each bubble rises with a constant velocity along the reactor height. The spread of the Residence Time Distribution (RTD) and the standard deviation of the velocity distribution are due to the various Lagrangian constant velocities instead of a random velocity change along the reactor height, which is the definition of the

dispersive mixing mechanism. The sedimentation-dispersion model follows the dispersive mixing mechanism. Representations of this kind of mixing mechanism are presented in Figure 4.2. The turbulent mixing mechanism (Grossman and Procaccia, 1984) is also shown in this figure. The turbulent mixing mechanism is characterized by the particles (or fluid elements) transferred from eddies to eddies. This mixing mechanism needs to be represented in at least 2D. In a 1D representation, a dispersive mixing behavior will be observed.

Larachi et al. (1995) demonstrated that particles often rise with a constant Lagrangian velocity in a three-phase fluidized bed. These particles are probably in the bubble wake. Cassanello et al. (1995) showed with Hursts' exponent analysis that the solid phase follows a superdispersive mechanism. This means the solid movement is faster than the dispersive movement (diffusion like process), which is the case of the convective mixing mechanism.

Larachi et al. (1995) have also shown that the particles often go downward with a constant Lagrangian velocity. This was attributed to a compensatory effect of the upward convective solid movement. They also observed a third kind of particle movement, i.e., particles having random movement. This random particle movement was linked to the vortical flow region identified by Tzeng et al. (1993) and Chen et al. (1994).

Based on the above literature finding, the structural wake model was modified in order to take into account the various bubble wake velocities and the random movement of the particles (Lefebvre et al., 2004). Figure 4.3 shows the updated version of the structural wake model. The emulsion phase is divided into two phases, i.e., the ***vortex-emulsion phase*** and the ***upfow/downflow-emulsion phase***. The bubble phase, i.e., the gas phase, is divided into various bubble classes. A particle/liquid wake class is

attached to each bubble class. Therefore, the liquid and solid in the bubble wake follows not only the average bubble velocity, but also the velocity distribution of the bubbles.

This flow representation is coherent when the convective is superimposed onto the dispersive mixing mechanism as observed in the liquid phase (Lübbert and Larson, 1990; Yang et al., 1993; Lefebvre and Guy, 1999) and solid phases (Larachi et al., 1995; Cassanello et al., 1995) in systems containing gas bubbles. With this flow representation it is possible to adjust the relative importance of the convective to the dispersive mixing mechanism, which depends on the relative importance of the mean and variance velocity distribution of the three particle phases. It also depends on the particle phase holdup and exchange between particle phases. These parameters were quantified with Radioactive Particle Tracking (RPT) data obtained at various superficial gas and liquid velocities, column diameters and particle systems.

4.2.4 EXPERIMENTAL

4.2.4.1 Experimental Setups

Data were obtained from two different size co-current upward three-phase fluidized bed reactors and for various particle systems. Water was used as the fluidized media and air was the gas phase. Experiments were done at ambient temperature and pressure.

The smaller column has a diameter of 0.10 m. RPT data obtained in this column have already been published in previous articles, e.g., Larachi et al. (1995), Larachi et al. (1996), Cassanello et al. (1995), Kiared et al. (1997). In a new larger column 0.292 m in diameter, 9 new sets of RPT data were obtained. In total, 18 sets of RPT data were used here. Table 4.1 shows the experimental conditions. The range of

superficial gas and liquid velocities was 0.010-0.106 m/s and 0.042-0.065 m/s, respectively. The particle systems used were:

- Single particle systems: 3 mm glass beads (GB, 2475 kg/m^3) ; 5.5 mm PVC (1320 kg/m^3)
- Binary particle systems: GB3GB0.9; GB3GB5; GB3PVC5.5

Table 4.1 lists some particle properties. Note that PVC particles had a hexagonal shape and were rendered wettable by chemically treating it with an $H_2SO_4/K_2Cr_2O_7$ aqueous solution according to a procedure described by Linek et al. (1974).

The 0.10 m column has a height of 1.5 m. To distribute the liquid, the water was first fed into a packed conical-base bed 0.15 m high containing 5 mm glass beads. Secondly, the water crossed a perforated plate (5.5 % open area with 0.74 mm holes arranged in a 2 mm triangular pitch) that supported another packed bed 0.20 m high containing 2 mm glass beads retained by a fine mesh screen. The fluidized particles were settled on the fine mesh screen. The air was fed at the conical-base with three horizontal tube injectors situated just beneath the perforated plate. These horizontal tube injectors were porous (20 μm pore size) and were spaced 120° apart. Gas and liquid were, therefore, pre-mixed before entering the fluidized bed. More details on the experimental setup may be found in Larachi et al. (1996).

The 0.292 m column has a height of 2.7 m. Contrary to the 0.10 m column, the air and water feed were separated. Figure 4.4 shows the distributor. The water distributor was a perforated plate. The water was fed into the column by a conical winbox and crossed 268 2-mm holes (4000 holes/m^2) in the perforated plate arranged in a rectangular pattern 9x27 mm. The liquid velocity through the holes was about 4 m/s for a superficial liquid velocity of 0.05 m/s, which was higher than that found in literature

(1-1.5 m/s). With this there were enough distributor pressure drops to distribute the liquid uniformly across all of the holes. The gas was fed into 11 horizontal conduits hollowed out directly in the perforated plate. The conduit diameter was 6.35 mm. The gas was fed into each side of the conduits and entered the bed via 94 1-mm holes (1400 holes/m^2). The square pitch was 27 mm. The gas distributor was designed so that the Weber number of the gas flows through the holes was larger than 2 (Nigam and Schumpe, 1996). Bubbles are, thus, form at each hole. This gas-liquid distributor provides very good distribution for both the gas and liquid phases.

For both reactors, the water was circulated in a closed loop. On top of the columns, an overflow system separated the gas from the liquid. A buffer vessel was installed in order to use the pumps properly. For the 0.10 m column, the fluid flow was controlled by rotameters. Homemade orifice flow meters were used to control the fluid flow in the 0.292 m column setup.

4.2.4.2 Radioactive Particle Tracking (RPT)

The noninvasive Radioactive Particle Tracking (RPT) technique developed by Chaouki's team was used (Larachi et al., 1994). This technique follows one radioactively marked particle having the same diameter and density as the bed particles. The 3D position of the particle versus time was obtained. Solid parameters, such as particle velocities, particle phase holdup and spending time can be computed to study solid phase hydrodynamics.

The RPT technique consists of arranging various 76x76 mm uncollimated and unshielded NaI(TI) cylindrical scintillation detectors around the studied reactor. Eight detectors were used for the 0.10 m column and 16 for the 0.292 m column. A ^{46}Sc filled particle (GB and PVC) was used as the traced particle and has the same diameter and density as the bed particles. The ^{46}Sc was obtained using neutron radiative capture

by ^{45}Sc in the Ecole Polytechnique Slowpoke nuclear reactor. Radioactivity of the ^{46}Sc was 50 and 200 μCi for the 0.10 and the 0.292 m columns, respectively. The γ-ray emitted by the ^{46}Sc was detected by the scintillation detectors. A detector photon count depends on the traced particle location in the bed, the corresponding subtended effective solid angle and the bed attenuation. Using the photon count of each detector, a triangulation techniquewas used to yield the instantaneous traced particle position at 30 ms intervals. Data were collected over 5-6 hours for each experiment.

Prior to each experiment, the bed was fluidized and a set of measurements of the γ-ray photon count was made to calibrate the system using the traced particle rigidly positioned at 150 representative and known locations throughout the bed. Three parameters were fitted for each experiment: the linear attenuation coefficient of the gas-liquid-solid emulsion, the detectors dead time and the source radioactivity.

4.2.5 RPT DATA TREATMENT AND PARAMETER DEFINITION

An example of the traced particle axial position time series obtained in the 0.292 m column was illustrated in Figure 4.5. The pattern was the same for the 0.10 m column, which was already shown in literature (Larachi et al. 1995; Larachi et al. 1996; Cassanello et al. 1996; Kiared et al. 1997). In Figure 4.5, constant Lagrangian velocity trajectories were identified as part of the particle wake and particle downflow-emulsion phases. It is clear that a fraction of the solid follows a convective mixing mechanism. Random movement trajectories of the traced particle were identified as part of the particle vortex-emulsion phase. In a 1D representation this behavior may be attributed to a dispersive mixing mechanism. Therefore, a fraction of the solid follows the dispersive mixing mechanism.

The overall importance of one mixing mechanism superimposed onto the other depends on the mean and variance of the velocity distribution of each particle phase. It also

depends on the holdup of each particle phase and the solid exchange between them. In order to quantify these parameters, the traced particle trajectory has to be separated into the three particle phases.

To do that, the Lagrangian axial velocities were calculated at 30 ms intervals, i.e., at each time step. If the Lagrangian velocities were positive for more than N steps, the trajectory was classified as a part of the particle wake phase. For N consecutive negative Lagrangian velocities, the trajectory was classified as a part of the particle downflow-emulsion phase. Otherwise, the trajectory was classified as a part of the vortex-emulsion phase. When two particle wake phase trajectories were separated by only one step, the two trajectories were linked in order to form one trajectory. The same rule was applied for the particle downflow-emulsion phase. Various N values were used, and above 4-5, the calculated parameters were nearly independent for N. Note that Larachi et al. (1996) obtained the same N-value

For the convective particle phases, Lagrangian particle velocities were calculated by linear regression of the z-t paths. For the particle vortex-emulsion phase, Lagrangian particle velocities were calculated at 30 ms intervals with a numerical central derivative scheme.

The times that the traced particle spent in a specific particle phase were computed. An example of the traced particle's spending time (t_{spend}) in the particle wake phase is shown in Figure 4.5. The spending time is simply the time interval from when the traced particle entered a particle phase to when it left the particle phase. A population of spending times for each particle phase was obtained for the various experimental conditions. Using these populations, particle phase holdup is calculated as the total spending time on the total time experiment. The spending time distribution function

for each particle phase was studied because of its link to solid exchange between particle phases.

The parameters are shown in two scales, i.e., the macroscale and the mesoscale. For the former, the parameters were averaged over the whole bed volume. This gives a good and simpler view of the parameters dependence on operating conditions, column diameter and particle system. The mesoscale results represent the parameters' average over smaller volume elements at sizes having an order of magnitude of a few centimeters, e.g., Δz = 0.050-0.080 m; Δr = 0.005-0.015 m; $\Delta\theta = 2\pi$. The parameters were averaged over annulus volume elements. It was then possible to refine the macroscale analysis. The particle velocity field was compared to the particle phase holdup field. The contribution of each phase (each mixing mechanism) to the velocity field was studied.

4.2.6 MACROSCOPIC HYDRODYNAMICS - RESULTS

4.2.6.1 Solid Velocity

This section contains discussions about particle velocities. The raw particle velocities were separated according to the particle phases discussed above. Figure 4.6 shows the raw particle velocity distribution, i.e., for all particle phases (black curve). The average value is obviously zero and the distribution looks like log-normal, but may be approximated by a Gaussian distribution. If this curve were obtained from Eulerian measurement, the velocity distribution shape would be wrongly attributed to turbulence. The turbulence mechanism supposes that the velocities of a particle randomly change over time from the vortices transfer mechanism as is often assumed in CFD modeling. With Lagrangian data from RPT measurement it is clear that this is not the case (Figure 4.5 and Cassanello et al., 1996). Particles often have a Lagrangian constant velocity, sometimes in the upflow direction and sometimes in the downflow

direction. Particles also experience random changes in their velocities in the downflow and upflow directions (particle vortex-emulsion phase). Therefore, the raw particle velocity distribution is a combination of various velocity distributions coming from various phenomena, separated into the three particle phases. The velocity distributions of each phase are shown in Figure 4.6 and discussed in the following three sub-sections.

4.2.6.1.1 Wake phase

Figure 4.6 shows the Lagrangian particle wake phase velocity distribution for one condition. It is clear that the distribution is log-normal as observed for the bubble phase velocity distribution in a three-phase fluidized bed (Matsuura and Fan, 1984) and bubble column (Hyndman and Guy, 1995a; Sikun et al., 2005). This analogy was already observed in the 0.10 m diameter three-phase fluidized bed reactor (Larachi et al., 1996). In the current work, the log-normal distribution function was fitted to obtain the mean and standard-deviation (STD) of the particle wake velocity distribution. These two first moments evolution with operating condition, column diameter and particle system were compared with literature concerning the bubble phase. This made it possible to identify whether particle wake and bubble phase have the same characteristics.

The log-normal distribution function is shown in equation (1). The relations between the first two moments of distribution and the function parameters (α,β) are shown in equations (2) and (3).

$$f\left(u_{pwd}\right)=\frac{1}{\beta u_{pwd}\sqrt{2\pi}}\exp\left[-\frac{\left(\ln\left(u_{pwd}\right)-\alpha\right)^2}{2\beta^2}\right] \qquad (1)$$

$$u_{pw} = \exp\left(\alpha + \frac{\beta^2}{2}\right) \quad (2)$$

$$\sigma_{pwd} = \exp\left(\alpha + \frac{\beta^2}{2}\right)\sqrt{\exp(\beta^2) - 1} \quad (3)$$

The fit quality is good (Figure 4.6). Figure 4.7 shows fitted particle wake phase velocity distribution for various operating conditions obtained in the 0.292 m column. The effect of the column diameter and the particle system is presented later. The wake phase velocity distribution becomes broader at higher superficial gas and liquid velocities. This point is discussed in more detail elsewhere in the text. It should be noted that particles might rise with a very low constant axial Lagrangian velocity, i.e., may be lower than 0.05 m/s (Figure 4.6 and Figure 4.7). This means that the particle may be entrained by a very slow bubble or that there is a slip velocity between some particles in the wake and the bubble.

The mean and STD of the particle wake velocity distribution are shown in Figure 4.8 at various operating conditions. The mean particle wake phase velocity increases when the superficial gas velocity increases as observed with a local probe measuring the mean bubble velocity (Rigby et al., 1970; Kim et al., 1977; Yu and Kim, 1998; Sikun et al., 2005). Mean bubble velocity increases due to the increase in bubble size with superficial gas velocity. Global mean bubble velocity obtained from RTD measurement versus superficial gas velocity (Hyndman and Guy, 1995b) is shown in Figure 4.8 in order to make a comparison with the mean particle wake phase velocity. Hyndman and Guy (1995b) values are obtained in an air/water batch bubble column, 0.2 m in diameter. The velocities of particle wake phase and bubbles are similar in magnitude. Furthermore, the effect of superficial gas velocity is the same.

At a small superficial gas velocity (Ug=0.031m/s), the effect of superficial liquid velocity is more important. The mean particle wake phase velocity increases from 0.2 to 0.3 m/s for a liquid velocity range from 0.042 to 0.062 m/s. At a higher superficial gas velocity (Ug≥0.051 m/s), superficial liquid velocity below 0.051 m/s has a negligible impact on mean particle wake phase velocity. However, at U_L=0.062 m/s, the mean particle wake phase increases significantly, e.g., from 0.35 to 0.45 m/s at Ug=0.080 m/s. Yu and Kim (1988) and Rigby et al. (1970) found a relatively small increasing effect of the superficial liquid velocity on the mean bubble velocity.

4.2.6.1.1.1 Bubble Properties – A Brief Review

To understand the effect of superficial gas and liquid velocities on particle wake phase velocity, a brief review of bubble characteristics is presented here. Bubble velocity (u_b, relative to the wall) can be expressed as follows:

$$u_b = \frac{U_L}{\varepsilon_L} + u_{br} \qquad (4)$$

Bubble velocity is represented by the bubble velocity relative to the liquid velocity (u_{br}), plus the interstitial liquid velocity (U_L/ε_L) that entrains the bubbles. For a **single bubble system**, Davis and Taylor (1950) proposed the following relation for the relative bubble velocity:

$$u_{br} = 0.71\sqrt{gd_b} \qquad (5)$$

In a **multi-bubble system**, the bubbles rise faster than a single bubble due to the bubble swarm drift effect. Several relative bubble velocity correlations may be found in literature for a **multi-bubble system**. Kim et al. (1977) (dp=1 and 6 mm glass beads)

found in a 2D system that the relative bubble velocity is correlated with the mean bubble diameter (d_b) as shown in equation (6).

$$u_{br} = 17 d_b^{0.989} \qquad (6)$$

Kim et al. (1977) also proposed a relation predicting the relative bubble velocity with operating conditions and fluid properties:

$$u_{br} = 1.609 U_L^{0.065} U_g^{0.339} \gamma^{0.025} \sigma^{0.179} \qquad (7)$$

Where σ is the surface tension in dyne/cm (the only one parameter not in SI) and γ is the generalized liquid viscosity constant in $N/s^n m^2$.

The local relative bubble velocity (v_{br}) was also correlated with the local bubble chord length (Lee and de Lasa, 1986) as shown in equation (8).

$$v_{br} = 1.655 l_b^{0.293} \quad \text{for } 0.2 < l_b < 1.01\ cm \qquad (8)$$

$$v_{br} = 6.357 l_b^{0.598} \quad \text{for } 1.01 < l_b < 4\ cm$$

A correlation of the local bubble chord length is needed to evaluate the impact of operating conditions. Rigby et al. (1970), Yu and Kim (1988), Lee et al. (1990) and Kwon et al. (1994) showed that l_b decreases when the superficial liquid velocity increases. Therefore, equation (8) shows that local relative bubble velocity decreases for every increase in the liquid velocity. This is in contradiction to what equation (7) predicts, i.e., a small increasing effect of the superficial liquid velocity on the relative bubble velocity. However, equation (7) came from a 2D system and most authors

have shown that reducing superficial liquid velocity decreases bubble size. Kwon et al. (1994) (dp=1 and 2.3 mm glass beads) proposed the following correlation to predict local bubble chord length (time-average at a given radial position):

$$l_b = 0.1682 D_T^{0.497} d_p^{0.503} \left(1+\frac{Ug}{U_L}\right)^{0.890} \left(1-\frac{r}{R}\right)^{0.01} \quad (9)$$

Kwon et al. (1994) correlated the bubble chord length radial profile with the Hurst exponent that, in turn, was correlated with operating conditions. Equation (9) is a combination of the two correlations.

Rigby et al. (1970) and Yu and Kim (1988) observed that bubble velocity (relative to the wall) increases as liquid velocity increases. Rigby et al. and Yu and Kim's correlations are shown in equation (10) and (11), respectively.

$$u_b = Ug + U_L + 373\left(\frac{\varepsilon}{1-\varepsilon}\right)^2 l_b^{1.53} \quad (10)$$

$$u_b = 1.772 d_p^{0.060} U_L^{0.024} U_g^{0.225} \quad (11)$$

4.2.6.1.1.2 Particle Wake Phase – Discussion and Correlations

According to the above discussions and correlations on bubble behavior, it is possible to explain the behavior of the particle wake phase velocity distribution mean and STD shown in Figure 4.8. When superficial gas velocity increases, the bubble size increases (equation (9)). That is, relative bubble velocity increases (equations (6) and (8)). This generates faster rising bubbles (equation (4)). It is well known that the liquid phase hold-up decreases with an increase of superficial gas velocity. For

a given superficial liquid velocity, interstitial liquid velocity, which entrains the bubbles, increases (equation (4)) with the superficial gas velocity. Hence, there are two contributions to the faster rising bubble at higher superficial gas velocity.

When superficial liquid velocity increases, bubble size (equation (9)) and relative bubble velocity (equations (6) and (8)) decrease. However, interstitial liquid velocity increases because the liquid hold-up is weakly dependent on the superficial liquid velocity. Since it was observed that the bubble velocity (relative to the wall) increases with the liquid superficial velocity (equations (10) and (11)), the interstitial liquid velocity increases even more than the decrease of the bubble relative velocity. The effect of the superficial liquid and gas velocity on the relative bubble and liquid interstitial velocity explains why the superficial gas velocity has a higher impact on the bubble rise velocity, i.e., both terms in equation (4) increase. However, particle phase velocity is slightly influenced only at a superficial liquid velocity lower than 0.051 m/s.

The STD of the particle wake phase velocity distribution increases with the superficial gas velocity (Figure 4.8) as for the bubble velocity distribution STD in a three-phase fluidized bed (Darton and Harrison, 1974a). Figure 4.8 shows the bubble velocity distribution STD according to superficial gas velocity obtained from Hyndman and Guy (1995b). Magnitude and trend are similar. Again, bubble and particle wake phases have the same behavior.

Superficial liquid and gas velocity effects on particle wake phase velocity distribution STD are very similar to the mean particle wake phase velocity. In fact, there is a strong correlation between mean and STD as shown in Figure 4.9a. Except for the cases of U_L=0.062 and Ug=0.080m/s (Dc=0.292 m), a linear relation with a zero abscissa coordinate describes the link between mean (u_{pw}) and STD (σ_{pwd}). The linear relation

is presented in equation (12) with K=0.60 for Dc=0.292 m and K=0.41 for Dc=0.10 m whatever the particle system used.

$$\sigma_{pwd} = K u_{pw} \qquad (12)$$

Therefore, the dimensionless velocity STD (σ_{pwd}/u_{pw}) is only a function of the reactor diameter. It increases with the reactor diameter as for the mixing extent observed in literature. It was often assumed that the mixing extent increases were due to an increase in the turbulence scale that was assumed to increase with reactor diameter. With the results shown here, the increase in the mixing extent is due more to an appearance of new particle Lagrangian constant velocities in the wake phase.

It is possible to correlate the STD to the mean and the reactor diameter with the following relation. The fit quality is shown in Figure 4.9b.

$$\sigma_{pwd} = 0.927 u_{pw} D_c^{0.355} \qquad (13)$$

For 0.100≤Dc≤0.292 m

u_{pw} = 0-0.35 m/s obtained at 0.042≤U_L≤0.051 m/s (Dc=0.292 m)

0.058≤U_L≤0.065 m/s (Dc=0.100 m)

0.010≤Ug≤0.110 m/s

For Dc=0.292 m, at U_L=0.062 and Ug=0.080m/s the dimensionless STD decreased from 0.6 to 0.5. The relative wideness of the particle wake phase velocity distribution became smaller at a high superficial liquid velocity for the larger reactor.

For Dc=0.292 m at a superficial liquid velocity above 0.051 m/s, the particle wake phase velocity distribution STD may be approximated using equation (14).

$$\sigma_{pwd} = 0.168 u_{pw} + 0.148 \qquad (14)$$

For Dc=0.292 m

u_{pw} = 0.35-0.45 m/s obtained at $0.051 \le U_L \le 0.062$ m/s

Ug=0.080 m/s

Note that Matsuura and Fan (1984) found that the bubble chord length distribution STD is directly proportional to the mean bubble size.

According to the above discussions, only the mean particle wake velocity needs to be correlated with operating conditions. Figure 4.10a shows that the mean particle wake velocity may be linearly correlated to the addition of the superficial gas and liquid velocities with a zero abscissa. The following equation shows the relation with K=1.8 for Dc=0.10 m and K=3.0 for Dc=0.292 m:

$$u_{pw} = K\left(Ug + U_L\right) \qquad (15)$$

Particle wake velocity is higher for a larger reactor. This may be explained by the fact that the bubble size increases with reactor diameter (equation (9)). This induces higher relative bubble velocity (equations (6) and (8)). This trend is also shown in equation (10) . Correlation of the mean particle wake phase velocity is shown in the following equation and the regression quality is shown in Figure 4.10b.

$$u_{pw} = 5.13\left(Ug + U_L\right) D_c^{0.450} \qquad (16)$$

The ratio $u_{pw}/\left(Ug + U_L\right)$ may be viewed as an indicator of the repartition of the energy feed to the reactor that is transferred to the particle wake phase. Assuming that, more energy is transferred to the particle wake phase at a higher reactor diameter.

For a given superficial gas velocity, the particle wake phase velocity distribution STD increases with the superficial liquid velocity. Rigby et al. (1970) and Kwon et al. (1994) demonstrated that the bubble size distribution STD decreases with an increase in the superficial liquid velocity. The following text explains this *apparent* contradiction.

Equation (4) may be modified to represent local measurement:

$$v_b = v_{le} + v_{br} \qquad (17)$$

Where v_b is the local bubble velocity (relative to the wall). The local liquid *emulsion* phase velocity, v_{le}, entrains the bubble with a certain bubble size. A local relative bubble velocity (v_{br}) may be calculated for each bubble size giving a certain *relative* bubble velocity distribution. A bubble with a given size (given local relative bubble velocity) is entrained at various local liquid *emulsion* phase velocity streamlines. Hence, the STD of the local liquid *emulsion* phase velocity streamline (the width of the liquid phase time-averaged axial velocity profile) increases the bubble velocity distribution STD. It is possible to link the bubble velocity distribution STD (σ_{v_b}) to

the liquid *emulsion* phase velocity distribution STD ($\sigma_{v_{le}}$) and the relative bubble velocity distribution STD ($\sigma_{v_{br}}$) with the following relation:

$$\sigma_{v_b} = (f_{le})\sigma_{v_{le}} + (f_b)\sigma_{v_{br}} \qquad (18)$$

Where f_{le} and f_b are weight functions depending on the liquid emulsion and bubble phase properties, respectively. It is, thus, clear that even if the relative bubble velocity distribution STD ($\sigma_{v_{br}}$) decreases due to an increase in the superficial liquid velocity, the bubble velocity distribution STD (σ_{v_b}) may increase as a result of an increase in the liquid emulsion phase turbulence due to a higher superficial liquid velocity.

Depending on the influence of the liquid superficial velocity on the bubble size distribution and the liquid emulsion phase turbulence, the bubble velocity distribution STD (σ_{v_b}) may increase, decrease or remain constant.

It is possible to say that the wideness of the particle wake phase velocity distribution depending on the superficial gas velocity is due to the increase in bubble size distribution due to bubble coalescence. Furthermore, the wideness of the particle wake phase velocity distribution depending on the superficial liquid velocity is due to the increase in liquid emulsion phase turbulence.

Discussions in this section show that the particle having a Lagrangian constant positive axial velocity is due to their entrainment in the bubble wake. Indeed, the bubble hydrodynamics can explain the behaviors of the particle wake phase velocity.

4.2.6.1.2 Downflow-Emulsion Phase

Figure 4.6 shows an example of particle downflow-emulsion phase velocity distribution. As for the particle wake phase, the distribution is log-normal. Particle downflow-emulsion phase velocity distribution data was fitted with equation (1). The effect of operating conditions and column diameter on the particle downflow-emulsion phase velocity distribution is very close to the effect on the particle wake phase velocity distribution. The distribution becomes wider for a larger column and at higher superficial liquid and gas velocities.

Mean and STD of the particle downflow-emulsion phase velocity distribution follow the same trend as shows in Figure 4.8 for the particle wake phase. In fact, as could be expected, there is a strong correlation between the particle wake and downflow-emulsion velocity. Indeed, since large particles are close to each other (small void fraction) in the fluidized bed, the convective upflow movement of the particle swarms induces an equivalent movement in the downflow direction, i.e., a convective downflow movement due to mass conservation. Figure 4.11 shows that the wake and downflow-emulsion velocities may be correlated by a linear function with a zero abscissa whatever the reactor size. The velocity of the particle in the downflow-emulsion phase (u_{pde}) is 10 % smaller than the velocity of the wake phase (u_{pw}). Equation (19) shows the relation between the velocities of the two particle phases whatever the reactor diameter.

$$u_{pde} = 0.90 u_{pw} \qquad (19)$$

This relation may be applied even at UL=0.062 m/s and Ug=0.080 m/s for the 0.292 m column. The fact that the slope is not equal to one is because the particle downflow-

emulsion phase fraction (ϕ_{pde}) is larger than the fraction of the particle wake phase (ϕ_{pw}). The particle phase fraction is shown elsewhere in the text. The net solid phase velocity (u_s) may be calculated from the following weight average relation:

$$u_s = \phi_{pde} u_{pde} + \phi_{pw} u_{pw} + \phi_{pve} u_{pve} \qquad (20)$$

In a solid batch system, the solid phase velocity should obviously be zero. All the calculated solid phase velocities were close to zero (from 0.001 to 0.008 m/s, less than 3 % of the mean velocity of the downflow-emulsion phase).

As for the case of the particles in the wake phase, there is a strong correlation between mean and STD as shown in Figure 4.12a. Except for the case of U_L=0.062 and Ug=0.080m/s, a linear relation with a zero abscissa coordinate describes the link between mean (u_{pde}) and STD (σ_{pded}). The linear relation is presented in equation (23) with K=0.37 for Dc=0.10 m and K=0.55 for 0.292 m.

$$\sigma_{pded} = K u_{pde} \qquad (21)$$

As for the wake phase, the STD increases with column diameter. The relative wideness of the particle wake phase velocity distribution depends only on the reactor diameter. It does not depend on operating conditions and particle size for one reactor. However, at a high superficial liquid velocity, the dimensionless STD decreases from 0.55 to 0.5 at U_L=0.062 and Ug=0.080m/s (Dc=0.292 m). The relative wideness of the particle downflow-emulsion phase velocity distribution becomes smaller at high superficial liquid velocity.

The following relation shows the correlation of the STD and Figure 4.12b illustrates the regression quality.

$$\sigma_{pded} = 0.873 u_{pde} D_c^{0.369} \qquad (22)$$

For 0.100≤Dc≤0.292 m

u_{pw} = 0-0.35 m/s obtained at 0.042≤U_L≤0.051 m/s (Dc=0.292 m)

0.058≤U_L≤0.065 m/s (Dc=0.100 m)

0.010≤Ug≤0.110 m/s

Coefficients of this equation are similar to the ones of equation 13. However, the dimensionless STD of the particle downflow-emulsion phase is systematically lower than for the particle wake phase. Therefore, it is not suitable to combine the two relations and estimate the dimensionless STD of the two convective phases by the same relation.

For a superficial liquid velocity above 0.051 m/s (Dc=0.292 m), the particle wake phase velocity distribution STD may be approximated by the following equation

$$\sigma_{pded} = 0.251 u_{pde} + 0.096 \qquad (23)$$

For Dc=0.292 m

u_{pde} = 0.35-0.45 m/s obtained at 0.051≤U_L≤0.062 m/s

Ug=0.080 m/s

The wideness of the downflow-emulsion phase is always smaller than that of the wake phase.

4.2.6.1.3 Vortex-emulsion phase

Figure 4.6 shows an example of particle vortex-emulsion phase velocity distribution. Contrary to the particle wake and downflow-emulsion phase, the log-normal distribution is not followed. In fact, the distribution follows a *double exponential* (Laplace) distribution, presented in the following equation (Rade and Westergren, 1999):

$$f\left(u_{pvd}\right)=\frac{\lambda}{2}\exp\left[-\left|\lambda\left(u_{pvd}-\kappa\right)\right|\right] \tag{24}$$

The vertical bars represent the absolute value operator. The mean and STD of the distribution are obtained by the following relations:

$$u_{pve}=\kappa \tag{25}$$

$$\sigma_{pved}=\frac{\sqrt{2}}{\lambda} \tag{26}$$

The fit quality is shown in Figure 4.6 and it is very good. Figure 4.13 shows the operating condition effect on the particle vortex-emulsion phase velocity distribution. The wideness of the distribution is more clearly seen with the maximum value of the distribution. Indeed, maximum occurs at $u_{pvd}=\kappa$ and that value corresponds to $\lambda/2$. Therefore, the distribution is larger at a smaller maximum value. It is, thus, clear that the particle vortex-emulsion phase velocity distribution becomes larger at a high superficial gas and liquid velocity as in the particle wake and downflow-emulsion

phases. This trend is shown in Figure 4.14. The value of the mean particle vortex-emulsion phase velocities is always nearly zero.

The velocity distribution of the vortex-emulsion phase is attributed to a random process. There are no Lagrangian constant velocities. Particles in this phase are transported by the liquid turbulence. Turbulence increases with superficial liquid and gas velocities (Figure 4.14). Superficial liquid velocity directly increases the turbulence intensity in the emulsion phase. Superficial gas velocity increases the vortex-emulsion phase turbulence intensity due to the bubble shear effect.

Comparing GB3mm system results from the 0.10 and 0.292 m columns at a small superficial gas velocity (Ug=0.03 m/s) makes it possible to observe a negligible effect of the column diameter on the turbulence in the particle vortex-emulsion phase. At a higher superficial gas velocity, turbulence is more intense in the larger column.

Turbulence in the vortex-emulsion phase follows the same trend as in the bubble mixing extent. In other words, the vortex-emulsion phase turbulence follows the mixing extent of the other particle phases as would be expected according to the previous relations shown.

There is no great impact of the particle system (GB vs PVC vs binary system) on the turbulence for the large particles used in this work. This was also observed for the other particle phases and the bubble phase in literature. However, {GB3}GB5 gives a different STD. According to the STD values obtained from a different system than the GB3mm system (ex.,: PVC5.5mm) and from a more similar system than the {GB3}GB5 system (GB3{GB5}), the difference may be due to experimental uncertainty.

4.2.6.1.4 Lagrangian to Eulerian velocity measurements

According to the above discussions, the STD of the local solid or liquid velocity measurement at one point (Eulerian measurement) should be not represented by only a random fluctuation process in CFD modeling. Turbulence theory is often used to represent liquid and solid velocity fluctuation in a three-phase fluidized bed CFD model (Gidaspow et al., 1994; Grevskott et al., 1996; Mitra-Mujumdar et al., 1997). Based on the above discussion, a mechanistic description of the measured Eulerian velocity fluctuation is proposed here.

Figure 4.15 shows an example of how an Eulerian particle velocity time series may be obtained from a Lagrangian particle description presented previously. At time t_1, a particle inside a bubble wake passes behind a velocity probe (see illustration at the top of Figure 4.15). Its positive velocity (u_{pw1}) is measured by the probe. Another particle, again inside a bubble wake, passes behind the probe with a positive velocity u_{pw2} at time t_2. At time t_3, the positive velocity of a particle in the particle vortex-emulsion phase is measured. For the vortex phase, the particle velocity may be either negative or positive. The negative velocity of a particle following a convective downflow trajectory (downflow-emulsion phase) is measured by the probe at t_4. The time series obtained from only random velocity fluctuations, as in the vortex phase, cannot be differentiated from the time series obtained by the Lagrangian mechanisms described above.

The Eulerian CFD and mixing model have to be coherent with Lagrangian mechanisms. Levenspiel and Fiztgerald (1983) and Levenspiel (1999) have demonstrated that it is possible to differentiate between various Lagrangian mechanisms with RTD data collected at various axial positions (Eulerian data obtained at various positions). Using this method it is possible to differentiate between the Lagrangian mechanisms as generalized by Lefebvre et al. (2004). The method was

used by Hyndman and Guy (1995a) to show that bubbles in a bubble column follow a convective behavior. Lübbert and Larson (1990) have shown that the liquid phase in the riser of an airlift reactor follows a superposition of the convective onto the dispersive mechanism. The convective contribution is due to the liquid entrained in the bubble wake at various Lagrangian constant bubble velocities as discussed before. Cassanello et al. (1995) obtained that the solid phase is superdispersive (faster than dispersive flow) in the axial direction. This superdispersive behavior is due to the particle transported in the Lagrangian constant bubble wake. In the CFD model, the velocity fluctuation term cannot be represented only by a turbulence effect as for the k-ε model often used. The CFD model has to take into account the contribution of the transport in the bubble wake at various Lagrangian constant bubble velocities.

The CFD Lagrangian model of Li et al. (1999) and Zhang et al. (2000) capture such transport bubble phenomena. The model solution, however, needed high computing time. The model was validated with a small 2-D gas/liquid/solid system, i.e., 0.1 m in height and 0.06 m in width containing only 1000 particles. For comparison purposes, a system 1 m in height and 0.29 m in diameter containing more than 2 000 000 particles 3 mm in diameter was used.

In Eulerian CFD modeling, the particle velocity fluctuation term may be separated into three terms, according to the wake, downflow-emulsion and vortex emulsion phases. However, turbulence theory may be used only for the vortex-emulsion phase. The convective momentum transport term in the momentum balance may be extended to a distribution of convective momentum transport terms for the wake and downflow-emulsion phases. Hence, a series of momentum balances may be written for each particle phase. Velocity distributions and the two first moment relations given in this report may be included in those types of CFD models. A coalescence/breakup model may also be included in the solution for the series of momentum balances for the

convective phases. Such a model needs the knowledge of the particle phase holdup. The approach that combined bubble coalescence/breakup model with CFD simulation was used by Olmos et al. (2001) for bubble column reactor.

4.2.6.2 Particle Phase Holdup and Spending Time

Particle phase holdup and spending time are presented together in this section because of their link. The spending time was defined previously in Figure 4.5 and in section 4.2.5. If the sum of the particle wake spending time is divided by the total time of the experiment (t_{tot}), the particle wake phase holdup is obtained:

$$\phi_{pw} = \frac{\sum t_{spw_i}}{t_{tot}} \qquad (27)$$

The particle phase holdup for the other particle phases are calculated in the same way. The mean particle spending time is calculated by the first moment of the spending time distribution function. Both particle holdup and mean spending time depend on wake shedding frequency. In fact, particle spending time is a parameter affecting the particle phase holdups. Moreover, particle wake phase holdup is related to the bubble wake holdup (ε_w) and the relative solid wake holdup ($\varepsilon_{w_s}/\varepsilon_{ls_s}$).

The particle phase holdup determines the relative importance (weight) of the mixing mechanism followed by each particle phase on the overall mixing mechanism. For example, if the particle wake and downflow-emulsion phase (convective mechanism) holdups are higher compared to the particle vortex phase (dispersive mechanism) holdup, the dominant mixing mechanism would be convective. This is true if the particle phase velocity STD is similar for all particle phases and exchange between particle phases is not too high (spending time should not be too short).

Figure 4.16a shows particle wake holdup for all experiments. Note that the particle downflow-emulsion phase holdup trend is almost the same as particle wake holdup. For the 0.292 m column, it is clear that the trend of the particle wake holdup with the superficial gas velocity depends on the superficial liquid velocity. At a small superficial liquid velocity, particle wake holdup increases with superficial gas velocity. It is the inverse at a larger superficial liquid velocity.

Table 4.2 explains this behavior. The table illustrates how superficial gas and liquid velocities affect ε_w and $\varepsilon_{w_s}/\varepsilon_{ls_s}$. An increase of superficial gas velocity decreases the relative volume of the wake compared with the gas holdup (Darton and Harrison (1975); Darton (1985)). The gas holdup, however, increases. Therefore, increasing superficial gas velocity may increase or decrease the wake holdup (ε_w), depending on the gas velocity range. Moreover, there is more and more solid in the wake compared with the emulsion phase when superficial gas velocity increases (Fan and Tsuchiya, 1990). The superficial liquid velocity has the inverse effect on the holdup parameters, giving the trend translation of the particle wake holdup with the superficial gas velocity. Furthermore, particle spending time (link to wake shedding frequency) dependency on the superficial velocity (shown in Figure 4.19a; discussed later) affects the trend of the particle wake holdup.

In terms of mixing mechanism predominance, according to Figure 4.16a, the contribution of the convective mechanism is not always an increasing function of the superficial gas velocity, as would be thought *a priori* due to the increase in the bubbles number. The maximum convective mixing contribution in terms of holdup is under intermediate superficial velocity (Ug+UL) conditions. In other words, at Ug+UL≈0.09 m/s, approximately 70 % of the solid follows a convective mixing behavior, i.e., less than 35 % in the particle wake phase and more than 35 % in the downflow-emulsion phase.

Observing the GB3mm systems at UL = 0.062-0.065 m/s, it is possible to remark that the trend of the particle wake holdup vs superficial velocity shifted to the right for the 0.10 m column compared with the 0.292 m column. In other words, the particle wake holdup increased with the superficial gas velocity at UL=0.065 m/s in the smaller column and this trend is, also, observed in the larger column at UL=0.042 m/s.

For the 0.10 m column and both the GB3mm and PVC5.5mm systems, Cassanello et al. (1995) have shown a slight increase in the particle axial velocity Hurst exponent with superficial gas velocity, i.e., Hurst's exponent from 0.63 to 0.68 for GB3mm and from 0.57 to 0.63 for PVC5.5mm. Hurst's exponent and the particle wake holdup trend are coherent while indicating an increase in the convective mixing mechanism with superficial gas velocity for the 0.10 m column. Yang et al. (1993) used the CARPT method with a neutrally buoyant radioactive particle to track the liquid phase in a batch bubble column. They found that the "liquid" axial velocity Hurst exponent decreased when the superficial gas velocity increased, i.e., from 0.7 to 0.6 depending on column diameter. This indicates that the system moves toward a dispersive mechanism (at 0.5 the Fickian model may apply) at a higher superficial gas velocity. This shows an opposite trend to that demonstrated by Cassanello et al. (1995) for the solid phase.

Systems with larger particles promote higher particle wake holdup, since larger particles in the emulsion phase keep more of the particles in the wake (Fan and Tsuchiya, 1990; Fan and Yang, 2002). Note that for an increase in particle diameter in the system having a particle diameter less than 500 μm (small solid holdup system), particle wake phase holdup decreased (Schlüter et al., 2004). Therefore, for a large range of particle diameters, the particle wake phase holdup will perhaps have a concave parabolic shape.

A correlation was developed to estimate the particle wake phase holdup. This correlation includes superficial gas and liquid velocities, the column diameter and the particle diameter. It was observed, for the binary system, that the maximum particle diameter better correlated the particle phase holdup. The correlation is shown here:

$$\phi_{pw} = \frac{A\left[1 - be^{-m(Ug+U_L)D_c^{0.916}}\right] d_p^{1.663}}{(Ug+U_L)D_c^{0.916}} \qquad (28)$$

Where parameters are in SI units and ϕ_{pw} is in percentage (%),

A = 1.237 x 10^4, m = 26.09 and b = 1.208 for 0.0083 < $(Ug+U_L)D_c^{0.916}$ < 0.0118 $m^{1.916}/s$

and

A = 2.563 x 10^4, m = 53.11 and b = 1.815 for 0.0118 ≤ $(Ug+U_L)D_c^{0.916}$ ≤ 0.0460 $m^{1.916}/s$

Figure 4.16b shows the correlation prediction quality. It is not as good as the previous relation shown for the particle velocities, but it is acceptable for approximation considering the much more complex trend of the particle holdup phase parameters.

To obtain the particle vortex phase holdup, a simple linear correlation with the particle wake holdup may be used:

$$100 - \phi_{pve} = 2.042\phi_{pw} \qquad (29)$$

The following relation may be used to calculate the downflow-emulsion phase holdup:

$$\phi_{pde} = 100 - \phi_{pve} - \phi_{pw} = 1.042\phi_{pw} \qquad (30)$$

Equation (30) shows, as previously discussed, that the downflow-emulsion phase holdup has somewhat larger values than the particle wake phase. This validates the assumption of the compensatory effect of the convective rising particle (in the wake) on the convective downward particle. In other words, the number of particles that rise at a constant Lagrangian velocity in the bubble wake is compensated for by almost the same number of particles going down also with a constant Lagrangian velocity.

Figure 4.16c shows the fit quality of equation (29), which is good. Note that the relation is independent of the column diameter and particle system.

Based on a combination of the particle velocity STD and holdup, an indicator quantifying the relative contribution of the convective over the dispersive mixing mechanism was developed. The definition of this indicator is shown here:

$$MMI = \frac{\phi_{pw}\sigma_{pwd} + \phi_{pde}\sigma_{pded}}{\phi_{pve}\sigma_{pved}} \qquad (31)$$

This indicator is simply the ratio of the weight average of the particle velocity STD of the convective phases to the weighted particle vortex-emulsion phase velocity STD. This indicator was named the Mixing Mechanisms Indicator (MMI). Normally, the exponent, N, of the relation between the residence time distribution STD, σ_{RTD}, and the length of the measuring points, L, is obtained in order to diagnose the mixing mechanism, i.e., fitting relation $\sigma_{RTD} = kL^N$. However, Lefebvre et al. (2004) demonstrated that even if a mixing model needs to follow the dependence of σ_{RTD} vs L, the N value does not always correctly diagnose the mixing mechanism for systems having a contribution of both convective and dispersive mixing mechanisms. The MMI was, therefore, preferred to diagnose the contribution of each mixing mechanism.

Figure 4.17 shows the MMI versus experimental conditions. The convective mixing mechanism dominates in the overall solid phase mixing mechanism for the larger reactor at most of the operating conditions. The trend of the MMI is more similar to the holdup trend than that of the velocity STD. For the 0.292 m column at low superficial liquid velocity, the contribution of the convective mixing mechanism increases with superficial gas velocity. However, when the superficial liquid velocity increases, this trend reverses, i.e., the convective mixing mechanism contribution decreases with the superficial gas velocity. This is due to various phenomena having the opposite effect on the mixing mechanisms. When the superficial gas velocity increases, the bubble holdup (ε_g) and the relative solid concentration in the bubble wake ($\varepsilon_{w_s}/\varepsilon_{ls_s}$) increase, but the relative volume of the bubble wake ($\varepsilon_w/\varepsilon_g$) decreases. Moreover, the turbulence in the liquid emulsion phase increases, that is, wake shedding increases due to the high flow instability surrounding the bubble wake. When the superficial liquid velocity increases, the bubbles become smaller and faster, leading to smaller bubble holdup. The wake shedding increases also due to an increase of the turbulence in the liquid emulsion phase. However, the relative volume of the bubble wake ($\varepsilon_w/\varepsilon_g$) increases. This complex behavior gives the parabolic-like shape of the MMI versus UL+Ug.

For the 0.10 m column, the convective mixing mechanism contribution is much smaller than for the 0.292 m column. The trend is also different. MMI continually increases over the same UL+Ug range. This means that smaller reactors have to be operated at a higher superficial velocity in order to have the same contribution of the convective mixing mechanism (same key hydrodynamic properties). Particle system properties have a negligible effect on the MMI. The extent of mixing (Figure 4.8 and Figure 4.14) and the overall mixing mechanism (Figure 4.17) does not follow the same trend.

The CFD and mixing model have to follow not only the mixing extent, which increases with superficial velocity and reactor diameter, but also the relative importance of the mixing mechanisms, which exhibit a more complex trend.

The ***particle spending time*** of the wake phase is an important parameter affecting the particle phase holdup and solid exchange between particle phases. The particle spending time in the wake phase is in turn dependent on bubble wake shedding and particle expulsion phenomena due to forces acting on the particles in the bubble wake. For large particles, a centrifugal force promoting particle expulsion is high, but particle inertia reduces particle entrainment in bubble wake vortices. Moreover, solid fraction in the emulsion phase is high for the large particle system that keeps particles in the bubble wake (Fan and Tsuchiya, 1990; Fan and Yang, 2002). It is possible that spending time would be close to the reciprocal of the bubble wake shedding for the particles used here (≥ 3 mm). In other words, wake shedding is assumed to be the most important phenomena affecting the solid exchange between the particle wake phase and the other phases.

In literature, reported wake shedding was obtained mostly for 2-D systems containing few bubbles and small particles (< 1 mm). Here, the wake shedding reciprocal, i.e., particle wake spending time, in multi-bubble 3-D systems containing large particles, is reported.

Particle spending time of the particle phases is also important in determining the predominant mixing mechanism. Indeed, if spending time is very short (high solid exchange between particle phases), a dispersive mixing mechanism may predominate even if the holdup of the convective particle phases (wake and downflow-emulsion phase) is very high. In that case the particle velocity change more randomly, as in the dispersive mixing system.

Figure 4.18 shows a cumulative distribution function of the particle phase spending time. Examples of two conditions are shown, one for each column. Wake spending time ranges from 0.15 to 2 sec (0.5 to 6.7 s^{-1}). These values are of the same order of magnitude as the wake shedding frequency reported in literature, i.e., about 3.5-6 s^{-1} (Fan and Tsuchiya, 1990) for the system discussed previously.

In the example given for the 0.292 m column, wake and downflow-emulsion particle phase distributions are wider than the vortex-emulsion particle phase distribution. The three distributions are more similar in the example given for the 0.10 m column and also for some conditions in the 0.292 m column.

Figure 4.19a and b show the evolution of the mean spending time for the wake and the vortex-emulsion particle phase, respectively. Again, the trend of the downflow-emulsion particle phase is close to the wake particle phase. The differences in the values are from 0 to 9 %.

For the 0.292 m column data, wake spending time increases for $Ug+U_L<0.082$ m/s and decreases for $Ug+U_L>0.082$ m/s. This parabolic-like shape may be explained by the opposite effect of the two phenomena. The bed expands as $Ug+U_L$ increases, giving a higher length for the bubble wake to transport the particles. However, the turbulence increases with $Ug+U_L$, promoting wake shedding (Fan, 1989). The turbulence at the top of the bed (in the reversal flow region) is more intense and particle shedding from the wake occurs often in that region. For the 0.10 m column data and GB3mm, wake spending time increases for the whole Ug+UL range. This indicates that the bed expansion effect dominates in this case.

The superficial velocity ($Ug+U_L$) at which the particle wake holdup begins to decrease is about 0.09 m/s (see Figure 4.16). This velocity is higher than the one at which spending time begins to decrease (0.082 m/s). This means that wake volume and/or particle concentration in the wake increase between 0.082 and 0.09 m/s.

Particle wake spending time is lower in the 0.10 m column. This would be due to a smaller bed height. Figure 4.20 shows particle wake spending time versus the expanded bed height. This figure shows a tendency of the particle wake spending time to increase with expanded bed height. This is obvious considering that bubble wakes have a longer length to transport a particle at a higher bed height. However, as discussed previously, turbulence intensity and particle diameter also affect spending time. It is possible all the same to say that the higher wake spending time values in the larger column are due more to the effect of the bed height than the column diameter.

As shown in Figure 4.18b for the 0.292 m column, vortex-emulsion spending time is parabolic with the superficial velocity (Ug+UL). The values are of the same order of magnitude as the wake and the downflow-emulsion spending time. Moreover, the spending time values are the same for all the particle phases in the velocity boundary range (Ug+UL = 0.073 and 0.142 m/s).

For the 0.10 m column, the vortex-emulsion spending time is much higher than the wake values (1-2 s vs 0.3-0.5 s) for a weak superficial gas velocity ($Ug<0.032$ m/s). In other words, under such conditions the vortex spending time is more affected by the superficial velocity ($Ug+U_L$) than the wake spending time. This can be easily explained. Wake spending time does not depend on the number of bubbles (or ε_g). It depends on the bubble wake properties and the flow surrounding the wake. Vortex spending time depends on the number of bubbles. For a low number of bubbles, the probability that a particle is trapped in a bubble wake obviously decreases. That

particle will remain in the vortex phase longer. This explains the high vortex phase spending time observed for the PVC5.5mm system, operated at low superficial gas velocity. For the particle wake phase, the spending time seems to be higher for larger particle systems. As discussed for the holdup, larger particles stabilize the solid in the bubble wake. Note that the trend shown for the MMI does not change while including the particle spending time.

For CFD model validation or CFD modeling development and Monte-Carlo simulation, knowing if the particle phase spending time depends on particle phase velocity is useful. Figure 4.21a shows an example of the particle wake and downflow-emulsion phase spending time versus the particle wake and downflow-emulsion phase velocity. The graph was constructed as follows: when the traced particle is in the wake phase, its spending time is plotted against its velocity. Positive values are used for the wake phase and negative values are used for the downflow-emulsion phase. Even if spending time and velocity versus time are irregular, a structure appears when plotting the two parameters together. This structure is not a simple direct correlation, but a relation between the domains of the spending time depending on the particle velocity. The same structure is observed for all conditions, column diameters and particle systems.

It is possible to represent the relation between spending time and particle velocity in terms of a spending time cumulative distribution function with mean and variance depending on particle Lagrangian velocity. Figure 4.21b and c show this cumulative distribution function. The probability that a particle stays in a bubble wake depends on the velocity of that bubble. The spending time cumulative distribution function is wider for intermediate velocities, i.e., between 0.2 and 0.6 m/s in absolute values. The cumulative distribution function becomes narrower for velocities leaving this range.

4.2.7 MESOSCOPIC HYDRODYNAMICS - RESULTS

In the previous section, the hydrodynamic parameters were averaged over the whole bed volume. This made it possible to investigate the contribution of the convective and dispersive mixing mechanisms under various conditions. The time-average velocity field and particle phase holdup field are shown here in order to study the space repartition of the particle phases, that is, of the mixing mechanism. In other words, the region where the convective mixing mechanism predominates is identified. The fields are shown in 2D for the radius and the axial coordinate. The average was computed over the complete circulation, i.e., integrated from 0 to 2π.

Figure 4.22 is an example of typical fields observed in the 0.292 m column. The time-averaged velocity field shows a clockwise solid circulation pattern as observed for the liquid phase in bubble columns (Devanathan et al., 1990 ; Degaleesan, 1997). Larachi et al. (1996) also showed such a pattern for the solid phase. The solid rises at the center of the column and goes down at the wall. The time-averaged velocity is zero at about 70-80% of the column radius as typically observed in literature for the liquid phase. Reversal flow regions are observed at the top and bottom of the bed. Remark the fountain shape at the top of the bed. It comes from the particles projection due to wake shedding above the bed surface. Particles are entrained above the bed surface in the bubble wake mostly at the center where the bubble density is higher. When the wake is shed, the particles rise a certain distance before going down due to a downward buoyancy force. The liquid drag force acting on the particles induces a fluctuating movement of the particles, which are pushed toward the wall by the bubble swarms that are more numerous at the center than at the wall.

The upward time-average velocity region frontiers do not follow a straight shape, but exhibit more of an egg-like shape. This particular shape is followed by the particle wake phase holdup shown to the right of the time-averaged velocity field. It is, thus,

clear that the high upward time-averaged velocities are mostly due to the solid transported in the bubble wake. The particle wake phase holdup is about 80 % in that region, with an expanse about 1/3 of the radius. The upward time-averaged velocity decreases when the particle wake phase holdup decreases. At the center in 1/3 of the column radius, approximately half of the 20 % contribution to the time-averaged velocity is due to the vortex-emulsion phase and the other half is due to the downflow-emulsion phase. Therefore, the convective mixing mechanism is mainly responsible for the high upward time-averaged velocity values.

Close to the wall, the zone where the downward time-averaged velocities are high coincides with the zone where the particle downflow-emulsion phase holdup is high, i.e., more than 60 %. The compensatory effect of the convective upward solid movement causes the high downward time-averaged velocity at the wall. The solid at the wall follows a convective mixing mechanism.

Between 0.05 and 0.10 m in the radius axis, the bed volume is occupied mostly by the convective phases, but the vortex-emulsion phase is also fairly present. Particle wake and downflow-emulsion phases gradually cancel each other the time-averaged velocity while reaching about 70-80% of the column radius.

At the top of the bed, the particle vortex-emulsion phase dominates. As described above, most of the particles are free from the bubble wake and go down toward the wall. In the bed bottom, particle vortex-emulsion phase holdup is higher than in each of the other two phases, but not as at the top of the bed. About 50 % of the solid randomly fluctuates at the bottom, in the whole column radius. At the center, the other 50 % of the solid rises in the wake phase. Close to the wall, the other 50 % of the solid goes down in the downflow-emulsion phase.

The solid in the established region (between the reversal flow regions) mainly follows a convective mixing mechanism. The dominated mixing mechanism followed by the solid at the top of the bed is the dispersive mixing mechanism. However, very few particles are present in the zone dominated by the vortex-emulsion phase. Figure 4.23 shows the axial profile of the particle vortex-emulsion phase holdup and the particle occurrence. The latter was defined as the total time the traced particle was present in one position, whatever the particle phase, based on the total experiment time. It seems that solid particles are less present in the bubble wake zone where the fraction of solid is very low. Again, solid in the wake is retained by the surrounding solid in the emulsion phase. Note the similarity with the axial profile shape of the liquid phase axial dispersion coefficient found by Gervais et al. (1995) for three-phase fluidized beds.

Figure 4.24 shows another example of the fields obtained from the 0.292 m column, but at a higher superficial liquid velocity. The fields shapes are the same, but the holdup values and the volume of the various regions are different. The particle vortex-emulsion phase holdup is higher and the wake phase holdup is lower at a high superficial liquid velocity, as is demonstrated in Figure 4.16. This is due to an increase in the particle vortex-emulsion phase turbulence. Indeed, the vortex-emulsion phase velocity distribution STD increases as shown in Figure 4.14. This decreases the particle wake spending time, because the wake shedding is promoted by the instability of the flow around the wake (see Figure 4.19). The volume of the region where the vortex-emulsion phase holdup exceeds 80 %, at the top of the bed, is higher at a higher superficial liquid velocity. That volume also increases at a higher superficial gas velocity. This zone may be viewed as the ***disengagement zone*** of the solid from the bubble wake (Bhatia and Epstein, 1974).

At a low superficial gas velocity, low bubble density combined with a low superficial liquid velocity induced a less structured flow pattern. Figure 4.25 shows the example at the lower superficial gas and liquid velocities. The velocity field follows two circulation cells instead of a single clockwise circulation cell. Devanathan et al. (1990) also reported one liquid phase circulation cell at the bottom of a bubble column and a larger one above the bottom circulation cell at a low superficial gas velocity. For a three-phase fluidized bed, the circulation pattern at the bed bottom may be due to the fact that there is less solid in the convective phase in that region. The particle vortex-emulsion phase holdup is higher at the bottom compared to the previous examples.

Particle vortex-emulsion phase is higher at a lower superficial gas velocity due to lower bubble density. Moreover, remember that the volume of the wake relative to the bubble volume is lower at a lower superficial liquid velocity. In other words, the higher particle vortex-emulsion phase holdup is not due to higher turbulence, as at high superficial gas and liquid velocities, but is due to a lower bubble wake phase holdup.

The particle wake phase is still more present at the center of the column. The holdup is, however, lower, i.e., about 50-60 %. The remainder is mostly occupied by the vortex-emulsion phase. In fact, at lower superficial gas and liquid velocities, the three particle phases coexist more in the whole bed volume. At a low superficial gas velocity, the flow pattern became more structured (single circulation) at a higher superficial liquid velocity. This is certainly due to the larger relative volume of the wake and the larger drag force acting on the particles. In the last case, the particles are more likely to be entrained by the bubble wake, because they are artificially "lighter".

For the 0.10 m column and at low superficial gas and liquid velocities, the pattern shown in Figure 4.26 is similar to the one for the 0.292 m column at low superficial gas and liquid velocities (Figure 4.25). However, the higher time-averaged velocities are

not at the column center, but in the middle of the column radius. What is interesting is that the higher time-averaged velocity region corresponds again to the region having the higher particle wake phase holdup, i.e., in the middle of the column radius. Most of the bed is in the particle vortex-emulsion phase.

At a higher superficial gas velocity (higher bubble density), the single circulation clockwise pattern appears. Figure 4.27 shows the fields under such conditions for the 0.10 m column. The particle wake phase is mostly at the center of the bed and the wake phase holdup is about 50 %. In that region, about 50 % of the remaining solid is in the particle vortex-emulsion phase.

Figure 4.28 illustrates the fields for the PVC5.5mm particle system at very low superficial liquid and gas velocities. The freeboard region volume is higher as expected for lighter particle systems. Solid in that region is mainly in the particle vortex-emulsion phase and follows a dispersive mixing mechanism. The solid in the established region is mainly in the particle wake and downflow-emulsion phases, but the amount of solid in the particle vortex-emulsion phase is fairly important. Even if the superficial gas and liquid velocities are lower than what were shown previously, the clockwise circulation and core/annulus patterns are observed. PVC particles are less dense and less spherical than glass beads. Hence, PVC particles are more likely to be entrained by the bubbles in the dense solid region, even if bubbles are less numerous as for the GB3mm at a higher superficial liquid velocity.

In summary, the solid follows a core/annulus/annulus pattern when the superficial gas and liquid velocities are enough relative to the particle buoyancy and drag due to sphericity. Under these conditions, the solid in the established region mainly follows the convective mixing mechanism. The particle wake phase dominates at the center and the particle downflow-emulsion phase dominates close to the wall. However, a

part of the solid in the established region follows a dispersive mixing mechanism in the particle vortex-emulsion phase. The relative importance of the mixing mechanism depends on the operating conditions, the reactor design used (eg., distributor configuration and column diameter) and the particle buoyancy. The particle vortex-emulsion phase is mainly present at the top of the bed (in fact, above the bed). Hence, the dispersive mixing mechanism dominates in that region and its volume depends again on the operating conditions, the reactor design used and the particle buoyancy. In some cases, the solid at the bottom of the bed mainly follows the dispersive mixing mechanism.

Therefore, the well-used k-ε turbulence model cannot be applied in CFD modeling in the established region, because the solid velocity STD is not due to vortice transports. The solid velocity STD came from the various bubble velocities that entrained the solid with a constant Lagrangian velocity. The momentum balance has to be applied on the various upward and downward constant Lagrangian velocities following a log-normal distribution (equation (1)).

4.2.8 CONCLUSIONS AND DISCUSSIONS

The objective of this work was to compute parameters to investigate the relative contribution of the convective and dispersive mixing mechanism on the overall solid phase mixing mechanism for CFD and mixing model development.

The structural wake model was updated while accounting for the bubble properties distribution that is linked to the liquid/particle wake property distribution. That phase was named for the solid, particle wake phase. The emulsion phase was divided into two liquid/particle phases, named for the solid in the three-phase fluidized bed reactors, particle downflow-emulsion phase and particle vortex-emulsion phase. It was shown previously with RPT data that the solid in the particle wake and downflow-emulsion

phases follows a convective mixing mechanism. Solid in the vortex-emulsion phase has random movement, attributed in a large sense to a dispersive mixing mechanism. RPT data were treated in order to obtain the parameters affecting the overall solid phase mixing mechanism for each of the three particle phases. The studied parameters are the mean and standard-deviation (STD) of the particle phases velocity distribution, particle phase holdup and spending time, which for the particle wake phase represents, in some cases, the reciprocal of the wake shedding. These parameters were examined at two different scales, i.e., macroscale, where the parameters were averaged over the whole bed volume and mesoscale, where the parameters were averaged over annulus elements, i.e., fields over r and z coordinates were obtained. Various operating conditions and particle systems were investigated in two different size three-phase fluidized bed reactors.

For the convective particle phases, the log-normal velocity distribution function gives a good representation of the particle axial velocity distribution in the bubble phase. Moreover, the mean and STD of the particle wake phase velocity distribution have the same trend and order of magnitude as the bubble phase. The double-exponential (Laplace) distribution function better fitted the particle vortex-emulsion phase axial velocity distribution. The mean and STD of the velocity distribution of each particle phase increase with the superficial liquid and gas velocities as well as the column diameter. This means, as is already known, that the solid phase mixing extent increases with operating conditions and reactor size. However, contrary of what is often assumed, the dispersive mixing mechanism is not solely responsible for the mixing extent. Indeed, the STD of the convective phase's particle velocity distributions is higher than the STD of the vortex-emulsion phase. The particle system has a negligible effect on particle velocity distribution. Simple relations to estimate the mean and STD of the velocity distribution for each particle phase were developed. It

was found that the dimensionless STD, i.e., STD/mean, of the convective particle phase's velocity distribution is only a function of the reactor diameter.

The particle velocity STD gives an indication of the predominant mixing mechanism, but must be weighted by the particle phase's holdup. Indeed, a particle phase may be characterized by a large velocity STD, but have a small contribution to the overall mixing mechanism when very few particles are present in that particle phase, i.e., very small holdup. The particle phase holdup has a much more complex trend than particle velocity mean and STD. For the larger column (Dc = 0.292 m), the relation between the particle phase's holdup and superficial gas velocity depends on the superficial liquid velocity. The particle phase holdup is a parabolic-like shape relative to UL+Ug. For the 0.10 m column, the wake and downflow-emulsion phase holdup increase with UL+Ug, that is, the particle vortex-emulsion phase decreases. The convective particle phase holdup increases with the reactor diameter. In other words, the number of particles moving randomly in the vortex-emulsion phase is higher in a smaller reactor. Relations estimating particle phase holdup were developed. These relations take into account the operating conditions, reactor diameter and particle system.

Based on a combination of the particle velocity STD and holdup, an indicator quantifying the relative contribution of the convective over the dispersive mixing mechanism was developed. This indicator is simply the ratio of the weight average of the particle velocity STD of the convective phases to the weighted particle vortex-emulsion phase velocity STD. This indicator was named the Mixing Mechanisms Indicator (MMI). With the MMI, it was found that the convective mixing mechanism dominates in the overall solid phase mixing mechanism for the larger reactor for most of the operating conditions. The particle phase holdup mostly affects the trend of the MMI. Therefore, at low superficial liquid velocity, contribution of the convective mixing mechanism increases with superficial gas velocity. However, when the

superficial liquid velocity increases, this trend reverses, i.e., the convective mixing mechanism contribution decreases with the superficial gas velocity. This is due to various phenomena having the opposite effect on mixing mechanisms. When the superficial gas velocity increases, the bubble holdup (ε_g) and the relative solid concentration in the bubble wake ($\varepsilon_{w_s}/\varepsilon_{ls_s}$) increase, but the relative volume of the bubble wake ($\varepsilon_w/\varepsilon_g$) decreases. Moreover, the turbulence in the liquid emulsion phase increases, that is, wake shedding increases due to the high flow instability surrounding the bubble wake. When the superficial liquid velocity increases, the bubbles become smaller and faster, leading to smaller bubble holdup. The wake shedding also increases due to an increase in the turbulence of the liquid emulsion phase. However, the relative volume of the bubble wake ($\varepsilon_w/\varepsilon_g$) increases. This complex behavior gives the parabolic-like shape of the MMI versus UL+Ug. For the 0.10 m column, the convective mixing mechanism contribution is much smaller than for the 0.292 m column. The trend is also different. MMI continually increases over the same UL+Ug range. This means that smaller reactors have to be operated at higher superficial velocity in order to have the same contribution of the convective mixing mechanism (same key hydrodynamic properties). Particle system properties have a negligible effect on the MMI. The extent of mixing and the overall mixing mechanism do not follow the same trend. The CFD and the mixing model have to follow not only the mixing extent, which increases with superficial velocity and reactor diameter, but also the relative importance of the mixing mechanisms, which exhibit a more complex trend.

The investigation of 2D velocity and particle phase holdup fields demonstrated that the convective mixing mechanism is followed mostly in the established region, i.e., between the reverse flow regions at the bottom and top of the bed. The particle wake phase is mostly present at the column center and the downflow-emulsion phase at

the wall. The particle vortex-emulsion phase is mostly present at the top of the bed, but it is not negligible in the established region and is fairly present at the bed bottom. The region at the top of the bed may be seen as a disengagement zone, where the particle leaves the bubble wake. This explains the low solid occurrence in that region. The volume of each region depends on the operating conditions, reactor diameter and particle system properties.

Particle wake phase spending time range is 0.15-2 seconds. This range gives a frequency range of 0.5-6.7 s^{-1}, which is similar to the wake shedding frequency found in literature (3.5-6 s^{-1}). The main solid exchange mechanism may be attributed to wake shedding for large particle systems, where high solid holdup and particle inertia stabilizes the solid in the bubble wake.

The next step is to develop a mixing model including the contribution of both the convective and dispersive mixing mechanism.

4.2.9 ACKNOWLEDGEMENTS

The authors gratefully acknowledge financial support from the Natural Science and Engineering Research Council of Canada and the Fond pour la Fond Québécois de Recherche sur la Nature et la Technologie. Dr G. Kennedy and Mr. Saint-Pierre are also gratefully acknowledged for activation of the tracer. A special acknowledgement to Pierre Sauriol who has performed useful modifications to the RPT software system and to Jean Huard and Robert Delisle who worked on the experimental setup and RPT facilities.

4.2.10 NOMENCLATURE

d_b : mean bubble equivalent diameter (m)

d_p : particle diameter (m)

D_T : column diameter (m)

f_b : weight functions depending on the bubble phase properties (-)

f_{le} : weight functions depending on the liquid emulsion phase properties (-)

l_b : local bubble chord length (m)

MMI : mixing mechanism indicator (-)

r : radial position (m)

R : column radius (m)

t_{spw} : spending time of the particle wake phase (s)

t_{tot} : total time of the experiment (s)

u_b : mean bubble velocity relative to the wall (m/s)

u_{br} : mean bubble velocity relative to the liquid phase (m/s)

$u_{b_{\phi_i}}$: bubble velocity of the class ϕ_i (m/s)

u_{pde} : mean solid velocity in the particle downflow-emulsion phase (m/s)

u_{pded} : solid velocity in the particle downflow-emulsion phase (m/s)

u_{pvd} : solid velocity in the particle vortex-emulsion phase (m/s)

u_{pve} : mean solid velocity in the particle vortex-emulsion phase (m/s)

u_{pw} : mean solid velocity in the particle wake phase (m/s)

u_{pwd} : solid velocity in the particle wake phase – in the log-normal velocity distribution (m/s)

u_s : net solid phase velocity (m/s)

U_g : superficial gas velocity (m/s)

U_L : superficial liquid velocity (m/s)

U_{sl} : superficial slurry velocity (m/s)

v_b : local bubble velocity relative to the wall (m/s)

v_{br} : local relative bubble velocity (m/s)

v_{le} : local liquid emulsion phase (m/s)

V_{ls} : liquid velocity in the particle/liquid downflow/upflow-emulsion phase (m/s)

V_s : solid velocity for the specified particle phase (m/s)

V_p : particle velocity in the particle/liquid emulsion phase (m/s)

Greek Letters

α : parameter of the log-normal distribution

α_v : ratio of $\varepsilon_v / \varepsilon_{ls}$

β : parameter of the log-normal distribution

ε : bed void fraction (-)

ε_e : particle/liquid downflow/upflow-emuslion phase holdup (-)

ε_g : bubble (or gas) phase holdup (-)

$\varepsilon_{g_{\phi_i}}$: holdup of the class ϕ_i in the bubble phase (-)

ε_L : liquid phase holdup (-)

ε_w : bubble wake holdup (-)

ε_{w_s} : solid holdup in the bubble wake phase (-)

ε_{w_L} : liquid holdup in the bubble wake phase (-)

$\varepsilon_{w_{\phi_i}}$: holdup of the class ϕ_i in the bubble wake phase (-)

ε_{ls} : particle/liquid emulsion phase holdup (-)

ε_{ls_L} : liquid holdup in the emulsion phase (-)

ε_{ls_s} : solid holdup in the particle/liquid downflow/upflow-emulsion phase (-)

ε_v : particle/liquid vortex-emulsion phase holdup (-)

ε_{v_s} : solid phase in the particle/liquid vortex-emulsion phase holdup (-)

ε_{v_L} : liquid phase in the particle/liquid vortex-emulsion phase holdup (-)

ϕ_{pde} : holdup of the particle downflow-emulsion phase (- or %)

ϕ_{pve} : holdup of the particle vortex-emulsion phase (- or %)

ϕ_{pw} : holdup of the particle wake phase (- or %)

γ : generalized liquid viscosity constant ($N/s^n m^2$)

κ : parameter of the double exponential distribution

λ : parameter of the double exponential distribution

σ : surface tension (dyne/cm)

σ_{pded} : solid velocity distribution standard-deviation of the particle downflow-emulsion phase (m/s)

σ_{pved} : solid velocity distribution standard-deviation of the particle vortex-emulsion phase (m/s)

σ_{pwd} : solid velocity distribution standard-deviation of the particle wake phase (m/s)

σ_{v_b} : bubble velocity (relative to the wall) distribution standard-deviation

$\sigma_{v_{le}}$: liquid emulsion phase velocity distribution standard-deviation

$\sigma_{v_{br}}$: bubble velocity (relative to the liquid emulsion phase) distribution standard-deviation

4.2.11 REFERENCES

Bhatia, V. K. and N. Epstein (1974). Three-phase fluidization: a generalized wake model. Fluidization and its application. H. Angélino, Couderc,J.P., Gilbert, H. Laguérie, C. Toulouse, France, Cépaduès-Editions: 380-392.

Cassanello, M., F. Larachi, M.-N. Marie, C. Guy and J. Chaouki, "Experimental characterization of the solid phase chaotic dynamics in three-phase fluidization.", Industrial and Engineering Chemistry Research, Vol. 34, 2971-2980 (1995).

Chen, R. C., J. Reese and L.-S. Fan, "Flow structure in a three-dimensional bubble column and three-phase fluidized bed.", American Institute of Chemical Engineering Journal, Vol. 40, 1093-1104 (1994).

Darton, R. C., "The physical behavior of three-phase fluidized beds, chapter 15 in Fluidization", Academic Press, (1985).

Darton, R. C. and D. Harrison, "The rise of single gas bubbles in liquid fluidised beds.", Transactions of the Institute of Chemical Engineers, Vol. 53, 301 (1974).

Davies, R. M. and G. I. Taylor, "The mechanics of large bubbles rising through extended liquids and through liquids in tubes.", Proc. Royal Soc., Vol. A200, 375 (1950).

Dayan, A. and S. Zalmanovich, "Axial dispersion and entrainment of particles in wakes of bubbles.", Chemical Engineering Science, Vol. 37, 1253-1257 (1982).

Degaleesan, S., "Fluid dynamic measurements and modelling of liquid mixing in bubble columns", Department of chemical engineering, Saint-Louis, Washington university (1997)

Devanathan, N., D. Moslemian and M. P. Dudukovic, "Flow mapping in bubble columns using CARPT.", Chemical Engineering Science, Vol. 45, 2285-2291 (1990).

El-Temtamy, S. A. and N. Epstein, "Simultaneous solids entrainment and de-entrainment above a three-phase fluidized bed.", Fluidization, Vol., 519-528 (1980).

Fan, L. S., "Gas-liquid-solid fluidisation engineering", Butterworths, Massachusetts Institute of Technology, (1989).

Fan, L.-S. and K. Tsuchiya, "Bubble wake dynamics in liquid and liquid-solid suspensions", Butterworths, Massachusetts institute of technology, (1990).

Fan, L.-S. and G. Yang (2002). Gas-liquid-solid three-phase fluidization. Handbook of fluidization and fluid-particle systems. Y. a. D. Wen-Ching, M. **Chapter 27**.

Gervais, A., C. L. Briens, J. C. André and G. Wild, "A modified axial dispersion model applied to three-phase fluidized bed reactors with a transition zone.", Transactions of the Institute of Chemical Engineers, Vol. 73(Part A), 745-750 (1995).

Gidaspow, D., M. Bahary and U. K. Jayaswal, "Hydrodynamic models for gas-liquid-solid fluidization.", Numerical Methods in multiphase flows, Vol. 185, 177-123 (1994).

Grace, J. R., "Fluidization", McGraw-Hill, (1982).

Grevskott, S., B. H. Sannaes, M. P. Dudukovic, K. W. Hjarbo and H. F. Svendsen, "Liquid circulation, bubble size distributions, and solids movement in two- and three-phase bubble columns.", Chemical Engineering Science, Vol. 51, 1703-1713 (1996).

Grossman, S. and I. Procaccia, "Unified theory of relative turbulent diffusion.", Physical review, Vol. A29, 1358-1365 (1984).

Hyndman, C. and C. Guy, "Gas phase flow in bubble columns: a convective phenomenon.", The Canadian Journal of Chemical Engineering, Vol. 73, 426-434 (1995a).

Hyndman, C. and C. Guy, "Gas-phase hydrodynamics in bubble columns.", Transactions of the Institute of Chemical Engineers, Vol. 73, 302-307 (1995b).

Jean, R. H., W. T. Tang and L. S. Fan, "The sedimentation-dispersion model for slurry bubble columns.", American Institute of Chemical Engineering Journal, Vol. 35, 662-665 (1989).

Kiared, K., F. Larachi, C. Guy and J. Chaouki, "Trajectory length and residence-time distributions of the solids in three-phase
fluidized beds.", Chemical Engineering Science, Vol. 52, 3931-3939 (1997).

Kim, S. D., C. G. J. Baker and M. A. Bergougnou, "Bubble characteristics in three-phase fluidized beds.", Chemical Engineering Science, Vol. 32, 1299-1306 (1977).

Knesebeck, A. and R. Guardani, "Estimation of particle concentration profiles in a three-phase fluidized bed from experimental data and using the wake model.", Brazilian Journal of Chemical Engineering, Vol. 21(1), 47-57 (2004).

Kwon, H. W., Y. Kang, S. D. Kim, M. Yashima and T. L. Fan, "Bubble-chord length and pressure fluctuations in three-phase fluidized beds.", Industrial and Engineering Chemistry Research, Vol. 33, 1852-1857 (1994).

Larachi, F., M. Cassanello, J. Chaouki and C. Guy, "Flow structure of the solids in a 3-D gas-liquid-solid fluidized bed.", American Institute of Chemical Engineering Journal, Vol. 42, 2439-2452 (1996).

Larachi, F., M. Cassanello, M.-N. Marie, J. Chaouki and C. Guy, "Solids circulation pattern in three-phase fluidized beds containing binary mixtures of particles as inferred from RPT.", Transactions of the Institute of Chemical Engineers, Vol. 73, 263-268 (1995).

Larachi, F., G. Kennedy and J. Chaouki, "A gamma-ray detection system for 3-D particle tracking in multiphase reactors.", Nucl. Instr. Meth., Vol. A338, 568 (1994).

Lee, S. L. P., A. Soria and H. I. de Lasa, "Evolution of bubble length distribution in three-phase fluidized beds.", AIChE J., Vol. 36, 1763-1767 (1990).

Lefebvre, S., J. Chaouki and C. Guy, "Phase mixing modeling in multiphase reactors containing gas bubble: a review.", International journal of chemical reactor engineering, Vol. 2 (2004).

Lefebvre, S. and C. Guy, "Characterization of bubble column hydrodynamics with local measurements.", Chemical Engineering Science, Vol. 54, 4895-4902 (1999).

Levenspiel, O., "Chemical reaction engineering", John Wiley & Sons, Oregon state university (1999).

Levenspiel, O. and T. L. Fitzgerald, "A warning on the misuse of the dispersion model.", Chemical Engineering Science, Vol. 38, 491-493 (1983).

Li, Y., J. Zhang and L.-S. Fan, "Numerical simulation of gas-liquid-solid fluidization systems using a combined CFD-VOF-DPM method: bubble wake behavior.", Chemical Engineering Science, Vol. 54, 5101-5107 (1999).

Linek, V., V. Stoy, V. Machon and Z. Krvsky, "Increasing the effective interfacial area in plastic-packed bed absorption column.", Chemical Engineering Science, Vol. 29, 1955 (1974).

Lübbert, A. and B. Larson, "Detailed investigations of the multiphase flow in airlift tower loop reactors.", Chemical Engineering Science, Vol. 45, 3047-3053 (1990).

Matsuura, A. and L. S. Fan, "Distribution of bubble properties in a gas-liquid-solid fluidized bed.", American Institute of Chemical Engineering Journal, Vol. 30, 894-903 (1984).

Mitra-Mudjumdar, D., B. Farouk and Y. T. Shah, "Hydrodynamic modeling of three-phase flows trough a vertical column.", Chemical Engineering Science, Vol. 52, 4485-4497 (1997).

Murray, P. and L. S. Fan, "Axial solid distribution in slurry bubble column.", Industrial and Engineering Chemistry Research, Vol. 28, 1697-1703 (1989).

Nigam, K. D. P. and A. Schumpe, "Three-phase sparged reactors", Gordon and Breach, (1996).

Olmos, E., C. Gentric, C. H. Vial, G. Wild and N. Midoux, "Numerical simulation of multiphase flow in bubble column reactors. Influence of bubble coalescence and break-up.", Chemical Engineering Science, Vol. 56, 6359-6365 (2001).

Rade, L. and B. Westergren, "Mathematics handbook for science and engineering, 4ed", Springer-verlans Berlin Heidelberg., (1999).

Rigby, G. R., G. P. Van Blockland, E. H. Park and C. E. Capes, "Properties of bubbles in three phase fluidized beds as measured by an electroresistivity probe.", Chemical Engineering Science, Vol. 25, 1729-1741 (1970).

Schiller, L. and A. Naumann, "Zeitschr.", V.D.I., Vol., 318-320 (cited by Nigam and Schumpe, 1996) (1933).

Schlüter, M., S. Scheid, S. John and N. Räbiger, "Fluidization of fine particles in bubble wake affects hydrodynamics in three-phase flows.", Journal of chemical engineering of Japan, Vol. 37(8), 947-954 (2004).

Sikun, X., J. Chaouki, C. Guy and Q. Yuhui, "Characterization of homogeneity of bubble columns using RPT and fiber optics.", International journal of chemical reactor engineering, Vol. 3, A54 (2005).

Tang, W. T. and L. S. Fan, "Hydrodynamics of a three-phase fluidized bed containing low-density particles.", American Institute of Chemical Engineering Journal, Vol. 35, 355-364 (1989).

Tsutsumi, A., T. Charinpanitkul and K. Yoshida, "Prediction of solid concentration profiles in three-phase reactors by a wake shedding model.", Chemical Engineering Science, Vol. 47, 3411-3418 (1992).

Turi, E. and K. M. Ng, "Axial distribution of soid particles in bubble column slurry reactors in the bubble flow regime.", Chemical Engineering Communications, Vol. 46, 323-345 (1986).

Tzeng, J. W., R. C. Chen and L.-S. Fan, "Visualisation of flow characteristics in a 2-D bubble column and three-phase fluidized bed.", AIChE J., Vol. 39, 733 (1993).

Villermaux, J., "Trajectory length distribution (TLD), a novel concept to characterize mixing in flow systems.", Chemical Engineering Science, Vol. 51, 1939-1946 (1996).

Yang, Y. B. and M. P. Dudukovic, "Liquid backmixing in bubble column via computer-automated radioactive particle tracking (CARPT).", Experiments in fluids, Vol. 16, 1-9 (1993).

Yu, Y. H. and S. D. Kim, "Bubble caracteristics in the radial direction of three-phase fluidized beds.", AIChE J., Vol. 34, 2069-2072 (1988).

Zhang, J., Y. Li and L.-S. Fan, "Numerical studies of bubble and particle dynsmics in a three-phase fluidized bed at elevated pressures.", Powder technology, Vol. 112, 46-56 (2000).

LIST OF FIGURES

Figure 4.1: Flow representation characterizing various solid phase mixing models. (Figure inspired by Murray and Fan, 1989). Dash arrows represent transferred solute between phases and the full arrows represent liquid and solid phase exchange between wake and emulsion phases.

Figure 4.2: Three mixing mechanisms.

Figure 4.3: Update of the flow representation shown in Figure 1. Dash arrows represent transferred solute between phases and the full arrows represent liquid and solid phase exchange between bubble/wake class and liquid/solid emulsion phase, and between liquid/solid emulsion phase and liquid/solid vortex phase.

Figure 4.4: Distributor of the 0.292 m three-phase fluidized bed. Dimensions are in mm.

Figure 4.5: Time series of the traced particle axial position. Particle phase examples. Illustration of the spending time (tspend) and axial trajectory length (lz). Dc=0.292 m ; GB3mm ; UL=0.042 m/s ; Ug=0.050 m/s.

Figure 4.6: Solid Velocity Distribution functions – Downflow-Emulsion Phase, Vortex-Emulsion Phase, Wake Phase and all phases. Fitting quality example for Dc=0.292 m ; GB3mm ; UL=0.042 m/s ; Ug=0.031 m/s.

Figure 4.7: Solid Velocity Distribution function – Wake Phase. Operating conditions effect. Dc=0.292 m ; GB3mm.

Figure 4.8: Average and standard deviation (STD) of the Solid Velocity Distribution function – Wake Phase. Dc=0.292 m ; GB3mm.

Figure 4.9: Relation between the average and standard deviation (STD) of the Solid Velocity Distribution function – Wake Phase. (a) Comparison between Dc=0.10m and 0.292m. (b) Correlation taking into account the column diameter (Dc).

Figure 4.10: Relation between the average of the solid velocity distribution function and superficial gas and liquid velocity – Wake Phase. (a) Comparison between Dc=0.10m and 0.292m. (b) Correlation taking into account the column diameter (Dc).

Figure 4.11: Relation between the average of the solid velocity distribution function – Wake Phase vs Downflow-Emulsion phase.

Figure 4.12: Relation between the Average and Standard Deviation of the Solid Velocity Distribution function – Downflow-Emulsion Phase. . (a) Comparison between Dc=0.10m and 0.292m. (b) Correlation taking into account the column diameter (Dc).

Figure 4.13: Solid Velocity Distribution function – Vortex Phase. Operating conditions effect. Dc=0.292 m ; GB3mm.

Figure 4.14: Standard deviation (STD) of the Solid Velocity Distribution function – Vortex Phase.

Figure 4.15: From Lagrangian to Eulerian velocity measurements. Contribution of the three particle phases.

Figure 4.16: Particle phase holdup. (a) Wake phase (b) wake phase correlation prediction quality (c) Relation between particle vortex-emulsion phase and particle wake phase holdup.

Figure 4.17: Relative contribution of the convective over dispersive mixing mechanism or Mixing Mechanism Indicator (MMI).

Figure 4.18: Cumulative distribution function of particle phase spending time. (a) Dc=0.292 m, GB3mm, UL=0.042 m/s, Ug=0.080 m/s (b) Dc=0.10 m, GB3mm, UL=0.065 m/s, Ug=0.069 m/s

Figure 4.19: Mean particle phase spending time. (a) Wake phase (b) Vortex-emulsion phase.

Figure 4.20: Mean particle wake phase particle spending time again bed height.

Figure 4.21: Relation between particle convective spending time and particle convective phases velocity. Negative values for downflow-emulsion phase and positive values for wake phase. (a) direct plotting. (b) and (c) are the cumulative distribution function versus convective velocity for the downflow-emulsion phase and wake phase, respectively. Dc=0.292 m, GB3mm, UL=0.042 m/s, Ug=0.080 m/s.

Figure 4.22: Solid phase velocity flow field and particle phase holdup field. Dc=0.292 m ; GB3mm ; UL=0.042 m/s ; Ug=0.080 m/s.

Figure 4.23: Solid phase velocity flow field and particle phase holdup field. Dc=0.292 m ; GB3mm ; UL=0.062 m/s ; Ug=0.080 m/s.

Figure 4.24: Solid phase velocity flow field and particle phase holdup field. Dc=0.292 m ; GB3mm ; UL=0.042 m/s ; Ug=0.031 m/s.

Figure 4.25: Solid phase velocity flow field and particle phase holdup field. Dc=0.100 m ; GB3mm ; UL=0.065 m/s ; Ug=0.032 m/s.

Figure 4.26: Solid phase velocity flow field and particle phase holdup field. Dc=0.100 m ; GB3mm ; UL=0.065 m/s ; Ug=0.069 m/s.

Figure 4.27: Solid phase velocity flow field and particle phase holdup field. Dc=0.100 m ; PVC5.5mm ; UL=0.058 m/s ; Ug=0.025 m/s.

LIST OF TABLES

Table 4.1: Experimental conditions.

Table 4.2: Effect of superficial gas and liquid velocity on holdup parameters.

FIGURES

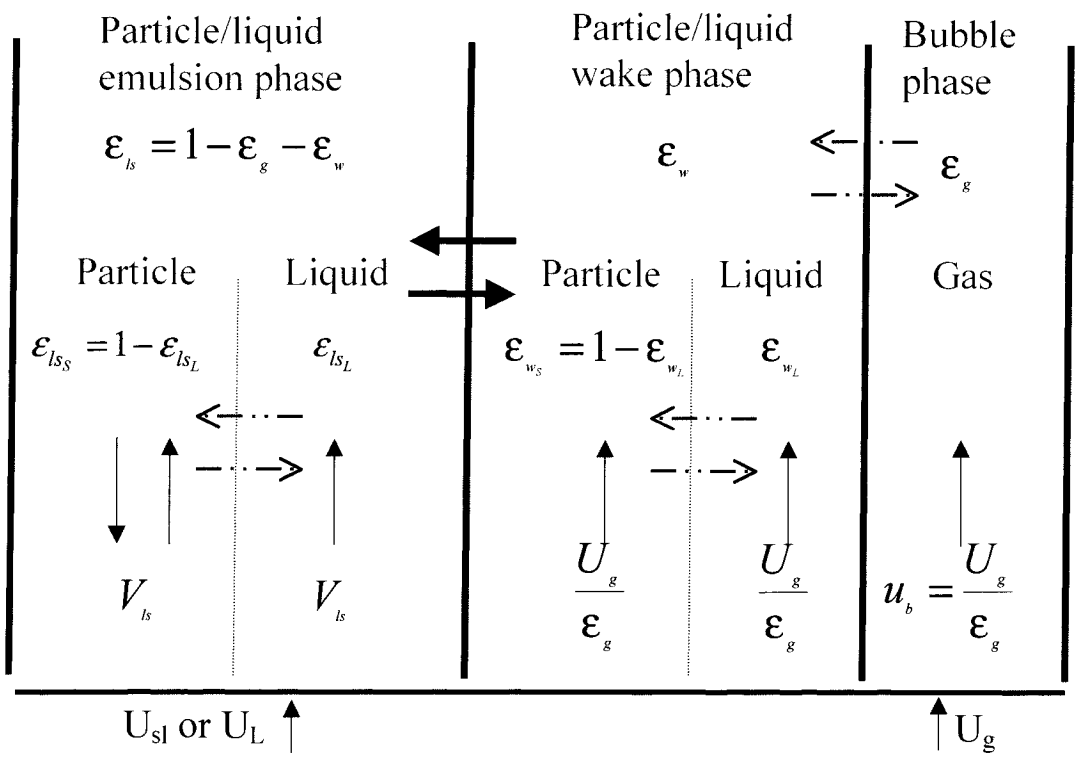


Figure 4.1: Flow representation characterizing various solid phase mixing models. (Figure inspired by Murray and Fan, 1989). Dash arrows represent transferred solute between phases and the full arrows represent liquid and solid phase exchange between wake and emulsion phases.

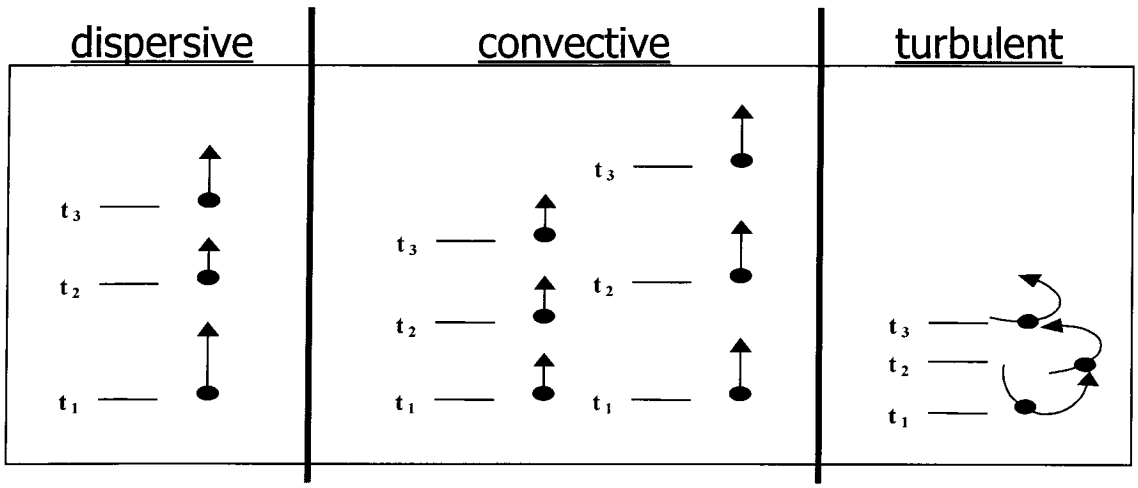


Figure 4.2: Three mixing mechanisms.

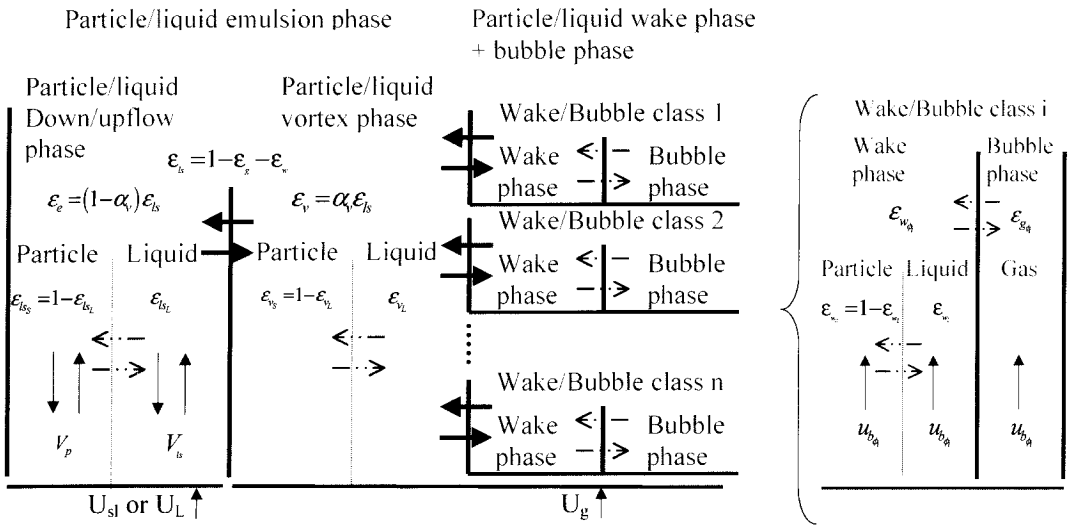


Figure 4.3: Update of the flow representation shown in Figure 4.1. Dash arrows represent transferred solute between phases and the full arrows represent liquid and solid phase exchange between bubble/wake class and liquid/solid emulsion phase, and between liquid/solid emulsion phase and liquid/solid vortex phase.

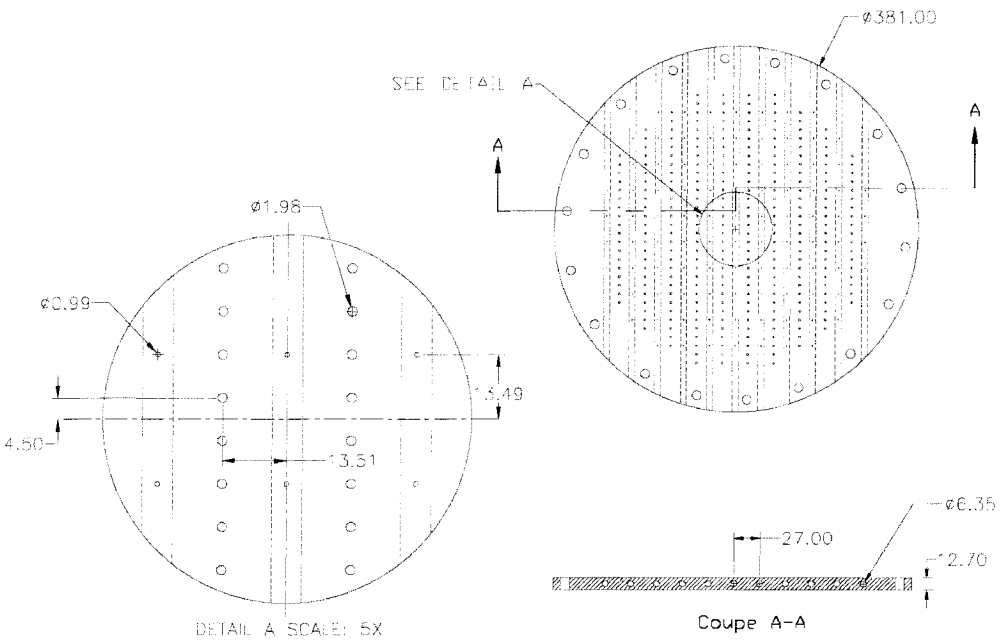


Figure 4.4: Distributor of the 0.292 m three-phase fluidized bed. Dimensions are in mm.

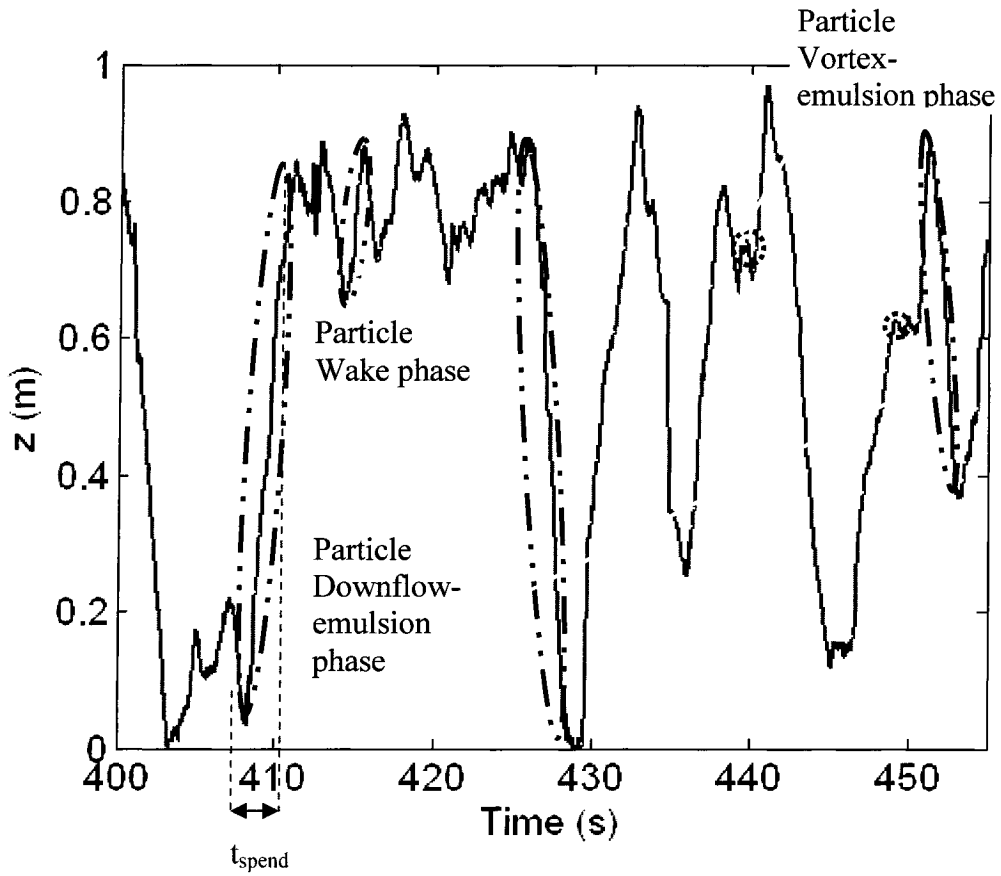


Figure 4.5: Time series of the traced particle axial position. Particle phase examples. Illustration of the spending time (t_{spend}) and axial trajectory length (l_z). Dc=0.292 m ; GB3mm ; UL=0.042 m/s ; Ug=0.050 m/s.

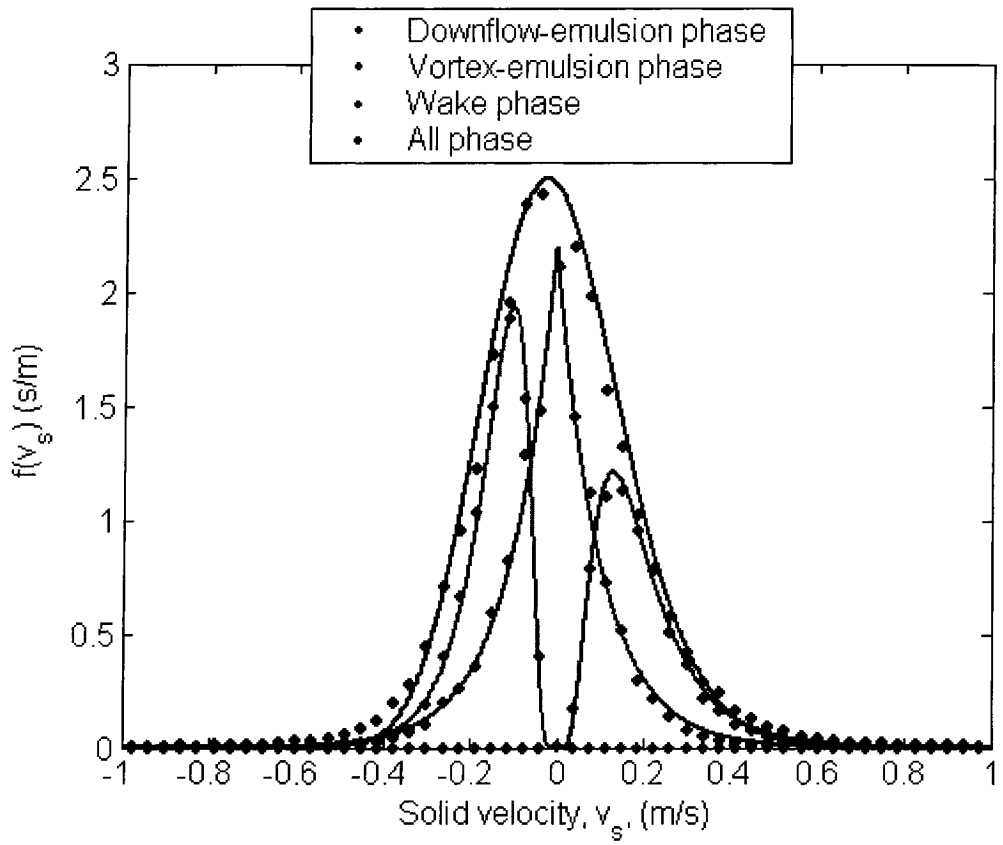


Figure 4.6: Solid Velocity Distribution functions – Downflow-Emulsion Phase, Vortex-Emulsion Phase, Wake Phase and all phases. Fitting quality example for Dc=0.292 m ; GB3mm ; UL=0.042 m/s ; Ug=0.031 m/s.

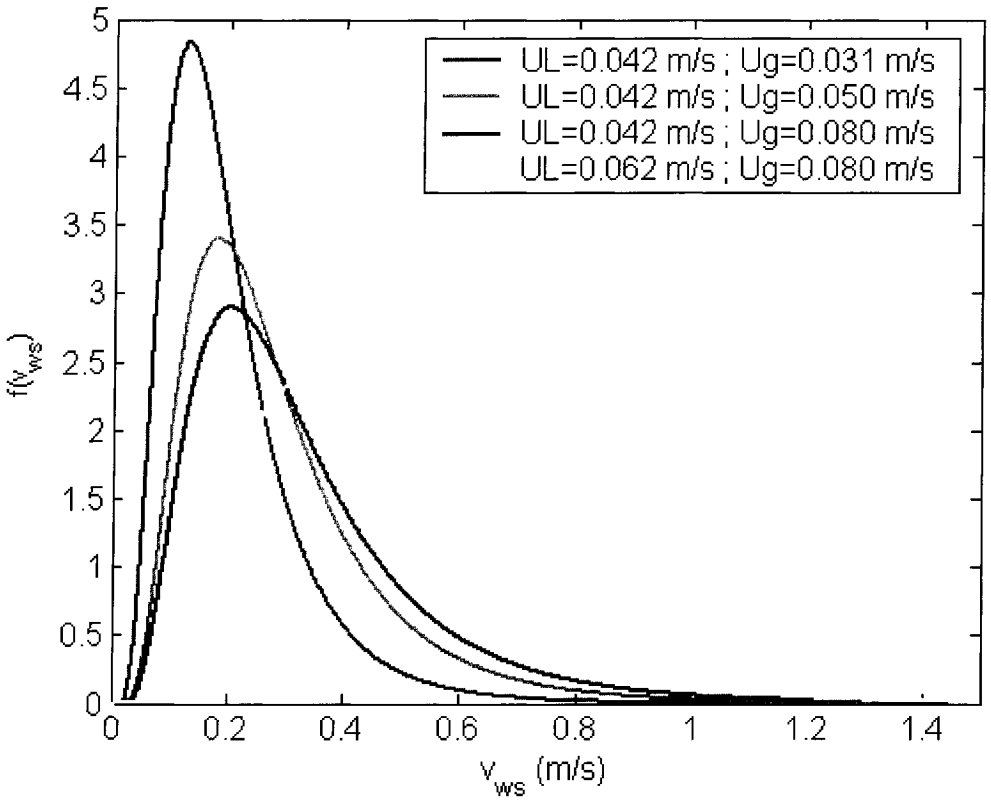


Figure 4.7: Solid Velocity Distribution function – Wake Phase. Operating conditions effect. Dc=0.292 m ; GB3mm.

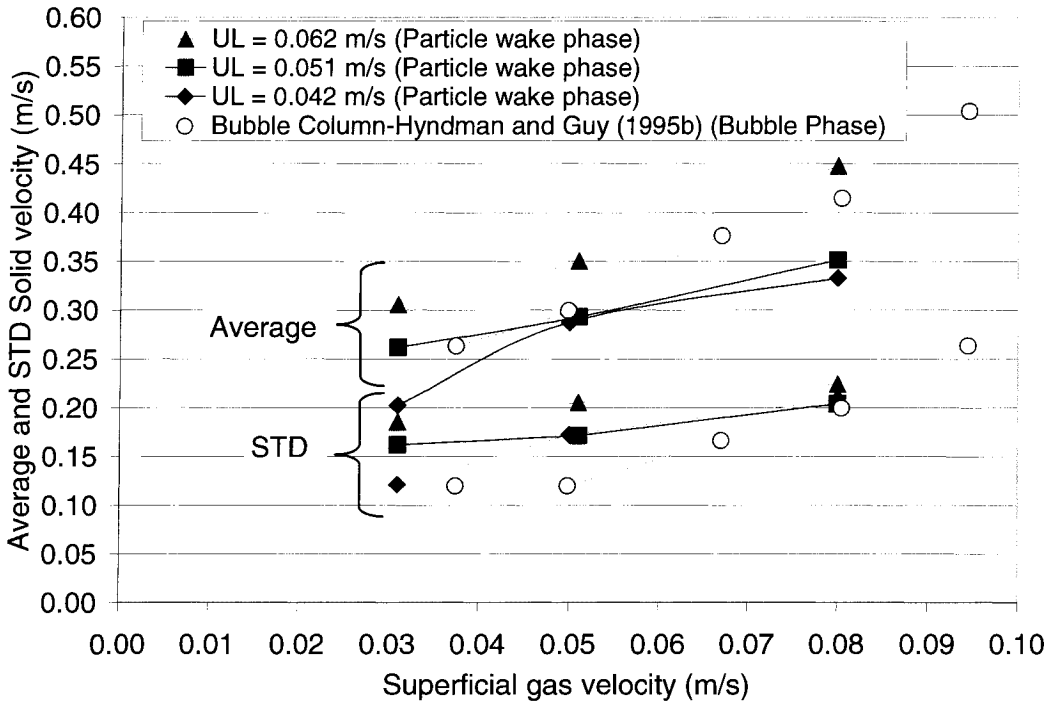
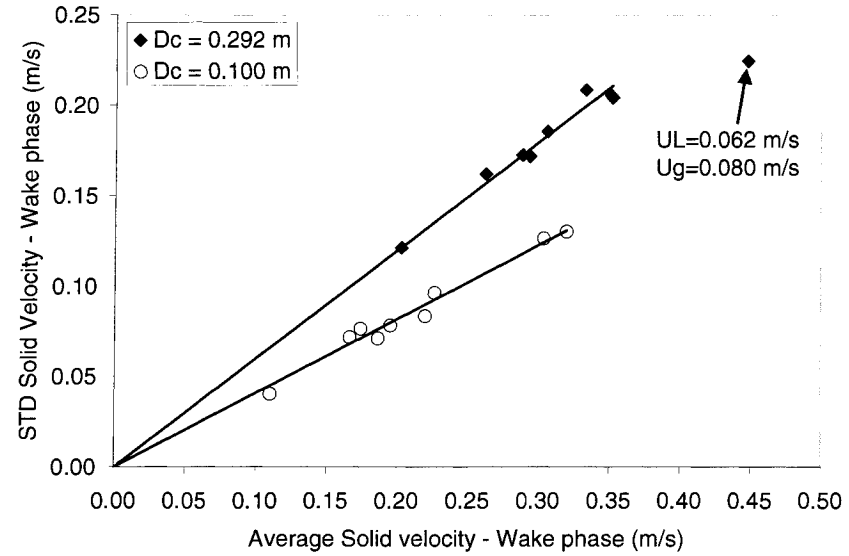
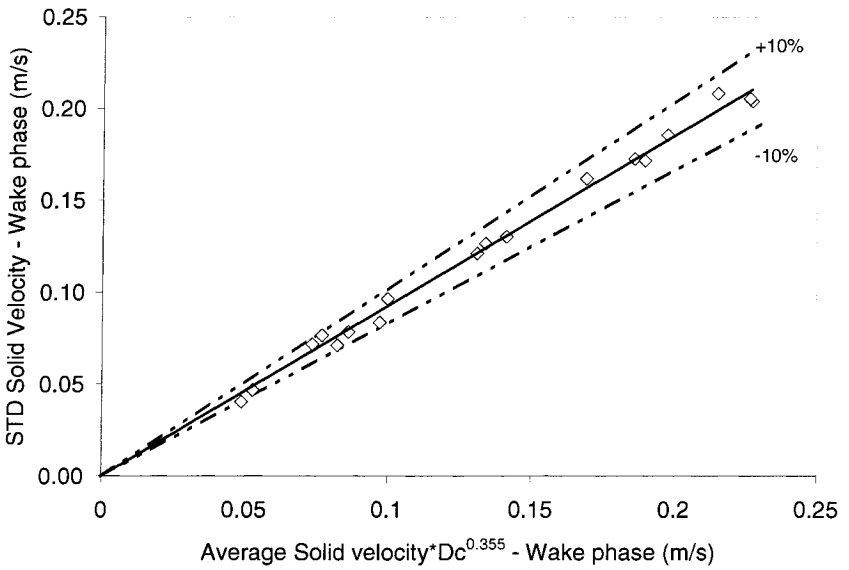


Figure 4.8: Average and standard deviation (STD) of the Solid Velocity Distribution function – Wake Phase. Dc=0.292 m ; GB3mm.

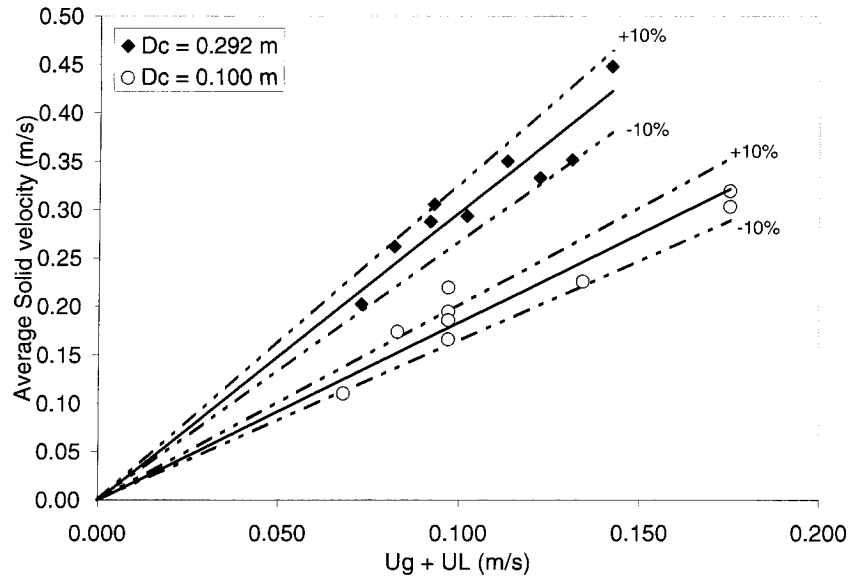


(a)

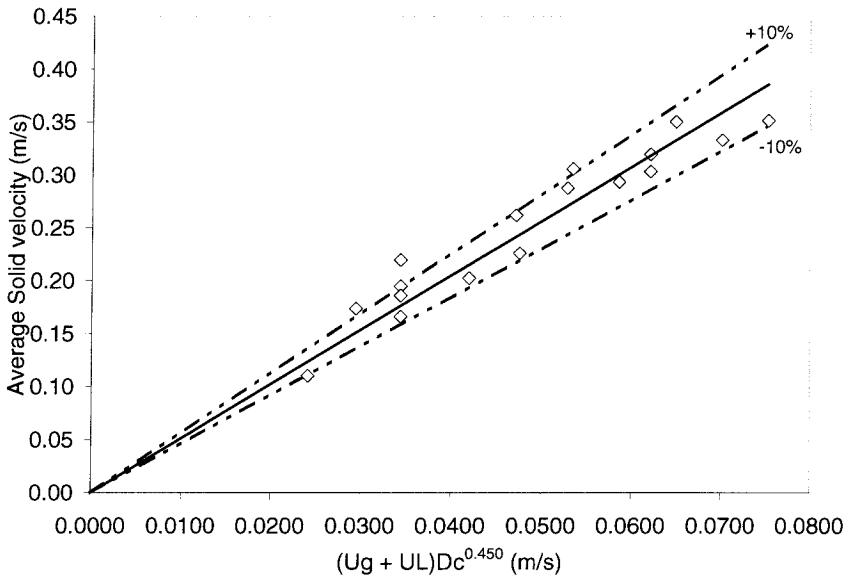


(b)

Figure 4.9: Relation between the average and standard deviation (STD) of the Solid Velocity Distribution function – Wake Phase. (a) Comparison between Dc=0.10m and 0.292m. (b) Correlation taking into account the column diameter (Dc).



(a)



(b)

Figure 4.10: Relation between the average of the solid velocity distribution function and superficial gas and liquid velocity – Wake Phase. (a) Comparison between Dc=0.10m and 0.292m. (b) Correlation taking into account the column diameter (Dc).

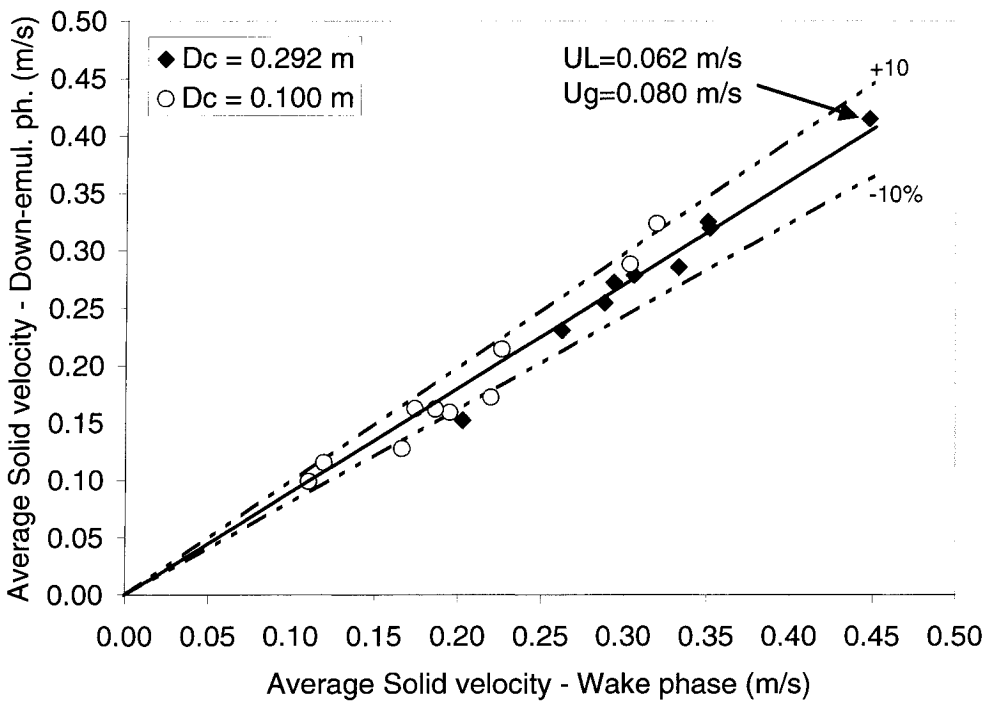
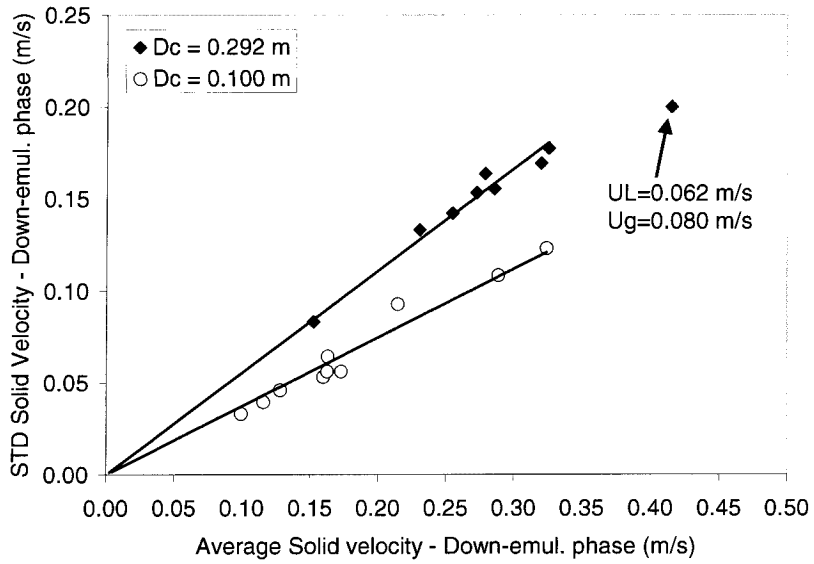
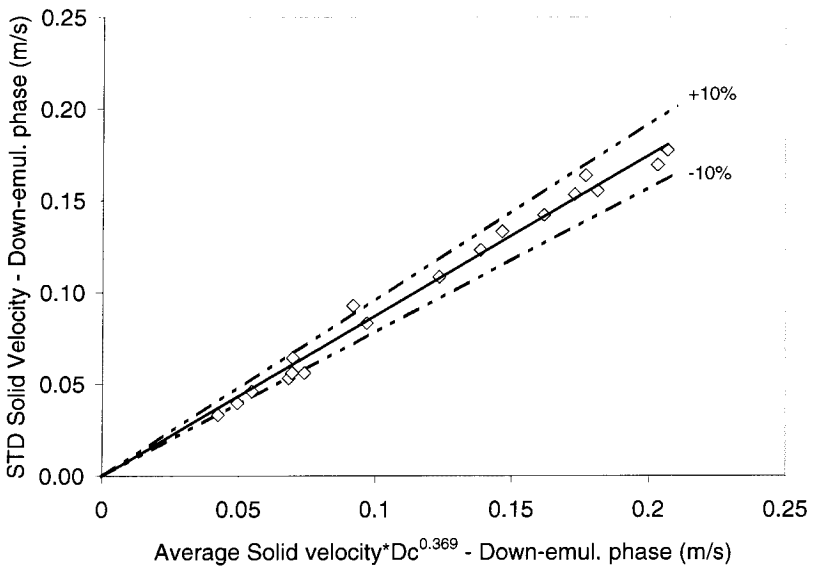


Figure 4.11: Relation between the average of the solid velocity distribution function – Wake Phase vs Downflow-Emulsion phase.



(a)



(b)

Figure 4.12: Relation between the Average and Standard Deviation of the Solid Velocity Distribution function – Downflow-Emulsion Phase. . (a) Comparison between Dc=0.10m and 0.292m. (b) Correlation taking into account the column diameter (Dc).

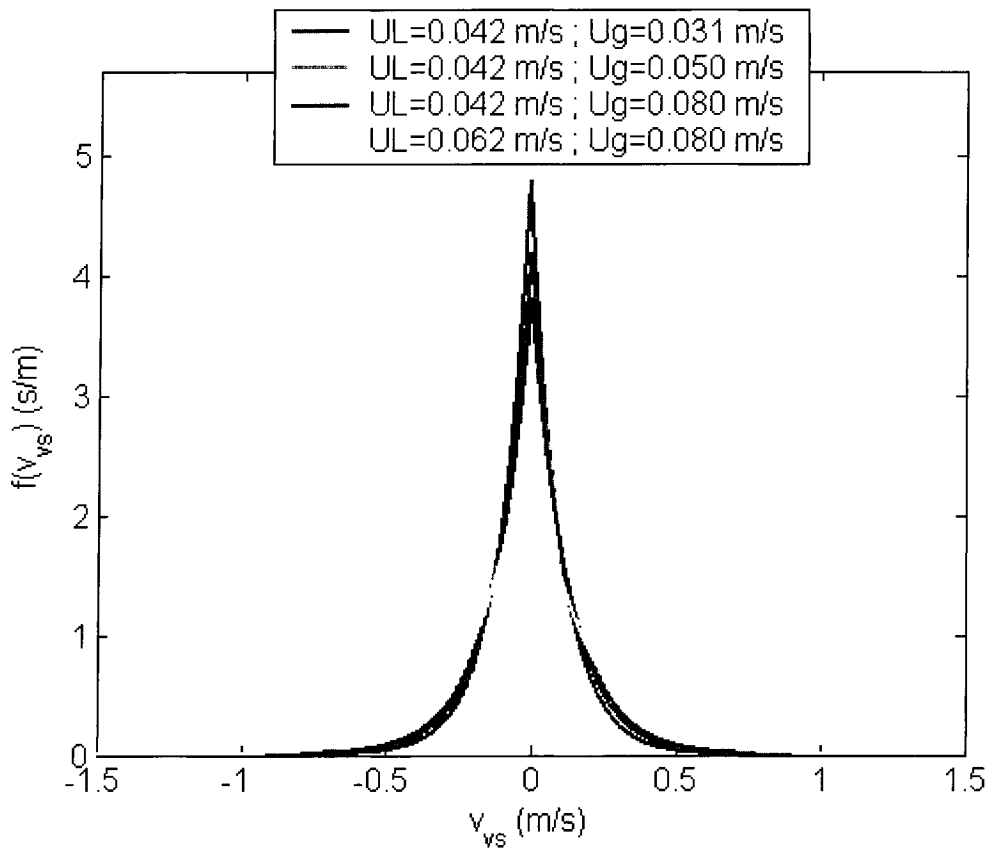


Figure 4.13: Solid Velocity Distribution function – Vortex Phase. Operating conditions effect. Dc=0.292 m ; GB3mm.

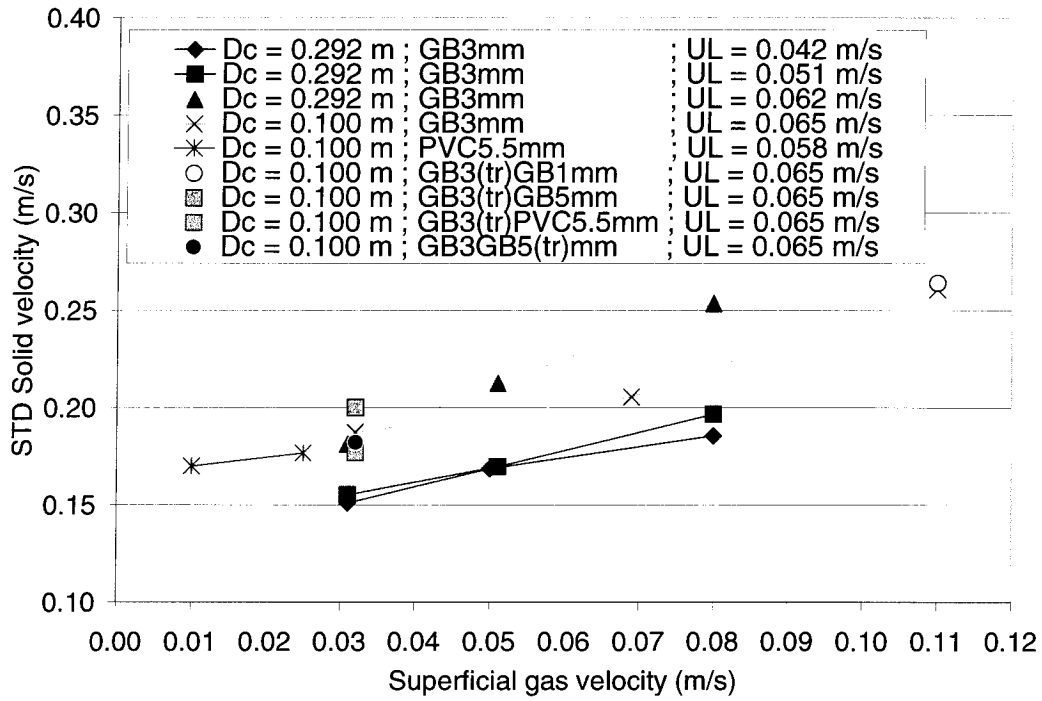


Figure 4.14: Standard deviation (STD) of the Solid Velocity Distribution function – Vortex Phase.

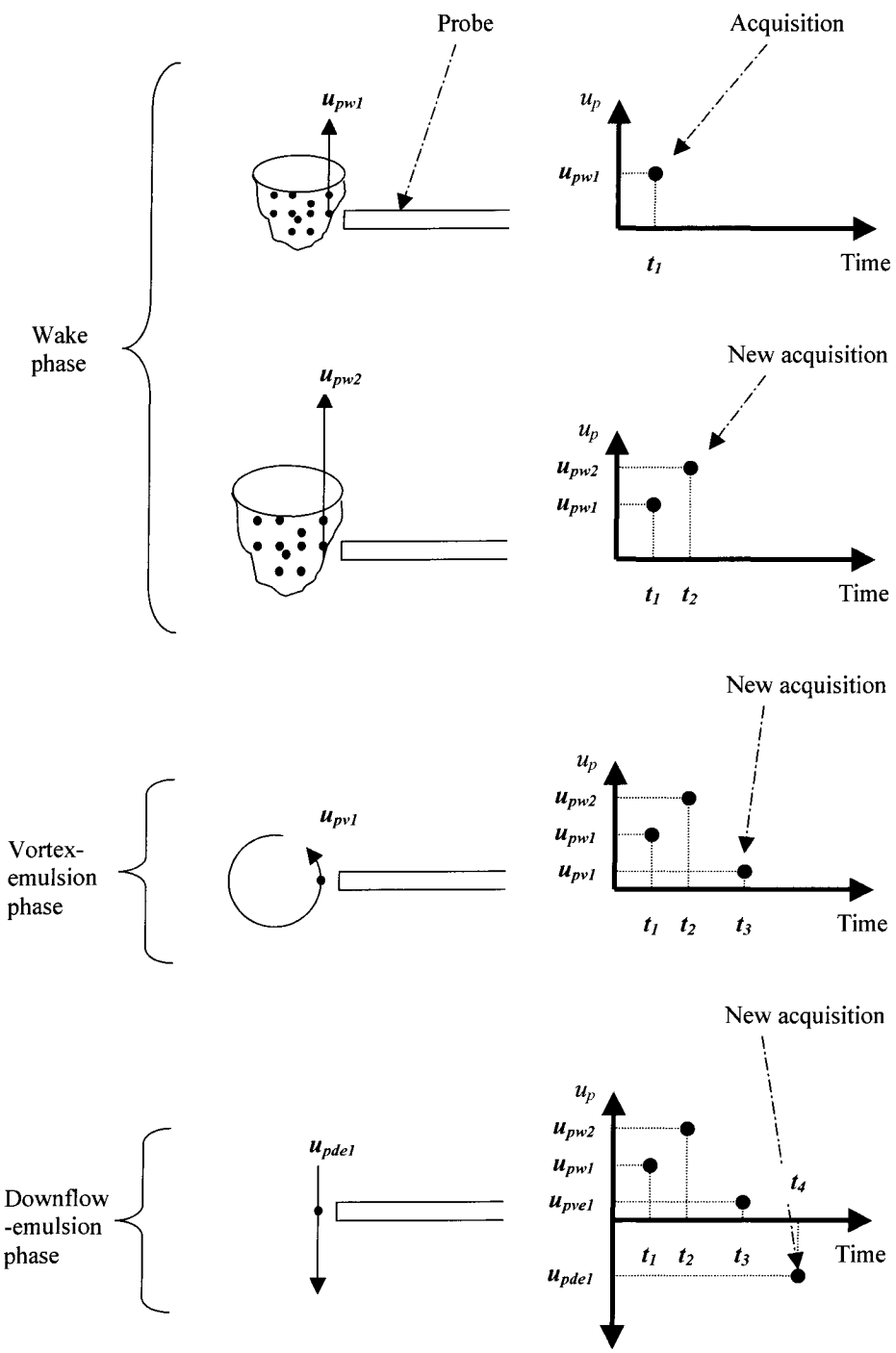
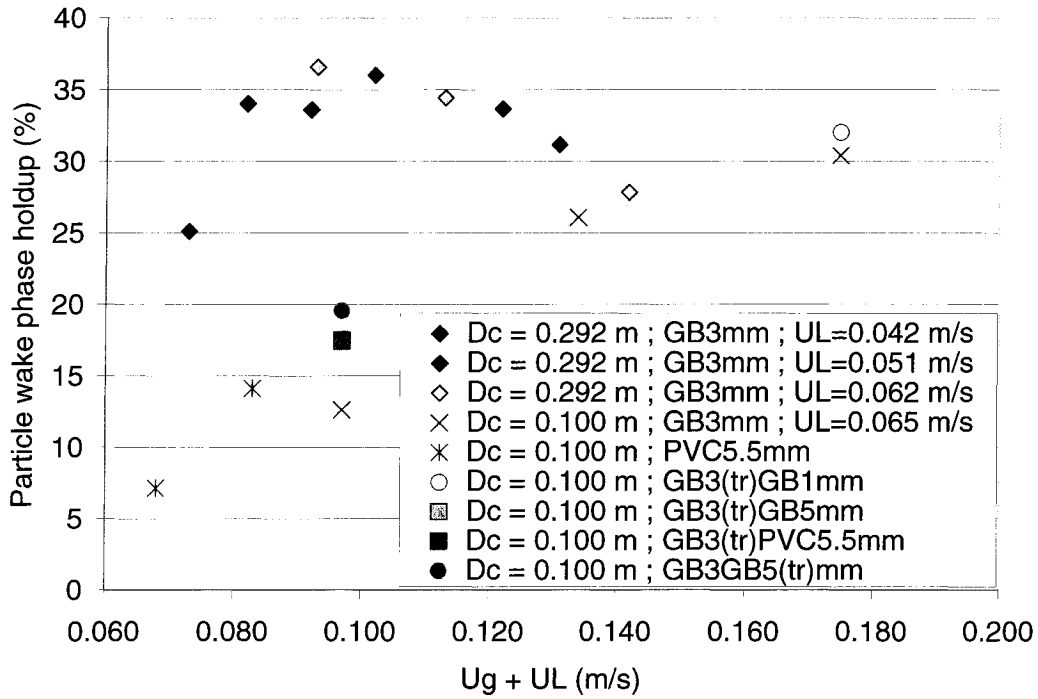
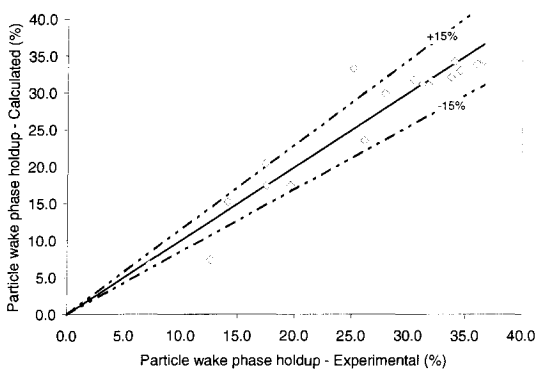


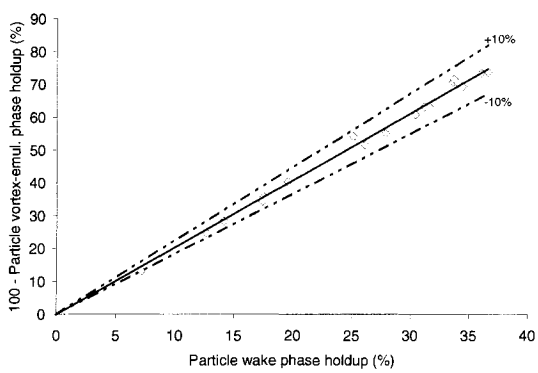
Figure 4.15: From Lagrangian to Eulerian velocity measurements. Contribution of the three particle phases.



(a)



(b)



(c)

Figure 4.16: Particle phase holdup. (a) Wake phase (b) wake phase correlation prediction quality (c) Relation between particle vortex-emulsion phase and particle wake phase holdup.

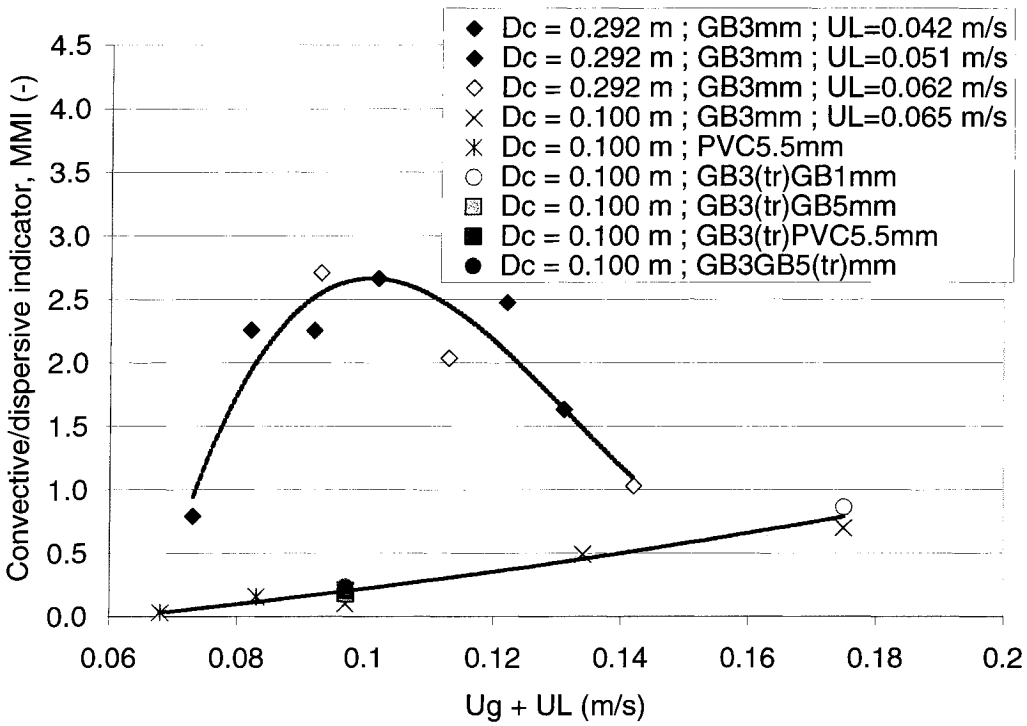
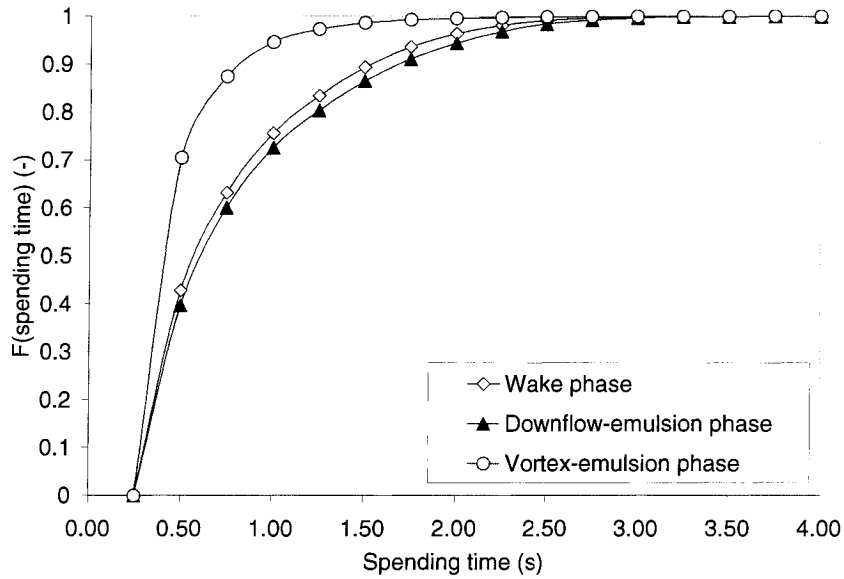
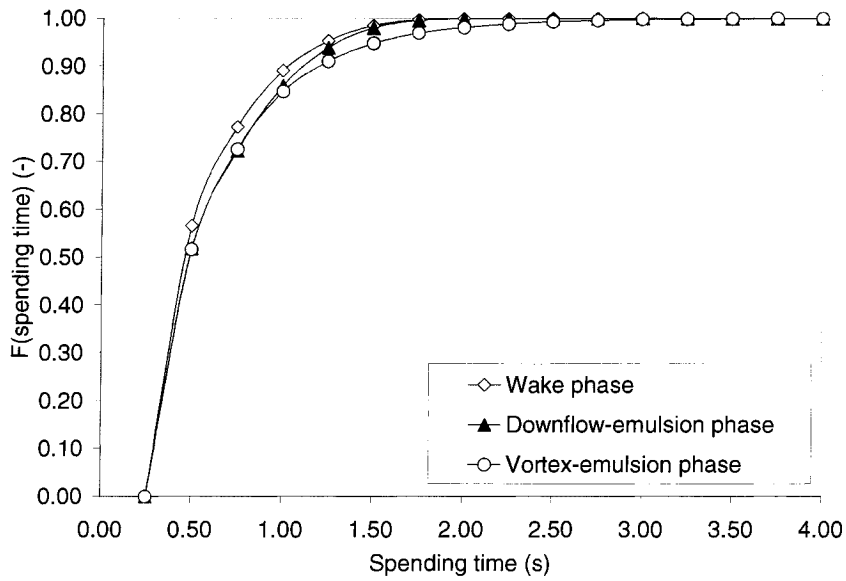


Figure 4.17: Relative contribution of the convective over dispersive mixing mechanism or Mixing Mechanism Indicator (MMI).

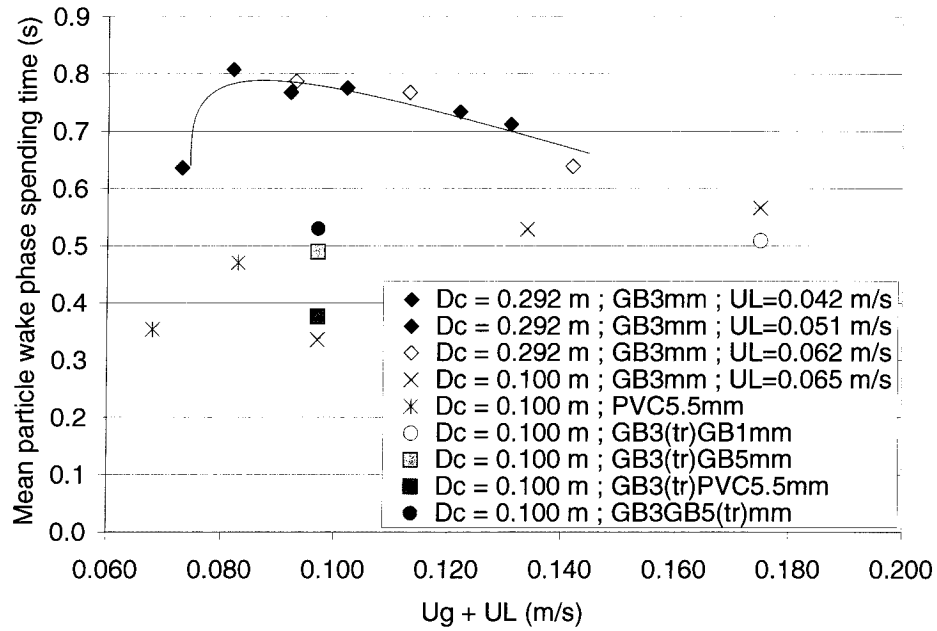


(a)

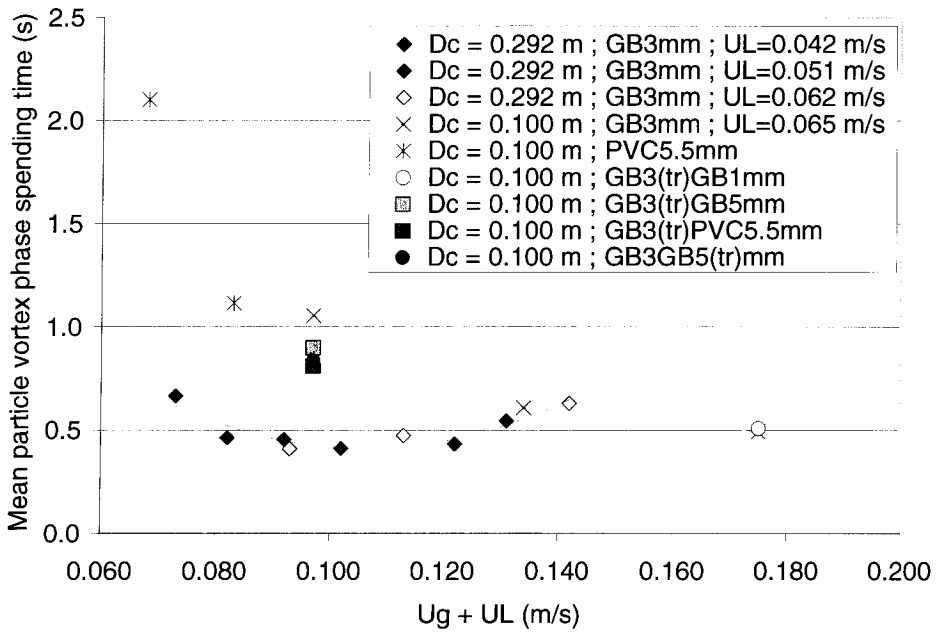


(b)

Figure 4.18: Cumulative distribution function of particle phase spending time. (a) Dc=0.292 m, GB3mm, UL=0.042 m/s, Ug=0.080 m/s (b) Dc=0.10 m, GB3mm, UL=0.065 m/s, Ug=0.069 m/s



(a)



(b)

Figure 4.19: Mean particle phase spending time. (a) Wake phase (b) Vortex-emulsion phase.

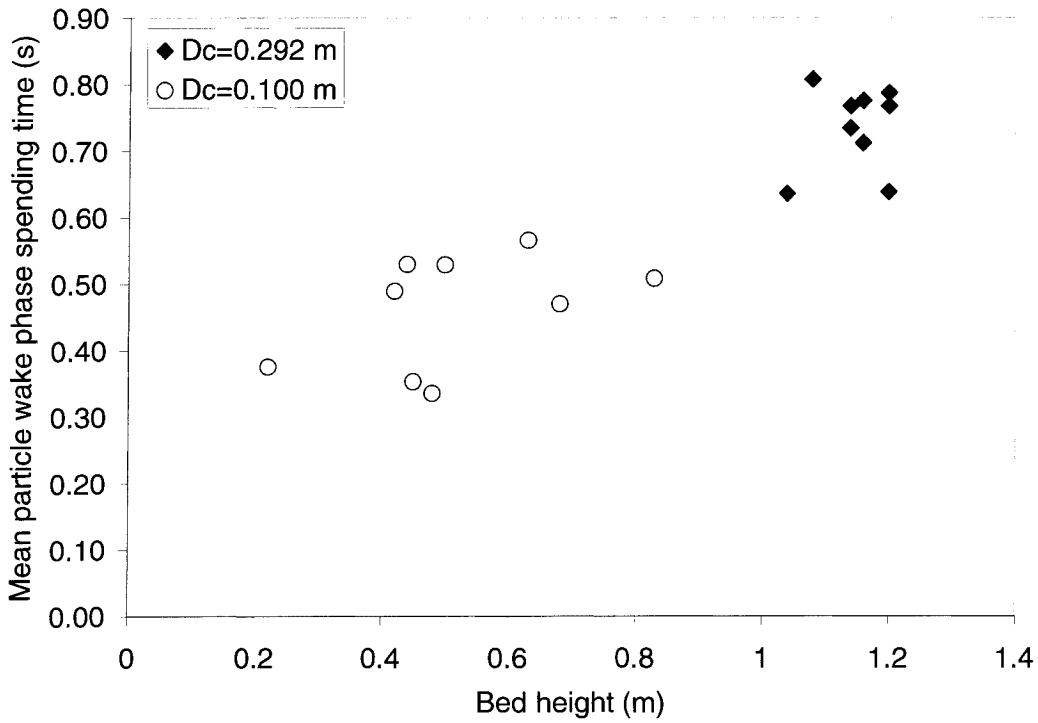
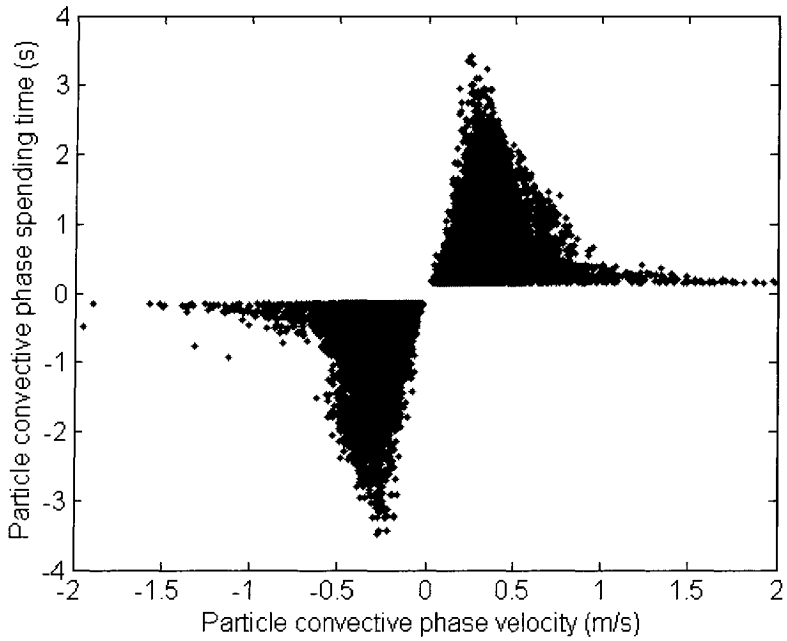
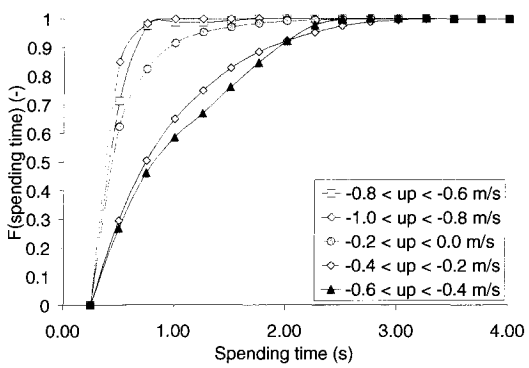


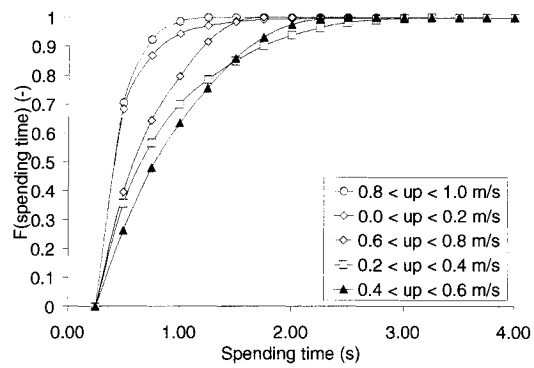
Figure 4.20: Mean particle wake phase particle spending time versus bed height.



(a)



(b)



(c)

Figure 4.21: Relation between particle convective spending time and particle convective phase velocity. Negative values for downflow-emulsion phase and positive values for wake phase. (a) direct plotting. (b) and (c) are the cumulative distribution function vs. convective velocity for the downflow-emulsion phase and wake phase, respectively. Dc=0.292 m, GB3mm, UL=0.042 m/s, Ug=0.080 m/s.

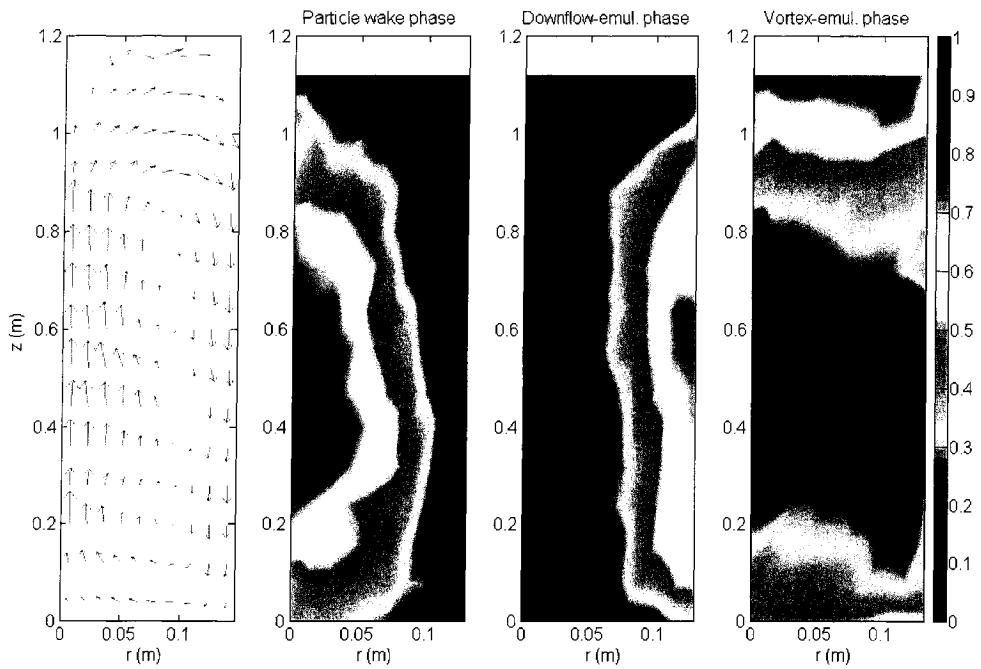


Figure 4.22: Solid phase velocity flow field and particle phases holdup field. Dc=0.292 m ; GB3mm ; UL=0.042 m/s ; Ug=0.080 m/s.

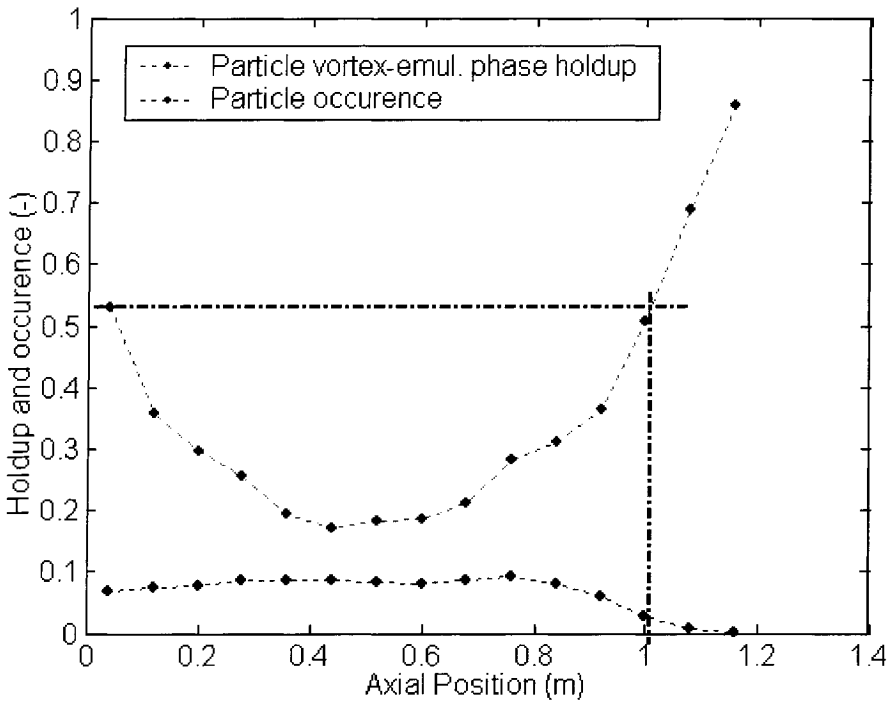


Figure 4.23: Comparison of the particle vortex-emulsion phase holdup axial profile and the particle occurrence axial profile. Dc=0.292 m ; GB3mm ; UL=0.042 m/s ; Ug=0.080 m/s.

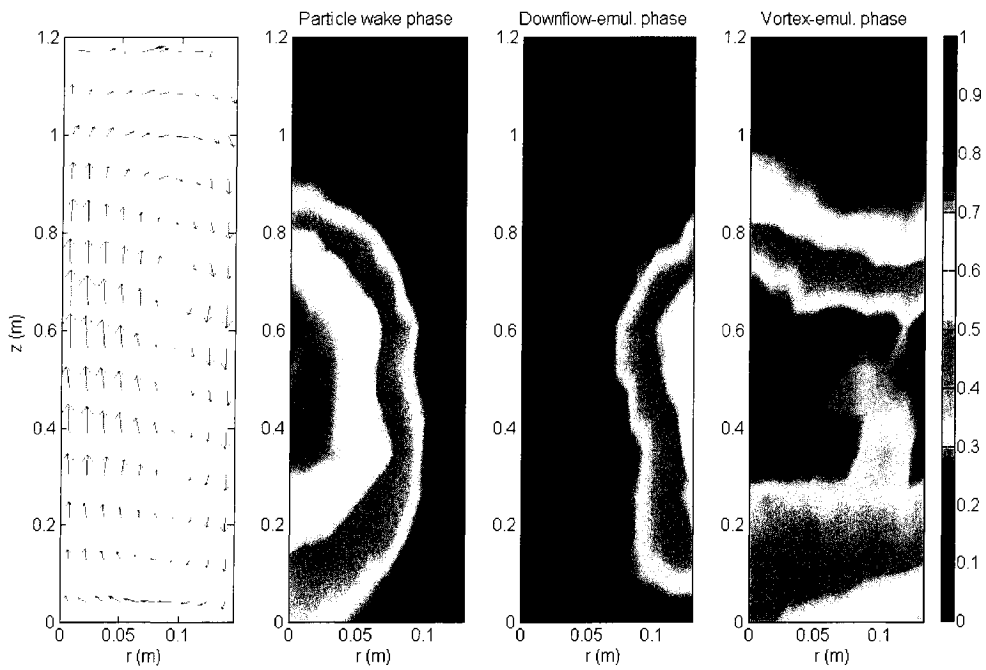


Figure 4.24: Solid phase velocity flow field and particle phase holdup field. Dc=0.292 m ; GB3mm ; UL=0.062 m/s ; Ug=0.080 m/s.

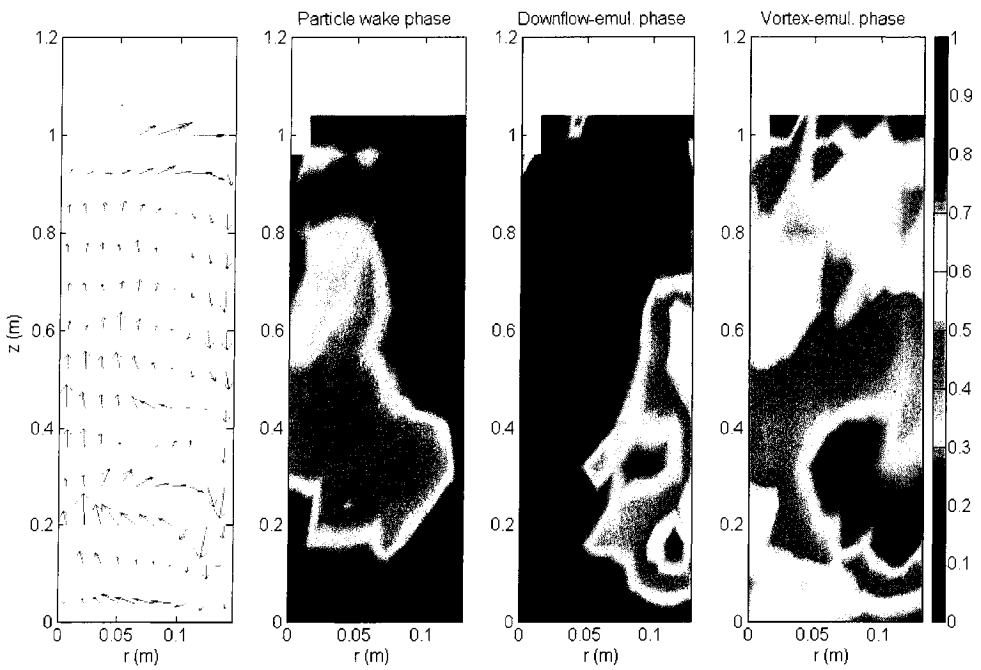


Figure 4.25: Solid phase velocity flow field and particle phase holdup field. Dc=0.292 m ; GB3mm ; UL=0.042 m/s ; Ug=0.031 m/s.

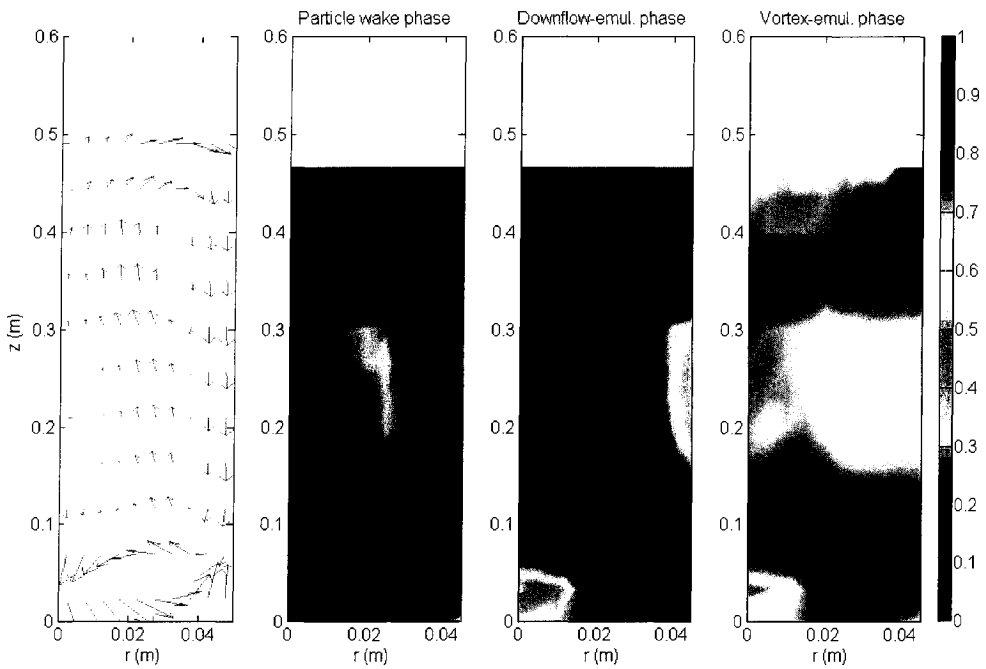


Figure 4.26: Solid phase velocity flow field and particle phase holdup field. Dc=0.100 m ; GB3mm ; UL=0.065 m/s ; Ug=0.032 m/s.

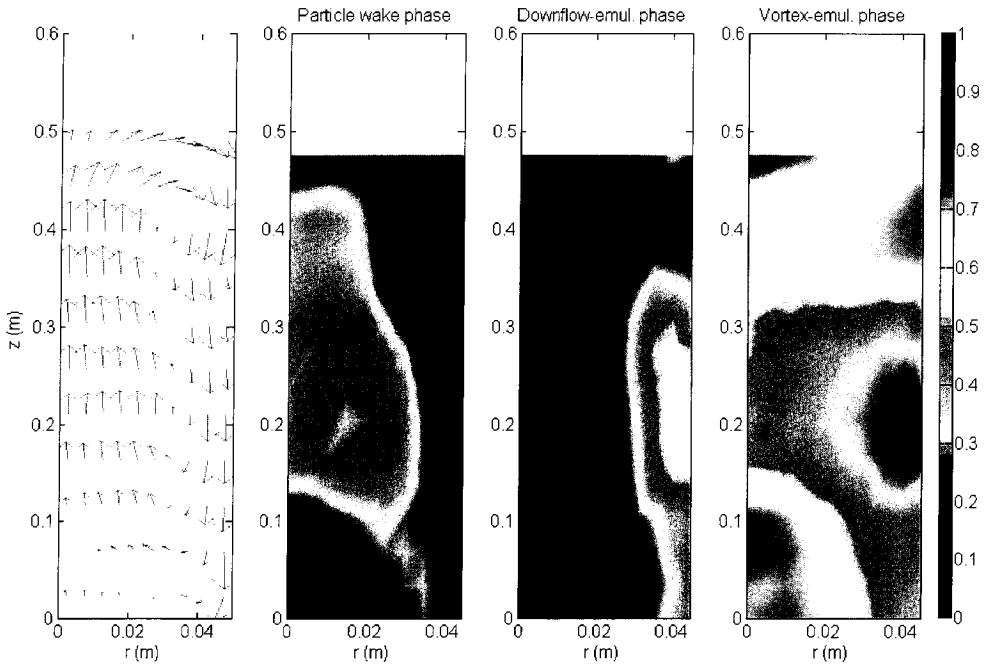


Figure 4.27: Solid phase velocity flow field and particle phase holdup field. Dc=0.100 m ; GB3mm ; UL=0.065 m/s ; Ug=0.069 m/s.

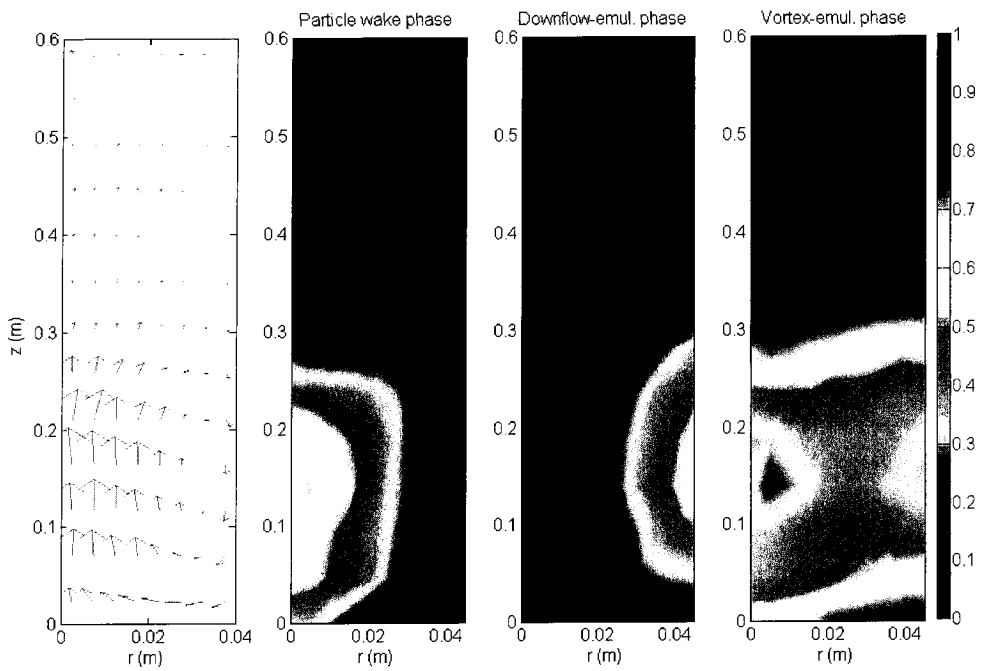


Figure 4.28: Solid phase velocity flow field and particle phase holdup field. Dc=0.100 m ; PVC5.5mm ; UL=0.058 m/s ; Ug=0.025 m/s.

TABLES

Table 4.1: Experimental Conditions.

Run	UL	Ug	Particle system [1]	Total bed mass [2]	$Umf_{Ug=0}$ [3]	u_t [4]
(#)	(m/s)	(m/s)		(kg)	(m/s)	(m/s)
Dc = 0.10 m						
1	0.065	0.032	GB3	4.0	0.036	0.37
2	0.065	0.069	GB3	4.0	0.036	0.37
3	0.065	0.106	GB3	4.0	0.036	0.37
4	0.065	0.106	{GB3}GB0.9	2.8	{0.036}0.009	{0.37}0.14
5	0.058	0.010	PVC5.5	0.8	0.023	0.23
6	0.058	0.025	PVC5.5	0.8	0.023	0.23
7	0.065	0.032	{GB3}GB5	3.0	{0.036}0.051	{0.37}0.47
8	0.065	0.032	GB3{GB5}	3.0	0.036{0.051}	0.37{0.47}
9	0.065	0.032	{GB3}PVC5.5	1.7	{0.036}0.023	{0.37}0.23
Dc = 0.292 m						
10	0.042	0.031	GB3	88	0.036	0.37
11	0.042	0.050	GB3	88	0.036	0.37
12	0.042	0.080	GB3	88	0.036	0.37
13	0.051	0.031	GB3	88	0.036	0.37
14	0.051	0.051	GB3	88	0.036	0.37
15	0.051	0.080	GB3	88	0.036	0.37
16	0.062	0.031	GB3	88	0.036	0.37
17	0.062	0.051	GB3	88	0.036	0.37
18	0.062	0.080	GB3	88	0.036	0.37

[1] GB: Glass Beads. The attached number represents the particle diameter in mm. { }: tracked particle.

[2] For binary system, the bulk volume ratio is approximately 1:1. 1.10 kg of glass beads and 0.62 kg of PVC particles composed the GB/PVC system. The void fraction at rest for glass beads and for PVC particles is, respectively, approximately 0.41 and 0.61.

[3] The liquid-solid minimum fluidization velocity was calculated by the Grace (1982)'s correlation.

[4] The terminal particle velocity was calculated by the Schiller and Nauman (1933)'s correlation.

Table 4.2: Effect of superficial gas and liquid velocity on holdup parameters.

Parameter	Ug ↑	UL ↑
$\varepsilon_w/\varepsilon_g$	↓	↑
ε_g	↑	↓
$\varepsilon_{w_s}/\varepsilon_{ls_s}$	↑	↓

CHAPITRE 5 : HYDRODYNAMIQUE DE LA PHASE SOLIDE – UN MODÈLE CONVECTIF/DISPERSIF[3]

5.1 Présentation de l'article

Les chapitres 2 et 4 ont permis d'identifier les caractéristiques clés qui doivent être respectées par un modèle de mélange de la phase solide. Parmi ces caractéristiques clés, il faut nommer l'effet des conditions opératoires sur la contribution relative du mécanisme convectif sur le mécanisme dispersif et le fait que cette contribution relative ne suit pas la même évolution que l'intensité de mélange. Les sous-phases de la phase solide sont réparties selon le mécanisme de mélange suivi par chacun. Afin d'avoir le modèle le plus simple possible, d'autres caractéristiques de l'hydrodynamique, comme le profil axial des fractions volumiques des sous-phases et l'évolution axiale des distributions de vitesse du solide, ont été négligées. Le développement et la validation du modèle proposé dans cette thèse font partie de ce chapitre. La comparaison avec d'autres modèles est également montrée dans ce chapitre.

---

[3] Soumis dans « Chemical Engineering Journal »

5.2 Solid Phase Hydrodynamics of Three-Phase Fluidized Beds – A Convective/Dispersive Mixing Model

Lefebvre, S., Guy, C., Chaouki, J.

5.2.1 Abstract

The main objective of this work was to develop a solid phase mixing model that followed not only the mixing extent, but also the overall mixing mechanism, i.e., the contribution of the convective onto the dispersive mixing mechanism. A non-invasive Radioactive Particle Tracking (RPT) technique was used to estimate the model parameters and generate tracer curves at various axial positions. The proposed model follows the tracer data well compared to the axial dispersion model. It has the flexibility to represent various contributions of the convective onto the dispersive mixing mechanism observed in three-phase fluidized beds and it is linked to the bubble velocity distribution. The convective/dispersive model successfully followed the evolution of the extent of particle mixing and the overall mixing mechanism at various superficial gas and liquid velocities as well as reactor diameters.

5.2.2 INTRODUCTION

Three-phase fluidized bed reactors are used in various industries, such as the petrochemical, biological and mineral industries. In order to design, optimize and scale-up three-phase fluidized bed reactors, models may be used. CFD models are great potential tools, but empirical closing equations and long computing times limit the utilization of such models. More simple models, called mixing models, which are based on assumptions about flow patterns, may be employed. These mixing models include the axial dispersion model, which is often relied on to model each phase without physical justification. Mixing models should be based on key hydrodynamic

properties, such as mixing mechanisms, e.g., convective and dispersive mechanisms (Levenspiel and Fitzgerald, 1983 and Levenspiel, 1999).

Lefebvre et al. (2004) reviewed phenomenological mixing models proposed in literature for reactors containing bubbles. The main conclusions were that the gas phase followed a convective mechanism (Hyndman and Guy, 1995), i.e., represented by a distribution of plug flow reactors in parallel. This means that bubbles are assumed to have constant Lagrangian rising velocities along the reactor length. This gives a convective mixing contribution to the liquid phase (Lübbert and Larson, 1990) due to the transport of the liquid in the bubble wake. Constant Lagrangian particle velocities were observed with radioactive particle tracking (RPT) measurements for the solid phase (Larachi et al., 1996) due, also, to the transport of the solid particles into the bubble wake. Based on these key hydrodynamic properties, Lefebvre et al. (2004) proposed an updated version of the structural wake model (Fan, 1989). There is no solid phase mixing model that takes into account the convective mixing contribution coming from the bubble wake transport at ***various*** Lagrangian constant velocities.

Lefebvre et al. (2006) relied on RPT data to compute parameters to investigate the relative contribution of the convective and dispersive mixing mechanisms on the overall solid phase mixing. One important finding discovered that the extent of mixing and the overall mixing mechanism (relative importance of the convective onto the dispersive mechanism) did not follow the same trend with experimental conditions, e.g., when the mixing extent increased, the relative importance of the convective mechanism might decrease or increase. A solid phase mixing model should follow not only the mixing extent, but also the overall mixing mechanism. The objective of this work was to develop such a mixing model.

5.2.3 EXPERIMENTAL

5.2.3.1 Experimental setups and operating conditions

Data were obtained from two different size co-current upward three-phase fluidized bed reactors and for various particle systems. Water was used as the fluidized medium and air was the gas phase. Experiments were conducted at ambient temperature and pressure.

The smaller column had a diameter of 0.10 m. RPT data obtained in this column have already been published in previous articles, e.g., Larachi et al. (1995), Larachi et al. (1996), Cassanello et al. (1995), Kiared et al. (1997). In a new, larger, three-phase fluidized bed, 0.292 m in diameter, 9 new sets of RPT data were obtained. In total, 15 sets of RPT data were used here. Table 5.1 shows the experimental conditions. The range of superficial gas and liquid velocities was 0.010-0.106 m/s and 0.042-0.065 m/s, respectively. Table 5.1 lists some particle properties. The 0.10 m and 0.292 m columns had a height of 1.5 m and 2.7 m, respectively. Description of the distribution systems and more details can be found in Lefebvre et al. (2006).

5.2.3.2 Radioactive Particle Tracking (RPT)

Our noninvasive Radioactive Particle Tracking (RPT) technique was used (Larachi et al., 1994). This technique followed one radioactively marked particle having the same diameter and density as the bed particles. The 3D position of the particle versus time was measured. Solid parameters, such as particle velocities and particle phase holdup, could then be computed to study solid phase hydrodynamics.

The RPT technique consisted of arranging various 76x76 mm uncollimated and unshielded NaI(TI) cylindrical scintillation detectors around the studied reactor. Eight detectors were used for the 0.10 m column and 16 for the 0.292 m column. A ^{46}Sc

filled particle was used as the traced particle and had the same diameter and density as the bed particles. The ^{46}Sc was obtained using neutron radioactive capture by ^{45}Sc in the Ecole Polytechnique Slowpoke nuclear reactor. Radioactivity of the ^{46}Sc was 50 and 200 μCi for the 0.10 and the 0.292 m columns, respectively. The γ-rays emitted by the ^{46}Sc were detected by the scintillation detectors. A detector photon count depends on the traced particle location in the bed, the corresponding subtended effective solid angle and the bed attenuation. This triangulation technique was used to yield the instantaneous traced particle position at 30 ms intervals. Data were collected over 5-6 hours for each experiment.

Prior to each experiment, the bed was fluidized and a set of measurements of the γ-ray photon count was made to calibrate the system using the traced particle rigidly positioned at 150 representative and known locations throughout the bed. Three parameters were fitted for each experiment: the linear attenuation coefficient of the gas-liquid-solid emulsion, the detectors dead time and the source radioactivity.

5.2.3.3 Mixing data from RPT

A tracer concentration curve generated after tracer injection was obtained from RPT data. This method assumed an ergodic motion process for the particles in the fluidized bed. It was already used by Cassanello et al. (1996) to obtain, as was done here, pulsed tracer data. The injection region was below 0.2 m in the axial direction (close to the distributor). Several radioactive particle trajectories starting below 0.2 m were collected. The positions of the collected trajectories were followed over 10 to 30 seconds. The first position of the collected trajectories was set at zero. At each time step (0.03 s), the number of particles in various axial regions, for example $0<z\leq0.2$ and $0.2<z\leq0.4$, was counted and divided by the volume of the region. The tracer concentration at each time step was divided by the tracer concentration at

homogenization. Normalized tracer curves were then obtained at various axial positions.

5.2.4 CONVECTIVE/DISPERSIVE MODEL DEVELOPMENT

5.2.4.1 Model concept

Based on the updated version of the structural wake model proposed by Lefebvre et al. (2004) and the study of Lefebvre et al. (2006), the solid phase mixing model shown in Figure 5.1 was proposed. The solid phase is separated into three sub-phases, i.e., the particle wake phase, the particle downflow-emulsion phase and the vortex-emulsion phase. The solid in the particle wake phase is transported at the various bubble wake Lagrangian constant velocities. This is demonstrated in Figure 5.2, which gives an example of RPT data. The upward constant Lagrangian velocity paths are identified as the particle wake phase and are due to transport in bubble wake. Therefore, the solid follows the convective mixing mechanism in that particle phase. The emulsion phase is divided into two particle phases. The particle downflow-emulsion phase represents the solid going down and following a convective mixing mechanism as a compensatory effect of the upward solid movement in the particle wake phase (Larachi et al., 1996). Therefore, the movement of the solid in the downflow-emulsion phase is indirectly linked to the gas phase hydrodynamics. The solid in the particle vortex-emulsion phase has a random movement, i.e., the particle position and velocity fluctuate erratically (dispersive mechanism). The solid in that particle phase is linked more to the liquid phase. Solid exchange occurs between the convective phases and the particle vortex-emulsion phase, but rarely between convective phases. In Figure 5.1, a large circulation pattern is represented by the arrow linking the convective phases at the top and bottom of the bed. This model agrees with the obvious superposition of the convective onto the dispersive mixing mechanism observed for the solid phase in three-phase fluidized bed reactors. It is also consistent with the result of Cassanello et

al. (1995) that the solid phase is superdispersive (faster than dispersive flow) in the axial direction.

5.2.4.2 Mathematical formulation

The model was applied onto a pulsed tracer test in batch mode constructed with the RPT data, as discussed previously. Mass balances on the solid phase convective/dispersive model were, therefore, made on an unsteady-state regime in a solid phase batch system.

The representation of multiple plug flows in parallel needed a velocity distribution function. Larachi et al. (1996) and Lefebvre et al. (2006) have shown that solid Lagrangian velocity distributions of the particle convective phases may be modelled after the log-normal distribution function shown in equation (32) for the particle wake phase. The Lagrangian velocity distribution of the particle wake phase may be viewed as the bubble velocity distribution. For the particle downflow-emulsion phase, replace u_{pwd}, u_{pw} and σ_{pwd} by u_{pded}, u_{pde} and σ_{pded}.

$$f\{u_{pwd}\} = \frac{1}{\beta u_{pwd}\sqrt{2\pi}} \exp\left[-\frac{\left(\ln\left(u_{pwd}\right) - \alpha\right)^2}{2\beta^2} \right] \qquad (32)$$

The relations linking the mean (u_{pw}) and the standard-deviation (σ_{pwd}) of the distribution to the function parameters (α,β) are shown in equations (33) and (34).

$$u_{pw} = \exp\left(\alpha + \frac{\beta^2}{2} \right) \qquad (33)$$

$$\sigma_{pwd} = \exp\left(\alpha + \frac{\beta^2}{2}\right)\sqrt{\exp(\beta^2) - 1} \qquad (34)$$

Unsteady-state regime mass balance applied on a fraction of the solid in the particle wake phase rising at a velocity u_{pwd} (one of the plug flow reactors) is shown in the following equation.

$$\frac{\partial C_{pw}\big|_{u_{pwd}}}{\partial t} = -u_{pwd}\frac{\partial C_{pw}\big|_{u_{pwd}}}{\partial z} + K_{pw-pve}\left[C_{pve} - C_{pw}\big|_{u_{pwd}}\right] \qquad (35)$$

With boundary conditions (B.C.) :

$$C_{pw}\{z=0\} = \frac{\phi_{pde}}{\phi_{pw}}\frac{\int_0^\infty u_{pded}C_{pde}\{z=0, u_{pded}\}f\{u_{pded}\}du_{pded}}{\int_0^\infty u_{pded}f\{u_{pded}\}du_{pded}}$$

Several differential equations, like equation (35), have to be solved. The number of differential equations depends on the discretization of the log-normal velocity distribution. This number has to be high enough to converge to the solution of the system of equations (discussed later).

An equivalent equation is obtained for the solid in the particle downflow-emulsion phase:

$$\frac{\partial C_{pde}\big|_{u_{pded}}}{\partial t} = -u_{pded}\frac{\partial C_{pde}\big|_{u_{pded}}}{\partial z} + K_{pde-pve}\left[C_{pve} - C_{pde}\big|_{u_{pded}}\right] \qquad (36)$$

$$\text{With B.C.}: C_{pde}\{z=L\}=\frac{\phi_{pw}}{\phi_{pde}}\frac{\int_0^{\infty}u_{pwd}C_{pw}\{z=L,u_{pwd}\}f\{u_{pwd}\}du_{pwd}}{\int_0^{\infty}u_{pwd}f\{u_{pwd}\}du_{pwd}}$$

Assuming that the solid mixing in the particle vortex-emulsion phase follows Fick's law, the unsteady-state regime mass balance gives:

$$\frac{\partial C_{pve}}{\partial t}=D_{ax_{pve}}\frac{\partial^2 C_{pve}}{\partial z^2}+\left(K_{pw-pve}\frac{\phi_{pw}}{\phi_{pve}}\right)\left[\int_0^{\infty}C_{pw}f\{u_{pwd}\}du_{pwd}-C_{pve}\right] \quad (37)$$

$$+\left(K_{pde-pve}\frac{\phi_{pde}}{\phi_{pve}}\right)\left[\int_0^{\infty}C_{pded}f\{u_{pded}\}du_{pded}-C_{pve}\right]$$

$$\text{B.C.1}: \left.\frac{\partial C_{pve}}{\partial z}\right|_{z=0}=0$$

$$\text{B.C.2}: \left.\frac{\partial C_{pve}}{\partial z}\right|_{z=L}=0$$

The average solid tracer concentration is obtained by:

$$C_S\{z\}=\phi_{pw}\frac{\int_0^{\infty}u_{pwd}C_{pw}\{z,u_{pwd}\}f\{u_{pwd}\}du_{pwd}}{\int_0^{\infty}u_{pwd}f\{u_{pwd}\}du_{pwd}} \quad (38)$$

$$+\phi_{pde}\frac{\int_0^{\infty}u_{pded}C_{pde}\{z,u_{pded}\}f\{u_{pded}\}du_{pded}}{\int_0^{\infty}u_{pded}f\{u_{pded}\}du_{pded}}+\phi_{pve}C_{pve}$$

Some explanations concerning the mass exchange terms have to be given. As a first formulation, the output flux of solid from one particle phase to another was assumed to

be proportional to the concentration of the "expulsing" phase, e.g., output flux from the particle wake phase to the vortex-emulsion phase equal to $K_{pw-pve}\, C_{pw}\big|_{u_{pwd}}$. This assumption came from developments of Dayan and Zalmanovich (1982), Turi and Ng (1986), Tang and Fan (1989) and Murray and Fan (1989). Depending on the authors, the value of K_{pw-pve} might be linked to the relative velocity of the particles close to the wake frontier, to the probability by unit length that the particles were discharged or to the axial velocity of the entrained particle. The total solid output flux from the particle vortex-emulsion phase to the wake phase was $K_{pve-pw}C_{pve}$. For one wake class defined by u_{pwd}, this total flux was weighted by the fraction of that class, i.e., $f\{u_{pwd}\}du_{pwd}$. Therefore, the first formulation of equation (37) contained the following exchange term for the mass transfer between the particle wake phase and the particle vortex-emulsion phase:

$$\left[K_{pw-pve} \frac{\phi_{pw}}{\phi_{pve}} \left\{ \int_0^{\infty} C_{pw} f\{u_{pw}\} du_{pw} \right\} - K_{pve-pw} C_{pve} \right] \qquad (39)$$

At an infinite time, the net flux should be zero (equation (39) is equal to zero) for three-phase fluidized beds having a constant solid concentration axial profile. In other words, the tracer concentration was the same everywhere in the reactor. The following relation between the constants was then obtained:

$$K_{pve-pw} = K_{pw-pve} \frac{\phi_{pw}}{\phi_{pve}} \qquad (40)$$

Replacing equation (40) with equation (39) gave the second term at the right of equations (37). The second term of equations (4) and (5) as well as the third term of equations (37) were also obtained in that way.

5.2.4.3 Model parameters

Table 5.2 contains the model parameters and how they were obtained. The mean particle wake phase velocity (u_{pw}) was fitted using the model predictions of RPT tracer data. For the convective phases, it was observed that the dimensionless standard-deviation (σ_{pwd}/u_{pw} and σ_{pded}/u_{pde}) of the particle velocity distribution was only a function of the reactor diameter (Lefebvre et al., 2006). These simple relationships were used to evaluate the particle velocity distribution standard-deviation (STD). The ratio of the particle mean velocities of the convective phases (u_{pde}/u_{pw}) was constant whatever the operating conditions, particle systems and reactor diameters. Particle vortex-emulsion phase holdup (ϕ_{pw}) was evaluated with RPT data (Lefebvre et al., 2006). Global mass balance linked the particle convective phases and made it possible to evaluate the particle downflow-emulsion phase holdup (ϕ_{pde}). Note that the mean particle velocity of the vortex-emulsion phase was zero. The particle vortex-emulsion phase holdup (ϕ_{pve}) was simply obtained by the definition of the holdup, i.e., $\phi_{pw}+\phi_{pde}+\phi_{pve}=1$. The expanded bed height (L_f) was obtained from RPT data. The axial dispersion coefficient of the particle vortex-emulsion phase ($D_{ax_{pve}}$) and the exchange coefficient from the particle wake phase to the vortex-emulsion phase (K_{pw-pve}) were fitted using model predictions and experimental RPT data. Hydrodynamic parameter values obtained for the convective phases were very close. Therefore, the assumption was made that the dimensionless number representing the ratio of the mass exchange between phases on the convective transport was the same

for the two convective phases. The exchange coefficient from the particle downflow-emulsion phase to the vortex-emulsion phase ($K_{pde-pve}$) was evaluated based on that dimensionless number. In summary, the model had 11 parameters, but only 9 independent parameters due to global mass balance and holdup definition. Only 3 parameters were fitted.

5.2.4.4 Numerical procedure

The fractional step method was used to solve the equation system (Yanenko, 1971). Using this method Renou et al. (2003) successfully solved a convective/dispersive/reactive system. The fractional step method is robust and stable if the methods used to solve the sub-system are adequate. It consists of separating the equations into sub-systems that can be solved with an efficient numerical or analytical method. For each time step, the solution of one sub-system becomes the initial condition of the next sub-system. For example, the convection sub-system of equation (35) was solved by simply shifting the matrix index for one time step (using $\Delta z = u_{pwd}\Delta t$) and the result became the initial condition for calculating the linear ordinary differential equation mass exchange sub-system. That sub-system was solved by the Runge-Kutta method with an adaptable time step. For solving the linear dispersion sub-system of the vortex-emulsion phase, the exponential matrix was used (Rugh, 1993).

The fractional step method converges toward a unique solution while decreasing the time step. The method is stable, i.e., the error does not increase with each time step and the solution is consistent with the results (see the results section). Various discretizations of the velocity distribution function (equation (32)) were used in order to converge toward a unique solution. A velocity step of 0.05 m/s is sufficient over a range from 0 to 1.3 m/s. A Nelder-Mead direct search method was used to fit the three parameters. The model was fitted onto various tracer concentration curves along the

reactor length. Fitting onto only one curve would have produced various sets of fitted parameters giving the same minimization of the objective function (Lefebvre et al., 2004).

5.2.5 RESULTS AND DISCUSSION

Figure 5.3 shows two examples of calculated data, one for each reactor diameter. The model was fitted simultaneously onto three curves above the region of the tracer injection, i.e., z>0.2 m. The objective function used is shown here:

$$r^2 = \frac{\sum_{j=1}^{j=Nb_z} \sum_{i=1}^{i=Nb_t} \left(C_{s\exp_i} - C_{s\mathrm{mod}_i} \right)_j^2}{\sum_{j=1}^{j=Nb_z} \sum_{i=1}^{i=Nb_t} \left(C_{s\exp_i} \right)_j^2} \qquad (41)$$

Where "*j*" represents the tracer concentration curve of the various axial positions, "*i*" represents the tracer concentration value for a given time; Nb_z and Nb_t are, respectively, the number of axial measurement positions and the number of time steps. This objective function forces the fitting procedure to obtain the parameter set respecting not only a tracer concentration curve at one axial position, but respecting the axial evolution of the tracer concentration curves as proposed by Lefebvre et al. (2004).

The increasing rank of difficulty for a model to fit the data is as follows: steady-state axial profile, one Residence Time Distribution (RTD), axial evolution of RTDs or batch tracer curves. In other words, more models can fit a steady-state axial profile better than an evolution of RTDs. A model following the tracer axial evolution would represent the mixing mechanism well (Levenspiel and Fitzgerald, 1983).

The fit quality for the 0.10 m reactor is good with a normalized square residual (r^2) ranging from 0,004 to 0,023. The fit quality for the 0.292 m reactor is fairly good with r^2 ranging from 0,017 to 0,093. For the larger reactor, the overshoot close to the injection zone is more pronounced due to the higher ratio of the solid circulation velocities to the exchange coefficient ($\phi_{pw} u_{pw} / K_{pw-pve}$). The axial evolution of the overshoot is difficult to fit. This is due to the assumption that the model parameters are not a function of the axial position. The authors' previous work (Lefebvre et al., 2006) indicated, for example, that the particle wake phase holdup is a parabolic function of the axial position. In order to have a number of parameters as low as possible and because the model captured the trend of the tracer curve evolution, the convective/dispersive model was not updated. The model respected the observed contribution of both the convective and dispersive mixing mechanisms (see Figure 5.2). Furthermore, the model gave a good estimation of the solid phase mixing time. Cassanello et al. (1995) used a model assuming one velocity for the particles going up and another for the particles going down. Solid particles in the vortex-emulsion phase were not considered. Solid mixing was represented by an exchange coefficient linking the upflow and downflow solid particles. Such a model overpredicted the solid phase mixing time, because it did not take into account the axial mixing.

Table 5.3 presents the three fitted parameters (u_{pw}, K_{pw-pve} and $D_{ax_{pve}}$) as well as the particle wake phase holdup (ϕ_{pw}) and the STD of the particle wake velocity distribution (σ_{pwd}). The other model parameters may be calculated with the relations given in Table 5.2. The particle wake phase holdup represents the contribution of the convective mixing mechanism in terms of relative volume of the convective phases (remember that $\phi_{pde} = \phi_{pw} / 0.90$ as shown in Table 5.2). The particle wake velocity distribution STD and the axial dispersion coefficient of the vortex-emulsion phase represent, in terms of mixing extent, the contribution of the convective and dispersive

mixing mechanism, respectively. The solid phase holdup is also given in Table 5.3 due to its link with the convective/dispersive model parameters (discussed later).

The axial dispersion model (equations (37) and (38) with $\phi_{pde} = \phi_{pw} = 0$) was also fitted onto the tracer curves. That model did not give a good fit quality as shown in Figure 5.4. This figure compares the fit quality of the axial dispersion model with the convective/dispersive model at the same operating conditions. The r^2 values for the axial dispersion model are about 2-4 times higher than the r^2 values for convective/dispersive model.

The axial evolution of the tracer curves was badly followed by the axial dispersion model. This means that the solid mixing has to be represented by more than only one parameter. The axial dispersion model is not appropriate as was expected from Cassanello et al. (1995), Lefebvre et al. (2004) and Lefebvre et al. (2006). The apparent axial dispersion coefficient ($D_{ax_{app}}$) values are shown in Table 5.3. A comparison of $D_{ax_{app}}$ between the two reactors should be made carefully, because the fit qualities were poor. Although the apparent axial dispersion coefficient is not correct to describe mixing and, especially, to be used to predict reactor conversion and selectivity when the kinetics are fast, it is often used in the literature. The values obtained here are similar with the ones obtained by Fan et al. (1987), i.e., 0.005-0.1 m^2/s, for 3 mm glass beads in a three-phase fluidized bed containing a binary system (3-4 mm and 3-6 mm glass beads).

For most cases, $D_{ax_{pve}} << D_{ax_{app}}$ and the extent of mixing is mainly due to the convective mixing mechanism. In other words, the extent of mixing is determined by the standard-deviation of the velocity distribution of the convective phases and not by Fick's law.

The difference between the two axial dispersion coefficients is more obvious for the larger reactor.

The convective mixing mechanism is more pronounced for the larger reactor, i.e., particle velocity distribution STD and holdup of the convective phases are higher. Knowing that is important for the scale-up of fast reacting systems from lab-scale ($Dc \leq 0.10$ m) to pilot-scale ($Dc \geq 0.3$ m) and from pilot-scale to commercial-scale ($Dc \geq 1$ m). The relative importance of the mixing mechanisms will change at each scale-up step.

As mentioned previously, the mean particle velocity of each convective particle phase was obtained directly from Lagrangian RPT data, i.e., z-t slope of the straight line shown in Figure 5.2. As seen in this figure, marked particle paths having constant Lagrangian velocity cover various lengths, called trajectory lengths (Villermaux, 1996). The trajectories start and stop at various axial positions. This causes an axial profile of the mean velocity distribution as presented in Figure 5.5. The proposed convective/dispersive model assumes that the trajectory lengths are equal to the expanded bed height. Figure 5.6 shows that the actual trajectory lengths are much smaller than the expanded bed height and that there is a large distribution of velocities. The proposed model is then a simplification of the reality: particles ascend the bed in the bubble wake, but need various lifts from bubbles to cross the whole height. Between those lifts, the particles spend some time in the vortex-emulsion phase resulting in an apparent lower value of their ascending velocity across the whole bed height. In the experiment presented in Figure 5.5 and Figure 5.6, the average value of the particle velocity across the bed height is 0.29 m/s, while the apparent velocity taking into account the various lifts and the time spent outside of the wakes is 0.24 m/s as obtained by the model. As expected, the apparent velocity is lower (about 20%) than the average velocity (Figure 5.7).

The apparent particle wake phase velocity has a tendency to decrease with solid phase holdup. Figure 5.8 reflects that tendency. Therefore, the overall solid circulation decreases for systems where the particles are closer. Indeed, the system inertia is higher for larger solid holdup. The particle wake phase velocity is higher in the larger column due to the fastest bubbles being there. The particle wake and particle downflow-emulsion phase velocity distribution STD follow the same trend with the solid phase holdup due to their relation with the particle wake phase velocity. This means that the extent of mixing decreases with the solid phase holdup.

The exchange coefficient from the particle wake phase to the vortex-emulsion phase (K_{pw-pve}) varied, in a general way, from 0.2 to 1.1 s^{-1}. These values are of the same order of magnitude as the solid mass exchange coefficient obtained by Cassanello et al. (1996). Figure 5.9 shows K_{pw-pve} vs the solid phase holdup. This figure reveals a tendency of K_{pw-pve} to decrease with the solid phase holdup. For large solid phase holdup, the particles are closer to each other and their interactions are more pronounced. This stabilizes (retains) the particles in the bubble wake as observed by Fan and Tsuchiya (1990) and Fan and Yang (2002). It is demonstrated in Figure 5.9 that the exchange K_{pw-pve} is higher for the smaller reactor. Solid particles are exchanged between phases less frequently in a larger reactor. This means that the particle velocity changes less frequently and randomly in larger reactors.

5.2.5.1 Limits of the convective/dispersive model

The relation between the two exchange coefficients shown in equation 40 is valid if the solid phase holdup axial profile is flat, as in this case. For slurry reactors and three-phase fluidized beds containing large/light particles, the solid phase holdup changes with the axial position. In that case, the convective/dispersive model may also be

applied in the mathematical form given here, but K_{pw-pve} and K_{pve-pw} have to be determined separately. As discussed previously, not taking into account the axial profile of the model parameters reduces the capacity of the model to follow the axial evolution of the tracer concentration curves for the 0.292 m reactor. Moreover, Lefebvre et al. (2006) showed that the parameters are also a function of the radial position. The solid particles having a time-averaged upward velocity in the center of the reactor are mostly in the particle wake phase. The solid having a time-averaged downward velocity close the wall (annulus) of the reactor is mostly in the particle downflow-emulsion phase. Between the two regions, the solid is about equally separated between the three particle phases. A more refined model would take into account this spatial repartition of the particle phases.

5.2.6 CONCLUSION

The main objective of this work was to develop a solid phase mixing model that follows not only the mixing extent, but also the overall mixing mechanism, i.e., the contribution of the convective onto the dispersive mixing mechanism. The developed model separates the solid phase into three sub-phases. Two sub-phases follow a convective mixing mechanism and are linked to the bubble velocity distribution. The third sub-phase follows a dispersive mixing mechanism and is subjected to random movement due to drag in the liquid emulsion phase. In the model, the relative contribution of the mixing mechanisms is weighted by the sub-phase holdup, the solid convective sub-phases velocity distribution standard-deviation and the axial dispersion coefficient of the dispersive solid sub-phase. Solid mass exchange and overall solid circulation are also considered in the convective/dispersive model. Some model parameters were obtained from the RPT data. Three model parameters were optimized by fitting the convective/dispersive model onto the axial evolution of tracer curves (generated by RPT data). Relations developed in a previous work were used to

estimate the remaining model parameters. The model estimated successfully the extent of solid mixing as well as followed the overall mixing mechanism.

In order to develop a predictive model for a three-phase fluidized bed reactor, the next step is to include the model parameters' axial profile functions into the model calculation. A bubble coalescence/breakup model should evaluate these axial profile functions. Local bubble size and bubble velocity distributions would be measured in order to develop a model that will be linked to the solid hydrodynamics in the particle wake phase. Relations found in literature for bubble wake holdup and solid holdup in the wake may be used. The solid hydrodynamics in the particle downflow-emulsion phase may be obtained from relations given by Lefebvre et al. (2006). The solid hydrodynamics in the particle vortex-emulsion phase has to be linked to the liquid phase hydrodynamics. Local measurement in the liquid for a three-phase fluidized bed should be obtained, but it is not an obvious task. There is a great lack of literature for the liquid phase local hydrodynamic in a three-phase fluidized bed.

5.2.7 Acknowledgements

The authors gratefully acknowledge financial support from the Natural Science and Engineering Research Council of Canada and the Fond pour la Fond Québécois de Recherche sur la Nature et la Technologie. Dr. G. Kennedy and Mr. Saint-Pierre are also gratefully acknowledged for activation of the tracer. A special acknowledgement to Pierre Sauriol, who has performed useful modifications to the RPT software system, and to Jean Huard and Robert Delisle, who worked on the experimental setup and RPT facilities.

5.2.8 Nomenclature

A : area of the solid phase, $\frac{D_c \pi}{4} \varepsilon_s$

$C_{pde}|_{u_{pded}}$: tracer concentrations in class defined by the particle velocity u_{pded} of the particle downflow-emulsion phase (kg/m^3) or normalized (-)

C_{pve} : tracer concentration in the particle vortex-emulsion phase. (kg/m^3) or normalized (-)

$C_{pw}|_{u_{pwd}}$: tracer concentration in the class defined by the particle velocity u_{pwd} of the particle wake phase (kg/m^3) or normalized (-)

$C_{s\exp}$: experimental tracer concentration ; normalized (-)

$C_{s\mathrm{mod}}$: model tracer concentration ; normalized (-)

C_{∞} : tracer concentration at homogenization – tracer test in batch (kg/m^3)

$D_{ax_{eff}}$: apparent axial dispersion coefficient of the axial dispersion model (m^2/s)

$D_{ax_{pve}}$: axial dispersion coefficient of the particle vortex-emulsion phase (m^2/s)

D_c : column diameter (m)

$f\{u_{pded}\}$: solid velocity distribution of the particle downflow-emulsion phase (s/m)

$f\{u_{pwd}\}$: solid velocity distribution of the particle wake phase (s/m)

K_{pve-pw} : proportional constant for the exchange from particle vortex-emulsion phase to particle wake phase (s^{-1})

K_{pw-pve} : proportional constant for the exchange from particle wake phase to particle vortex-emulsion phase (s^{-1})

$K_{pve-pde}$: proportional constant for the exchange from particle vortex-emulsion phase to particle downflow-emulsion phase (s^{-1})

$K_{pde-pve}$: proportional constant for the exchange from particle downflow-emulsion phase to particle vortex-emulsion phase (s^{-1})

L_f : fluidized bed height (m)

MMI : mixing mechanism index (-)

Nb_z : number of axial measurement positions

Nb_t : number of time steps

u_{pded} : solid velocity in class defined by particle velocity u_{pded} of the particle downflow-emulsion phase (m/s)

u_{pde} : mean particle velocity of the velocity distribution for the downflow-emulsion phase (m/s)

u_{pwd} : solid velocity in class defined by particle velocity u_{pwd} of the particle wake phase (m/s)

u_{pw} : mean particle velocity of the velocity distribution for the wake phase (m/s)

r^2 : normalized square residual (-)

t : time (s)

z : axial position (m)

Greek

α : parameter of the log-normal distribution function (-)

β : parameter of the log-normal distribution function (-)

ε_s : solid fraction (-)

ϕ_{pde} : particle downflow-emulsion phase holdup (-)

ϕ_{pve} : particle vortex-emulsion phase holdup (-)

ϕ_{pw} : particle wake phase holdup (-)

σ_{pwd} : standard deviation of the velocity distribution for the downflow-emulsion phase (m/s)

σ_{pwd} : standard deviation of the velocity distribution for the wake phase (m/s)

Δt : time step (s)

Δz : axial length step (m)

5.2.9 References

Cassanello, M., F. Larachi, C. Guy and J. Chaouki. 1996. << Solids mixing in gas-liquid-solid fluidized beds: experiments and modelling. >>. Chemical engineering Science. Vol. 51. 2011-2020.

Cassanello, M., F. Larachi, M.-N. Marie, C. Guy and J. Chaouki. 1995. << Experimental characterization of the solid phase chaotic dynamics in three-phase fluidization. >>. Industrial and Engineering Chemistry Research. Vol. 34. 2971-2980.

Dayan, A. and S. Zalmanovich. 1982. << Axial dispersion and entrainment of particles in wakes of bubbles. >>. Chemical Engineering Science. Vol. 37. 1253-1257.

Fan, L. S. 1989. << Gas-liquid-solid fluidisation engineering >>. Butterworths, Massachusetts Institute of Technology.

Fan, L.-S. and K. Tsuchiya. 1990. << Bubble wake dynamics in liquid and liquid-solid suspensions >>. Butterworths, Massachusetts institute of technology.

Fan, L.-S., T. Yamashita and R. H. Jean. 1987. << Solids Mixing and Segregation in a Gaz-Liquid-Solid Fluidized Bed >>. Chemical Engineering Science. Vol. 42. 17-25.

Fan, L.-S. and G. Yang (2002). Gas-liquid-solid three-phase fluidization. Handbook of fluidization and fluid-particle systems. Y. a. D. Wen-Ching, M. **Chapter 27**.

Grace, J. R. 1982. << Fluidization >>. McGraw-Hill.

Hyndman, C. and C. Guy. 1995a. << Gas phase flow in bubble columns: a convective phenomenon >>. The Canadian Journal of Chemical Engineering. Vol. 73. 426-434.

Kiared, K., F. Larachi, C. Guy and J. Chaouki. 1997. << Trajectory length and residence-time distributions of the solids in three-phase fluidized beds >>. Chemical Engineering Science. Vol. 52. 3931-3939.

Larachi, F., M. Cassanello, J. Chaouki and C. Guy. 1996. << Flow structure of the solids in a 3-D gas-liquid-solid fluidized bed >>. American Institute of Chemical Engineering Journal. Vol. 42. 2439-2452.

Larachi, F., M. Cassanello, M.-N. Marie, J. Chaouki and C. Guy. 1995. << Solids circulation pattern in three-phase fluidized beds containing binary mixtures of particles as inferred from RPT >>. Transactions of the Institute of Chemical Engineers. Vol. 73. 263-268.

Larachi, F., G. Kennedy and J. Chaouki. 1994. << A gamma-ray detection system for 3-D particle tracking in multiphase reactors. >>. Nucl. Instr. Meth. Vol. A338. 568.

Lefebvre, S., J. Chaouki and C. Guy. 2004. << Phase mixing modeling in multiphase reactors containing gas bubble: a review >>. International journal of chemical reactor engineering. Vol. 2, R2, http://www.bepress.com/ijcre/vol2/R2.

Lefebvre, S., J. Chaouki and C. Guy. 2006. << Solid Phase Hydrodynamic of Three-Phase Fluidized Bed - A Convective/Dispersive Mixing Mechanism Representation >>. International journal of chemical reactor engineering. Vol. Submited.

Levenspiel, O. 1999. << Chemical reaction engineering >>. John Wiley & Sons. Oregon state university.

Levenspiel, O. and T. L. Fitzgerald. 1983. << A warning on the misuse of the dispersion model >>. Chemical Engineering Science. Vol. 38. 491-493.

Lübbert, A. and B. Larson. 1990. << Detailed investigations of the multiphase flow in airlift tower loop reactors >>. Chemical Engineering Science. Vol. 45. 3047-3053.

Murray, P. and L. S. Fan. 1989. << Axial solid distribution in slurry bubble column. >>. Industrial and Engineering Chemistry Research. Vol. 28. 1697-1703.

Renou, S., M. Perrier, M. Dochain and S. Gendron. 2003. << Solution of the convection-dispersion-reaction equation by a sequencing method >>. Computer Chemical Engineering. Vol. 27. 615-629.

Rugh, W. J. 1993. << Linear System Theory >>. Prentice Hall Information and System Science Series. Toronto.

Schiller, L. and A. Naumann. 1933. << Zeitschr. >>. V.D.I. Vol. 318-320 (cited by Nigam and Schumpe, 1996).

Tang, W. T. and L. S. Fan. 1989. << Hydrodynamics of a three-phase fluidized bed containing low-density particles. >>. American Institute of Chemical Engineering Journal. Vol. 35. 355-364.

Turi, E. and K. M. Ng. 1986. << Axial distribution of soid particles in bubble column slurry reactors in the bubble flow regime. >>. Chemical Engineering Communications. Vol. 46. 323-345.

Villermaux, J. 1996. << Trajectory length distribution (TLD), a novel concept to characterize mixing in flow systems >>. Chemical Engineering Science. Vol. 51. 1939-1946.

Yanenko, N. N. 1971. << The Method of Fractional Steps: The Solution of the Problems of Mathematical Physics in Several Variables. >>. Springer-Verlag. Berlin.

List of figures

Figure 5.1: Schematics of the solid phase convective/dispersive model.

Figure 5.2: Time series of the traced particle axial position. Particle phases examples. Dc=0.292 m ; GB3mm ; UL=0.042 m/s ; Ug=0.050 m/s.

Figure 5.3: Convective/dispersive model fitting quality example for GB3mm. (a) Dc=0.10 m, UL=0.065 m/s, Ug=0.11 m/s. (b) Dc=0.292 m, UL=0.051 m/s, Ug=0.051 m/s. Dot: experimental result, line: model result.

Figure 5.4: Convective/dispersive vs axial dispersion model fitting quality example for GB3mm, Dc=0.10 m, UL=0.065 m/s, Ug=0.069 m/s. (a) Convective/dispersive model (b) Axial dispersion model. Dot: experimental result, line: model result.

Figure 5.5: Axial profile of the mean velocity distribution from RPT data. Dc=0.292 m, UL=0.051 m/s, Ug=0.051 m/s.

Figure 5.6: Particle wake phase Lagrangian velocity (slope of z vs t) vs axial trajectory length.

Figure 5.7: Particle wake phase velocity – fitted vs RPT values. The dashed line has a slope of 1. The solid line is a linear fit of the data and the slope is 0.8.

Figure 5.8: Fitted particle wake phase velocity vs solid phase holdup

Figure 5.9: Fitted exchange coefficient from the particle wake phase to the vortex-emulsion phase vs solid phase holdup

List of tables

Table 5.1: Experimental conditions.

Table 5.2: Model parameters.

Table 5.3: Model parameter values and apparent axial dispersion coefficient.

FIGURES

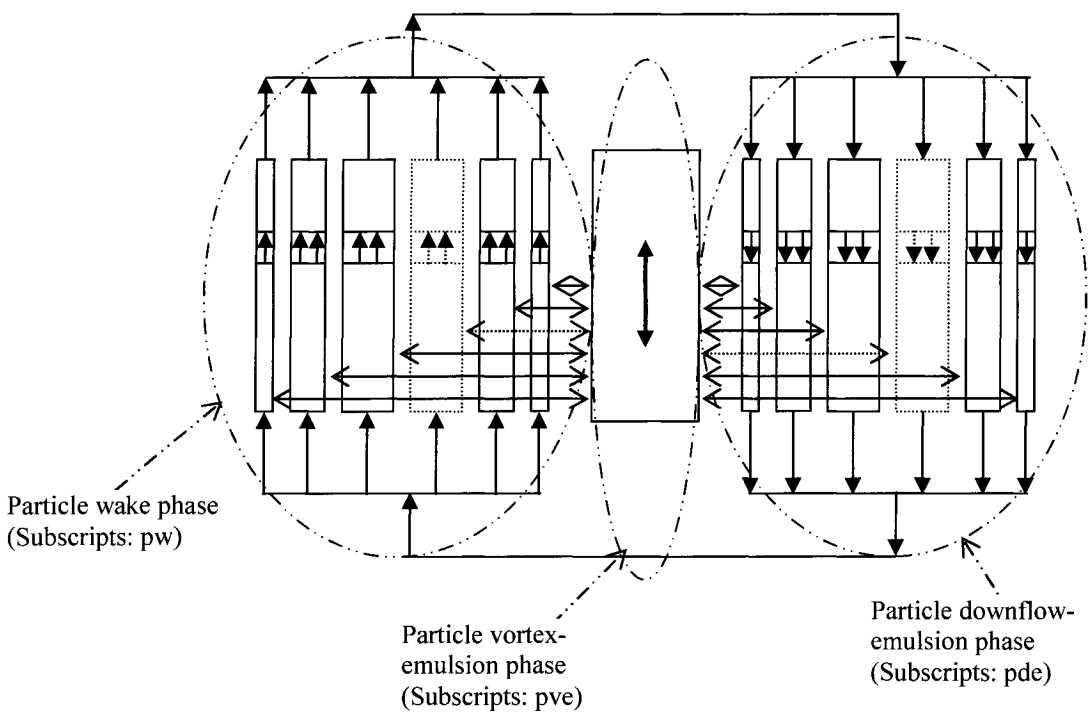


Figure 5.1: Schematics of the solid phase convective/dispersive model.

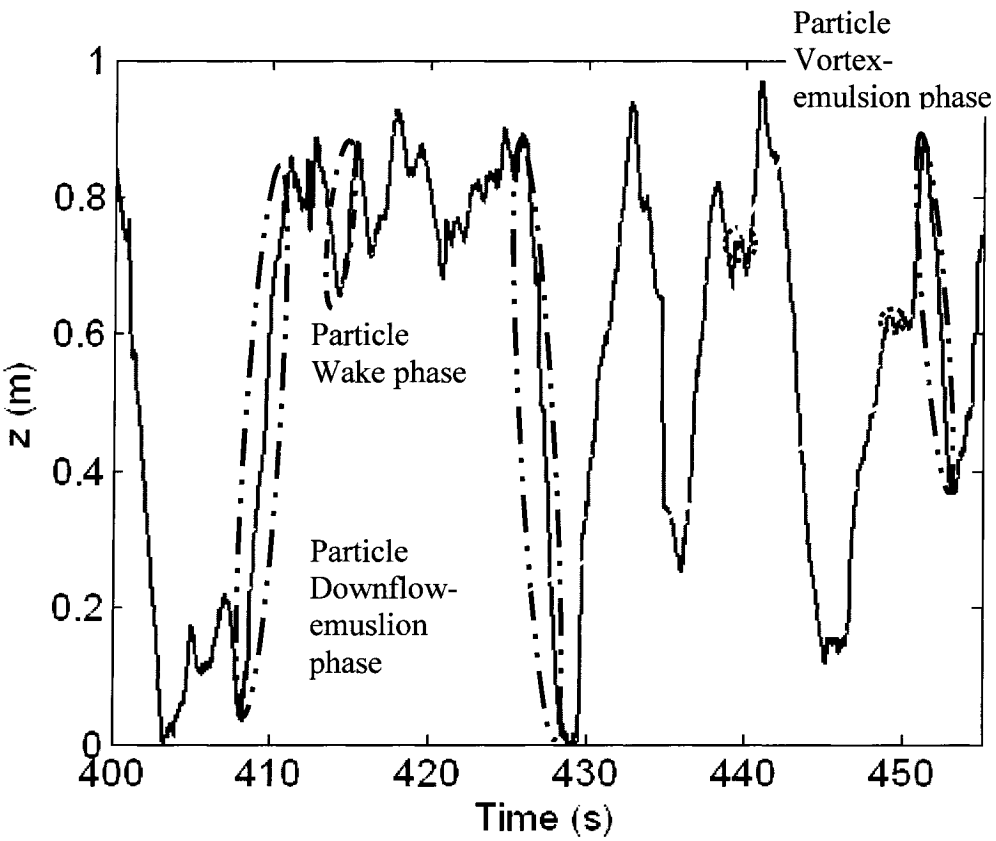
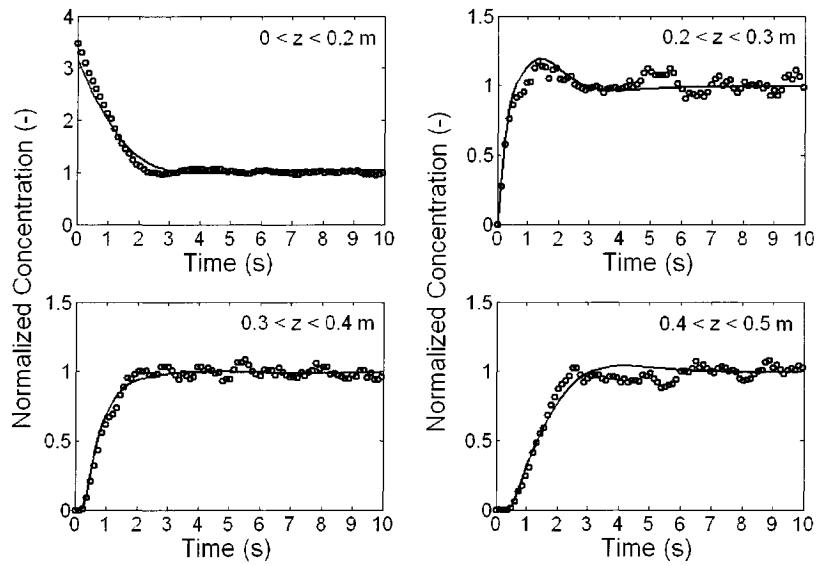
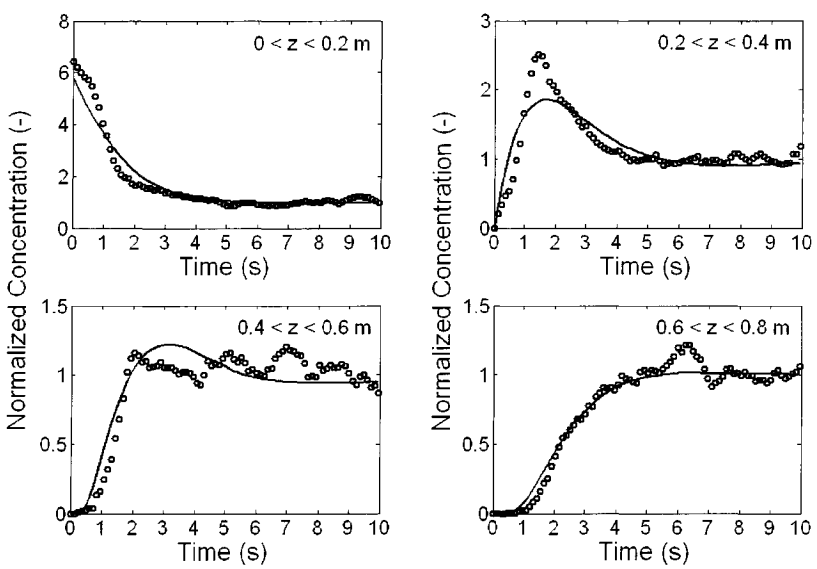


Figure 5.2: Time series of the traced particle axial position. Particle phases examples. Dc=0.292 m ; GB3mm ; UL=0.042 m/s ; Ug=0.050 m/s.

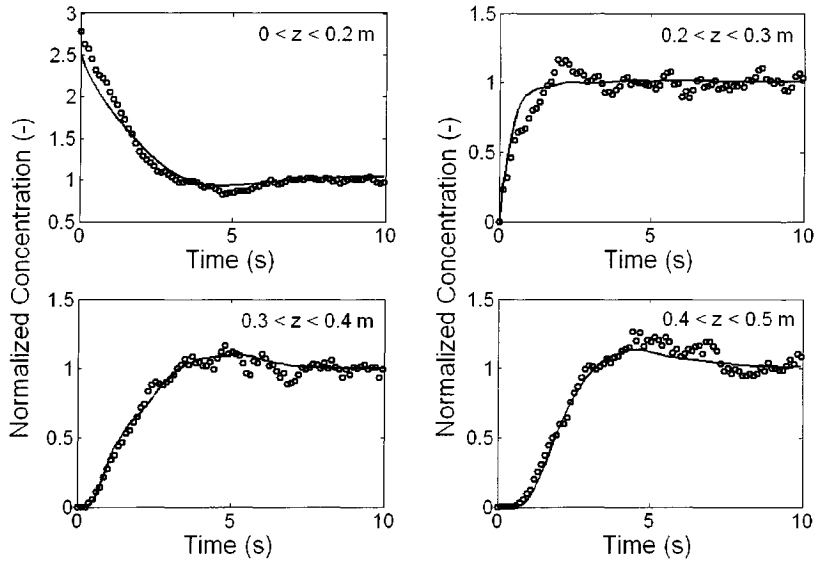


(a)

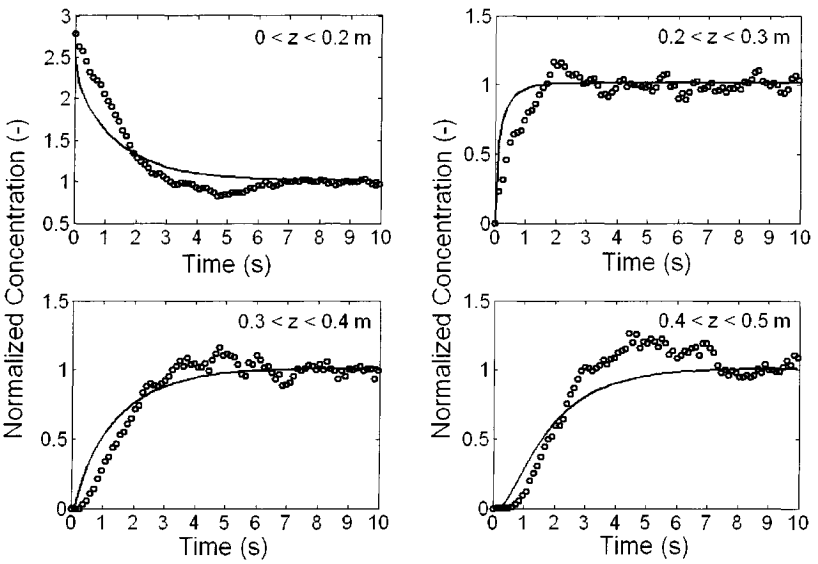


(b)

Figure 5.3: Convective/dispersive model fitting quality example for GB3mm. (a) run 3: Dc=0.10 m, U_L=0.065 m/s, Ug=0.106 m/s. (b) run 11: Dc=0.292 m, U_L=0.051 m/s, Ug=0.051 m/s. Dot: experimental result, line: model result.



(a)



(b)

Figure 5.4: Convective/dispersive vs axial dispersion model fitting quality example for run 2: GB3mm, Dc=0.10 m, U_L=0.065 m/s, Ug=0.069 m/s. (a) Convective/dispersive model (b) Axial dispersion model. Dot: experimental result, line: model result.

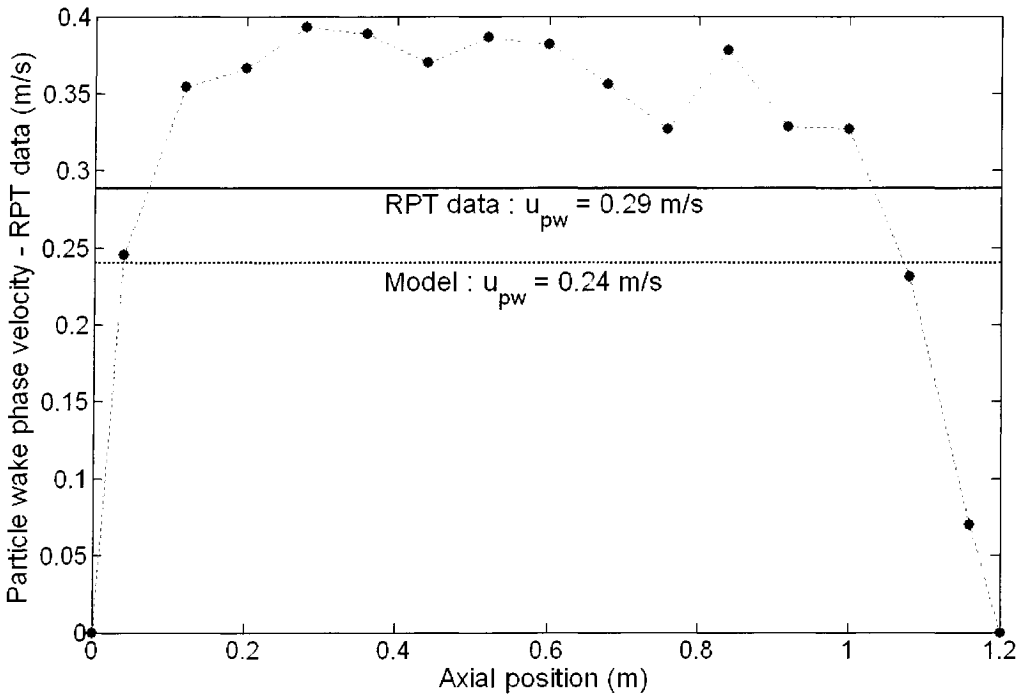


Figure 5.5: Axial profile of the mean velocity distribution from RPT data. Run 11 : Dc=0.292 m, U_L=0.051 m/s, Ug=0.051 m/s.

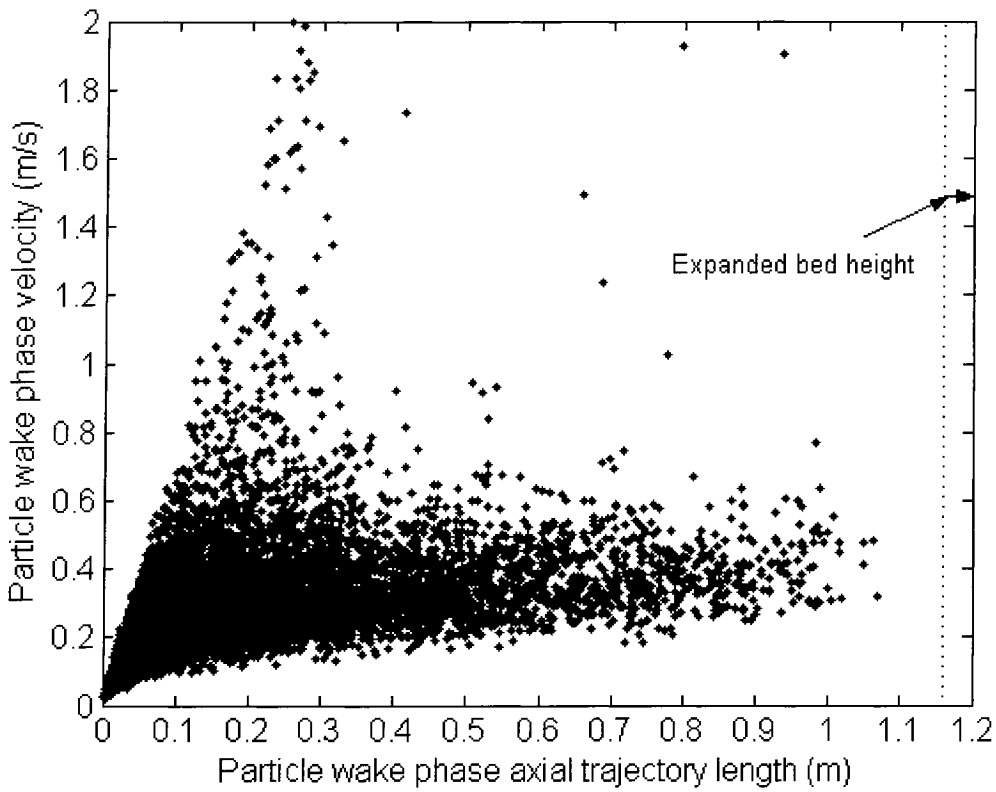


Figure 5.6: Particle wake phase Lagrangian velocity (slope of z vs t) vs axial trajectory length. Run 11 : Dc=0.292 m, U_L=0.051 m/s, Ug=0.051 m/s.

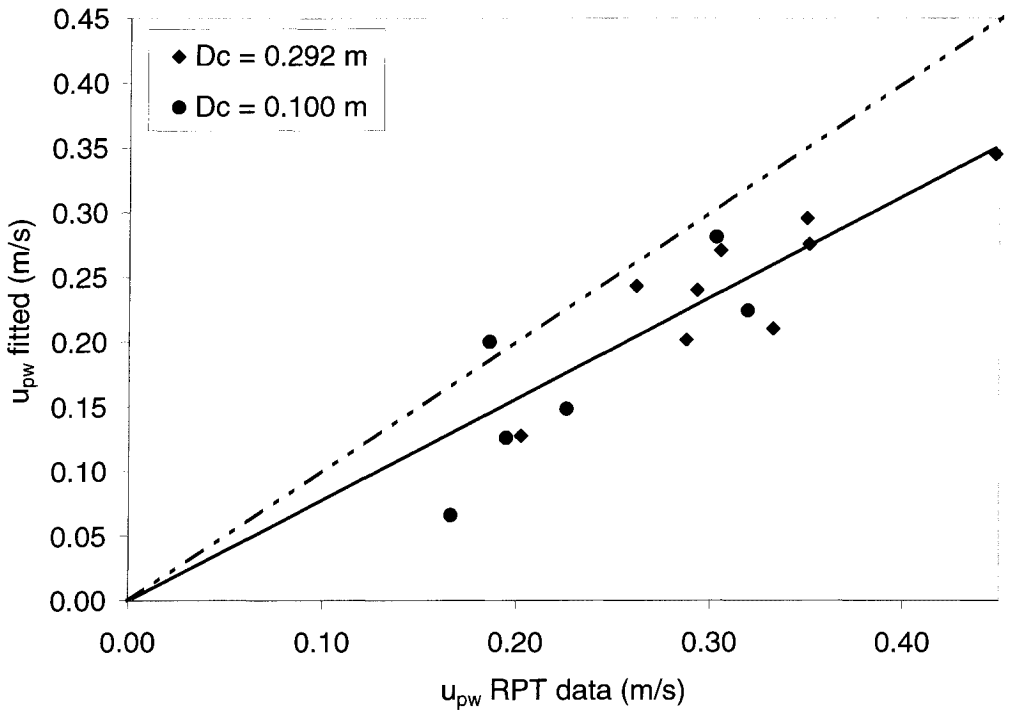


Figure 5.7: Particle wake phase velocity – fitted vs RPT values. The dashed line has a slope of 1. The solid line is a linear fit of the data and the slope is 0.8.

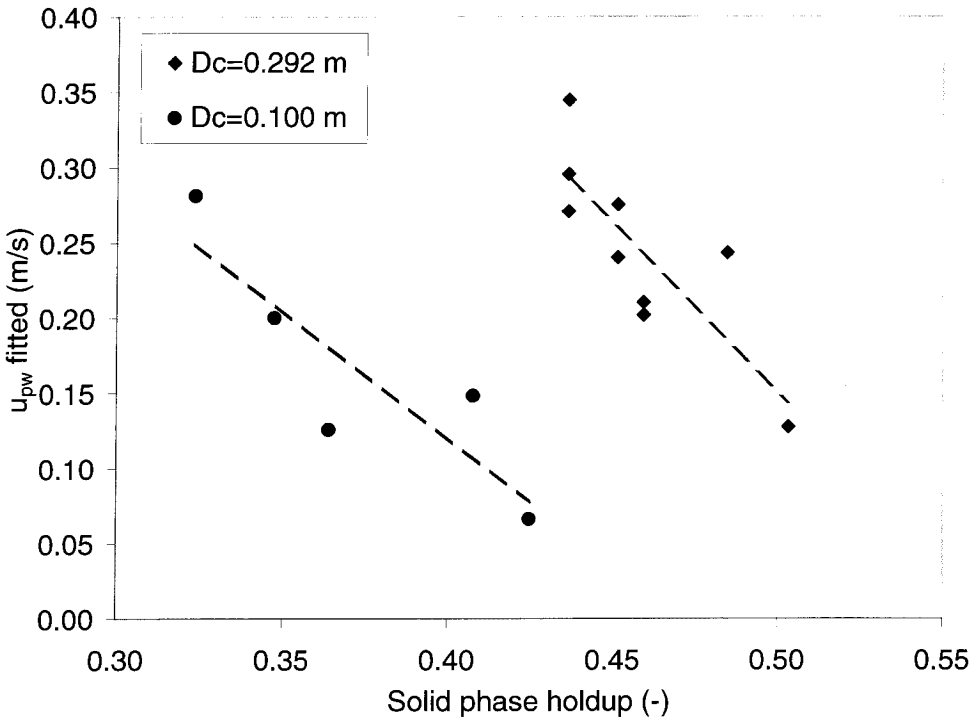


Figure 5.8: Fitted particle wake phase velocity vs solid phase holdup

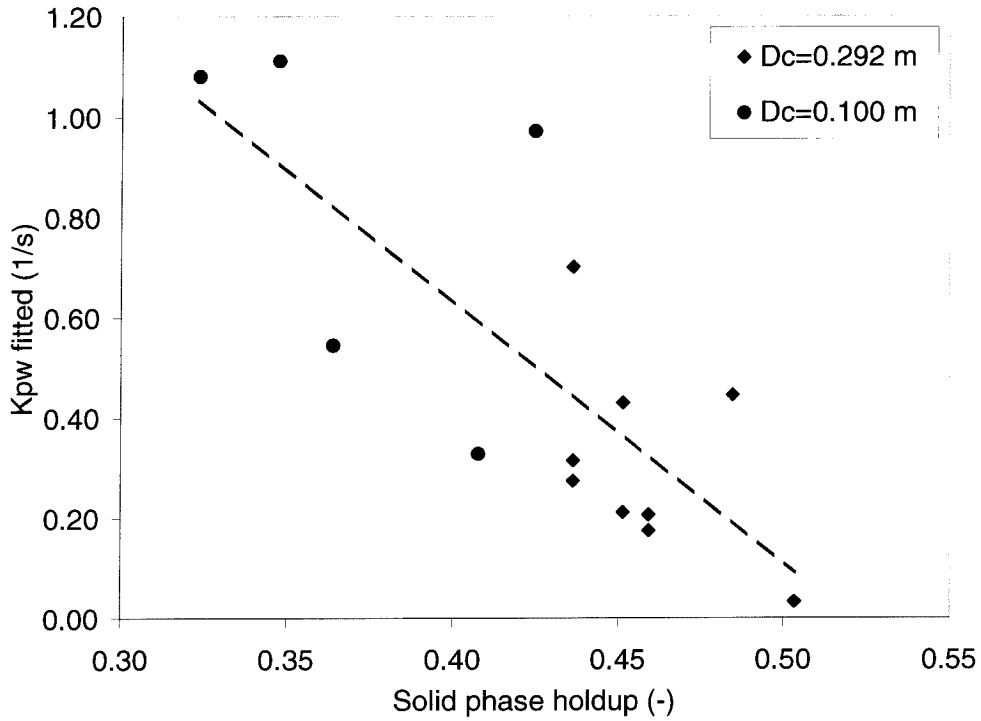


Figure 5.9: Fitted exchange coefficient from the particle wake phase to the vortex-emulsion phase vs solid phase holdup

TABLES

Table 5.1: **Experimental conditions.**

Run	UL	Ug	Particle system [1]	Total bed mass [2]	$Umf_{Ug=0}$ [3]	u_t [4]
(#)	(m/s)	(m/s)		(kg)	(m/s)	(m/s)
Dc = 0.10 m						
1	0.065	0.032	GB3	4.0	0.036	0.37
2	0.065	0.069	GB3	4.0	0.036	0.37
3	0.065	0.106	GB3	4.0	0.036	0.37
4	0.065	0.106	{GB3}GB0.9	2.8	{0.036}0.009	{0.37}0.14
5	0.065	0.032	{GB3}GB5	3.0	{0.036}0.051	{0.37}0.47
6	0.065	0.032	GB3{GB5}	3.0	0.036{0.051}	0.37{0.47}
Dc = 0.292 m						
7	0.042	0.031	GB3	88	0.036	0.37
8	0.042	0.050	GB3	88	0.036	0.37
9	0.042	0.080	GB3	88	0.036	0.37
10	0.051	0.031	GB3	88	0.036	0.37
11	0.051	0.051	GB3	88	0.036	0.37
12	0.051	0.080	GB3	88	0.036	0.37
13	0.062	0.031	GB3	88	0.036	0.37
14	0.062	0.051	GB3	88	0.036	0.37
15	0.062	0.080	GB3	88	0.036	0.37

[1] GB: Glass Beads. The attached number represents the particle diameter in mm. { }: tracked particle.

[2] For binary system, the bulk volume ratio is approximately 1:1. The solid phase holdup at rest for glass beads particles is approximately 0.59.

[3] The liquid-solid minimum fluidization velocity was calculated by the Grace (1982)'s correlation.

[4] The terminal particle velocity was calculated by the Schiller and Nauman (1933)'s correlation.

Table 5.2: **Model parameters.**

Parameter	Unit	Evaluation [1]	Note
u_{pw}	m/s	**Fitted**	
σ_{pwd}	m/s	$\frac{\sigma_{pwd}}{u_{pw}} = 0.927 D_c^{0.355}$	Use $\frac{\sigma_{pwd}}{u_{pw}} = 0.49$ for run 15
u_{pde}	m/s	$\frac{u_{pde}}{u_{pw}} = 0.90$	
σ_{pded}	m/s	$\frac{\sigma_{pded}}{u_{pde}} = 0.873 D_c^{0.369}$	Use $\frac{\sigma_{pded}}{u_{pde}} = 0.48$ for run 15
ϕ_{pw}	-	RPT data	
ϕ_{pde}	-	$\phi_{pde} = \frac{u_{pw}}{u_{pde}} \phi_{pw}$	Global mass balance
ϕ_{pve}	-	$\phi_{pve} = 1 - \phi_{pw} - \phi_{pde}$	
L_f	m	RPT data	
$D_{ax_{pve}}$	m^2/s	**Fitted**	
K_{pw-pve}	s^{-1}	**Fitted**	
$K_{pde-pve}$	s^{-1}	$\frac{L_f K_{pde-pve}}{u_{pde}} = \frac{L_f K_{pw-pve}}{u_{pw}}$	Assumption based on symmetry observed between the convective phases

[1] : the correlations came from Lefebvre et al. (2006).

Table 5.3: **Model parameters values and apparent axial dispersion coefficient.**

Run	ε_s	ϕ_{pw}	u_{pw}	σ_{pwd}	K_{pw-pve}	$D_{ax_{pve}}$	$D_{ax_{app}}$
	RPT data	RPT data	**Fitted**	Relation	**Fitted**	**Fitted**	Fitted
(#)	(-)	(-)	(m/s)	(m/s)	(s^{-1})	(m^2/s)	(m^2/s)
Dc = 0.10 m							
1	0.425	0.126	0.07	0.027	0.97	3.29E-02	0.037
2	0.408	0.261	0.15	0.061	0.33	4.44E-02	0.147
3	0.324	0.304	0.28	0.115	1.08	4.79E-12	0.135
4	0.172	0.320	0.22	0.092	0.29	7.85E-12	0.110
5	0.364	0.175	0.13	0.052	0.55	4.15E-02	0.095
6	0.347	0.196	0.20	0.082	1.11	9.34E-03	0.101
Dc = 0.292 m							
7	0.503	0.251	0.13	0.077	0.03	2.85E-02	0.037
8	0.459	0.336	0.20	0.121	0.21	4.83E-14	0.074
9	0.459	0.337	0.21	0.126	0.18	2.63E-12	0.096
10	0.485	0.340	0.24	0.146	0.45	2.23E-11	0.071
11	0.451	0.360	0.24	0.144	0.43	5.47E-06	0.073
12	0.451	0.312	0.28	0.165	0.21	1.40E-03	0.111
13	0.436	0.366	0.27	0.162	0.70	2.31E-14	0.076
14	0.436	0.345	0.30	0.177	0.28	2.90E-12	0.117
15	0.436	0.279	0.35	0.169	0.32	2.84E-03	0.133

CHAPITRE 6 : DISCUSSION GÉNÉRALE

La revue critique de la littérature a permis d'atteindre, de façon qualitative ou conceptuelle, le premier objectif de la thèse, soit d'identifier les caractéristiques clés liées à l'hydrodynamique des phases dans les lits fluidisés à trois phases. Les interactions entre les phases et la façon dont elles influencent leurs mécanismes de mélange ont été identifiées. La revue a fait ressortir que le modèle piston-dispersif n'est pas adéquat pour représenter le mélange des phases lorsque les cinétiques sont rapides et les transferts de masse limitants. Le modèle piston-dispersif suit un seul type de mécanisme de mélange, soit le mécanisme dispersif (Levenspiel and Fitzgerald (1983)). Le mécanisme dispersif représente un système dont les éléments (bulles, particules ou éléments de liquide) ont des vitesses qui changent de façon aléatoire. Le mouvement aléatoire des éléments génère le mélange qui peut être représenté par la loi de Fick lorsque le mouvement est de type Brownien (Nauman, 1981). Ce mécanisme de mélange doit être différencié du mécanisme convectif (Levenspiel and Fitzgerald, 1983), dont chaque élément a une vitesse constante. Le mélange est généré par la distribution de vitesse, comme par exemple la ségrégation de particules en chute ayant différentes tailles.

Dans le cas où les cinétiques sont rapides et les transferts de masse limitants, il faut utiliser des modèles plus phénoménologiques. Pour la phase gazeuse, Hyndman and Guy (1995a) ont montré que les bulles suivent un mécanisme de mélange convectif. Autrement dit, le mélange du gaz peut être décrit par une série de réacteurs pistons en parallèle. La distribution de vitesse caractérisant la vitesse de chaque réacteur piston suit une fonction de distribution log-normale. En conséquence du mécanisme convectif suivi par la phase gazeuse, une fraction du liquide (Lübbert and Larson, 1990; Yang et al. 1993; Lefebvre and Guy, 1999) et du solide (Larachi et al., 1996), contenus dans le sillage des bulles, suit un mécanisme convectif. Pour le solide dans un lit fluidisé à

trois phases, une fraction du solide qui descend suit aussi un mécanisme convectif (Larachi et al., 1996) dû à un mouvement compensatoire du solide qui monte en suivant un mécanisme convectif. Une autre fraction du solide suit un mouvement erratique et se déplace sur de plus courtes distances axiales par rapport au solide qui suit le mécanisme convectif. Les particules dans cette fraction de solide sont transportées par le liquide de la phase émulsion. Ces particules suivent plus ou moins le mouvement du liquide, en fonction de l'inertie des particules, de la fraction volumique de solide (interactions entre particules) et du transfert de quantité de mouvement à l'interface solide/liquide. Les particules peuvent être entraînées par les vortex de liquide observés entre la zone de montée au centre d'une colonne et la zone de descente formant un anneau près des parois (Tzeng et al., 1993 ; Chen et al., 1994). Un modèle d'écoulement schématique (conceptuel) respectant la description qui vient d'être donnée a été développé pour répondre au premier objectif de la thèse. Ce modèle schématique est présenté à la Figure 2.15. Ce modèle est une mise à jour du « structural wake model » (Fan, 1989).

Des analyses effectuées à l'aide de l'exposant de Hurst sont cohérentes avec l'écoulement des phases décrit plus haut. Dans la direction axiale, l'exposant de Hurts indiquait que le mélange du liquide (Yang et al., 1993) et du solide (Cassanello et al., 1995) est superdispersif, à savoir que le mouvement est plus rapide que le mouvement dû à un mécanisme dispersif. L'exposant de Hurts changeait avec les conditions opératoires, indiquant une évolution dans l'importance relative du mécanisme convectif sur le mécanisme dispersif.

L'exposant de Hurst n'est cependant pas pratique pour faire un lien quantitatif transparent entre les mécanismes de mélange et les modèles de mélange. Afin de répondre quantitativement au premier objectif de la thèse, des données obtenues à l'aide de la technique de suivi d'une particule radioactive (RPT) ont servi à extraire des

paramètres influençant l'importance relative du mécanisme convectif sur le mécanisme dispersif, et ce à travers le modèle schématique développé lors de la thèse (Figure 2.15). Les données de RPT ont été obtenues dans deux lits fluidisés de diamètres différents, soit 0.10 et 0.292 m. Pour le lit de 0.10 m de diamètre, les données de RPT viennent de travaux antérieurs à cette thèse (Cassanello et al., 1995 ; Larachi et al., 1996). Les autres données de RPT (lit de 0.292 m) ont été obtenues à partir d'expériences réalisées sur un nouveau montage dimensionné et construit lors de la présente thèse. Le modèle schématique relie les propriétés hydrodynamiques du gaz aux phases liquide et solide en terme de population de bulles. Le liquide et le solide dans le sillage d'une bulle ont les mêmes propriétés hydrodynamiques, à l'échelle du sillage, que la bulle transporteuse. Autrement dit, les propriétés des phases sont décrites pour des populations. Il y a un échange dynamique du liquide et du solide entre la sous-phase sillage et la phase émulsion. Cette dernière est divisée en deux sous-phases, soit une sous-phase où on retrouve un mouvement net de montée et/ou de descente du liquide et du solide ainsi qu'une phase où le liquide et le solide n'ont pas de déplacement net (vortex ou mouvement erratique ayant une vitesse moyenne nulle). Pour le solide, les sous-phases ont été nommées, dans l'ordre de leur description : la sous-phase particule-sillage, la sous-phase particule-émulsion-descente et la sous-phase particule-émulsion-vortex.

Les distributions de vitesse du solide ont été obtenues pour chacune des sous-phases du solide. Pour les sous-phases convectives (particule-sillage et particule-émulsion-descente), ce sont les vitesses Lagrangiennes qui ont été obtenues par régression linéaire des parcours convectifs « z vs t » mesurés à l'aide de la RPT. La moyenne et l'Écart-Type (ÉT) des distributions de vitesse de solide ont été calculés. La fraction volumique des trois sous-phases a été calculée. Ces paramètres ont un lien quantitatif transparent entre les mécanismes de mélange et les modèles de mélange.

6.1 Distributions de vitesse du solide

Le mécanisme de mélange convectif observé par Larachi et al. (1996) pour un lit fluidisé triphasique de 0.10 m de diamètre a aussi été observé dans le lit fluidisé triphasique de 0.292 m utilisé pour la présente thèse. La distribution de vitesse était également log-normale, comme la distribution de vitesse des bulles (Matsuura and Fan, 1984, Hyndman and Guy, 1995a). La moyenne et l'ÉT de la distribution de vitesse du solide sont du même ordre de grandeur que ceux de la distribution de vitesse des bulles observés dans la littérature (Hyndman and Guy, 1995a). Il faut noter que l***a vitesse moyenne et l'ÉT représentent l'importance relative du mécanisme convectif sur le mécanisme dispersif en terme d'intensité de mélange de chacune des sous-phases de la phase solide.*** La vitesse moyenne du solide varie entre 0.11 et 0.45 m/s. L'ÉT va de 0.04 à 0.22 m/s. L'évolution de la vitesse moyenne et de l'ÉT du solide suit les mêmes tendances que celle des bulles, à savoir qu'ils augmentent avec les vitesses superficielles de liquide et de gaz, ainsi qu'avec le diamètre du lit fluidisé. Une observation intéressante est que l'ÉT adimensionnel des phases convectives n'est fonction que du diamètre du réacteur à lit fluidisé, i.e.

$$\frac{\sigma_i}{u_i} \propto D_c^n \qquad (1)$$

où i représente une des deux phases convectives; $i = pw$ pour la sous-phase particule-sillage et $i = pde$ pour la sous-phase particule-émulsion-descente. Il faut noter que Matsuura and Fan (1984) ont trouvé que l'ÉT de la distribution des longueurs de corde des bulles est directement proportionnel à la longueur de corde moyenne des bulles. L'équation (1) montre que l'intensité de mélange convectif augmente avec le diamètre du réacteur. Cet effet du diamètre a souvent été observé à travers le modèle piston-dispersif. Cependant, l'interprétation souvent faite était que la longueur

caractéristique de la turbulence suivait le diamètre du réacteur. En considérant l'intensité du mélange convectif représenté par l'équation (1), une autre interprétation doit être faite, à savoir que l'intensité globale du mélange suit en partie la distribution de taille de bulle (mécanisme de mélange convectif). La théorie de la turbulence ne peut, à elle seule, être utilisée pour expliquer l'évolution de l'intensité du mélange.

La vitesse adimensionnelle du solide pour les sous-phases convectives suit aussi une relation simple avec le diamètre des lits fluidisés :

$$\frac{u_i}{Ug + U_L} \propto D_c^m \qquad (2)$$

Les équations (1) et (2) sont des critères simples de mise à l'échelle pouvant être utilisés pour les lits fluidisés à trois phases. Il existe également une relation simple entre la vitesse du solide des sous-phases convectives, c'est-à-dire entre les sous-phases particule-sillage et particule-émulsion-descente :

$$\frac{u_{pde}}{u_{pw}} = 0.90 \qquad (3)$$

La vitesse moyenne du solide dans la sous-phase particule-émulsion-vortex est nulle et l'ÉT de sa distribution de vitesse augmente avec les vitesses superficielles de liquide et de gaz ainsi qu'avec le diamètre des lits fluidisés, à l'instar des sous-phases convectives.

6.2 Fraction volumique des trois sous-phases

La fraction volumique de chacune des phases donne l'importance relative du mécanisme convectif sur le mécanisme dispersif en terme de poids de chaque sous-phases. L'effet des conditions opératoires et du diamètre des lits fluidisés sur la fraction volumique des sous-phases est plus complexe que leur effet sur les deux premiers moments de la distribution de vitesse du solide. Pour le lit de 0.292 m, la fraction volumique de la sous-phase particule-sillage augmente avec la vitesse superficielle du gaz pour de faibles vitesses superficielles du liquide, mais diminue avec la vitesse superficielle du gaz pour de grandes vitesses superficielles du liquide. En fait, la relation entre la fraction volumique de la sous-phase particule-sillage et $Ug+U_L$ suit une forme de type parabolique. Les causes de cette forme ont été expliquées dans le corps de la thèse et sont liées à l'effet des conditions opératoires sur l'évolution du volume relatif du sillage des bulles et de la fraction volumique du solide dans le sillage des bulles.

La fraction volumique de la sous-phase particule-sillage diminue avec le diamètre du lit fluidisé. Pour le lit de 0.10 m de diamètre, la fraction volumique de la sous-phase particule-sillage augmente avec les vitesses superficielles de gaz et de liquide. Des corrélations permettant d'estimer la fraction volumique des trois sous-phases ont été développées :

$$\phi_{pw} = \frac{A\left[1-be^{-m(Ug+U_L)D_c^{0.916}}\right]d_p^{1.663}}{(Ug+U_L)D_c^{0.916}} \qquad (4)$$

A = 1.237 x 10^4, m = 26.09 et b = 1.208 pour 0.0083 < $(Ug+U_L)D_c^{0.916}$ < 0.0118 $m^{1.916}/s$

and

A = 2.563 x 10^4, m = 53.11 et b = 1.815 pour 0.0118 ≤ $(Ug+U_L)D_c^{0.916}$ ≤ 0.0460 $m^{1.916}/s$

$$100 - \phi_{pve} = 2.042\phi_{pw} \qquad (5)$$

$$\phi_{pde} = 100 - \phi_{pve} - \phi_{pw} = 1.042\phi_{pw} \qquad (6)$$

Où les unités sont en SI et les fractions volumiques en pourcentage. L'indice *pve* représente la sous-phase particule-émulsion-vortex.

6.3 Évolution de l'importance relative du mécanisme convectif sur le mécanisme dispersif

Un indicateur de l'importance relative du mécanisme convectif sur le mécanisme dispersif a été développé :

$$MMI = \frac{\phi_{pw}\sigma_{pwd} + \phi_{pde}\sigma_{pded}}{\phi_{pve}\sigma_{pved}} \qquad (7)$$

Ce critère est le rapport de la moyenne pondérée de l'ÉT des sous-phases convectives sur la moyenne pondérée de l'ÉT de la sous-phase dispersive. Le critère a été nommé le MMI (en anglais : « Mixing Mechanism Indicator »). Ce critère a été utilisé à la place de la méthode des moments à cause des limitations de cette méthode montrée à la revue critique de la littérature.

Pour le lit à 0.292 m de diamètre, la relation entre le MMI et $Ug + U_L$ suivait une forme de type parabolique, comme pour la fraction volumique de la sous-phase particule-sillage. En fait, les tendances observées pour le MMI étaient les mêmes que pour la fraction volumique de la sous-phase particule-sillage. L'importance du mécanisme convectif sur le mécanisme dispersif augmentait avec la vitesse superficielle du gaz à de faibles vitesses superficielles du liquide, mais diminuait avec

la vitesse superficielle du gaz à de grandes vitesses superficielles du liquide. Cette évolution complexe vient de plusieurs phénomènes hydrodynamiques ayant des effets opposés. Lorsque la vitesse superficielle du gaz augmente, la fraction de bulle et la concentration relative de solide dans le sillage des bulles augmentent, mais le volume relatif du sillage diminue. De plus, la turbulence du liquide dans la phase émulsion augmente, entraînant une augmentation de la fréquence de largage du sillage des bulles (« wake shedding »), elle-même causée par l'écoulement instable autour du sillage des bulles. Lorsque la vitesse superficielle du liquide augmente, les bulles deviennent plus petites et plus rapides (entraînement par le liquide), causant une diminution de la fraction volumique des bulles. Le largage du sillage des bulles augmente aussi à cause d'une turbulence plus intense dans la phase liquide. Cependant, le volume relatif du sillage des bulles augmente.

Le mécanisme convectif domine moins sur le mécanisme dispersif dans le plus petit lit fluidisé. L'évolution de l'importance relative du mécanisme convectif est plus simple dans ce cas, à savoir qu'il augmente avec $Ug+U_L$ sur la gamme de conditions étudiées.

6.4 Représentation 2D de l'écoulement du solide et des fractions volumiques des sous-phases

L'étude des champs en 2D de vitesse du solide et de la fraction volumique des sous-phases a montrée que le mécanisme de mélange convectif est principalement suivi par le solide s'écoulant dans la région de « régime établi », i.e. entre les régions d'inversion de l'écoulement, en haut et en bas du lit. Le solide dans la sous-phase particule-sillage se retrouve principalement au centre du lit et le solide dans la sous-phase particule-émulsion-descente près des parois du réacteur. La région où les vitesses moyennes de solide sont les plus grandes coïncide avec la région où le solide suit un mécanisme convectif. Un modèle doit en conséquence tenir compte de ce mécanisme. Le solide

s'écoulant entre le centre et l'anneau convectifs se retrouve en fraction non négligeable dans la sous-phase particule-émulsion-vortex. La région où le solide est principalement dans la sous-phase particule-émulsion-vortex se retrouve surtout dans le haut du lit. Cette région se situe dans le « freeboard » du lit et contient peu de solide. Le haut du lit tient lieu de zone de désengagement du solide des sillages de bulles (El-Temtamy and Epstein, 1980). Le volume de chaque région dépend des conditions opératoires, du diamètre du réacteur et des propriétés du solide.

6.5 Modèle de mélange de la phase solide

En première approximation, un modèle de mélange 1D (axial) a été développé afin d'atteindre le deuxième objectif de la thèse, soit de développer un modèle de mélange le plus simple possible, mais qui respecte les caractéristiques clés liées à l'hydrodynamique. L'idée était de monter à un autre niveau de complexité par rapport aux modèles de mélange de la phase solide basés sur le « structural wake model ». Par exemple, Cassanello et al. (1995) ont exploité le modèle suivant :

Pour le solide qui monte dans le sillage des bulles :

$$\frac{\partial C_W}{\partial t} = -\frac{\partial (u_B C_W)}{\partial z} + K_{EW}(C_E - C_W) \qquad (8)$$

Pour le solide qui descend :

$$\frac{\partial C_E}{\partial t} = -\frac{\partial (u_E C_E)}{\partial z} - K_{EW}(C_E - C_W) \qquad (9)$$

Où C_W et C_E représentent la concentration de traceur solide par unité de volume de réacteur pour, respectivement, le solide dans le sillage des bulles et le solide qui descend dans la phase émulsion. u_B et u_E sont, respectivement, la vitesse de sillage de bulles et la vitesse de solide dans la sous-phase émulsion. K_{EW} est le coefficient

d'échange du solide entre le sillage des bulles et la sous-phase émulsion. Ce modèle ne considère que le transport piston à une seule vitesse pour le solide qui monte et pour celui qui descend. Le mélange axial n'est donc pas considéré. L'intensité de mélange est représentée uniquement par l'échange de solide entre le sillage des bulles et la sous-phase émulsion.

Appuyé par ce qui a été décrit jusqu'à maintenant, le modèle proposé dans cette thèse ajoute l'effet du mélange axial par deux mécanismes, soit les mécanismes convectif et dispersif. L'intensité du mélange du premier mécanisme s'ajuste avec la largeur (ÉT) de la distribution de vitesse des bulles et celui du mécanisme dispersif s'ajuste avec le coefficient de dispersion axiale du solide dans la sous-phase particule-émulsion-vortex. Le poids de chaque mécanisme est caractérisé par la fraction volumique des sous-phases. L'échange du solide entre les sous-phases particule-sillage et particule-émulsion-vortex, ainsi que celui entre les sous-phases particule-émulsion-descente et particule-émulsion-vortex sont considérés par le modèle. La circulation globale du solide est également considérée par le modèle.

L'idée était de vérifier si ce nouveau niveau de complexité était suffisant, avant de passer à une représentation en 2 ou en 3D et/ou de considérer l'évolution axiale des paramètres du modèle, par exemple, l'évolution axiale de la fraction volumique des sous-phases et/ou de la distribution de vitesse des sous-phases.

Le modèle développé au cours de cette thèse est montré sous forme schématique à la Figure 5.1 et sous forme mathématique par les équations suivantes pour le solide en cuvé. La distribution log-normale de vitesse du solide de la sous-phase particule-sillage est :

$$f\{u_{pwd}\} = \frac{1}{\beta u_{pwd}\sqrt{2\pi}} \exp\left[-\frac{\left(\ln\left(u_{pwd}\right) - \alpha\right)^2}{2\beta^2} \right] \qquad (10)$$

Les relations reliant la vitesse moyenne (u_{pw}) et l'ÉT (σ_{pwd}) de la distribution aux paramètres de la distribution log-normale (α,β) sont :

$$u_{pw} = \exp\left(\alpha + \frac{\beta^2}{2} \right) \qquad (11)$$

$$\sigma_{pwd} = \exp\left(\alpha + \frac{\beta^2}{2} \right) \sqrt{\exp\left(\beta^2\right) - 1} \qquad (12)$$

Une distribution équivalente est utilisée pour le solide de la sous-phase particule-émulsion-descente. Le bilan de masse en régime transitoire sur la fraction du solide de la sous-phase particule-sillage correspondante à la vitesse u_{pwd} (une des vitesses des réacteurs pistons) est montré ici :

$$\frac{\partial C_{pw}\big|_{u_{pwd}}}{\partial t} = -u_{pwd} \frac{\partial C_{pw}\big|_{u_{pwd}}}{\partial z} + K_{pw-pve}\left[C_{pve} - C_{pw}\big|_{u_{pwd}} \right] \qquad (13)$$

$$\text{Avec C.F. : } C_{pw}\{z=0\} = \frac{\phi_{pde}}{\phi_{pw}} \frac{\int_0^\infty u_{pded} C_{pde}\{z=0, u_{pded}\} f\{u_{pded}\} du_{pded}}{\int_0^\infty u_{pded} f\{u_{pded}\} du_{pded}}$$

Une série d'équations différentielles comme l'équation (13), dont les vitesses doivent suivre la distribution de vitesse, doit être résolue. Pour le solide de la sous-phase particule-émulsion-descente, une série d'équations différentielles comme l'équation (13) doivent aussi être résolues.

Les deux séries d'équations différentielles doivent être résolues avec l'équation différentielle décrivant le solide de la sous-phase particule-émulsion-vortex :

$$\frac{\partial C_{pve}}{\partial t} = D_{ax_{pve}} \frac{\partial^2 C_{pve}}{\partial z^2} + \left(K_{pw-pve} \frac{\phi_{pw}}{\phi_{pve}} \right) \left[\int_0^\infty C_{pw} f\{u_{pwd}\} du_{pwd} - C_{pve} \right] \qquad (14)$$

$$+ \left(K_{pde-pve} \frac{\phi_{pde}}{\phi_{pve}} \right) \left[\int_0^\infty C_{pded} f\{u_{pded}\} du_{pded} - C_{pve} \right]$$

$$\text{C.F.1 : } \left. \frac{\partial C_{pve}}{\partial z} \right|_{z=0} = 0$$

$$\text{C.F.2 : } \left. \frac{\partial C_{pve}}{\partial z} \right|_{z=L} = 0$$

La concentration moyenne du traceur solide est :

$$C_S\{z\} = \phi_{pw} \frac{\int_0^\infty u_{pwd} C_{pw}\{z, u_{pwd}\} f\{u_{pwd}\} du_{pwd}}{\int_0^\infty u_{pwd} f\{u_{pwd}\} du_{pwd}} + \phi_{pde} \frac{\int_0^\infty u_{pded} C_{pde}\{z, u_{pded}\} f\{u_{pded}\} du_{pded}}{\int_0^\infty u_{pded} f\{u_{pded}\} du_{pded}} + \phi_{pve} C_{pve} \quad (15)$$

Le modèle contient 11 paramètres dont 9 indépendants, i.e. le bilan de masse globale et la définition des fractions volumiques des sous-phases relient certains paramètres. À l'aide de relations (montrées précédemment) reliant les paramètres et d'estimations de paramètres faites à l'aide des données de RPT, seulement 3 paramètres ont été obtenus par régression non-linéaire, soit la vitesse du solide dans la sous-phase particule-sillage, le coefficient d'échange de la sous-phase particule-sillage à la sous-phase particule-émulsion-vortex et le coefficient de dispersion axiale du solide dans la sous-phase particule-émulsion-vortex.

Les régressions ont été faites sur l'évolution axiale des courbes de traceur, C_s vs t, pour un système en cuvée. Ces courbes ont été obtenues à l'aide des données de la RPT. Suivre l'évolution de ces courbes est plus exigeant pour un modèle que faire une régression sur une seule distribution de temps de séjours ou sur un profil axial de traceur en régime permanent. Les courbes « C_s vs t » générées par le modèle suivent assez bien l'évolution des données expérimentales. Le modèle de dispersion axiale (modèle piston-dispersif avec vitesse nulle : système en cuvé) a aussi été exploité afin d'étudier de quelle façon il pouvait suivre l'évolution axiale des courbes expérimentales « C_s vs t ». Le modèle de dispersion axiale suivait moins bien les courbes expérimentales, indiquant qu'un seul paramètre n'est pas suffisant pour représenter le mélange du solide. Cassanello et al. (1995) ont montré que leur

modèle (équations (8) et (9)) sous-estimait le temps de mélange du solide parce que le mélange axial n'était pas considéré. Leur modèle et le modèle de dispersion axiale, étant des cas particuliers du modèle proposé dans cette thèse, ne peuvent mieux suivre les courbes expérimentales. Le modèle de mélange de la phase solide proposé dans cette thèse est celui qui suit le mieux l'intensité du mélange et le seul qui peut suivre l'importance relative des mécanismes de mélange, mais il peut quand même être amélioré. Pour le lit de 0.292 m de diamètre, l'évolution des courbes expérimentales « C_s vs t » était moins bien suivie par le modèle que pour le lit de 0.10 m. Le modèle pourrait mieux suivre les courbes expérimentales en considérant l'évolution axiale de certains paramètres comme la fraction volumique des sous-phases et les moyennes et ÉT des distributions de vitesse de solide. Les meilleurs résultats obtenus par le modèle de Cassanello et al. (1995) l'ont été lorsque l'évolution axiale des vitesses a été considérée.

La vitesse moyenne du solide dans la sous-phase particule-sillage obtenue directement des données de RPT n'a pas été utilisée comme valeur de paramètre du modèle pour la raison suivante : les trajets de la particule radioactive ayant une vitesse Lagrangienne constante, ils parcouraient très rarement toute la hauteur de lit, pouvant débuter et finir à différents endroits le long de l'axe de la colonne. En conséquence, l'utilisation des valeurs obtenues de la RPT aurait eu pour résultat de surestimer l'effet du mécanisme convectif et de la circulation globale du solide. La vitesse obtenue par régression représente donc une vitesse axiale moyenne ou apparente de circulation du solide, décrivant mieux l'évolution des courbes « C_s vs t ». Il a été observé que cette vitesse effective du solide de la sous-phase particule-sillage suit les mêmes tendances que la vitesse obtenue directement des données de RPT, à savoir qu'elle augmente avec les vitesses superficielles du gaz et du liquide ainsi qu'avec le diamètre du réacteur. Les valeurs de vitesse effective sont généralement plus faibles de 7 à 35 % par rapport aux vitesses obtenues directement des données de RPT. Il a été observé que la vitesse du

solide diminue avec l'augmentation de la fraction volumique du solide. Ce dernier varie de 0.2 à 0.5. Autrement dit, la vitesse de circulation du solide diminue lorsque l'inertie de l'ensemble des particules solides augmente (l'interaction entre les particules augmente). Le coefficient d'échange a également tendance à être plus faible à des fractions volumiques de solide plus importantes. La valeur du coefficient d'échange varie de 0.03 à 1 s^{-1}.

La valeur du coefficient de dispersion axiale du solide dans la phase particule-émulsion-vortex varie considérablement. Elle passe de $2x10^{-14}$ à $3x10^{-2}$ m^2/s. Evidemment, le coefficient de dispersion axiale du solide dans la phase particule-émulsion-vortex est systématiquement plus faible que le coefficient de dispersion effectif obtenu par régression du modèle de dispersion axiale à cause que le mécanisme convectif domine sur le mélange du solide. La valeur de ce dernier passe de $4x10^{-2}$ à $1x10^{-1}$ m^2/s (même ordre de grandeur que Fan et al. (1987)). Bien que le modèle de dispersion axiale ne soit pas adéquat pour représenter le mélange des phases, spécialement pour prédire la conversion et la sélectivité quand les réactions chimiques sont rapides, il est beacoup utilisé dans la litérature.

CHAPITRE 7 : CONCLUSION ET RECOMMANDATIONS

7.1 Conclusion

Le premier objectif de la thèse était d'identifier les caractéristiques clés liées à l'hydrodynamique des phases dans les lits fluidisés à trois phases. Deux moyens ont été utilisés afin de répondre au premier objectif, soit de réaliser une revue critique de la littérature et des tests de suivi d'une particule radioactive (RPT). Le premier moyen a permis de répondre qualitativement (conceptuellement) au premier objectif en développant un modèle schématique montrant l'interaction entre les phases. Ce modèle est une mise à jour du « structural wake model ». Dans la mise à jour, le liquide et le

solide dans le sillage des bulles ne montent pas seulement à la vitesse moyenne des bulles, ils suivent aussi la distribution de vitesse des bulles et le même mécanisme de mélange que la phase gazeuse, i.e. le mécanisme convectif. Le liquide et le solide dans la phase émulsion sont divisés en deux sous-phases, soit une sous-phase où le liquide et le solide ont un mouvement net de montée ou de descente et une sous-phase où le liquide et le solide ont un déplacement net nul (vitesse moyenne nul). Une fraction du liquide et du solide suivent donc en plus un mécanisme dispersif.

Les paramètres du modèle schématique ont été mesurés pour la phase solide à l'aide de la technique de suivi d'une particule radioactive (RPT) sur deux lits fluidisés à trois phases, soit de 0.10 et de 0.292 m de diamètre. La vitesse moyenne et l'écart-type (ÉT) des distributions de vitesse du solide ont été obtenus pour chacune des sous-phases de la phase solide. De plus, la fraction volumique des sous-phases a été calculée. La valeur de tous ces paramètres donne l'importance relative du mécanisme convectif sur le mécanisme dispersif. Cette étude a permis de répondre quantitativement au premier objectif de la thèse. Voici les principales conclusions de cette étude.

La distribution de vitesse du solide ainsi que sa moyenne et son ÉT ont été obtenus pour les trois sous-phases de la phase solide. Pour un lit fluidisé à trois phases, le solide dans la sous-phase où les particules ont un mouvement net de descente, nommée la sous-phase particule-émulsion-descente, suit un mécanisme de mélange convectif. Cela est causé par un effet compensatoire du solide montant dans le sillage des bulles, nommée la sous-phase particule-sillage, qui suit un mécanisme convectif provenant du mélange convectif des bulles. Le solide dans la sous-phase où le solide n'a pas de mouvement net, nommée la sous-phase particule-émulsion-vortex, suit un mouvement erratique attribué à un mécanisme dispersif. L'ÉT de la distribution de vitesse du solide dans les sous-phases convectives (particule-sillage et particule-émulsion-

descente) représente donc l'importance relative du mécanisme convectif en terme d'intensité de mélange. L'ÉT de la sous-phase particule-émulsion-vortex représente l'intensité de mélange générée par le mécanisme dispersif. Une observation qui pourrait être utile pour une mise à l'échelle est que l'ÉT adimensionnel (ÉT/vitesse moyenne) des sous-phases convectives n'est fonction que du diamètre du lit fluidisé. L'ÉT et la vitesse moyenne du solide des sous-phases convectives augmentent avec les vitesses superficielles du gaz et du liquide ainsi qu'avec le diamètre du lit fluidisé. La vitesse moyenne du solide dans la sous-phase particule-émulsion-vortex est nulle et l'ÉT augmente avec les vitesses superficielles du gaz et du liquide ainsi qu'avec le diamètre du lit fluidisé.

La fraction volumique de chacune des phases donne l'importance relative du mécanisme convectif sur le mécanisme dispersif en terme de poids de chaque sous-phase (chaque mécanisme de mélange). La fraction volumique des sous-phases a un comportement plus complexe que la moyenne et l'ÉT des distributions de vitesse du solide. Pour le lit de 0.292 m, la fraction volumique de la sous-phase particule-sillage augmente avec la vitesse superficielle du gaz pour de faibles vitesses superficielles du liquide, mais diminue avec la vitesse superficielle du gaz pour de grandes vitesses superficielles du liquide. En fait, la relation entre la fraction volumique de la sous-phase particule-sillage et $Ug+U_L$ suit une forme de type parabolique. Les causes de cette forme ont été expliquées dans le corps de la thèse et sont liées à l'effet des conditions opératoires sur l'évolution du volume relatif du sillage des bulles et de la fraction volumique du solide dans le sillage des bulles. La fraction volumique de la sous-phase particule-sillage diminue avec le diamètre du lit fluidisé. Pour le lit de 0.10 m de diamètre, la fraction volumique de la sous-phase particule-sillage augmente avec les vitesses superficielles de gaz et de liquide.

Des corrélations ont été développées pour estimer les différents paramètres discutés. Un indicateur montrant l'importance relative du mécanisme convectif sur le mécanisme dispersif a été développé. Cet indicateur, nommé MMI, a permis de montrer que l'importance relative du mécanisme convectif suit un comportement complexe comme la fraction volumique du solide dans la sous-phase particule-sillage. L'intensité de mélange ne suit pas le même effet des conditions opératoires que l'importance relative du mécanisme convectif. Autrement dit, lorsque l'intensité de mélange augmente, l'importance relative du mécanisme convectif peut augmenter ou diminuer, selon les conditions opératoires et le diamètre du lit fluidisé. Un modèle de mélange doit pouvoir suivre tant l'intensité que l'importance relative des mécanismes de mélange. Tout cela consiste en des caractéristiques clés liées à l'hydrodynamique.

Le deuxième objectif de la thèse était de développer un modèle de mélange le plus simple possible, mais qui respecte les caractéristiques clés liées à l'hydrodynamique. Un modèle de mélange de la phase solide contenant les paramètres qui viennent d'être discutés et pouvant suivre tant l'évolution de l'intensité de mélange que l'importance relative du mécanisme convectif sur le mécanisme dispersif a été développée. À l'aide de relations reliant les paramètres et d'estimations de paramètres faites à partir des données de RPT, seulement 3 paramètres ont été obtenus par régression non-linéaire. Les régressions ont été faites sur l'évolution axiale des courbes de traceur, C_s vs t, pour un système en cuvé. Ces courbes ont été obtenues à l'aide des données de la RPT. Suivre l'évolution de ces courbes est plus exigeant pour un modèle que faire une régression sur une seule distribution de temps de séjours ou sur un profil axial de traceur en régime permanent. Les courbes « C_s vs t » générées par le modèle suivent assez bien l'évolution des données expérimentales. Le modèle de dispersion axiale (modèle piston-dispersif avec vitesse nulle : système en cuvé) a aussi été exploité afin d'étudier de quelle façon il pouvait suivre l'évolution axiale des courbes expérimentales « C_s vs t ». Le modèle de dispersion axiale suivait moins bien les

courbes expérimentales, indiquant qu'un seul paramètre n'est pas suffisant pour représenter le mélange du solide. Cassanello et al. (1995) ont montré que leur modèle, basé sur le « structural wake model », sous-estimait le temps de mélange du solide parce que le mélange axial n'était pas considéré. Leur modèle et le modèle de dispersion axiale, étant des cas particuliers du modèle proposé dans cette thèse, ne peuvent suivre mieux les courbes expérimentales. Le modèle de mélange de la phase solide proposé dans cette thèse est celui qui suit le mieux l'intensité du mélange et le seul qui peut suivre l'importance relative des mécanismes de mélange, mais il peut quand même être amélioré. Pour le lit de 0.292 m de diamètre, l'évolution des courbes expérimentales « C_s vs t » était moins bien suivie par le modèle que pour le lit de 0.10 m. Le modèle pourrait mieux suivre les courbes expérimentales en considérant l'évolution axiale de certains paramètres comme la fraction volumique des sous-phases et les moyennes et ÉT des distributions de vitesse de solide. Les meilleurs résultats obtenus par le modèle de Cassanello et al. (1995) l'ont été lorsque l'évolution axiale des vitesses a été considérée.

7.2 Recommandations

Des recommandations visant principalement l'amélioration du modèle proposé dans cette thèse et le développement d'autres modèles sont présentées ici.

- Inclure le profil axial des paramètres du modèle dans l'exploitation du modèle de mélange. Le profil des paramètres peut être obtenu à l'aide des données de RPT. Dans ce cas, la vitesse du solide dans le sillage des bulles ne serait pas obtenue par régression, mais plutôt fournie dans la résolution des équations différentielles. Si l'évolution des courbes expérimentales « C_s vs t » est mieux suivie, des relations quantifiant le profil des paramètres identifiés comme améliorant les prédictions du modèle pourraient être développées.

- Mettre en compétition le modèle de mélange avec les résultats d'une simulation Monte-Carlo. La simulation devrait utiliser les distributions de vitesse du solide, les profils de fraction volumique des sous-phases ainsi que les distributions de « spending time ». Des simulations en 1D, 2D et 3D pourraient être faites. Pour les simulations en 2D et 3D, les champs de vitesses moyennes estimées pourraient être comparés aux champs obtenus expérimentalement lors de cette thèse.

- Effectuer des mesures locales de distribution de vitesses de bulles à l'aide de fibres optiques par exemple. Ces mesures devraient être faites aux mêmes conditions opératoires qui ont servi à obtenir les données de RPT. Ces mesures serviraient à développer un modèle de coalescence/rupture de bulles.

- Le modèle de coalescence/rupture de bulles pourrait être inclu dans un modèle CFD simulant la variabilité des vitesses avec une contribution du mécanisme convectif (une série de termes de transport de quantité de mouvement par convection en parallèle (comme une série de réacteurs piston en parallèle) et une contribution pourrait être modélisée par la théorie de la turbulence. La contribution du mécanisme convectif serait liée par le modèle de coalescence/rupture de bulles.

RÉFÉRENCES

AUFDERHEIDE, E. and A. VOGELPOHL. (1986) << Convective model to interpret dispersed-phase residence time measurements in pulsed liquid/liquid extractors >>. Chemical Engineering Science. Vol. 41. 1747-1757.

BAIRD, M. H. and R. G. RICE. (1975) << Axial dispersion in large unbaffled columns >>. Chemical Engineering Journal. Vol. 9. 171-174.

BECKER, S., A. SOKOLICHIN and G. EIGENBERGER. (1994) << Gas-liquid flow in bubble columns and loop reactors: part II. Comparison of detailed experiments and flow simulations. >>. Chemical Engineering Science. Vol. 49. 5747-5762.

BHAGA, D. and M. WEBER. (1981) << Bubbles in viscous liquids: shapes, wakes and velocities. >>. Journal of Fluid Mechanics. Vol. 105. 61-85.

BHAGA, D. and M. E. WEBER. (1980) << In-line interaction of pair of bubbles in a viscous liquid >>. Chemical Engineering Science. Vol. 35. 2467-2474.

BHATIA, V. K. and N. EPSTEIN (1974). Three-phase fluidization: a generalized wake model. Fluidization and its application. H. Angélino, Couderc,J.P., Gilbert, H. Laguérie, C. Toulouse, France, Cépaduès-Editions: 380-392.

BRIAN, B. and P. N. DYER (1984). The effect of gas and liquid velocities and solid size on solid suspension in a three-phase bubble column reactor. Symposium series ACS Chem. Catal. React. Model.

CASSANELLO, M., F. LARACHI, C. GUY and J. CHAOUKI. (1996) << Solids mixing in gas-liquid-solid fluidized beds: experiments and modelling. >>. Chemical engineering Science. Vol. 51. 2011-2020.

Cassanello, M., F. Larachi, C. Guy and J. Chaouki. (1996) << Solids mixing in gas-liquid-solid fluidized beds: experiments and modelling. >>. Chemical engineering Science. Vol. 51. 2011-2020.

CASSANELLO, M., F. LARACHI, M.-N. MARIE, C. GUY and J. CHAOUKI. (1995) << Experimental characterization of the solid phase chaotic dynamics in three-phase fluidization. >>. Industrial and Engineering Chemistry Research. Vol. 34. 2971-2980.

Cassanello, M., F. Larachi, M.-N. Marie, C. Guy and J. Chaouki. (1995) << Experimental characterization of the solid phase chaotic dynamics in three-phase fluidization. >>. Industrial and Engineering Chemistry Research. Vol. 34. 2971-2980.

CHEN, R. C., J. REESE and L. S. FAN. (1994) << Flow structure in a three-dimensional bubble column and three-phase fluidized bed >>. American Institute of Chemical Engineering Journal. Vol. 40. 1093-1104.

COCKX, A., Z. DO-QUANG, A. LINE and M. ROUSTAN. (1999) << Use of computational fluid dynamics for simulating hydrodynamics and mass transfer in industrial ozonation tower. >>. Chemical Engineering Science. Vol. 54. 5085-5090.

COVA, D. R. (1966) << Catalyst suspension in gas-agitated tubular reactors. >>. Industrial and Engineering Chemistry. Process Design and Development. Vol. 5. 20-25.

DARTON, R. C. (1985) The physical behavior of three-phase fluidized beds, chapter 15 in Fluidization. Academic Press.

DARTON, R. C. and D. HARRISON. (1974) << The rise of single gas bubbles in liquid fluidised beds >>. Transactions of the Institute of Chemical Engineers. Vol. 53. 301.

DAVIES, R. M. and G. I. TAYLOR. (1950) << The mechanics of large bubbles rising through extended liquids and through liquids in tubes. >>. Proc. Royal Soc. Vol. A200. 375.

DAYAN, A. and S. ZALMANOVICH. (1982) << Axial dispersion and entrainment of particles in wakes of bubbles. >>. Chemical Engineering Science. Vol. 37. 1253-1257.

Dayan, A. and S. Zalmanovich. (1982) << Axial dispersion and entrainment of particles in wakes of bubbles. >>. Chemical Engineering Science. Vol. 37. 1253-1257.

DECKWER, W.-D., R. BURCKHART and G. ZOLL. (1974) << Mixing and mass transfer in tall bubble columns. >>. Chemical Engineering Science. Vol. 29. 2177-2188.

DECKWER, W.-D. and A. SCHUMPE. (1987) << Bubble columns - the state of the art and current trends >>. International Chemical Engineering. Vol. 27. 405-422.

DECKWER, W.-D. and A. SHUMPE. (1993) << Improved tools for bubble column reactor design and scale-up. >>. Chemical Engineering Science. Vol. 48. 889-911.

DEGALEESAN, S. (1997) Fluid dynamic measurements and modelling of liquid mixing in bubble columns Department of chemical engineering. Saint-Louis. Washington university.

DEGALEESAN, S., M. P. DUDUKOVIC, B. A. TOSELAND and B. L. BHATT. (1997) << A two-compartment convective-diffusion model for slurry bubble column reactors >>. Industrial and Engineering Chemistry Research. Vol. 36. 4670-4680.

DEGALEESAN, S., S. ROY, B. KUMAR and M. P. DUDUKOVIC. (1996) << Liquid mixing based on convection and turbulent dispersion in bubble columns >>. Chemical Engineering Science. Vol. 51. 1967-1976.

DELNOIJ, E., J. A. M. KUIPERS and W. P. M. VAN SWAAIJ. (1997) << Computional fluid dynamics applied to gas-liquid contactors >>. Chemical Engineering Science. Vol. 52. 3623-3638.

DEVANATHAN, N., D. MOSLEMIAN and M. P. DUDUKOVIC. (1990) << Flow mapping in bubble columns using CARPT >>. Chemical Engineering Science. Vol. 45. 2285-2291.

EL-TEMTAMY, S. A., Y. O. EL-SHARNOUBI and M. M. EL-HALWAGI. (1979a) << Liquid dispersion in gas-liquid fluidized beds Part I: Axial dispersion. The axially dispersed plug-flow model. >>. The Chemical Engineering Journal. Vol. 18. 151-159.

EL-TEMTAMY, S. A. and N. EPSTEIN. (1978) << Bubble wake solids content in three-phase fluidized beds. >>. Int J Multiphase Flow. Vol. 4. 19-31.

EL-TEMTAMY, S. A. and N. EPSTEIN. (1980) << Simultaneous solids entrainment and de-entrainment above a three-phase fluidized bed >>. Fluidization. Vol. 519-528.

EPSTEIN, N. (1981) << Three-phase fluidization : some knowledge gaps. >>. The Canadian Journal of Chemical Engineering. Vol. 59. 649-657.

FAN, L.-S. (1989) Gas-liquid-solid fluidisation engineering. Butterworths, Massachusetts Institute of Technology.

FAN, L. S. (1989) Gas-liquid-solid fluidisation engineering. Butterworths, Massachusetts Institute of Technology.

Fan, L. S. (1989) Gas-liquid-solid fluidisation engineering. Butterworths, Massachusetts Institute of Technology.

FAN, L.-S. and K. TSUCHIYA. (1990) Bubble wake dynamics in liquid and liquid-solid suspensions. Butterworths, Massachusetts institute of technology.

Fan, L.-S. and K. Tsuchiya. (1990) Bubble wake dynamics in liquid and liquid-solid suspensions. Butterworths, Massachusetts institute of technology.

FAN, L.-S., T. YAMASHITA and R. H. JEAN. (1987) << Solids Mixing and Segregation in a Gaz-Liquid-Solid Fluidized Bed >>. Chemical Engineering Science. Vol. 42. 17-25.

Fan, L.-S., T. Yamashita and R. H. Jean. (1987) << Solids Mixing and Segregation in a Gaz-Liquid-Solid Fluidized Bed >>. Chemical Engineering Science. Vol. 42. 17-25.

FAN, L.-S. and G. YANG (2002). Gas-liquid-solid three-phase fluidization. Handbook of fluidization and fluid-particle systems. Y. a. D. Wen-Ching, M. **Chapter 27**.

Fan, L.-S. and G. Yang (2002). Gas-liquid-solid three-phase fluidization. Handbook of fluidization and fluid-particle systems. Y. a. D. Wen-Ching, M. **Chapter 27**.

FAN, L. T. and Y. CHANG. (1979) << Mixing of large particles in two-dimesional gas fluidized beds. >>. The Canadian Journal of Chemical Engineering. Vol. 57. 88-97.

FARKAS, E. and P. F. LEBLOD. (1969) << Solids concentration profile in the bubble column slurry reactor. >>. The Canadian Journal of Chemical Engineering. Vol. 47. 215-217.

FIELD, R. W. and J. F. DAVIDSON. (1980) << Axial dispersion in bubble columns. >>. Institution of Chemical Engineers. Vol. 58. 228-236.

FISCHER, J., H. KUMAZAWA and E. SADA. (1994) << On the local gas holdup and flow pattern in standard-type bubble columns >>. Chemical Engineering and Processing. Vol. 33. 7-21.

FRANZ, K., T. BÖRNER, H. J. KANTOREK and R. BUCHHOLZ. (1984) << Flow structures in bubble columns >>. German Chemical Engineering. Vol. 7. 365-374.

GERVAIS, A., C. L. BRIENS, J. C. ANDRÉ and G. WILD. (1995) << A modified axial dispersion model applied to three-phase fluidized bed reactors with a transition zone >>. Transactions of the Institute of Chemical Engineers. Vol. 73. (Part A). 745-750.

GIDASPOW, D., M. BAHARY and U. K. JAYASWAL. (1994) << Hydrodynamic models for gas-liquid-solid fluidization. >>. Numerical Methods in multiphase flows. Vol. 185. 177-123.

GODBOLE, S. P., M. F. HONATH and Y. T. SHAH. (1982) << Holdup structure in highly viscous newtonian and non-newtonian liquids in bubble columns. >>. Chemical Engineering Communications. Vol. 16. 119-134.

GODBOLE, S. P., S. JOSEPH and Y. T. SHAH. (1984) << Hydrodynamics and mass transfer in a bubble column with an organic liquid. >>. The Canadian Journal of Chemical Engineering. Vol. 62. 440-445.

GRACE, J. R. (1982) Fluidization. McGraw-Hill.

Grace, J. R. (1982) Fluidization. McGraw-Hill.

GRANDJEAN, B. P. A. and J. CHAOUKI. (1993) << Application of a monte carlo method to solid flow pattern visualization in CFB. >>. Chemical Reactor Technology for Environmentally Safe Reactors and Products. Vol. 537-546.

GRANDJEAN, B. P. A., C. HYNDMAN and C. GUY. (1995) << A monte-carlo simulation of gas phase hydrodynamics in bubble columns. >>. Chemical Engineering Communications. Vol. 133. 93-105.

GREVSKOTT, S., B. H. SANNAES, M. P. DUDUKOVIC, K. W. HJARBO and H. F. SVENDSEN. (1996) << Liquid circulation, bubble size distributions, and solids movement in two- and three-phase bubble columns. >>. Chemical Engineering Science. Vol. 51. 1703-1713.

GROEN, J. S., R. G. C. OLDEMAN, R. F. MUDDE and H. E. A. VAN DEN AKKER. (1996) << Coherent structures and axial dispersion in bubble column reactors >>. Chemical Engineering Science. Vol. 51. 2511-2520.

GROSSMAN, S. and I. PROCACCIA. (1984) << Unified theory of relative turbulent diffusion. >>. Physical review. Vol. A29. 1358-1365.

HEBRARD, G., D. BASTOUL and M. ROUSTAN. (1996) << Influence of gas sparger on hydrodynamic behaviour of bubble columns >>. Transactions of the Institute of Chemical Engineers. Vol. 74. 406-414.

HIKITA, H. and H. KIKUKAWA. (1974) << Liquid-phase mixing in bubble columns: effect of liquid properties >>. Chemical Engineering Journal and the Biochemical Engineering Journal. Vol. 8. 191-197.

HYNDMAN, C. (1995) Gas phase hydrodynamics of bubble columns, Ph.D. Thesis Chemical engineering department. Montréal. École Polytechnique de Montréal.

HYNDMAN, C. and C. GUY. (1995a) << Gas phase flow in bubble columns: a convective phenomenon >>. The Canadian Journal of Chemical Engineering. Vol. 73. 426-434.

Hyndman, C. and C. Guy. (1995a) << Gas phase flow in bubble columns: a convective phenomenon >>. The Canadian Journal of Chemical Engineering. Vol. 73. 426-434.

HYNDMAN, C. and C. GUY. (1995b) << Gas-phase hydrodynamics in bubble columns >>. Transactions of the Institute of Chemical Engineers. Vol. 73. 302-307.

HYNDMAN, C., F. LARACHI and C. GUY. (1997) << Understanding gas-phase hydrodynamics in bubble columns: a convective model based on kinetic theory >>. Chemical Engineering Science. Vol. 52. 63-77.

IMAFUKU, K., T.-Y. WANG, K. KOIDE and H. KUBOTA. (1968) << The behavior of suspended solid particles in the bubble column. >>. Journal of Chemical Engineering of Japan. Vol. 1. 153-158.

JEAN, R. H., W. T. TANG and L.-S. FAN. (1989) << The sedimentation-dispersion model for slurry bubble columns. >>. American Institute of Chemical Engineering Journal. Vol. 35. 662-665.

JEAN, R. H., W. T. TANG and L. S. FAN. (1989) << The sedimentation-dispersion model for slurry bubble columns. >>. American Institute of Chemical Engineering Journal. Vol. 35. 662-665.

JOSEPH, S. and Y. T. SHAH. (1986) << Errors caused by tracer solubility in the measurement of gas phase axial dispersion. >>. The Canadian Journal of Chemical Engineering. Vol. 64. 380-386.

JOSEPH, S., Y. T. SHAH and B. G. KELKAR. (1984) << Simple experimental technique to measure gas phase dispersion in bubble columns. >>. Chemical Engineering Communications. Vol. 28. 223-230.

JOSHI, J. B. (1980) << Axial mixing in multiphase contactors -a unfied correlation. >>. Institution of Chemical Engineers. Vol. 58. 155-165.

JOSHI, J. B. (1982) << Gas phase dispersion in bubble columns >>. The Chemical Engineering Journal. Vol. 24. 213-216.

JOSHI, J. B. and Y. T. SHAH. (1981) << Hydrodynamic and mixing models for bubble column reactors >>. Chemical Engineering Communications. Vol. à voir. 165-199.

JOSHI, J. B. and M. M. SHARMA. (1978) << Liquid phase backmixing in sparged contactors >>. The Canadian Journal of Chemical Engineering. Vol. 56. 116-119.

JOSHI, J. B. and M. M. SHARMA. (1979) << A circulation cell model for bubble columns >>. Transactions of the Institute of chemical Engineers. Vol. 57. 244-251.

KAFAROV, V. V., V. P. VOROB'EV and V. A. KLIPINISTER. (1973) << Modeling of a flow reactor for a two-phase liquid-liquid system. >>. Journal of Applied Chemistry of the USSR (English translation of Zhurnal Prikladnoi Khimii). Vol. 46. 2645-2649.

KAGO, T., T. SARUWATARI, S.-I. OHNO, S. MOROOKA and Y. KATO. (1987) << Axial mixing of liquid in horizontal two phase slug flow. >>. Journal of Chemical Engineering of Japan. Vol. 20. 252-256.

KANG, Y., K. J. WOO, M. H. KO and S. D. KIM. (1997) << Particle dispersion and pressure fluctuations in three-phase fluidized beds >>. Chemical Engineering Science. Vol. 52. 3723-3732.

KANTAK, M. V., R. P. HESKETH and B. G. KELKAR. (1995) << Effect of gas and liquid properties on gas phase dispersion in bubble columns >>. The Chemical Engineering Journal. Vol. 59. 91-100.

KANTAK, M. V., S. A. SHETTY and B. G. KELKAR. (1994) << Liquid phase backmixing in bubble column reactors-a new correlation. >>. Chemical engineering Communications. Vol. 127. 23-34.

KARA, S., B. KELKAR, Y. T. Shah and N. L. CARR. (1982) << Hydrodynamics and axial mixing in a three-phase bubble column. >>. Industrial and Engineering Chemistry. Process Design and Development. Vol. 21. 584-594.

KATO, Y., S. MOROOKA, M. OYAMA, T. KAGO and S. Z. YANG. (1985) << Longitudinal dispersion coefficient of liquid in three-phase bed for gas-liquid-solid systems. >>. Journal of Chemical Engineering of Japan. Vol. 18. 313-318.

KATO, Y. and A. NISHIWAKI. (1972) << Longitudinal dispersion coefficient of a liquid in bubble column. >>. International Chemical Engineering. Vol. 12. 82-187.

KATO, Y., A. NISHIWAKI, T. FUKUDA and S. TANAKA. (1972) << The behavior of suspended solid particles and liquid in bubble columns. >>. Journal of Chemical Engineering of Japan. Vol. 5. 112-118.

KAWAGOE, M., T. OTAKE and C. W. ROBINSON. (1989) << Gas-phase mixing in bubble columns. >>. Journal of Chemical Engineering of Japan. Vol. 22. 136-142.

KAWASE, Y. and M. MOO-YOUNG. (1986) << Liquid phase mixing in bubble columns with Newtonian and non-Newtonian fluids >>. Chemical Engineering Science. Vol. 41. 1969-1977.

KELKAR, B. G., S. P. GODBOLE, M. F. HONATH, Y. T. SHAH, N. L. CARR and W.-D. DECKWER. (1983) << Effect of addition of alcohols on gas holdup and backmixing in bubble columns. >>. American Institute of Chemical Engineering Journal. Vol. 29. 361-369.

KIARED, K., F. LARACHI, C. GUY and C. CHAOUKI. (1997) << Trajectory length and residence-time distributions of the solids in three-phase fluidized beds >>. Chemical Engineering Science. Vol. 52. 3931-3939.

KIARED, K., F. LARACHI, C. GUY and J. CHAOUKI. (1997) << Trajectory length and residence-time distributions of the solids in three-phase fluidized beds >>. Chemical Engineering Science. Vol. 52. 3931-3939.

Kiared, K., F. Larachi, C. Guy and J. Chaouki. (1997) << Trajectory length and residence-time distributions of the solids in three-phase fluidized beds >>. Chemical Engineering Science. Vol. 52. 3931-3939.

KIM, C. H., H. DELMAS and J. P. RIBA. (1991) << Liquid-solid mass transfer and axial dispersion in three-phase fluidization. >>. International Chemical engineering. Vol. 31. 303-314.

KIM, C. H. and S. D. KIM. (1981) << Liquid phase dispersion in three phase fluidized beds. >>. Proceeding of the 2nd world congress of chemical engineering. Vol. III. 1-4.

KIM, S. D., C. G. J. BAKER and M. A. BERGOUGNOU. (1977) << Bubble characteristics in three-phase fluidized beds >>. Chemical Engineering Science. Vol. 32. 1299-1306.

KIM, S. D., G. J. BAKER and M. A. BERGOUGNOU. (1972) << Hold-up and axial mixing characteristics of two and three phase fluidized beds. >>. The Canadian Journal of Chemical Engineering. Vol. 50. 695-701.

KIM, S. D. and Y. KANG. (1997) << Heat and mass transfer in three-phase fluidized-bed reactors- an overview. >>. Chemical Engineering Science. Vol. 52. 3639-3660.

KNESEBECK, A. and R. GUARDANI. (2004) << Estimation of particle concentration profiles in a three-phase fluidized bed from experimental data and using the wake model >>. Brazilian Journal of Chemical Engineering. Vol. 21. (1). 47-57.

KOJIMA, H., A. IGUCHI and K. ASANO. (1984) << Solid hold-up in bubble column with suspended solid particles under continuous operation. >>. The Canadian Journal of Chemical Engineering. Vol. 62. 346-351.

KRISHNA, R., J. W. A. DE SWART, D. E. HENNEPHOF and J. ELLENBERGER. (1994) << Influence of increased gas density on hydrodynamics of bubble-column reactors >>. American Institute of Chemical Engineering Journal. Vol. 40. 112-119.

KWON, H. W., Y. KANG, S. D. KIM, M. YASHIMA and T. L. FAN. (1994) << Bubble-chord length and pressure fluctuations in three-phase fluidized beds >>. Industrial and Engineering Chemistry Research. Vol. 33. 1852-1857.

LAPIN, A. and A. LÜBBERT. (1994) << Numerical simulation of the dynamics of two-phase gas-liquid flows in bubble columns. >>. Chemical Engineering Science. Vol. 49. 3661-3674.

LARACHI, F., M. CASSANELLO, J. CHAOUKI and C. GUY. (1996) << Flow structure of the solids in a 3-D gas-liquid-solid fluidized bed >>. American Institute of Chemical Engineering Journal. Vol. 42. 2439-2452.

Larachi, F., M. Cassanello, J. Chaouki and C. Guy. (1996) << Flow structure of the solids in a 3-D gas-liquid-solid fluidized bed >>. American Institute of Chemical Engineering Journal. Vol. 42. 2439-2452.

LARACHI, F., M. CASSANELLO, M.-N. MARIE, J. CHAOUKI and C. GUY. (1995) << Solids circulation pattern in three-phase fluidized beds containing binary mixtures of particles as inferred from RPT >>. Transactions of the Institute of Chemical Engineers. Vol. 73. 263-268.

Larachi, F., M. Cassanello, M.-N. Marie, J. Chaouki and C. Guy. (1995) << Solids circulation pattern in three-phase fluidized beds containing binary mixtures of particles as inferred from RPT >>. Transactions of the Institute of Chemical Engineers. Vol. 73. 263-268.

LARACHI, F., G. KENEDY and J. CHAOUKI. (1994) << A gamma-ray detection system for 3-D particle tracking in multiphase reactors. >>. Nucl. Instr. Meth. Vol. A338. 568.

Larachi, F., G. Kennedy and J. Chaouki. (1994) << A gamma-ray detection system for 3-D particle tracking in multiphase reactors. >>. Nucl. Instr. Meth. Vol. A338. 568.

LEE, S. L. P., A. SORIA and H. I. DE LASA. (1990) << Evolution of bubble length distribution in three-phase fluidized beds. >>. AIChE J. Vol. 36. 1763-1767.

LEFEBVRE, S., J. CHAOUKI and C. GUY. (2004) << Phase mixing modeling in multiphase reactors containing gas bubble: a review >>. International journal of chemical reactor engineering. Vol. 2, R2, http://www.bepress.com/ijcre/vol2/R2.

Lefebvre, S., J. Chaouki and C. Guy. (2004) << Phase mixing modeling in multiphase reactors containing gas bubble: a review >>. International journal of chemical reactor engineering. Vol. 2, R2, http://www.bepress.com/ijcre/vol2/R2.

LEFEBVRE, S., J. CHAOUKI and C. GUY. (2006) << Solid Phase Hydrodynamic of Three-Phase Fluidized Bed - A Convective/Dispersive Mixing Mechanism Representation >>. International journal of chemical reactor engineering. Vol. Submited.

Lefebvre, S., J. Chaouki and C. Guy. (2006) << Solid Phase Hydrodynamic of Three-Phase Fluidized Bed - A Convective/Dispersive Mixing Mechanism Representation >>. International journal of chemical reactor engineering. Vol. Submited.

LEFEBVRE, S. and C. GUY. (1999) << Characterization of bubble column hydrodynamics with local measurements. >>. Chemical Engineering Science. Vol. 54. 4895-4902.

LEVENSPIEL, O. (1999) Chemical reaction engineering. John Wiley & Sons. Oregon state university.

Levenspiel, O. (1999) Chemical reaction engineering. John Wiley & Sons. Oregon state university.

LEVENSPIEL, O. and T. L. FITZGERALD. (1983) << A warning on the misuse of the dispersion model >>. Chemical Engineering Science. Vol. 38. 491-493.

Levenspiel, O. and T. L. Fitzgerald. (1983) << A warning on the misuse of the dispersion model >>. Chemical Engineering Science. Vol. 38. 491-493.

LI, Y., J. ZHANG and L.-S. FAN. (1999) << Numerical simulation of gas-liquid-solid fluidization systems using a combined CFD-VOF-DPM method: bubble wake behavior. >>. Chemical Engineering Science. Vol. 54. 5101-5107.

LINDT, J. T. (1972) << On the periodic nature of the drag on a rising bubble. >>. Chemical Engineering Science. Vol. 27. 1775-1781.

LINDT, J. T. and R. G. F. DE GROOT. (1974) << Drag on a single bubble accompanied by periodic wake. >>. Chemical Engineering Science. Vol. 29. 957-962.

LINEK, V., V. STOY, V. MACHON and Z. KRVSKY. (1974) << Increasing the effective interfacial area in plastic-packed bed absorption column. >>. Chemical Engineering Science. Vol. 29. 1955.

LÜBBERT, A. and B. LARSON. (1987) << A new method for measuring local velocities of the continous liquid phase in strongly aerated gas-liquid multiphase reactors >>. Chemical Engineering and technologies. Vol. 10. 27-32.

LÜBBERT, A. and B. LARSON. (1990) << Detailed investigations of the multiphase flow in airlift tower loop reactors >>. Chemical Engineering Science. Vol. 45. 3047-3053.

Lübbert, A. and B. Larson. (1990) << Detailed investigations of the multiphase flow in airlift tower loop reactors >>. Chemical Engineering Science. Vol. 45. 3047-3053.

MANGARTZ, K. H. and T. PILHOFER. (1980) << Untersuchungen zur gasphasendispersion in blasensaeulenreaktoren (Studies of the Gas Phase Dispersion in Bubble Column Reactors) >>. Verfahrenstechnik. Vol. 14. 40-44.

MANGARTZ, K. H. and T. PILHOFER. (1981) << Interpretation of mass transfer measurements in bubble columns considering dispersion of both phases. >>. Chemical Engineering Science. Vol. 36. 1069-1077.

MATSUMOTO, T., N. HIDAKA, H. KAMIMURA, M. TSUCHIYA, T. SHIMIZU and S. MOROOKA. (1988) << Turbulent mixing-length model for axial turbulent diffusion of liquid in three-phase fluidized bed. >>. Journal of Chemical Engineering of Japan. Vol. 21. 256-261.

MATSUURA, A. and L.-S. FAN. (1984) << Distribution of bubble properties in a gas-liquid-solid fluidized bed. >>. American Institute of Chemical Engineering Journal. Vol. 30. 894-903.

MATSUURA, A. and L. S. FAN. (1984) << Distribution of bubble properties in a gas-liquid-solid fluidized bed. >>. American Institute of Chemical Engineering Journal. Vol. 30. 894-903.

MITRA-MUDJUMDAR, D., B. FAROUK and Y. T. SHAH. (1997) << Hydrodynamic modeling of three-phase flows trough a vertical column. >>. Chemical Engineering Science. Vol. 52. 4485-4497.

MIYAHARA, T., M. KURIHARA, M. ASODA and T. TAKAHASHI. (1990) << Gas-liquid interfacial area and liquid-phase mass transfer coefficient in sieve plate columns without downcomer operating at high gas velocities >>. Journal of Chemical Engineering of Japan. Vol. 23. 280-285.

MODAK, S. Y., V. A. JUVEKAR and V. C. RANE. (1993) << Dynamics of the gas phase in bubble columns >>. Chemical Engineering technologies. Vol. 16. 303-306.

MODAK, S. Y., V. A. JUVEKAR and V. C. RANE. (1994) << Comparison of the single-bubble-class and modified two-bubble-class models of bubble column reactors >>. Chemical Engineering and technologies. Vol. 17. 313-32.

MOLERUS, O. and M. KURTIN. (1986) << Modelling of residence time distributions of the gas phase in bubble columns in the liquid circulation regime. >>. Chemical Engineering Science. Vol. 41. 2693-2698.

MUDDE, R. F., J. S. GROEN and H. E. A. VAN DEN AKKER. (1997) << Liquid velocity field in a Bubble Columns: LDA experiments >>. Chemical Engineering Science. Vol. 52. 4217-4224.

MUDDE, R. F. and O. SIMONIN. (1999) << Two- and three-dimensional simulation of bubble plume using a two-fluid model. >>. Chemical Engineering Science. Vol. 54. 5061-5069.

MUROYAMA, K. and L.-S. FAN. (1985) << Fundamentals of gas-liquid-solid fluidization. >>. American Institute of Chemical Engineering Journal. Vol. 31. 1-34.

MURRAY, P. and L.-S. FAN. (1989) << Axial solid distribution in slurry bubble column. >>. Industrial and Engineering Chemistry Research. Vol. 28. 1697-1703.

MURRAY, P. and L. S. FAN. (1989) << Axial solid distribution in slurry bubble column. >>. Industrial and Engineering Chemistry Research. Vol. 28. 1697-1703.

Murray, P. and L. S. Fan. (1989) << Axial solid distribution in slurry bubble column. >>. Industrial and Engineering Chemistry Research. Vol. 28. 1697-1703.

MYERS, K., M. P. DUDUKOVIC and P. A. RAMACHANDRAN. (1987) << Modelling churn-turbulent bubble columns - I. Liquid-phase mixing >>. Chemical Engineering Science. Vol. 42. 2301-2311.

NACEF, S., G. WILD, A. LAURANT and S. D. KIM. (1992) << Scale effects in gas-liquid-solid fluidisation. >>. International Chemical Engineering. Vol. 32. 51-72.

NASSAR, R., J. SCHMIDT and A. LÜBBERT. (1992) << A stochastic dispersion model in gas-liquid flow systems >>. Chemical Engineering Science. Vol. 47. 3657-3664.

NAUMAN, E. B. (1981) << Residence time distyribution in systems governed by the dispersion equation. >>. Chemical engineering Science. Vol. 36. 957-966.

NIGAM, K. D. P. and A. SCHUMPE. (1996) Three-phase sparged reactors. Gordon and Breach.

OHKI, Y. and H. INOUE. (1970) << Longitudinal mixing of the liquid phase in bubble coumns. >>. Chemical Engineering Science. Vol. 25. 1-16.

OLMOS, E., C. GENTRIC, C. H. VIAL, G. WILD and N. MIDOUX. (2001) << Numerical simulation of multiphase flow in bubble column reactors. Influence of bubble coalescence and break-up. >>. Chemical Engineering Science. Vol. 56. 6359-6365.

PARULEKAR, S. J. and T. Y. SHAH. (1980) << Steady-state behavior of gas-liquid-solid fluidized-bed reactors. >>. Chemical Engineering Journal and the Biochemical Engineering Journal. Vol. 20. 21-33.

PATEL, S. A., J. G. DALY and D. B. BUKUR. (1989) << Holdup and interfacial area measurements using dynamic gas disengagement >>. American Institute of Chemical Engineering Journal. Vol. 35. 931-942.

PFLEGER, D., S. GOMES, N. GILBERT and H.-G. WAGNER. (1999) << Hydrodynamics simulations of laboratory scale bubble columns fundamental studies of the eulerian- eulerian modelling approach. >>. Chemical Engineering Science. Vol. 54. 5091-5099.

RADE, L. and B. WESTERGREN. (1999) Mathematics handbook for science and engineering, 4ed. Springer-verlans Berlin Heidelberg.

RENOU, S., M. PERRIER, M. DOCHAIN and S. GENDRON. (2003) << Solution of the convection-dispersion-reaction equation by a sequencing method >>. Computer Chemical Engineering. Vol. 27. 615-629.

RICE, R. G. and M. A. LITTLEFIELD. (1987) << Dispersion coefficients for ideal bubbly flow in truly vertical bubble columns. >>. Chemical Engineering Science. Vol. 42. 2045-2053.

RICHARDSON, J. F. and W. N. ZAKI. (1954) << Sedimentation and fluidization-Part 1 >>. Transactions of the Institute of Chemical Engineers. Vol. 32. 35-53.

RIGBY, G. R., G. P. VAN BLOCKLAND, P. E.H. and C. E. CAPES. (1970) << Properties of bubbles in three phase fluidized beds as measured by an electroresistivity probe. >>. Chemical Engineering Science. Vol. 25. 1729-1741.

RIQUARTS, H. P. (1981) << A physical model for axial mixing of the liquid phase for heterogeneous flow regime in bubble columns >>. German Chemical Engineering. Vol. 4. 18-23.

ROGALEWICZ, V. and I. FORT. (1991) << Stochastic model of an agitated gas-liquid system. >>. Computers Chemical Engineering. Vol. 15. 437-444.

RUGH, W. J. (1993) Linear System Theory. Prentice Hall Information and System Science Series. Toronto.

Rugh, W. J. (1993) Linear System Theory. Prentice Hall Information and System Science Series. Toronto.

RUSTEMEYER, U., J. PAULI, T. MENZEL, R. BUCHHOLZ and U. ONKEN. (1989) << Liquid-Phase Mixing Model for Hydrodynamics of Bubble Columns >>. Chemical Engineering and Processing. Vol. 26. 165-172.

SANYAL, J., S. VASQUEZ, S. ROY and M. P. DUDUKOVIC. (1999) << Numerical simulation of gas-liquid dynamics in cylindrical bubble column reactors. >>. Chemical Engineering Science. Vol. 54. 5071-5083.

SCHILLER, L. and A. NAUMANN. (1933) << Zeitschr. >>. V.D.I. Vol. 318-320 (cited by Nigam and Schumpe, 1996).

Schiller, L. and A. Naumann. (1933) << Zeitschr. >>. V.D.I. Vol. 318-320 (cited by Nigam and Schumpe, 1996).

SCHLÜTER, M., S. SCHEID, S. JOHN and N. RÄBIGER. (2004) << Fluidization of fine particles in bubble wake affects hydrodynamics in three-phase flows >>. Journal of chemical engineering of Japan. Vol. 37. (8). 947-954.

SCHLÜTER, S., A. STEIFF and P. M. WEINSPACH. (1992) << Modeling and simulation of bubble column reactors >>. Chemical Engineering and Processing. Vol. 31. 97-117.

SCHMIDT, J., R. NASSAR and A. LÜBBERT. (1992a) << Influence of the wakes in bubble driven multiphase flow systems >>. Chemical Engineering Science. Vol. 47. 2295-2300.

SCHMIDT, J., R. NASSAR and A. LÜBBERT. (1992b) << Local dispersion in the liquid phase of gas-liquid reactors >>. Chemical Engineering Science. Vol. 47. 3363-3370.

SCHUMPE, A. and W.-D. DECKWER. (1982) << Gas holdups, specific interfacial areas, and mass transfer coefficients of aerated carboxymethyl cellulose solutions in a bubble column. >>. Industrial and Engineering Chemistry. Process Design and Development. Vol. 21. 706-711.

SCHUMPE, A. and G. GRUND. (1986) << The gas disengagement technique for studying gas holdup structure in bubble columns. >>. The Canadian Journal of Chemical Engineering. Vol. 64. 891-896.

SHAH, Y. T., S. JOSEPH, D. N. SMITH and A. J. RUETHER. (1985a) << Two-bubble class model for churn-turbulent bubble-column reactors >>. Industrial and Engineering Chemistry. Process Design and Development. Vol. 24. 1096-1104.

SHAH, Y. T., S. JOSEPH, D. N. SMITH and A. J. RUETHER. (1985b) << On the behavior of the gas phase in bubble column with ethanol-water mixtures >>. Industrial and Engineering Chemistry. Process Design and Development. Vol. 24. 1140-1148.

SHAH, Y. T., B. G. KELKAR, S. P. GODBOLE and W.-D. DECKWER. (1982) << Design parameters estimation for bubble column reactors. >>. American Institute of Chemical Engineering Journal. Vol. 28. 353-379.

SHAH, Y. T., G. J. STIEGEL and M. M. SHARMA. (1978) << Backmixing in gas-liquid reactors. >>. American Institute of Chemical Engineering Journal. Vol. 24. 369-400.

SHETTY, S. A., M. V. KANTAK and B. G. KELKAR. (1992) << Gas-phase backmixing in bubble-columns reactors. >>. American Institute of Chemical Engineering Journal. Vol. 38. 1013-1026.

SIKUN, X., J. CHAOUKI, C. GUY and Q. YUHUI. (2005) << Characterization of homogeneity of bubble columns using RPT and fiber optics >>. International journal of chemical reactor engineering. Vol. 3. A54.

SIRAM, K. and R. MANN. (1977) << Dynamic gas disengagement: a new technique for assessing the bahaviour of bubble columns. >>. Chemical Engineering Science. Vol. 32. 571-580.

SMITH, D. N. and A. J. RUETHER. (1985) << Dispersed solid dynamics in a slurry bubble column. >>. Chemical Engineering Science. Vol. 40. 741-754.

SMITH, D. N., J. A. UETHER, Y. T. SHAH and BADGUJAR. (1986) << Modiefied sedimentation-dispersion model for solids in a three-phase slurry column. >>. American Institute of Chemical Engineering Journal. Vol. 32. 426-436.

SOKOLICHIN, A. and G. EIGENBERGER. (1994) << Gas-liquid flow in bubble columns and loop reactors: part I. Detailed modelling and numerical simulation. >>. Chemical Engineering Science. Vol. 49. 5735-5746.

SOKOLICHIN, A., G. EIGENBERGER, A. LAPIN and A. LÜBBERT. (1997) << Dynamics numerical simulation of gas-liquid two-phase flows. >>. Chemical Engineering Science. Vol. 52. 611-626.

STEWART, C. W. (1995) << Bubble interaction in low-viscosity liquids >>. International Journal of Multiphase Flow. Vol. 21. 1037-1046.

TANG, W. T. and L.-S. FAN. (1989) << Hydrodynamics of a three-phase fluidized bed containing low-density particles. >>. American Institute of Chemical Engineering Journal. Vol. 35. 355-364.

Tang, W. T. and L. S. Fan. (1989) << Hydrodynamics of a three-phase fluidized bed containing low-density particles. >>. American Institute of Chemical Engineering Journal. Vol. 35. 355-364.

TARMY, B. L. and C. A. COULALOGLOU. (1992) << Alpha-omega and beyond industrial view of gas/liquid/solid reactor development. >>. Chemical Engineering Science. Vol. 47. 3231-3246.

TOWELL, G. D. and G. H. ACKERMAN. (1972) << Axial mixing of liquid and gas in large bubble reactors. >>. Proceeding of the symposium on chemical reaction engineering. Vol. Amsterdam, Holland, B3-1-B3-13.

TSUTSUMI, A., T. CHARINPANITKUL and K. YOSHIDA. (1992) << Prediction of solid concentration profiles in three-phase reactors by a wake shedding model. >>. Chemical Engineering Science. Vol. 47. 3411-3418.

TURI, E. and K. M. NG. (1986) << Axial distribution of soid particles in bubble column slurry reactors in the bubble flow regime. >>. Chemical Engineering Communications. Vol. 46. 323-345.

Turi, E. and K. M. Ng. (1986) << Axial distribution of soid particles in bubble column slurry reactors in the bubble flow regime. >>. Chemical Engineering Communications. Vol. 46. 323-345.

TZENG, J. W., R. C. CHEN and L.-S. FAN. (1993) << Visualisation of flow characteristics in a 2-D bubble column and three-phase fluidized bed. >>. AIChE J. Vol. 39. 733.

UEYAMA, K. and T. MIYAUCHI. (1979) << Properties of recirculating turbulent two phase flow in gas bubble columns >>. American Institute of Chemical Engineering Journal. Vol. 25. 258-266.

UEYAMA, K., N. TAMURA and S. FURUSAKI. (1985) << Distribution of hold-up of particles in a three-phase fluidized bed. >>. Fluidization 85 science and Technology. Vol. Amsterdam, 274-282.

VAN DER LAAN, G. P., A. A. C. M. BEENACKERS and R. KRISHNA. (1999) << Multicomponent reaction engineering model for Fe-catalyzed Fischer-Tropsch synthesis in comercial scale slurry bubble column reactors. >>. Chemical Engineering Science. Vol. 54. 5013-5019.

VERMEER, D. J. and R. KRISHNA. (1981) << Hydrodynamics and mass transfer in bubble columns operating in the churn-turbulent regime. >>. Industrial and Engineering Chemistry. Process Design and Development. Vol. 20. 475-482.

VILLERMAUX, J. (1996) << Trajectory length distribution (TLD), a novel concept to characterize mixing in flow systems >>. Chemical Engineering Science. Vol. 51. 1939-1946.

Villermaux, J. (1996) << Trajectory length distribution (TLD), a novel concept to characterize mixing in flow systems >>. Chemical Engineering Science. Vol. 51. 1939-1946.

WACHI, S. and Y. NOJIMA. (1990) << Gas-phase dispersion in bubble columns >>. Chemical Engineering Science. Vol. 45. 901-905.

WEBER, M. E. and D. BHAGA. (1982) << Fluid drift caused by a rising bubble. >>. Chemical Engineering Science. Vol. 37. 113-116.

WILD, G., M. SABERIAN, J.-L. SCHWARTZ and J.-C. CHARPENTIER. (1984) << Gas-liquid-solid fluidized-bed reactors. State of the art and industrial possibilities. >>. International Chemical Engineering. Vol. 24. 639-678.

YANENKO, N. N. (1971) The Method of Fractional Steps: The Solution of the Problems of Mathematical Physics in Several Variables. Springer-Verlag. Berlin.

Yanenko, N. N. (1971) The Method of Fractional Steps: The Solution of the Problems of Mathematical Physics in Several Variables. Springer-Verlag. Berlin.

YANG, S. Z. (1986) << A correlation of liquid dispersion in three phase fluidized beds. >>. Proceeding of the 3rd world congress of chemical engineering. Vol. III. 496-499.

Yang, Y. B. and M. P. Dudukovic. (1993) << Liquid backmixing in bubble column via computer-automated radioactive particle tracking (CARPT) >>. Experiments in fluids. Vol. 16. 1-9.

YANG, Y. B., M. P. DUDUKOVIC and M. P. DUDUKOVIC. (1993) << Liquid backmixing in bubble column via computer-automated radioactive particle tracking (CARPT) >>. Experiments in fluids. Vol. 16. 1-9.

YAO, B. P., C. ZHENG, H. E. GASCHE and H. HOFMANN. (1991) << Bubble behaviour and flow structure of bubble columns >>. Chemical Engineering and Processing. Vol. 29. 65-75.

YU, Y. H. and S. D. KIM. (1988) << Bubble caracteristics in the radial direction of three-phase fluidized beds. >>. AIChE J. Vol. 34. 2069-2072.

ZAHRADNIK, J. and M. FIALOVA. (1996) << Effect of bubbling regime on gas and liquid phase mixing in bubble column reactors >>. Chemical Engineering Science. Vol. 51. 2491-2500.

ZEHNER, P. (1986a) << Momentum, mass and heat transfer in bubble columns. Part 1. Flow model of the bubble column and liquid velocities >>. International Chemical Engineering. Vol. 26. 22-28.

ZEHNER, P. (1986b) << Momentum, mass and heat transfer in bubble columns. Part 2. Axial blending and heat transfer >>. International Chemical Engineering. Vol. 26. 29-35.

ZEHNER, P. and G. SCHUCH. (1985) << Concept for the description of gas phase mixing in buble column >>. German Chemical Engineering. Vol. 8. 282-289.

ZHANG, J., Y. LI and L.-S. FAN. (2000) << Numerical studies of bubble and particle dynsmics in a three-phase fluidized bed at elevated pressures >>. Powder technology. Vol. 112. 46-56.